2023

Age-associated Collagen Crosslinking and its Role in Skeletal Muscle Regeneration

Lucas C. Olson
Virginia Commonwealth University

College of Engineering
Biomedical Engineering

Age-associated Collagen Crosslinking and its Role in Skeletal Muscle Regeneration

By

Lucas Christian Olson

A dissertation submitted in partial fulfillment of the requirements for the degree of Doctor of Philosophy in Biomedical Engineering at Virginia Commonwealth University.

Advisor
Michael J. McClure, Ph.D.
Assistant Professor, Department of Biomedical Engineering

Advisory Committee

[1]Zvi Schwartz, D.M.D., Ph.D.; [1]Jennifer L. Puetzer, Ph.D.; [1]Rebecca L. Heise, Ph.D.; [3]Vamsi K. [4]Yadavalli, Ph.D.; Mary S. Shall, P.T., Ph.D.

[1]Department of Biomedical Engineering, VCU College of Engineering; [2]Department of Periodontics, University of Texas Health Science Center at San Antonio; [3]Department of Chemical and Life Science Engineering, Virginia Commonwealth University; [4]Department of Physical Therapy, Virginia Commonwealth University

Acknowledgments

A Ph.D. is more than what one person can do and achieve. I am indebted to a host of mentors, friends, and family for the person, and the “Doctor”, I am today. First, I’d like to thank VCU as a whole for giving me a chance to chase my dreams of becoming a tissue engineer. While this journey has been full of twists, turns, and unexpected difficulties, it has also been marked by hard work, amazing individuals, and second chances.

Dr. Zvi Schwartz, thank you for supporting me with the dual merit scholarship my last semester of undergrad. As always, thank you for teaching me how to stand on an idea scientifically, and for training me how to be organized and efficient. Without your support and mentorship, I would not have made it where I am today! Dr. Josh Cohen, thank you for taking me on as an undergrad in the LMRI lab, and for supporting me through all the growing pains as I learned how to be an organized, regimented scientist. Because of your mentorship, I have been able to study at the doctoral level. Additionally, I am indebted to all of your assistance with the numerous *in vivo* studies during my doctoral training. Next, I’d like to acknowledge my advisor, Dr. Michael McClure. I am grateful to have been your first Ph.D. student, and I thank you for your support of my ideas and believing in me. You have enabled me to be confident as a researcher and a thinker. Also, you have taught me to be bold in my ideas and aspirations.

Next, I’d like to thank my friends in the Ph.D. program. Jingyao, Cydney, Franck, Mario and I have all been through the toughest courses and periods of the Ph.D. program together. Thank you for your friendship outside of work, and for how you have all been team players when it comes to studying, prepping for presentations, or troubleshooting experiments. Additionally, there are other friends that have played crucial roles during my doctoral training. Mark Lewis, my Best Man and compadre, I’ve thoroughly enjoyed all the times where we kicked back and played video games or grabbed food, or when we’ve had long conversations that have helped me unwind and reflect on life. I’d like to thank my groomsmen (in no particular order) Finn Smyth, Seung Kim, Takoda Crawford, Kobe Frimpong, and Matthew Johnson Jr. for sharing in friendship and brotherhood with me. I will always cherish our times together.

I’d like to acknowledge my parents, Larry and Anna Olson, for how they have always supported me academically and for their sacrifices that made it possible for me to reach this point. Dad, thank you for instilling in me a sense of curiosity and a dedication to do my best. Mom, thank you for your

unconditional love and for showing me through example what it means to work hard. I love you both. My sister, Cassady Olson, is a Ph.D. candidate at the University of Chicago studying computational neuroscience. As such, we have been able to uniquely share and bond over the joys and challenges of biological research. Thank you for your love and support, and concern for me to take care of myself when life gets way too busy. I love you. Also, I'd like to thank my father and mother-in-law, Matthew Johnson Sr. and Jennice Johnson, for encouraging me to stick it out in my doctoral studies. Thank you for your love and hospitality and for raising an amazing daughter!

Lastly, I'd like to acknowledge Jenica Olson, my wife. She has supported me throughout my doctoral training, from when we were dating till after we were married. She's inquisitive, curious, intuitive, intelligent, kind, loyal, unique, and ever-so-beautiful. She has truly made this time special, always showering me with love and encouragement. Without her, I don't think I would have remained as emotionally grounded, especially during the hardest moments of this journey. I love you to the moon and back!

Table of Contents

Abstract

Advanced glycation end-products (AGEs) non-enzymatically accumulate on skeletal muscle collagen in old age via the Maillard reaction, causing an increase in intramuscular collagen and a stiffening of the muscle's microenvironment. AGEs abrogate muscle regeneration through stiffening the muscle stem cell (MuSC) microenvironment and by binding to the receptor for advanced glycation end products (RAGE). Stiffer substrates promote MuSC proliferation at the expense of differentiation, and soluble AGEs are known to abrogate myogenic differentiation. Previously our group has demonstrated that decellularized muscle matrix (DMM), a type of extracellular matrix (ECM) scaffold extracted from skeletal muscle, encourages regeneration in a challenging rat volumetric muscle loss (VML) injury. Clinically, most human tissue for organ transplantation is sourced from older donors. My dissertation addresses whether old age is an important factor for DMM, and if this concern is AGE dependent. We isolated DMM from an aged murine model, and proved that AGE cross-links are present and that they are associated with increased stiffness. Further, we demonstrate that AGE-cross-linked collagen is stiffer, and disrupts myoblasts' proliferation and differentiation in a RAGE-dependent manner. Curiously, AGE cross-links reduced RAGE in myoblasts, and RAGE inhibition shut down late myogenesis. Impressively, when myoblasts were challenged with the RAGE agonist S100b, myofiber formation was restored. We next proved that RAGE is significantly regulated in VML injuries, and we could regulate this with adipose-derived stromal cell delivery. Interestingly, AGEs were reduced in VML injuries, most likely due to an increase in new collagen deposition. Finally, we proved that an AGE-laden DMM disrupts muscle regeneration in a VML model and promotes inflammation while downregulating ECM synthesis. This was associated with upregulations in the AGE receptors RAGE and Galectin-3. Altogether, this dissertation provides strong evidence that age matters in the clinical translation of DMM, and AGEs are a prime target for rejuvenation therapies in skeletal muscle aging. Also, future study is warranted into the role that S100b can play in countering the AGE-RAGE axis in old age.

Chapter 1. Specific Aims

Musculoskeletal aging in individuals over 65 years impacts independence, increases the risk for fall-related injuries, and reduces life quality.[1] This is partly caused by a deterioration of the muscle's strength and mass that culminates in sarcopenia, an age-dependent muscle wasting disease.[2] Closely associated with sarcopenia is a reduced regenerative ability that is caused in part by reduced levels of tissue-resident stem cells, called satellite cells.[3] Satellite cells reside underneath the basal lamina in a prolonged quiescent state, and when activated by injury or disease, they create progeny to repair, increase fiber size, and generate new muscle while renewing their stem cell pool.[2] Yet, for reasons that are not fully understood, the number of quiescent satellite cells deplete as we age, reducing our ability to heal, regenerate, and increase muscle mass.[3] One possible mechanism is the effect that aging has on the extracellular matrix (ECM), which can alter satellite cell behavior.[3–7]

This proposal's primary focus is to elucidate mechanisms of skeletal muscle ECM aging and understand how this perturbs skeletal muscle regeneration. In a young environment, skeletal muscle ECM's anisotropic structure and biochemical composition exert a spatiotemporal regulatory role over the activation, differentiation, and subsequent fusion of muscle progenitor cells.[3–5,7] Satellite cells are heavily influenced by their extracellular niche, and while intrinsic aging does impact these multipotent cells, there is copious evidence suggesting that age-related alterations to the extracellular space drive the decline in satellite cell number and ability typical to sarcopenia.[6,8–16] Specifically, increased fibrosis and stiffness of aged skeletal muscle ECM dysregulates the healing process and could hinder the ability of ECM to support myogenesis (Figure 1).[6,17]

Advanced glycation end-products (AGEs), the final derivative of the Maillard or browning reaction, are known to accumulate in musculoskeletal tissues in old age.[18–20] AGEs stochastically modify proteins and are prevalent moieties in diabetes and age-associated pathologies.[20,21] The random nature of the Maillard reaction combined with the constant presence of the precursors (glucose and proteins) causes AGEs to preferentially accumulate on the ECM's long-lived proteins, especially the collagens, which results in an accumulation of sugar cross-links that hinder normal ECM turnover.[21] In addition to having a long half-life, collagens are rich in repeating arginine and lysine amino acids that potentiate the reaction between collagen and AGE precursors, further predisposing collagen to these glycation cross-links.[21] Non-enzymatic cross-linking by AGEs decreases collagen's susceptibility to degradation by matrix metalloproteinases, causing the build-up of collagen and subsequent stiffening of the usually

pliant skeletal muscle ECM.[21] The age-related increase in ECM stiffness decreases satellite cell self-renewal and differentiation, leading to the depletion of the satellite cell pool.[6] Conversely, activated satellite cells express the receptor for advanced glycation end-products (RAGE) that promotes satellite cell differentiation, which could explain the age increase in activated proliferating myoblasts.[16,22–24] If ECM contains age-related modifications, then satellite cell response could be poor, leading to lower regeneration. We hypothesize that non-enzymatic collagen cross-linking by AGEs in old age hinders the ability of ECM to promote regeneration of skeletal muscle.

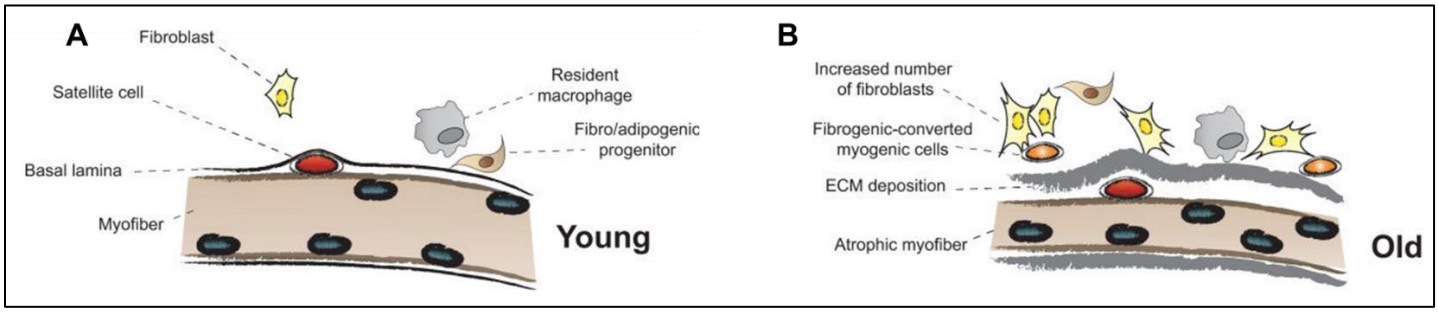

Figure 1. The aged skeletal muscle. In young age (A) the myofiber is hypertrophic and the extracellular matrix is thin and pliant. In old age (B) the myofiber atrophies and the ECM thickens and stiffens. Adapted from Mann et. al.

The overall working hypothesis for this thesis is that the accumulation of advanced glycation end-products (AGEs) in skeletal muscle extracellular matrix (ECM) modifies collagen fibers in a way that impairs myoblast function and inhibits muscle regeneration.

Previous research in our lab has found in a murine model that there is an increase in muscle collagen cross-linking with age, and this effect is retained in processed skeletal muscle ECM.[25] Furthermore, there is a greater presence of collagen and fibrotic mass when examined histologically in native muscle and processed muscle ECM.[25] These data indicated that muscle collagen levels might be elevated due to reduced collagen turnover and increased cross-linking. Decoupling whether cross-linking in muscle ECM independently activates cell receptors that sense biochemical signals or ECM stiffness due to cross-linking has not been determined. This led us to hypothesize that collagen cross-linking, and specifically, AGEs, limit muscle progenitor cell differentiation and regeneration.

Specific Aim 1: Characterize aging muscle and whether AGE-driven alterations to muscle ECM are elevated.

Old muscle ECM contains elevated levels of AGEs that compared to muscle fibers. A model of muscle aging is used, with a focus on the gastrocnemius from 5-week (immature), 10-week (mature), and 90-week (old mature) C57BL/6 mice. Muscles will be decellularized into a testable matrix termed decellularized muscle matrix (DMM). Histology will be used to qualify morphology, as well as the amount of fibrosis and collagen. Fibrosis will be assessed with scanning electron microscopy (SEM) and atomic force microscopy (AFM). The stiffness of these muscles and DMM will be determined with AFM. Levels of collagen cross-linking will be indirectly quantified by measuring the amount of hydroxyproline released from tissue digest. The number of AGEs present in muscle and DMM will be measured using an AGE enzyme-linked-immunosorbent assay (ELISA) normalized to hydroxyproline.

Specific Aim 2: Determine whether AGEs in skeletal muscle ECM impair myoblast differentiation *in vitro* via the receptor for AGEs (RAGE) and integrin signaling.

We will develop a collagen membrane model of AGE cross-linking to test the hypothesis that *AGE cross-links in muscle ECM reduce muscle progenitor cell differentiation and increase proliferation via RAGE and integrin signaling.* Mouse and human myoblasts will be cultured on the AGE-collagen, and the effect of AGEs assessed using proliferation and differentiation assays. RAGE, Nf-kB, and P38 MAPK will be measured to determine their role in the AGE-collagen model. The role of the RAGE receptor will be tested by culturing RAGE mouse myoblasts on AGE-collagen in the presence of RAGE inhibitors and agonist to determine if the phenotype matches control myoblasts on unmodified collagen.

Specific Aim 3: Determine the role of AGEs in skeletal muscle regeneration in vivo.

Whether the presence of AGEs will negatively impact a muscle injury model repaired with DMM will be determined. To test this, AGEs will be measured in a VML injury site. Following this, the role of AGE cross-linked ECM will be tested using a murine injury model repaired with DMM and AGE-DMM. Healing and regeneration in these muscle injury models will be assessed using muscle function tests, histology, and protein analysis.

Chapter 2. Background

Abstract

Advanced age causes skeletal muscle to undergo deleterious changes including muscle atrophy, fast-to-slow muscle fiber transition, and an increase in collagenous material that culminates in the age-dependent muscle wasting disease known as sarcopenia. Advanced glycation end-products (AGEs) non-enzymatically accumulate on the muscular collagens in old age via the Maillard reaction, potentiating the accumulation of intramuscular collagen and stiffening the microenvironment through collagen cross-linking. This review contextualizes known aspects of skeletal muscle extracellular matrix (ECM) aging, especially the role of collagens and AGE cross-linking, and underpins the motor nerve's role in this aging process. Specific directions for future research are also discussed, with the understudied role of AGEs in skeletal muscle aging highlighted. Despite more than a half century of research, the role that intramuscular collagen aggregation and cross-linking plays in sarcopenia is well accepted yet not well integrated with current knowledge of AGE's effects on muscle physiology. Furthermore, the possible impact that motor nerve aging has on intramuscular cross-linking and muscular AGE levels is posited.

Introduction

Musculoskeletal injury increases due to falls and other accidental injuries in old age, and age-dependent alterations to skeletal muscle structure and function are the primary causal factors of such incidents.[26] The etiology of muscle atrophy due to aging, or sarcopenia, includes loss in muscle strength, muscle fiber wasting, increased intramuscular connective tissue, and a disruption of the muscle stem cell population that results in muscle that is weaker, stiffer, and less able to regenerate.[27–33] Muscular aging is multifactorial, involving extrinsic and intrinsic mechanisms that attack both the cellular components and extracellular matrix (ECM). Advanced glycation end-products (AGEs), the final derivative of the Maillard or browning reaction, are known to accumulate in musculoskeletal tissues in old age and are thought to play a role in the development of sarcopenia.[18–21] AGEs preferentially accrue on the long-lived extracellular matrix (ECM) proteins, especially collagens, since their formation relies on its precursors' stochastic reaction (glucose and proteins) via the Maillard reaction. In addition to having a long half-life, collagens are rich in repeating arginine and lysine amino acids that potentiate the reaction between collagen and AGE precursors, further predisposing collagen to these glycation cross-links.[21] Non-enzymatic cross-linking by AGEs decrease collagen's susceptibility to degradation

by matrix metalloproteinases, causing the build-up of collagen and subsequent stiffening of the usually pliant skeletal muscle ECM.[34] There are only a handful of reviews that focus on the aging and cross-linking of the sclerotic collagens in skeletal muscle, and even fewer that address the role of AGEs in sarcopenic decline.[35–40] Furthermore, it has been 10 years since the last time this topic was reviewed in-depth, thus a purview of the literature in this space is warranted.[41] In addition, muscle-nerve interactions play an integral role in muscle health, and a discussion of motor neurons is included in this review in support of the critical role that AGEs have in the aging motor endplate.

Skeletal Muscle and the Aging Extracellular Matrix

Skeletal muscle ECM is highly structured and regulated to maintain its force-bearing properties and spatial-temporal regulation of muscle-specific stem cells, muscle fibers, and a host of other cell types including fibroblasts, endothelial cells, and nerve fibers.[3–5,7,34] The entire muscle is encased by the epimysium, which consists of type I and III collagen fibers that run perpendicular to the muscle and are responsible for maintaining the muscle girth.[34,42,43] Skeletal muscle is further cordoned off by the perimysium into muscle fiber groupings known as fascicles. The perimysium consists of type I and III collagen that runs both parallel to the muscle fibers, coalescing at the tendons, and perpendicular collagen that resists fascicular expansion.[21,42] Each muscle fiber is surrounded by the endomysium, which includes the basal and reticular laminae, that contain collagen orientated perpendicular to the muscle fibers during contraction and longitudinally orientated during relaxation.[44–47]

ECM Composition Is Unique to the Muscle Fiber Type

Oxidative muscle fibers (types 1 and 2a) have a rich vascular supply, and as such have higher amounts of collagen in their endomysium, especially type IV, compared to glycolytic fibers (type 2b).[48] In addition, the basal lamina is made up of laminin, fibronectin, vitronectin, entactin/nidogen, collagen type VI, and proteoglycans and is a reservoir for many soluble factors (including transforming growth factor beta (TGF-β)).[49,50] Between the basal lamina and the muscle fiber resides the satellite cell, or the adult resident muscle stem cell, and the satellite cell modifies and maintains its basal lamina niche through the excretion of MMPs and laminin.[3,51–53] The reticular lamina is rich in type 1 collagen and is in-between adjacent basal laminae and is responsible for force transfer from the fiber.[34,49,54]

Satellite Cells and Aging

Adult myogenesis is a series of highly coordinated events that follow a defined transcriptional template.[55] Adult muscle stem cells are known as satellite cells, and they lie quiescent between the muscle fiber and its apposed basal lamina and highly express Pax7, a pioneering transcription factor

that maintains the myogenic potential of the cells.[51,55] Upon activation due to injury or other disruptive event, the satellite cells undergoes asymmetrical apical-basal division where the daughter cell close to the muscle fiber begins to express MyoD and Myf5 as the cell closer to the basal lamina remains solely a Pax7 positive cell for maintenance of the satellite cell pool (self-renewal).[55–57] Other satellite cells undergo symmetrical division where both daughter cells either remain solely Pax7 positive to renew the quiescent population or both become activated MyoD positive myoblasts. Due in part to Myf5 upregulation, the activated myoblasts proliferate to expand the available pool of regenerative cells. Over time, the proliferating myoblasts sequentially lose Pax7, Myf5, and MyoD expression as Myogenin (MyoG) begins to be upregulated. As a result, the committed myoblast phenotype emerges where the myoblasts are less proliferative and are preparing for fusion. MyoG supports the expression of Myosin Heavy Chain type 1 (MyHC1) and the other contractile proteins as the cells begin to fuse into muscle fibers.[58–60] Dysregulation of the myogenic program is known to occur in the aging process, resulting in homeostatic decompensation, whereby the expression of myogenic factors such as MyoD and MyoG are upregulated.[61–63] It is thought that homeostatic decompensation, in part, explains the aberrant activation and depletion of the satellite cell niche. However, the mechanisms behind age-dependent satellite cell decline are still being elucidated.

The AGE-RAGE Axis in Skeletal Muscle Aging

The receptor for advanced-glycation end-products (RAGE) is a pattern-recognition receptor expressed in activated satellite cells and myoblasts, and was originally discovered in bovine lung homogenate due to its ability to bind AGEs.[22,64] RAGE is expressed in several cell types at a basal level.[65–67] However, it is not normally expressed in adult muscle fibers, but is upregulated after acute injury, in dystrophic muscles, and in cancer cachexia condition.[22,23,68,69] Further, RAGE signaling plays a normal role in skeletal muscle maintenance and regeneration.[22] Over time, other ligands in addition to AGEs were discovered such as amphoterin (HMGB1) and S100B, and it was observed that RAGE elicits a ligand-dependent response in cultured myoblasts.[22–24,70–72] Activated myoblasts respond to S100B via RAGE in the early phases of differentiation with enhanced proliferation via extracellular signal-regulated kinase 1/2 (ERK1/2) while priming the myogenic program through p38 mitogen activated protein kinase (MAPK).[24] In the later phases of differentiation, HMGB1 upregulates myogenin via RAGE-dependent stimulation of p38 MAPK pathways, prepping the myoblasts for fusion by suppressing Pax7.[23] In cases where AGEs are pathologically upregulated, such as in aging, AGE-RAGE signaling dominates normal RAGE processes, leading to an aberrant increase in satellite cell proliferation at the expense of differentiation (Figure 2).[22] Moreover, systemic levels of soluble RAGE

increase in individuals with sarcopenia.[73] AGE-RAGE signaling stimulates the phosphorylation of nuclear factor kappa B (NF-κB), upregulating extracellular matrix genes (e.g., collagen type I) and inflammatory cytokine production.[74] P-38 MAPK phosphorylation is upregulated by AGE-RAGE signaling and elevated p-38 MAPK signaling been implicated as a factor that disrupts satellite cell signaling in old age.[2,23,24]

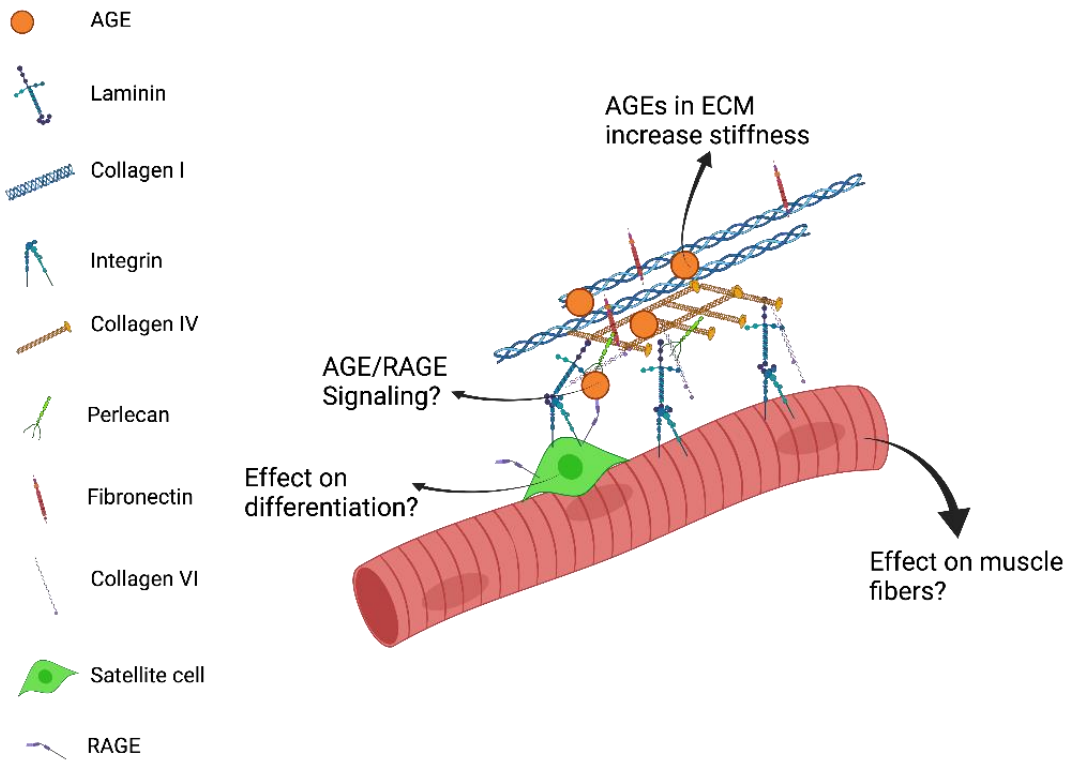

Figure 2. Advanced glycation end-products (AGEs) in skeletal muscle are associated with receptor for advanced glycation end-products (RAGE) activation and have been associated with muscle aging. RAGE plays a normal role in supporting adult myogenesis; however, when there is a pathological increase in RAGE activation due to AGEs, muscle wasting, increased muscular inflammation, and deleterious satellite cell signaling occurs. What remains unclear is whether effects from AGEs are due to soluble factors that activate RAGE signaling or from extracellular matrix cross-links that signal via RAGE as well. This figure proposes answered questions due to AGE cross-linking in muscle ECM.

Aging of Skeletal Muscle Collagen

Collagen is the most abundant structural protein found in mammals, and is highly conserved between species.[75–77] As such, collagen aging in skeletal muscle has been investigated in humans, rats, mice, rabbits, lizards, seals, pigs, and cows.[78–86] A common feature is that the total amount of intramuscular collagen, as assayed by hydroxyproline, increases in old age.[79,83] In contrast, the acid-soluble fraction of collagen decreases in old age, indicating elevated collagen cross-linking.[79,83,87] As

muscle develops, collagen is laid down and then fully cross-linked by the enzyme lysyl oxidase (LOX) which ceases by the end of sexual maturity.[88] Since the mature LOX cross-links (hydroxypyridine and pyridine) are enzymatic-dependent, they are destroyed and remade in humans following the normal 2 year half-life of skeletal muscle collagen (as determined by the ^{14}C bomb-pulse technique).[88,89] Interestingly, the half-life of skeletal muscle collagen increases with age, due to a reduction in the proteostasis of collagen.[90] Altogether, these phenomena indicate either a dysregulation in LOX-gelatinase control in the muscle or an increase in non-enzymatic cross-linking such as advanced glycation end-product (AGE) cross-linking. Gelatinases A and B (MMP-2 and MMP-9) lose their responsiveness to exercise-initiated ECM remodeling in old age.[91] Further, LOX protein levels increase in aged dystrophic mice, and there is a recent conference abstract reporting that LOX was increased in old female mice.[92,93] In addition, these data were correlated with decreased collagen solubility. However, there is opposing evidence found in a study on human muscle that the LOX-dependent cross-link hydroxylysylpyridinoline is unchanged in old age, while the AGE pentosidine is increased by 200%.[78] Furthermore, glycation cross-links were not investigated in the studies that measured LOX levels.

AGEs are non-enzymatic post-translational modifications to proteins in the body. AGE formation follows the stochastic browning, or Maillard, reaction where a monosaccharide (e.g., glucose, fructose, lactose, or ribose) in its open-ring conformation interacts with a protein to form an unstable Amadori product.[18] Over the course of a few days, the Amadori product matures and forms a very stable, irreversible AGE. Since AGE formation is a drawn-out, random process dependent on the concentration and probability of the monosaccharide existing in an open-ring conformation, most proteins in the body are degraded and turned over before appreciable AGE accumulation can occur. Due to collagen's long life-span, AGEs are able to accumulate and have biological consequence resulting in stiffer collagen that is resistant to enzymatic degradation.[21] Furthermore, collagen is rich in lysine and arginine amino acids that potentiate AGE formation.[21] Interestingly, despite the high relevance of AGE's role in skeletal muscle aging, there have been only a few studies characterizing the role of AGEs in this context.[25,94]

Basal Lamina Aging

Age-dependent changes to the basal laminae alter muscle health, impact force production, and change how muscle stem cells respond to injury.[41] Many age-dependent changes in the composition and organization of the basal lamina occur. Fibronectin is depleted from the basal lamina in old age, reducing the integrin attachment points for satellite cells.[5,15,95] Laminin increases in fast-twitch muscle with age, while it is depleted from slow-twitch.[96] Additionally, collagen type VI, which acts as a bridge

between the basal lamina and reticular lamina, is aberrantly increased in old age, disrupting the overall structure of the laminae.[96] Collagen type I increases significantly in the reticular laminae, and invades the basal laminar space. Furthermore, there is an increase in aberrant glycation cross-links that stiffens all collagens and other ECM components, which dysregulates quiescent muscle stem cells and muscle force transmission.[6,78,85] Collagen type IV, which forms a net-like structure in the basal lamina, serves as a scaffolding protein for the laminins and other cell-anchoring proteins.[97] Old age increases collagen type IV levels while decreasing the ability of muscle to regulate collagen type IV following injury.[96,98] AGE-modifications to ECM components reduces cell adhesion and disrupts the assembly of fibronectin to collagen type IV.[99,100] Further, AGE-modified basal lamina proteins caused mesangial cells to overexpress fibronectin matrix assembly, which implies that AGEs dysregulate the basal lamina structure.[101]

ECM Aging Is Muscle-Specific

As mentioned previously, muscle ECM composition is highly dependent on the muscle fiber type. As such, muscles that are predominantly fast-twitch will age differently than muscles that are primarily slow-twitch. Thus, aging is dependent on the location of the muscle in the body, with the hind-limb muscles aging at a faster rate than the forelimb.[32] Fast-twitch muscles are especially sensitive to the aging process as there is a fast-to-slow muscle fiber transition that is coordinated by the aging of the motor neurons.[21,33,71,102–108] An immediate consequence of this is that these fast-twitch muscle become enriched with ECM components more typical of slow-twitch muscles, namely, the collagens.[103,109] Curiously, the fast-to-slow transition does not replicate the increased density of satellite cells found in slow-twitch muscles.[4,110–118] Increases in deleterious modifications to the ECM, such as cross-linking and an imbalance in ECM components, may be more responsible for the decrease in satellite cells seen in the fast-to-slow transition than the actual modification to the muscle fibers themselves. Slow-twitch muscles are more resistant to aging, and this is thought to be due to their role as postural muscles, which are constantly activated throughout life.[119] However, any fast-twitch glycolytic fibers found in slow-twitch muscles are reduced in old age.[105] AGE cross-linking accumulation is ubiquitous to slow and fast-twitch muscles, albeit there was a greater staining intensity observed in the myofibers of slow-twitch muscles.[120] However, no one has examined if the increased AGE presence in slow-twitch muscles is related to the increased collagen content, moreover, if the fast-to-slow twitch increase in collagen is partially driven by AGE cross-linking.

Peripheral Nerve Involvement in Aging and Atrophy

Overview and Neuromuscular Junction Anatomy

The neuromuscular junction (NMJ) is a highly regulated microenvironment maintained by cross-talk between glial, motor nerve, and skeletal muscle. The NMJ is comprised of three major segments, the pre-synaptic, post-synaptic, and synaptic extracellular space. Vesicle packaged acetylcholine is localized in the pre-synaptic space inside the peripheral nerve terminal. Following membrane depolarization, acetylcholine is released into the synaptic cleft binding to the acetylcholine receptor, activating sodium ion channels, which results in skeletal muscle contraction.

While development of the NMJ is not completely understood, pre-patterning of acetylcholine receptors on the muscle membrane occurs before the motor nerve reaches the immature site.[121] Moreover, it is important to understand how the NMJ forms in order to address disruptions or degeneration of motor endplates due to disease or even AGEs (Figure 3). Interaction between motor nerves, leader Schwann cells, and skeletal muscle triggers the NMJ maturation and stabilization process. The pre-patterned acetylcholine receptors then enter a pruning phase and begin to consolidate to a centralized area on the muscle local to the motor neuron. Invaginations begin forming that increase the synaptic surface area while the acetylcholine receptors switch to mature subunits.[122] Additionally, during the maturation process, a carefully regulated extracellular matrix comprised heavily of collagen type IV and laminin develops in the region of the motor end plate, and is thought to contribute to NMJ development and maturation.[123,124]

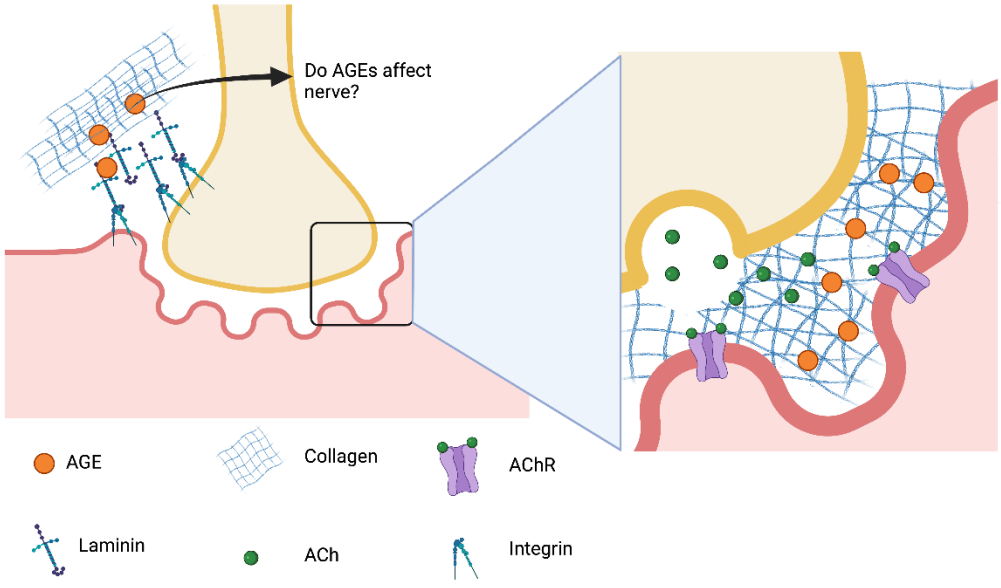

Figure 3. The role of AGEs at the neuromuscular junction are unclear and could have effects on synaptic vesicle release, acetylcholine diffusion to their receptors and an effect on signaling that may contribute to motor end-plate fragmentation and muscle aging.

Laminins play major roles in motor neuron pathfinding and are known to be critical in synaptogenesis. Peripheral motor neurons traverse the body through their basal laminar tube comprised of laminin α2β1γ1 and α5β1γ1.[125] Myelinating Schwann cells in the endoneurium cover the peripheral nerve and use the mechano-sensitive cues from the basal laminar tube for polarization and directionality.[126] Since mechanical queues play a critical role in Schwann cell pathfinding and subsequent regeneration, any disruptions to the connective tissue intramuscularly (e.g., AGE cross-linking) can drastically alter the peripheral nerve's ability and speed of muscle innervation.[127]

Endplate Fragmentation and Aging

Endplate fragmentation is a multi-stage disassociation of the NMJ typically seen during aging. This process is marked by a dispersal of clustered AChRs, AChR type switching, and increased turnover rates of the receptor.[128,129] As a way to compensate for fragmentation, increased enzyme levels of acetylcholinesterase and increased levels of acetylcholine (ACh) release from the synaptic terminal were detected.[129] Surprisingly, the receptor's ability to bind to acetylcholine has not been shown to be inhibited with age, suggesting that ACh release into the synaptic cleft is a critical feature of endplate fragmentation and helps to explain increases in ACh release during fragmentation. Moreover, research from Carlson et al. indicated that fragmentation may play a part in fiber type switching due to age, a process referred to as homeostatic decompensation.[61]

There is mounting evidence that the atrophy observed during aging is caused more by signaling disruptions than disuse. The disruption of cross-talk between the muscle and nerve can trigger downstream activation of atrogenes Murf-1 and Fbxo32 via TNF- α activation.[130] In more severe cases of atrophy like denervation, TNF-α synthesis increases, contributing to endplate breakdown. Similarly, circulating levels of TNF- α increase with age, and TNF-α is a major factor associated with endplate fragmentation and with activation of the RAGE pathway.[131]

Insights from Diabetic Neuropathy, AGEs, and RAGE

Diabetes may support an early onset aging phenotype.[132,133] Comparisons between diabetic muscle and aging muscle may be drawn, and aging is an independent factor that is predictive of diabetic neuropathy severity.[132–134] Similar to aging, diabetes also produces a pro-AGE environment in muscle and provides an alternative perspective for studying the impact of AGE-related changes. AGEs play a major role in diabetic neuropathy but its effects still need to be parsed.[135,136] Sensory nerves are highly affected by age-induced neuropathy, mirroring diabetic neuropathy.[137] Curiously, diabetic neuropathy causes the muscles of the distal limbs (foot to knee) of humans to undergo atrophy whereas the proximal limb (thigh muscles) preferentially undergo atrophy in sarcopenic individuals while the upper limbs in both conditions are relatively unaffected.[138–141] Further, AGE levels are correlated to sarcopenic muscle in the distal limb of older individuals with type 1 and type 2 diabetes.[142,143] However, it is unknown if the age-dependent atrophy of the lower limb is also driven by neuropathy or AGEs independent of diabetes. Like in diabetes, the number of motor units decrease in number but increase in size with age.[144,145] Intramuscular connective tissue increases in both aging and diabetes, and this is tied to AGE accumulation (Figure 4).[25,146] There is untapped potential in using correlated knowledge on geriatric and diabetic motor nerve neuropathy to elucidate the role of AGEs in age-dependent changes to muscle-nerve interactions.

Hyperglycemic conditions in diabetes mellitus causes global AGE formation in the body, leading to diabetic neuropathy and a host of other complications.[147] Sensory neurons preferentially undergo dysfunctional Wallerian degeneration that leads to chronic denervation, and sensory nerve deficits are seen in 70% of diabetic patients.[148] In contrast, motor nerve deficits are seen in only 1–6% of patients and are confined to the distal limbs.[149] As such, much of the diabetic body of literature focuses on sensory neuropathy as this is the primary clinical concern, but the contributive impact of AGEs in diabetic neuropathogenesis needs further study. It has been posited that motor neurons are partially protected by the central nervous system blood–brain barrier from the glycolytic attack that sensory nerve cell bodies experience in the diabetic state.[150,151] Additionally, other compensatory mechanisms likely exist for motor nerves (e.g., single motor unit action potential enlargement) that sensory nerves lack.[152]

Severe deficits in motor neurons are not seen until late in diabetic pathology where severe force deficits and motor neuron loss is observed.[152] However, there are minute, observable changes such as axonal sprouting, demyelination, and a decrease in both NMJ and motor unit number that occur in the beginning stages of diabetes.[152,153] AGEs destroy the microvasculature around motor nerves, slowing

the conduction velocity.[148,154–156] However, there is little research into AGE's direct effects on motor neuron diabetic neuropathy due to most of the literature concentrating on sensory neurons. In vitro study has been valuable in the effort to posit AGE-specific effects on sensory neurons. Rat sensory neurons grown on glycated collagen type IV, collagen type I, laminin, and fibronectin show a decrease in neurite outgrowth and dorsal root ganglion explants grown in high glucose conditions have decreased neurite outgrowth.[157–159] However, dorsal root ganglion explants from diabetic mice showed increased axonal sprouting, which better mirrors the in vivo reality where excessive axonal outgrowth interferes with successful re-innervation.[160–164] Moreover, AGEs are known to accumulate in the peripheral endonerium in diabetic mice.[158] Whether these results translate to motor neurons is not known. Additionally, it is known that AGEs are highly cytotoxic to Schwann cells via the P38 MAPK and NF-κB pathways.[159,165–169] Further, it is clear that the motor nerve neuropathy can be driven by AGE cross-linked ECM components.

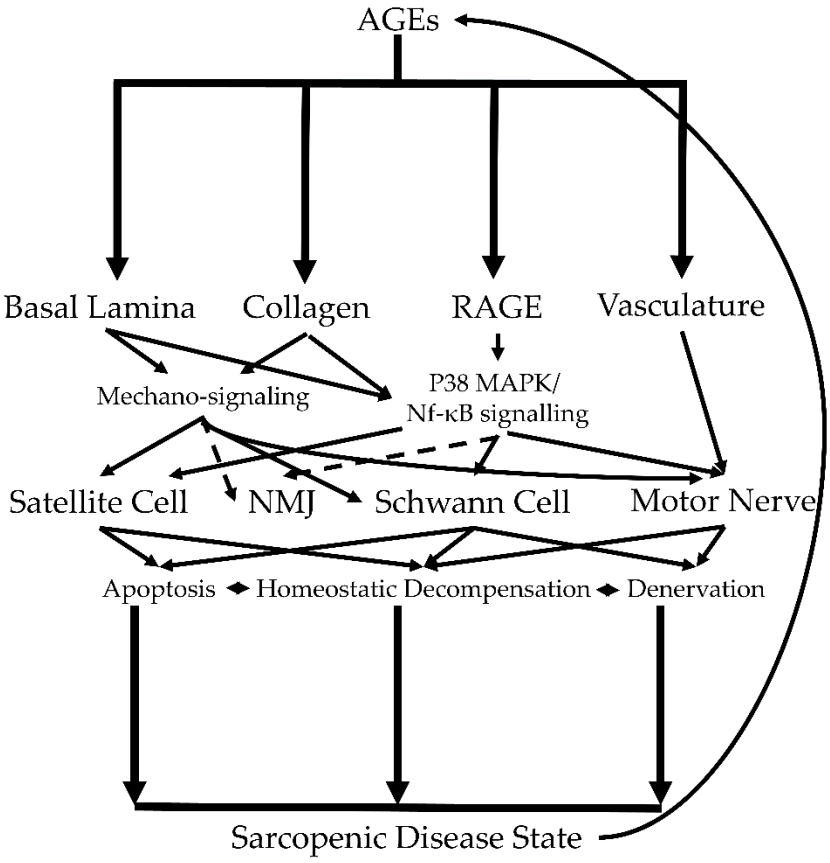

Figure 4. AGEs support a sarcopenic disease state in muscle by altering the basal lamina, collagen, RAGE signaling, and vasculature. These AGE-dependent changes accumulate and result in deleterious effects to satellite cells, NMJs, Schwann cells, and the motor nerve that culminate in

sarcopenia. Known mechanisms are indicated by solid arrows while proposed mechanisms (future directions) are indicated with dashed arrows.

Conclusions

Skeletal muscle aging is a process influenced by deterministic and stochastic processes, and is characterized by muscle wasting, fast-to-slow muscle fiber transition, and an increase in the skeletal muscle collagens. AGE collagen cross-linking clearly plays a role in sarcopenia; however, much study is warranted in further elucidating the impact of AGEs in skeletal muscle. Furthermore, age-related changes to motor nerves drive much of sarcopenia, and may involve AGE cross-linking.

Chapter 3. Advanced Glycation End Products Are Retained in Decellularized Muscle Matrix Derived from Aged Skeletal Muscle

Abstract

The overall goal of these experiments was to determine whether AGEs were elevated in older muscle and if those AGEs were specifically located in muscle ECM. While whole muscle provides a reliable readout for AGEs, it does not specify where those AGEs are located. Thus, using decellularized tissue allowed us to measure AGEs in muscle ECM. Decellularized tissues are also biocompatible materials that engraft well, but the age of their source has not been explored for clinical translation. Advanced glycation end products (AGEs) are chemical cross-links that accrue on skeletal muscle collagen in old age, stiffening the matrix and increasing inflammation. Whether decellularized biomaterials derived from aged muscle would suffer from increased AGE collagen cross-links is unknown. We characterized gastrocnemius muscles of 1-, 2-, and 20-month-old C57BL/6J mice before and after decellularization to determine age-dependent changes to collagen stiffness and AGE cross-linking. Total and soluble collagen was measured to assess if age-dependent increases in collagen and cross-linking persisted in decellularized muscle matrix (DMM). Stiffness of aged DMM was determined using atomic force microscopy. AGE levels and the effect of an AGE cross-link breaker, ALT-711, were tested in DMM samples. Our results show that age-dependent increases in collagen amount, cross-linking, and general stiffness were observed in DMM. Notably, we measured increased AGE-specific cross-links within old muscle, and observed that old DMM retained AGE cross-links using ALT-711 to reduce AGE levels. In conclusion, deleterious age-dependent modifications to collagen are present in DMM from old muscle, implying that age matters when sourcing skeletal muscle extracellular matrix as a bio-material.

Introduction

The deterioration of muscle's strength and mass with increasing age culminates in a condition known as sarcopenia, an age-dependent muscle wasting disease.[28–31,33,170] Advanced glycation end products (AGEs) are thought to play a role in the development of sarcopenia.[18–20] AGEs preferentially accrue on the long-lived extracellular matrix (ECM) proteins, especially collagens, decreasing collagen's susceptibility to degradation by matrix metalloproteinases and causing the build-up of collagen and subsequent stiffening of the usually pliant skeletal muscle ECM.[34]

The endomysium ECM surrounding muscle fibers plays an important role in regulation of satellite cells, a muscle stem cell source, and in regulation of muscle health.[3–5,7,45] Within this endomysium are two laminae, the basal lamina and the reticular lamina. As previously mentioned, the basal lamina is ECM that contacts muscle fibers and is composed primarily of laminin, fibronectin, collagen type IV, and VI. The reticular lamina is ECM that separates conjoined basal laminae and is mainly composed of type I collagen that runs parallel to the muscle fibers, coalescing at the ends of the muscle into the tendons.[34] Skeletal muscle ECM plays a critical role in muscle function, and as such age-dependent changes in the ECM have considerable implications for muscle performance.[171] Furthermore, the basal and reticular laminae are important regulators of muscle regeneration by providing the appropriate spatiotemporal cues to satellite cells.[4,6,17,51] Increased fibrosis and stiffness of the aged laminae dysregulates this healing process and could hinder the ability of ECM to support myogenesis.[5,7]

In young muscle, satellite cells are a resident stem cell population and endow muscle with a remarkable ability to regenerate, but there is little information about the impact of aged ECM on satellite cells and muscle regeneration.[2,3,172,173] Furthermore, less is known about whether AGE ECM cross-links could play an important role in muscle regeneration in older individuals with muscle injuries. The ECM is a critical mediator for satellite cell guidance cues and regulates the inflammatory response to determine whether fibrosis or regeneration occurs following injury. More, the regeneration of muscle injuries is dependent on the size of the injury itself, where larger injuries are more difficult to heal and often result in fibrosis.[174] Decellularized muscle matrix (DMM) is ideal for studying ECM-specific effects in muscle and as a regenerative tool to repair both small and large skeletal muscle injuries because its muscle-specific composition and anisotropy recapitulate the basal lamina environment. Decellularization is a method to procure an ECM scaffold rich in components specific to the tissue to which it is applied.[175] Skeletal muscle can be decellularized through several salt, enzymatic, and detergent soaks to lyse the cells, freeing them from the surrounding matrix, and washing them out of the tissue.[174–181] The white,

ghost-like scaffolds that result encourage myogenesis due to muscle-specific moieties and lack of immunogenic material, making these scaffolds an ideal source to study age-dependent effects on muscle ECM.[174–181] Furthermore, DMM can be processed into versatile hydrogels useful for tissue engineering and other cell culture strategies because of its biocompatibility, body temperature-dependent polymerization, and potential as a cell delivery vehicle. The ability of DMM as a reviver of the myogenic process is dependent on the host's age and immune capacity.[182–184] However, no studies have investigated whether deriving DMM from older individuals changed its myogenic characteristics, an important area of research that could underpin age-dependent ECM effects on muscle. We hypothesized that AGEs play a role in age-related collagen cross-linking and that those cross-links are retained in DMM sourced from old muscle. The aim of this study is to characterize age-dependent changes in AGE cross-linking in muscle and whether these changes persist in DMM.

Results

Histological Assessment of Whole Muscle

We characterized the muscle before decellularization to determine if an aging phenotype was present. The myofiber diameter was noticeably smaller in 1-month samples compared to 2-month and 20-month. Nuclei were counted in all samples, and we determined there to be a reduction in the number of total nuclei with age. We also observed a lipofuscin-like deposition or tubular aggregates inside the myofibers at 20 months of age (Figure 5A).[185,186] However, further histological investigations with lipid-detecting stains are needed to positively verify the presence of lipofuscin. In Masson's trichrome, we did not observe any qualitative morphological differences. The variation in color shade and intensity in the Masson's Trichrome is a technical staining artifact. Picrosirius red stains demonstrated a significant increase in collagen thickening and staining intensity at 20 months (Figure 5A).

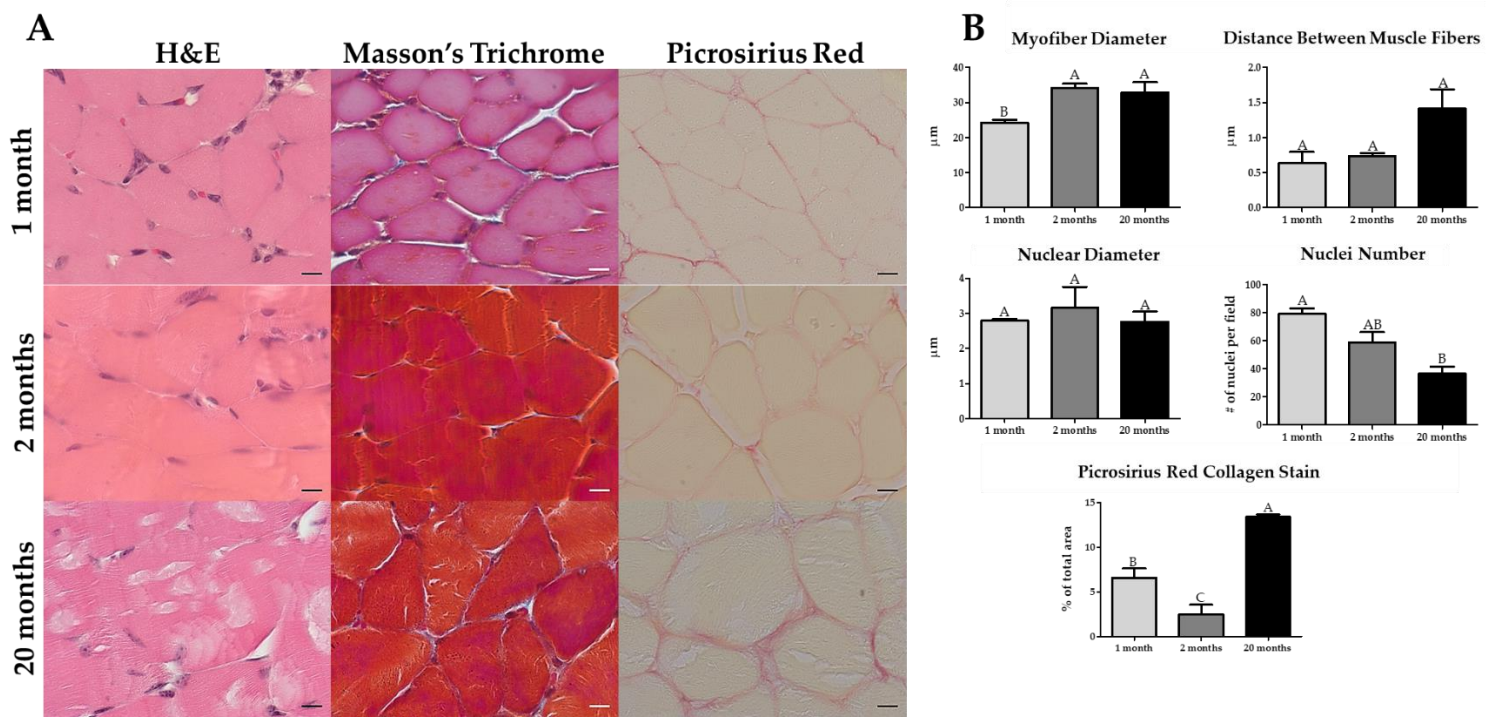

Figure 5. The gastrocnemius shows histomorphometric differences in old age. (**A**) Hematoxylin and Eosin (H&E) staining (*n* = 3) revealed a reduction in nuclei and the presence of lipofuscin-like or tubular aggregates inside the muscle fibers with old age. Masson's Trichrome (*n* = 3) had no apparent differences with age. Picrosirius Red staining (*n* = 4) displayed a pronounced increase in collagen staining in old age. (**B**) When quantified histomorphometrically, the gastrocnemius had a smaller myofiber diameter in immature muscle, an increase in the distance between muscle fibers and a decrease in the number of nuclei in old age, and a bimodal amount of collagen staining where immature and old have higher levels of collagen than young adult, albeit older also has higher amounts than immature muscle. Scale bar = 10 µm. Groups that do not share a letter (e.g. A, B, or C) are statistically different according to a one-way ANOVA followed by a two-tailed Tukey's correction ($p < 0.05$, n = 3 for H&E and Masson's, n = 4 for Picrosirius Red).

With histomorphometry, we confirmed an increase in muscle fiber diameter from 1-month to 2 months of age, and we observed an increase, albeit not significant, in the distance between the muscle fibers at 20 months of age, and there was a reduction in the number of nuclei from 1-month to 20 months of age (Figure 5B and Table 1). The area of Picrosirius red collagen stain was significantly elevated at 20 months compared to 1 and 2 months, also 1-month was significantly higher than 2 months (Figure 5B and Table 1). Whole muscle sections, stained using Hematoxylin and Eosin (H&E) and Picrosirius red (Figure 6), showed an overall increase in muscle size between 1-month and 2-month, and 1-month and

20-month samples. Picrosirius red staining also showed increased collagen staining between 2- and 20-month muscles.

Group	# of myofibers (mean+/-SEM)	Myofiber diameter (mean+/-SEM)	# of nuclei (mean+/-SEM)
1 month	25+/-5.57	24.25+/-0.82 μm	79.33+/-3.84
2 months	11.33+/-0.33	34.27+/-1.12 μm	58.67+/-7.42
20 months	13.33+/-2.03	32.90+/-2.84 μm	36.67+/-4.91

Table 1: Histomorphometry parameters from gastrocnemius muscles muscle of differently aged mice.

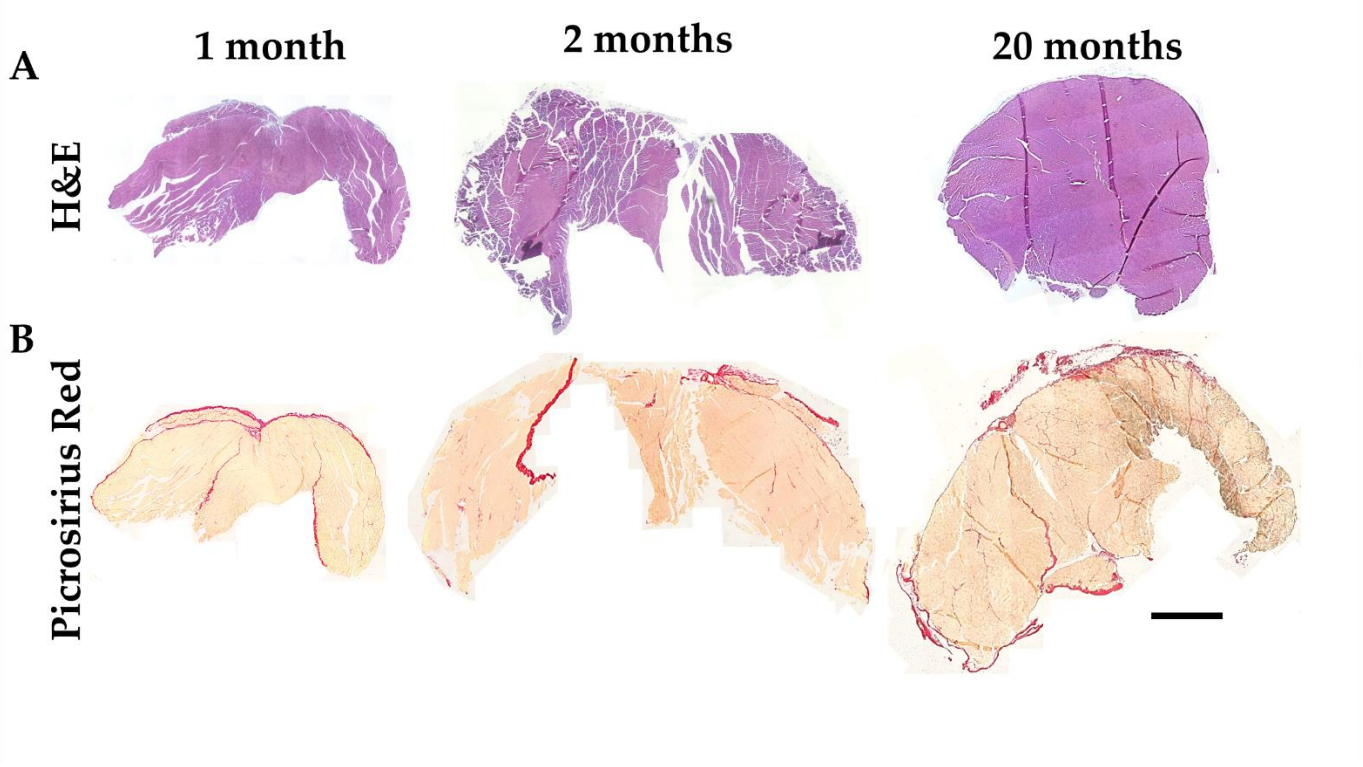

Figure 6: Whole histological cross-sections of gastrocnemius muscles muscles from differently aged mice. A) Muscles were stained with H&E. B) Muscles were stained with Picrosirius red (red=collagen, yellow=muscle). Scale bar= 1mm.

Age-Associated Effects in Whole Muscle Proteins

We examined the gastrocnemius muscles at different ages using Western blotting to determine if there was an age-dependent effect on muscle-specific proteins. Pax7 levels, a marker of satellite cells, were unchanged with age, indicating that the satellite pool was not affected (Figure 7A). MyoD was not detected in 1- and 2-month muscle but was upregulated at 20 months (Figure 7B). Myogenin was not different between the age groups (Figure 7C). Interestingly, RAGE was highest at 2 months and significantly lower at 1 and 20 months, indicating that RAGE may not play a significant role in our system (Figure 7D).

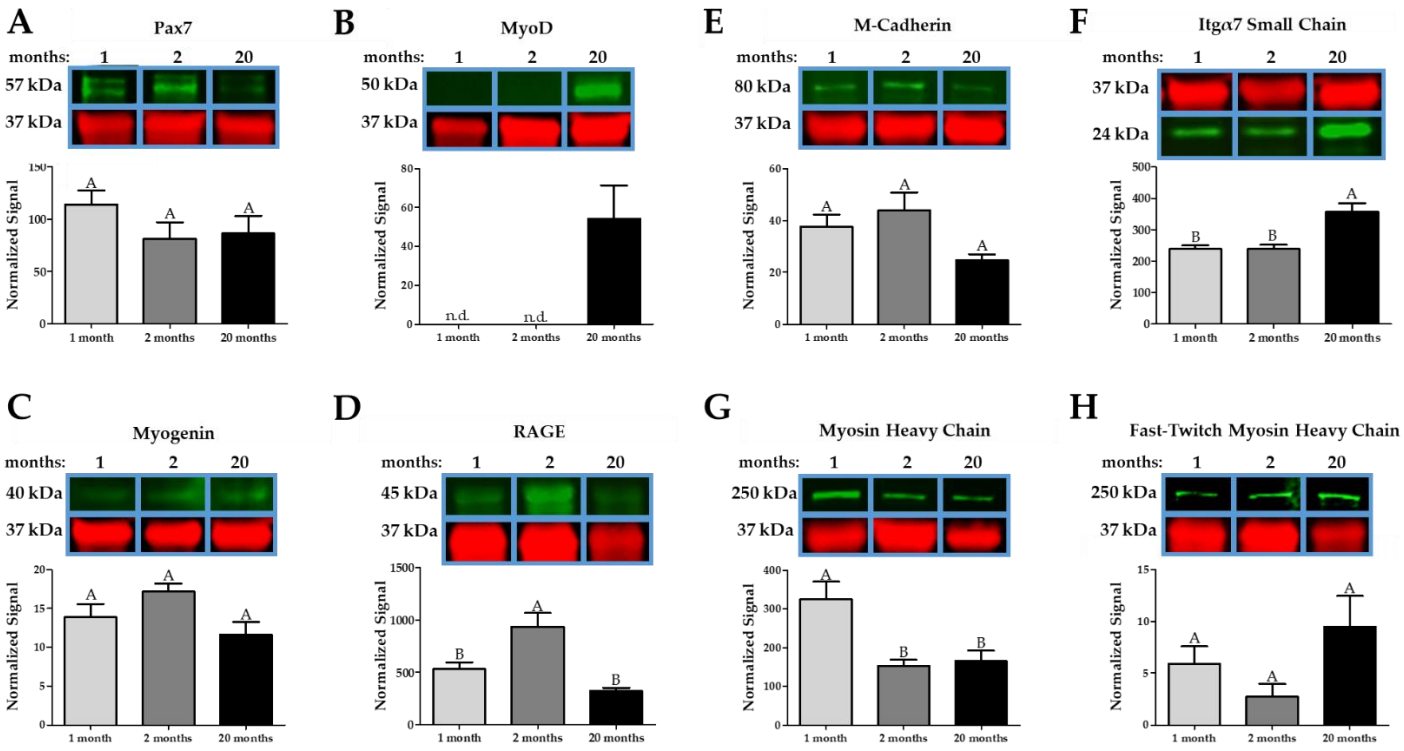

Figure 7. Western blotting differences in muscle-specific factors with age. (**A**,**B**) Pax7 does not change with age, suggesting that the satellite pool is unchanged at 20 months, while MyoD remains undetected (n.d. indicates not detected) until 20 months, indicating homeostatic compensation of the muscle. (**C**) Myogenin is marginally reduced at 20 months. (**D**) Curiously, RAGE (receptor for advanced glycation end products) decreased from 2 to 20 months. (**E**) M-cadherin is decreased in old age. (**F**) Integrin α7 is increased at 20 months, which might be a compensatory response by the muscle. (**G**) Myosin Heavy Chain is unchanged in old age compared to 2 months, indicating that muscle aging does not affect

contractile units at 20 months. (**H**) There is no difference in the Fast-Twitch Myosin Heavy Chain, further indicating that 20 months is not old enough to see sarcopenic effects. The red bands are GAPDH. Groups that do not share a letter (e.g. A or B) are statistically different according to a one-way ANOVA followed by a two-tailed Tukey's correction ($p < 0.05$, n = 6).

M-cadherin was reduced, albeit not significantly, at 20 months compared to 1 and 2 months (Figure 7E), while integrin α7 was upregulated at 20 months compared to 1 and 2 months (Figure 7F). Interestingly, myosin heavy chain was lower at 2 months and 20 months of age compared to 1-month, but there was no difference in myosin heavy chain staining between 2 and 20-month muscle lysates (Figure 7G). Fast-twitch, though not significantly different, had an elevated level at 20 months compared to 1 and 2 months (Fig. 7H).

Histological Assessment of Decellularized Muscle

We assessed DMM with histology to observe age-dependent changes to porosity and collagen content. Gastrocnemius muscles were decellularized and stained using hematoxylin and eosin. No nuclei were observed, indicating successful decellularization (Figure 8A).

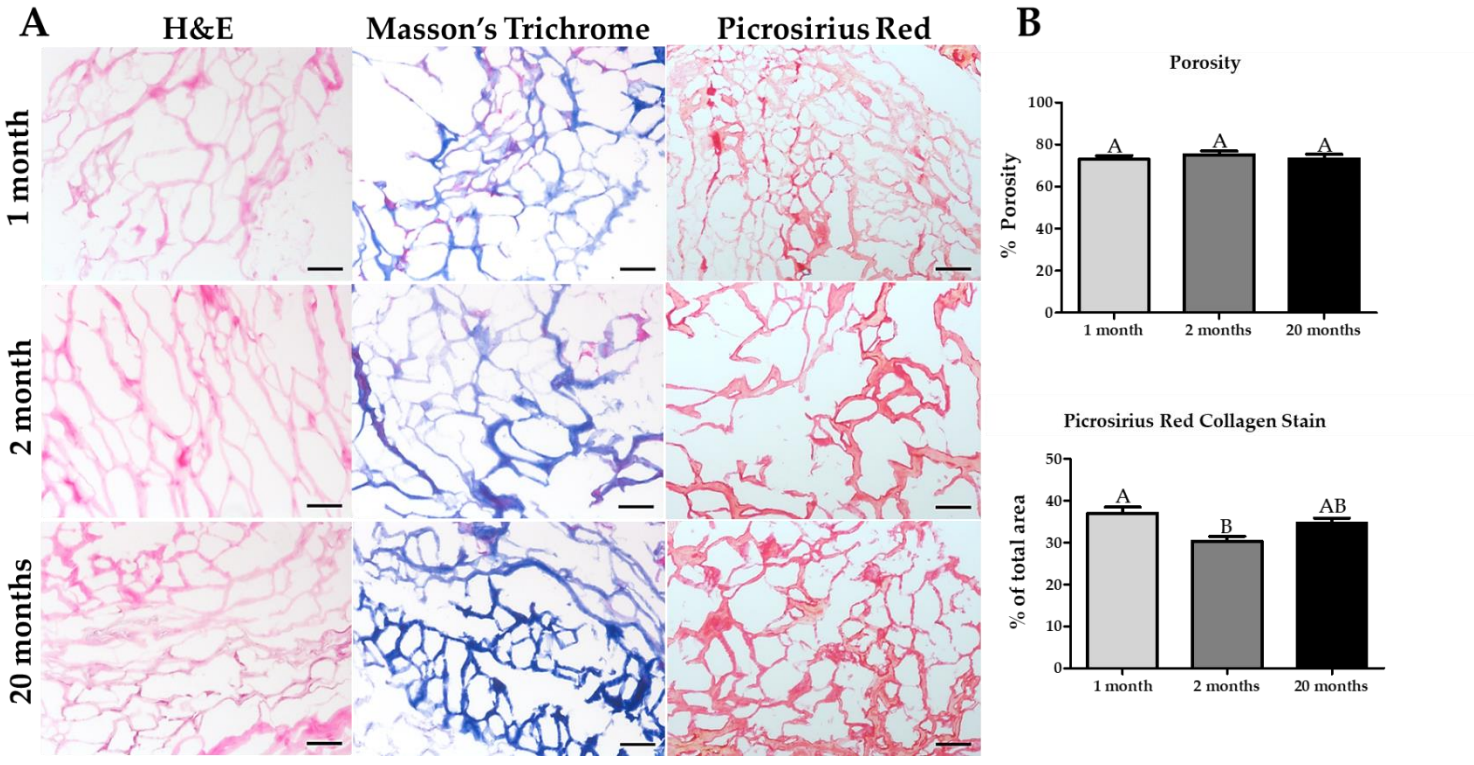

Figure 8. Decellularized muscle matrix (DMM) had no differences in collagen staining with old age. (**A**) Hematoxylin and Eosin (H&E) staining confirmed the absence of cell nuclei at all ages, indicating

successful decellularization. Masson's trichrome did not show age differences, while Picrosirius Red staining shows a thickening of the collagen with age in DMM. (**B**) There is no difference in porosity with age as measured with H&E staining. The amount of collagen area stained with Picrosirius Red staining is more significant in immature muscle compared to young adult. Although the mean area in old age is higher than in young adults, it is not statistically higher nor different from the immature muscle. Scale bar = 100 μm. Groups that do not share a letter (e.g. A or B) are statistically different according to a one-way ANOVA followed by a two-tailed Tukey's correction ($p < 0.05$, n = 6).

To confirm decellularization, we measured levels of dsDNA in the pregel of the processed DMM gel and showed there was significantly less dsDNA in all age groups when compared to whole muscle (Figure 9A). There was also no noticeable difference in Masson's trichrome amongst the three age groups; however, Picrosirius red staining demonstrated increased collagen thickening in the 20-month group (Figure 8A) compared to 1, and 2-month decellularized muscle. Surprisingly, when we quantified Picrosirius red staining, we observed the highest levels of collagen staining in 1-month ECM. In contrast, sexually mature 2-month decellularized muscle staining was lower. While 20-month ECM stains were thicker and at higher levels, there was no statistical difference between 20 and 2 -months. ECM porosity was unchanged with age.

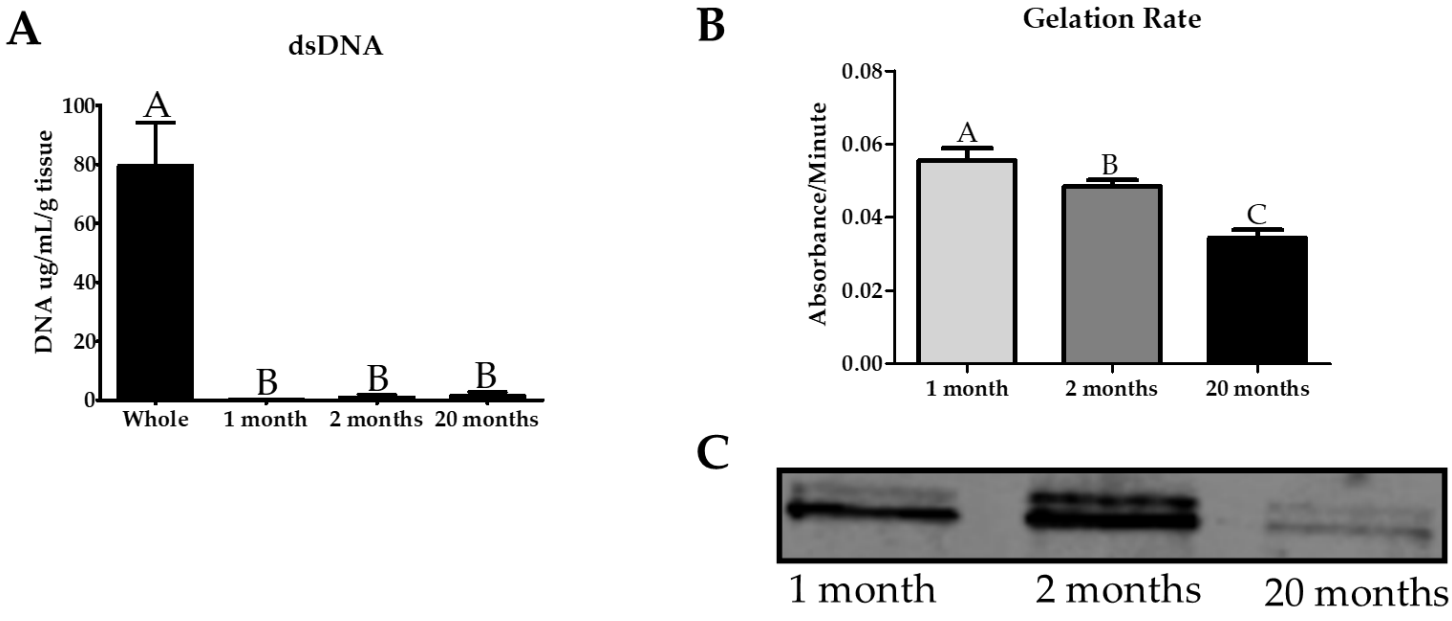

Figure 9: Decellularization was successful, as confirmed by reduced DNA (A), and old age was associated with reduced gelation kinetics (B) and reduced procollagen (C).

Ultrastructural Properties of Whole Muscle, DMM, and DMM Gels at Different Ages

Cryosections were processed for scanning electron microscopy imaging to assess age-dependent changes in the ultrastructure of the ECM, and whether these changes persist in DMM. Muscle fibers in all whole muscle samples appeared normal with a polygonal morphology. We observed distinct areas of ECM between the muscle fibers as well, demonstrating successful imaging of the endomysium. Spacing between muscle fibers appeared to increase, however not significantly, while the endomysium remained unchanged between ages (Figure 10A,B).

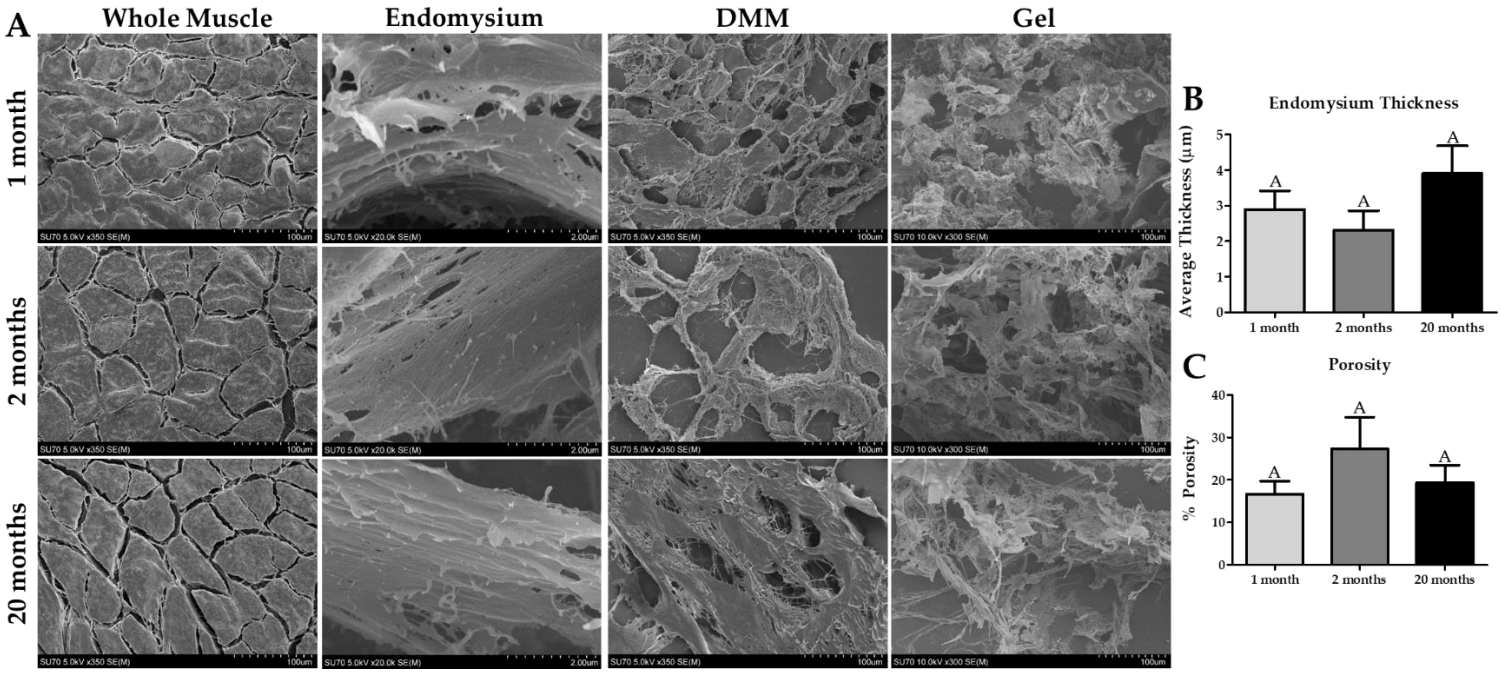

Figure 10. Scanning Electron Imaging shows distinctions in ECM structure with age in native muscle, decellularized muscle matrix (DMM), and processed DMM gels. (**A**) The muscle fibers are surrounded by endomysium in the whole muscle images, and the space between the muscle fibers appear to increase with age, however not significantly. DMM (n = 4 for 20-month DMM) and processed DMM gels, there is an obvious sclerotic structure indicating the presence of polymerized ECM such as collagen. (**B**) Endomysium thickness trends upwards with age but is not significantly different. (**C**) The porosity of DMM is not affected by age. Groups that do not share a letter (e.g. A) are statistically different according to a one-way ANOVA followed by a two-tailed Tukey's correction ($p < 0.05$, n = 6 except the 20-month-old muscle has n = 4).

In the processed DMM gels, we observed no differences in ultrastructure (Figure 10A). However, the gelation rate significantly decreased with increasing age, indicating that though collagen structure is similar differences in other age-dependent parameters such as collagen cross-linking may be at play (Figure 9B). In addition, we measured porosity in DMM and did not observe any age-dependent differences (Figure 10C).

Age-Dependent Effects in Collagen Are Preserved in Processed Muscle

To confirm the measured increase in Picrosirius red collagen staining with age and explore the age-dependent changes in collagen cross-linking, we used hydroxyproline-based assays. Hydroxyproline (the hydroxylated amino acid proline) is widely used as an indicator for the amount of collagen in tissue.[187] We measured increased total hydroxyproline amount in 20-month samples compared to 2-month in the whole muscle, DMM, and the processed DMM gels (Figure 11A). There was a higher amount of hydroxyproline in 1-month whole muscle and processed DMM gels (Figure 11A). To assay cross-linking, we digested our samples in proteinase K. Sample homogenates consisted of dissolved supernatant and a small pellet. We observed that the size of the pellet increased with sample age. Next, we quantified the amount of solubilized hydroxyproline in the supernatant. We detected reduced enzymatic-soluble hydroxyproline at 20 months in the whole muscles. A similar decrease was observed in DMM and the processed DMM gels, albeit only significant to 1-month samples in DMM gel (Figure 11B). To confirm our data, we processed the samples for SDS-PAGE and immuno-stained with a collagen type 1 antibody (which binds to the collagen molecule) and showed a significant decrease in the amount of collagen type 1 at 20 months compared to 1 month in the whole-muscle samples (Figure 11C). In contrast, collagen I in DMM and DMM gels was unchanged (Figure 11C). However, when we assayed the pregel solution, we observed a decrease in procollagen in the 20-month pre-gels compared to 2 months (Figure 9C).

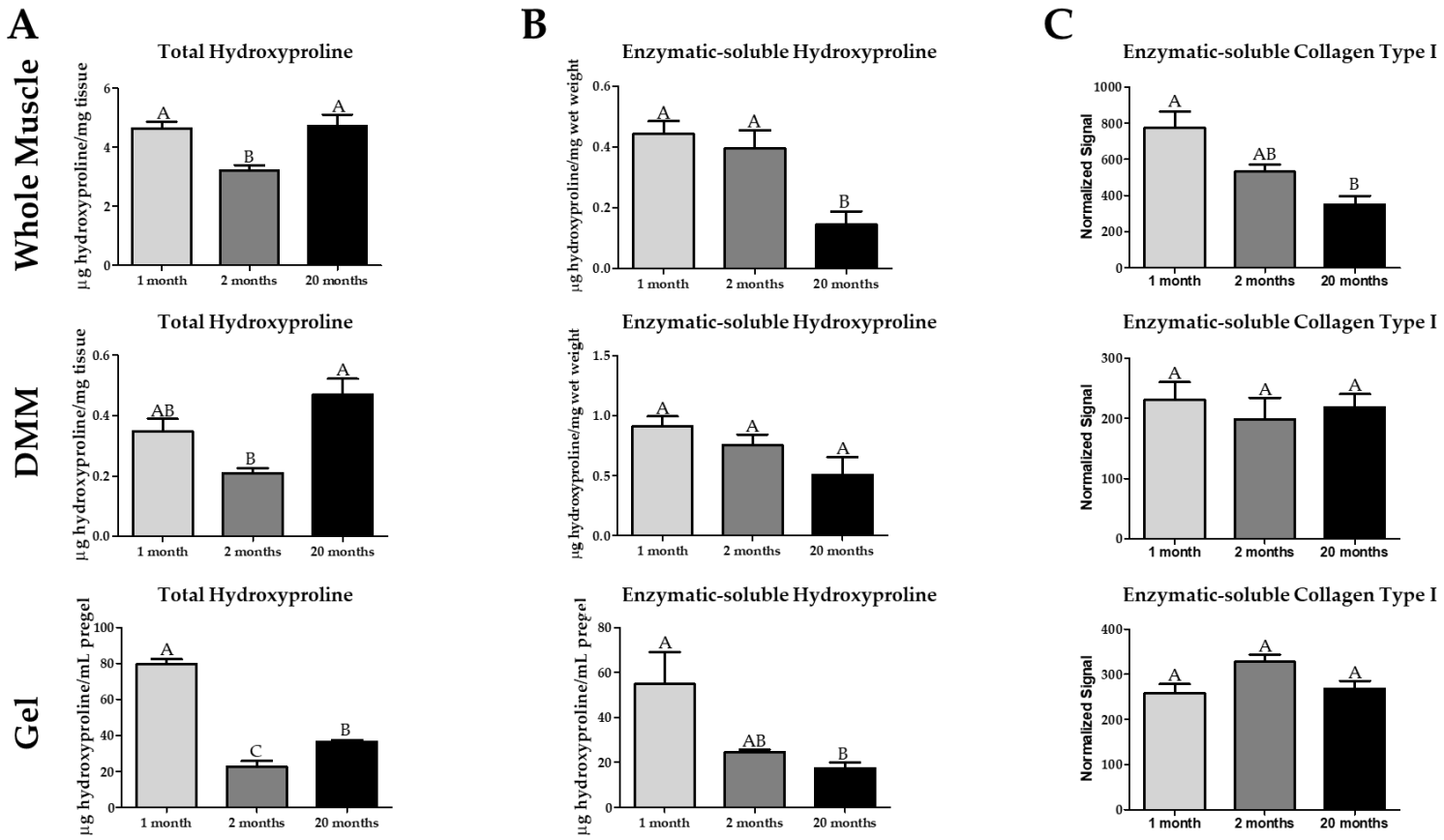

Figure 11. Total collagen is elevated in old age while soluble collagen is reduced as seen by hydroxyproline assays and SDS-PAGE. (**A**) Total hydroxyproline is increased at 1 month and 20 months compared to 2 months in whole muscle (n = 5 for 1 and 20 months, n = 6 for 2 months), decellularized muscle matrix (DMM) (n = 5 for 1-month, n = 6 for 2 and 20 months), and processed DMM gels (n = 3 for all groups), except 1 month is not higher than 2-month levels in DMM. Furthermore, total hydroxyproline levels are higher at 1 month in processed DMM gels compared to 20 months. (**B**) The amount of hydroxyproline soluble to the enzyme proteinase K is reduced in 20 months in whole muscle compared to 1 and 2 months and to 1 month in DMM (n = 5 for all groups) and processed DMM gels (n = 3 for all groups), indicating increased levels of cross-linking. (**C**) There is a decreased amount of proteinase K-soluble Collagen Type I at 20 months as determined by SDS-PAGE immunostaining compared to 1 month in whole muscle, indicating an increase in cross-linking. In DMM (n = 5 for all groups) and DMM processed gels (n = 3 for all groups), there is no difference in soluble Collagen Type I due to age, which could be due to the processing of the collagen denaturing the structural epitopes that the collagen antibody recognizes. Groups that do not share a letter (e.g. A, B, or C) are statistically

different according to a one-way ANOVA followed by a two-tailed Tukey's correction ($p < 0.05$, n value is detailed in each section).

Increased Stiffness in DMM from Old Muscle

We used atomic force microscopy imaging to test for age-dependent changes to muscle and DMM topography and stiffness. Cross-sectional muscle fiber topography was unchanged with age (Figure 12A). However, average fiber modulus was lower in 1-month muscle, and we observed a leftward shift in the modulus frequency distribution in 1-month muscle (Figure 12B). In addition, average roughness appeared to decline with age, and we observed an age-dependent decrease in percent maximum height (Figure 12B). In DMM, we demonstrated increased collagen structure with increasing age and an increased modulus with increasing age (Figure 12C). When we measured the average modulus, we detected an age-dependent increase in stiffness which was also observed in the modulus frequency distribution plots, where 20-month DMM was shifted toward higher moduli values compared to 1- and 2-month DMM (Figure 12D). In contrast to muscle fibers, average roughness increased in 20-month DMM compared to 1- and 2-month DMM. Height distribution was similar for 1- and 2-month DMM, while it appeared shifted to a lower maximum height for 20-month DMM (Figure 12D).

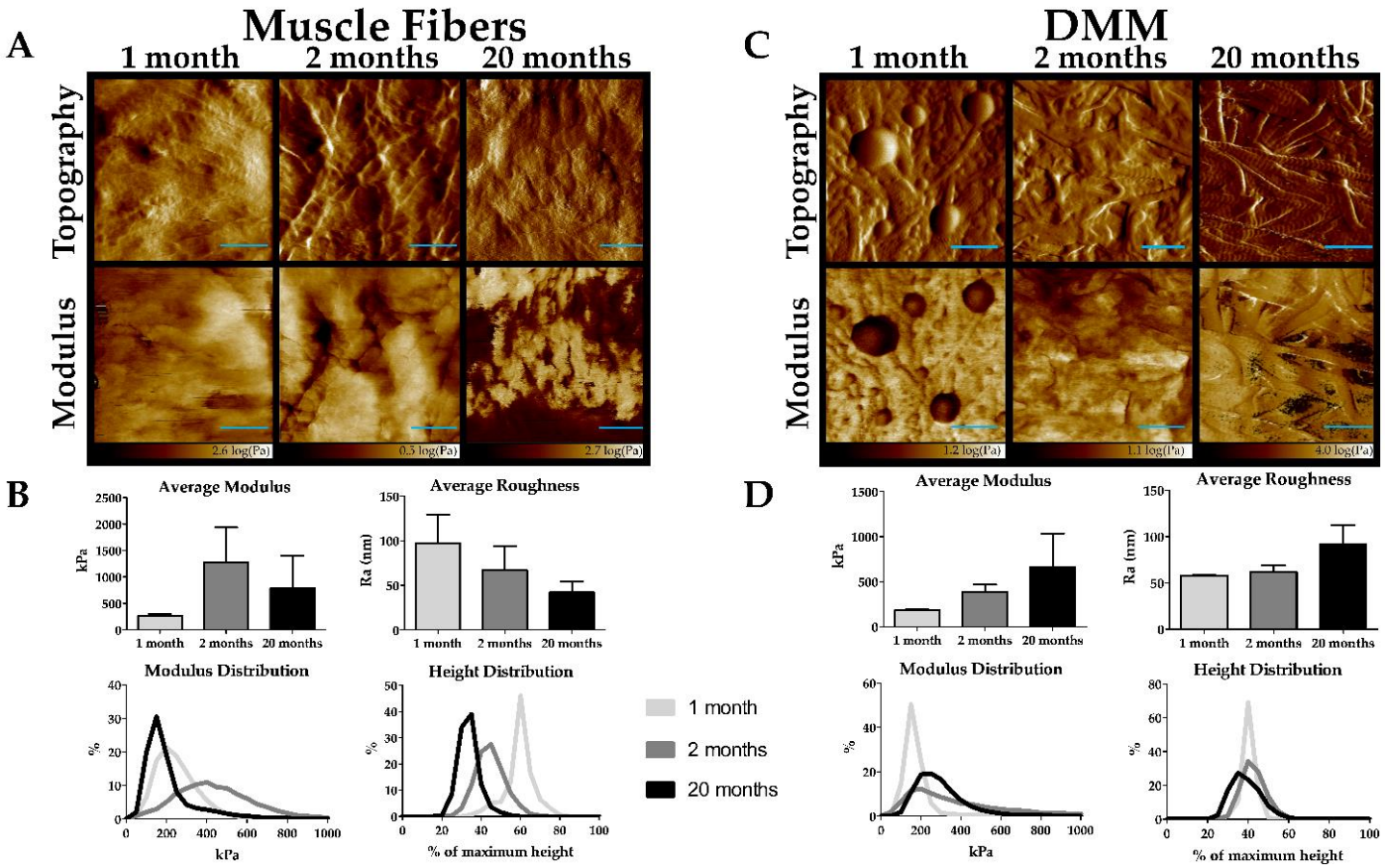

Figure 12. Atomic Force Microscopy imaging shows an increase in stiffness with age in decellularized muscle matrix (DMM). (**A**) The topography and modulus maps of muscle fibers show no noticeable difference with age. (**B**) The modulus of immature muscle fibers is reduced compared to 2 and 20 months. The average roughness of muscle fibers decreased with age, and the peak of the height distribution decreases with age. (**C**) The topography of DMM shows an increase in collagen structure with age. The topography of modulus is increased in old age. (**D**) The average modulus increased with age in DMM, and the peak of the modulus distribution is shifted to a higher value in old age. The average roughness is increased in old age compared to immature and young adult DMM. The peak of the height distribution is shifted slightly lower in old age. (n = 3 for all data in this figure). Scale bar = 500 nm.

Advanced Glycation End Products Are Retained in DMM

To test whether the increased cross-linking we observed in whole muscle is due to glycation cross-links (AGEs), we used the AGE ELISA kit. We quantified the amount of mechanically soluble hydroxyproline, and AGEs were normalized to hydroxyproline in our samples. Mechanical solubilization is not as

effective at extracting hydroxyproline using proteinase K due to the cross-links. This is supported by our data where we observed a decrease in the amount of mechanically soluble hydroxyproline in 2-month and 20-month whole muscle and DMM compared to the 1-month (Figure 13A). We demonstrated a significant increase in AGEs in 20-month whole muscle compared to 1- and 2-month muscle (Figure 13A). In contrast, we did not observe an age-dependent increase in AGEs in DMM (Figure 13B). No differences in total AGEs were observed in whole muscle and DMM, while there was a decrease in AGEs relative to wet weight in 2 and 20-month whole muscle and DMM samples compared to 1-month (Figure 14A,C). A decrease in AGEs per protein was measured in whole muscle between 1-month and 20 months, while there was no difference in DMM (Figure 14E). In addition, the wet weight increased with increasing age in whole muscle, while wet weight was reduced in 1-month compared to 2 and 20 months in DMM (Figure 14B). The same amount of protein was extracted from each age in whole muscle, while more protein was extracted in 1-month DMM compared to the other groups (Figure 14D). To further determine whether AGEs were responsible for reducing hydroxyproline with age, we treated DMM with an AGE cross-link breaker (ALT-711). ALT-711 incubation increased the amount of soluble hydroxyproline in 2-month and 20-month DMM, albeit only significant in the 2-month samples (Figure 13C). We also observed a significant decrease in the number of AGEs in the 1-month and 20-month group compared to the untreated age-matched DMM (Figure 13C). Lastly, we treated human DMM with ALT-711 and determined that ALT-711 reduced AGEs (relative to protein and hydroxyproline levels) in a clinically relevant human-derived DMM (Figure 15).

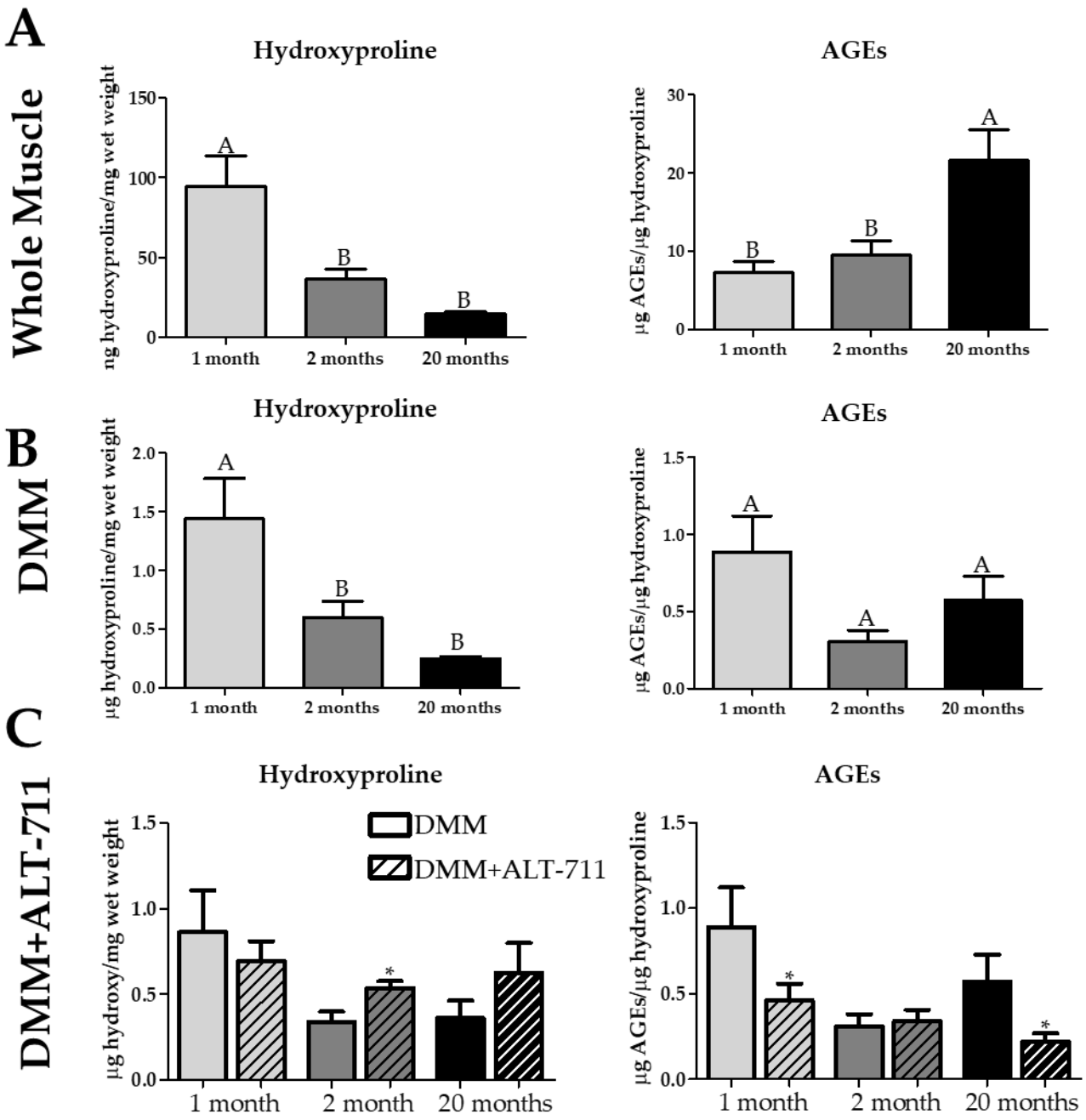

Figure 13. Advanced glycation end products (AGEs) are increased on old age in whole muscle but not in decellularized muscle matrix (DMM). However, the AGE cross-link breaker ALT-711 reduces the amount of AGEs in aged DMM. (**A**) The amount of detergent and mechanically soluble hydroxyproline is decreased in 2 and 20 months in whole muscle, indicating more cross-linking. AGEs are increased in old whole muscle relative to hydroxyproline (n = 6 in all groups). (**B**) The amount of detergent and mechanically soluble hydroxyproline is decreased in 2 and 20 months in DMM, indicating more cross-linking. However, there is no significant difference in AGEs relative to hydroxyproline with age in DMM

(n = 5 for 1- and 2-month groups, n = 6 for 20 months). (**C**) After treatment with ALT-711, the amount of detergent and mechanically soluble hydroxyproline was increased in 2-month samples compared to untreated age-matched DMM, and there was a reduction in the number of AGEs per hydroxyproline in 1-month and 20-month DMM treated with ALT-711 compared to untreated age-matched DMM, indicating that AGE reduction was effective at all ages. Groups that do not share a letter (e.g. A or B) are statistically different according to a one-way ANOVA followed by a two-tailed Tukey's correction ($p < 0.05$). * = statistically different to the age-matched control group (DMM without ALT-711) according to a two-tailed unpaired t-test ($p < 0.05$, n value detailed in each section).

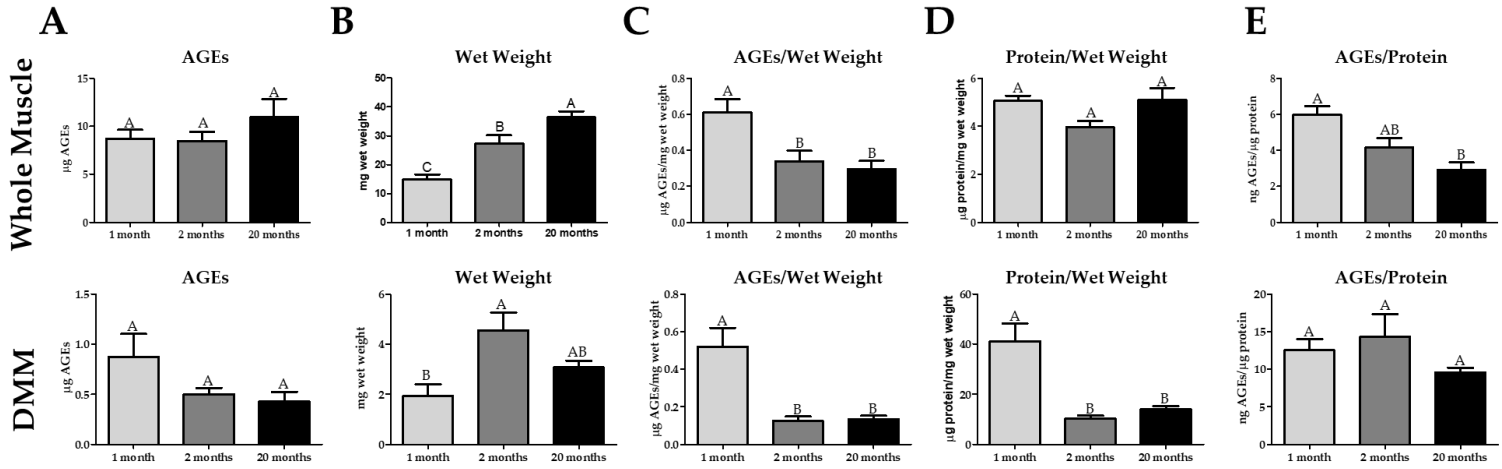

Figure 14: AGE levels were not different between 2 month mouse gastrocnemius muscles and 20 month gastrocnemius muscles. A) AGEs without normalization showed no difference. B) Wet weight increased with age in whole muscle, however wet weight was higher at 2 month DMM than 1 month. C) AGEs per wet weight was reduced from 1 month compared to 2 and 20 months. D) Protein per wet weight was not different in whole muscle, but was reduced from 1 to 2 and 20 months in DMM. E) AGEs per protein were reduced in whole muscle from 20 to 1 months, while there was no difference in DMM.

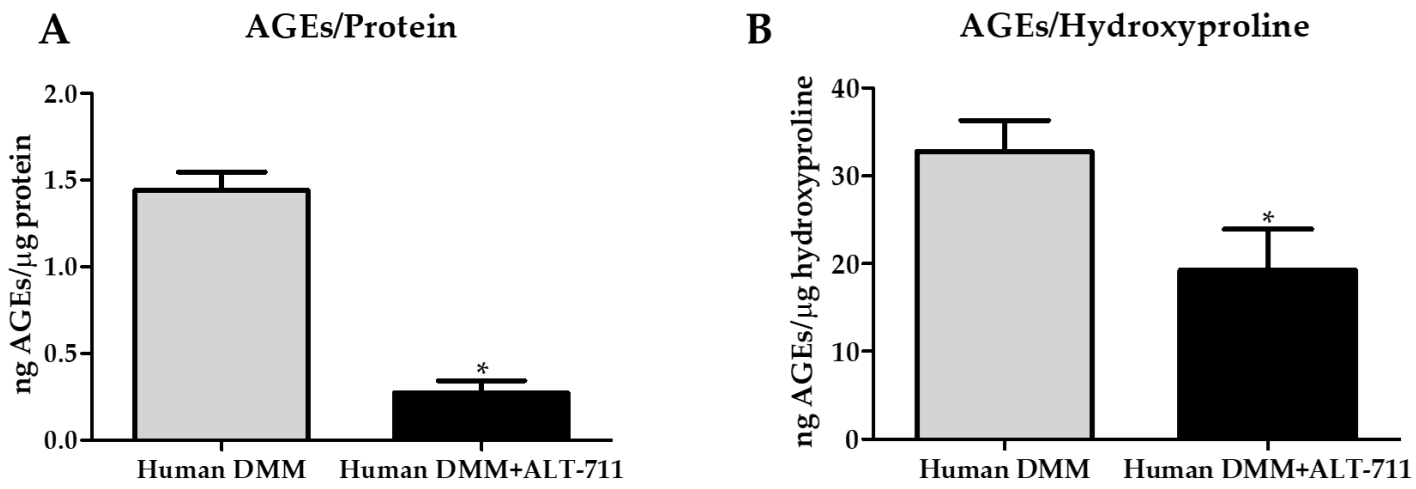

Figure 15: ALT-711 treatment reduced AGEs in human DMM. A) AGEs per protein was reduced with ALT-711 treatment. B) AGEs per hydroxyproline was reduced with ALT-711 treatment.

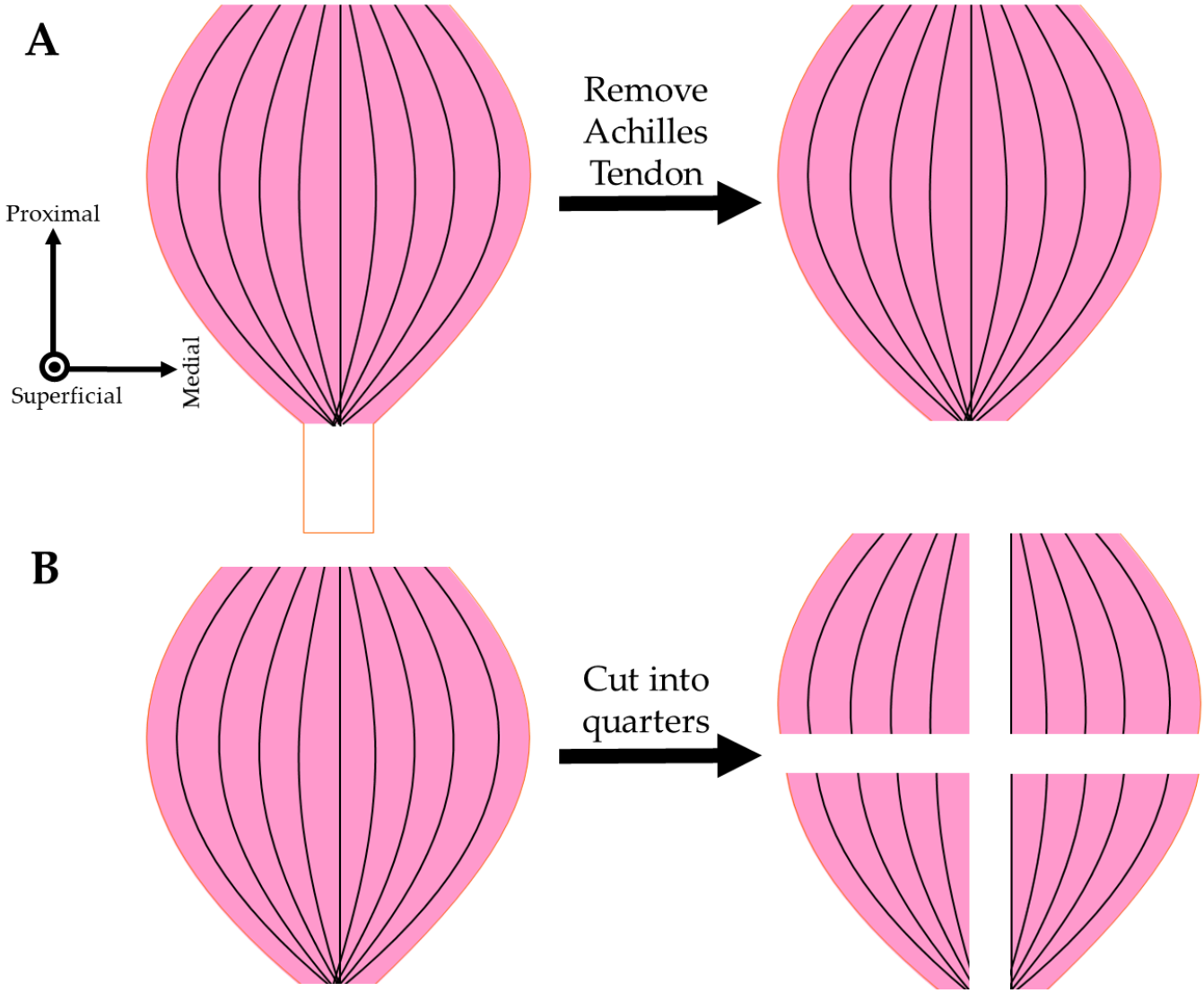

Figure 16: Gastrocnemius muscles were prepared for decellularization by Achilles' tendon (A) removal followed by quartering (B).

Challenges

AGE cross-links, by nature, are difficult to measure since they resist homogenization, and are often discarded as part of the irreducible matrix after centrifugation. Our initial experiments relied on total protein as the normalization factor for AGEs in the supernatant. We were unable to reliably measure an age-dependent increase of AGEs with age in whole muscle (data not shown). We hypothesized that we needed a more reliable normalization factor that held explanatory power over incomplete AGE extraction. We subsequently discovered that hydroxyproline, a proxy measurement for collagen, produced results that were in line with previously recorded literature.

Discussion

The overall goal of this study was to determine if collagen and AGE accumulation in skeletal muscle was specifically found in muscle ECM and retained in DMM. We captured muscle characteristics during various stages of maturation and aging using 1-month, 2-month, and 20-month gastrocnemius muscles from *C57BL/6J* mice. Characterization of these muscle specimens was an important step to identify whether AGE accumulation was detectable in older whole muscle and if it was specifically increased in relation to muscle ECM. Additionally, we chose the gastrocnemius as it has a heterogeneous distribution of fiber types to capture aspects of slow and fast-twitch muscle aging.[188,189] Furthermore, the gastrocnemius is among the hind limb muscles reported to be more susceptible to the aging process in rats, and was shown to be affected in 70-week-old mouse models of McArdle disease.[32,190] Next, we examined how muscle ECM was affected by aging. To do so, we decellularized the muscles, confirmed a successful decellularization, and characterized these matrices. In support of our hypothesis, we determined that AGEs accumulated in both old whole muscle and decellularized muscle ECM, indicating that AGE cross-links were conserved following decellularization. This was an important finding because it demonstrated that AGE cross-links in muscle ECM were detected and could have further implications in aged satellite cell and muscle fiber biology.

Investigation of 1-month, 2-month, and 20-month muscle captured various stages of collagen aging. During muscle maturation, collagens are not fully cross-linked, allowing the ECM to have a soft and spacious environment.[79,81,83] However, at sexual maturity (~ 2 months in murine models), stable lysyl oxidase (LOX) cross-links form and persist throughout adult life. As we age, collagen cross-links slowly accumulate, but remain at low levels relative to tissue weight. At about 20 years in humans AGEs begin to accumulate at a constant rate, dictated by the specific collagen turn-over time of each tissue type, and this process continues into old age.[191] Furthermore, starting at about 70 years of age, AGE accumulation on muscle collagen is correlated to loss of muscle function.[78] For this reason, we selected 20-month muscle as our aging model because unlike extreme old age (geriatric) only some of the aging features are present, which is more representative of an average older population.[192–194] In addition, it was previously reported that increased levels of AGE cross-links in the body is an early indicator of later pathological aging events.[195]

Furthermore, 20-month-old *C57BL/6J* mice are within the published accepted range for old age (18–24 months) with the maximum of 24 months based on 85% survivorship.[196,197] Selecting *C57BL/6J* mice older than 24 months is not advisable because of the increased prevalence of age-specific disease that

could lead to confounding results.[196,197] 18-22-month-old *C57BL/6J* mice have also been published as "old" age groups in multiple tissue types, including the lung, gut, spleen, skin, ovaries, eyes, brain, nails, tendon, meniscus, cartilage, bone, and skeletal muscle.[190,198–206] Additionally, senescence-like changes, a marker of old age, are observed between 18 and 24 months in *C57BL/6J* mice.[198,207–209]

Specific morphometric changes are expected in old age with skeletal muscles that reflect a reduction in cellularity with an increase in the ECM component.[210] We did not observe a decrease in the muscle fiber diameter with age, but there was a decrease in the number of nuclei, indicating that at 20 months an aging phenotype was not as pronounced as has been tested in other studies that use older mice.[211] The apparent increase in the amount of collagen at 20 months indicates changes in the ECM that precede changes in the muscle fibers themselves, even at this earlier stage of aging. In the immature 1-month group, we showed increased collagen levels that coincided with a decrease in muscle fiber diameter. Reduced dimensions of the muscle fibers could explain the increased amount of collagen relative to total area. However, it is also possible that the collagen occupied a larger volume due to less mature collagen cross-links.[88,210] This was confirmed quantitatively by measuring the amount of total hydroxyproline relative to weight at each age group.

Over time, there is an age-dependent decline in satellite cells that is associated with dysregulated differentiation and cell to cell fusion in the generation of new muscle fibers.[16] These age-dependent declines in the satellite cell pool are mirrored in the level of Pax7 detected in the tissue. Surprisingly, we did not measure a reduction in Pax7, suggesting that the number of satellite cells has not yet reached a sarcopenic decline at 20 months. However, another satellite and progenitor cell marker, m-cadherin, was reduced at 20 months of age. M-cadherin plays a role in maintaining the satellite cell niche in uninjured muscle and its decline could indicate that satellite cells may be at the beginning of sarcopenic decrease.[212–215] The transcription factors MyoD and myogenin are known to be upregulated in old age in a process known as homeostatic decompensation in a final attempt at recovering the muscle late in life.[61–63] Normally the myogenic transcription factors are at a low basal level in adult muscle, but when injury occurs, they are upregulated again and are responsible for patterning the myogenic process. Furthermore, in cases of denervation injury these transcription factors upregulate to form new muscle fibers in a recovery response to the atrophy and muscle fiber degradation typical to denervated muscle.[61] The aging environment in muscle is multifactorial but it is conjectured that the increase in MyoD and myogenin in aged muscle is in response to the retreat and fast-to-slow transition of the motor nerves.[61] Since MyoD was upregulated at 20 months and myogenin downregulated

slightly, the gastrocnemius at 20 months of age may be in the beginning stages of homeostatic decompensation.

The receptor for advanced glycation end products (RAGE) is thought to play a role in skeletal muscle aging by mediating the proinflammatory effects of AGEs and other RAGE ligands.[22] While we expected RAGE levels to increase in older animals, RAGE levels were actually lower in 20-month lysates compared to 2-month lysates. In muscle, RAGE is primarily expressed in activated satellite cells and differentiated myoblasts. As myoblasts fuse with existing muscle fibers, RAGE expression decreases dramatically, indicating that its expression in muscle is related to the progenitor cell pool.[23,71] In addition, there is a decrease in the amount of RAGE measured in human satellite cells in old age, and this is partially due to an increase in truncation of RAGE that makes it not detectable via immunostaining.[70] Furthermore, RAGE levels in 2-month muscle could be vastly different compared to middle aged muscle. In order to fully determine why 20-month muscle was reduced compared to 2-month would require more study.

Integrin α7 is a transmembrane protein responsible for transmitting force, is upregulated in differentiated myoblasts, and protects against sarcolemmal damage.[216,217] Integrin signaling has been implicated in muscle aging. Targeting β1-integrin signaling improved regeneration in dystrophic muscle and demonstrated that its deletion resulted in sarcopenic-like muscle.[218] Muscle's β1-integrin counterpart, α7, has less known effects during aging. Recent evidence suggests no differences between levels of α7B in 3- and 22-month murine muscle.[219] In contrast, our data show an increase in total *α7* at 20 months, suggesting a compensatory mechanism to protect muscle from sarcolemmal damage. Whether differences in α7B also exist in our model was not investigated. Slow-twitch muscle fibers are known to increase relative to fast-twitch muscle fibers with age, especially in sarcopenia.[27,90] We did not observe an increase in the level of total myosin heavy chain nor did we observe a change in fast-twitch myosin heavy chain levels in 20-month muscle compared to 2-month samples, suggesting that the degree of age-related changes in muscle has not yet affected muscle fibers. This supports our use of 20-month aged mice in order to assess the accumulation of AGE-crosslinks independent of other mechanisms associated with frail, sarcopenic muscle phenotypes. In addition, changes in fiber composition were found to be subtle and specific to fast twitch fiber type in the early stages of aging.[220] Additionally, recent evidence reported that fast-twitch muscle from *C57BL/6J* mice displayed subtle changes in myofiber type composition at 24 months of age.[185] Furthermore, *C57BL/6J* mice are known

to show age-dependent loss in muscular strength at an older relative age than humans, and as such may not be the best sarcopenic model.[29,221]

Since we observed age-dependent changes in ECM, we anticipated that these could carry over to DMM. In support of our hypothesis, we observed a significant increase in collagen at 20 months in DMM, indicating that additional age-related cross-links attenuated normal collagen turnover. Skeletal muscle collagen is heavily cross-linked by glycation in aged muscles, stiffening the matrix and causing it to be resistant to enzymatic turn-over.[6,17,20] Furthermore, no considerable differences in enzymatic cross-linking have been observed with age.[78,222] To test whether cross-links were increased in old muscle, we digested our samples in proteinase K and measured the amount of soluble hydroxyproline. There was a reduction in enzymatic-soluble hydroxyproline in 20-month whole muscle, implying an increase in the amount of collagen cross-linking. Interestingly, this effect was lost after decellularization, indicating that decellularization destroyed collagen cross-linking or otherwise caused the collagen to be more susceptible to protease degradation. If aberrant collagen cross-linking is reduced by decellularization, this would be an advantage as DMM would not “remember” the age of its collagen. However, an alternative explanation is that DMM lacks intracellular proteins to inhibit the proteinase K, thus the collagen cross-linking is overtaken by proteolytic cleavage in this case. We further processed our DMM into a gel and observed that both 2 and 20 months had significantly less enzymatic-soluble hydroxyproline, which could be due to a concentrating of the heavily cross-linked, irreducible parts of the matrix.

Collagen cross-linking significantly regulates the mechanical properties of tissues.[223] In old age, skeletal muscle stiffens and dysregulates the satellite cell niche, abrogating regeneration.[6,17] Whether this increase in stiffness is related to muscle fiber stiffness or the ECM is unclear. In addition, studies that investigate muscle stiffness in vivo rely on bulk material properties, which may miss minute mechanical features that cells would experience.[17,224] We used the AFM method to overcome these limitations of bulk mechanical testing and we observed that the increase in stiffness with age is specific to DMM, supporting our hypothesis that increased stiffness was ECM-related. Table 2 gives literary context to the exact moduli values recorded in our experimentation.

Citation	Method	Stiffness
Zhu, Yanxia et al. “Determination of mechanical properties of soft tissue scaffolds by atomic force microscopy	collagen–chitosan (80%/20%, v/v) scaffold; symmetric triangle tip (radius= 20 nm)	3.69 kPa

nanoindentation." Journal of biomechanics vol. 44,13 (2011): 2356-61.		
Luque, T et al. "Local micromechanical properties of decellularized lung scaffolds measured with atomic force microscopy." Acta biomaterialia vol. 9,6 (2013): 6852-9.	Cryosectioned decellularized lung (7 µm); V-shape Au-coated cantilever with a four-sided pyramidal tip on its apex	~20 kPa
Asgari, Meisam et al. "Revealing Layer-Specific Ultrastructure and Nanomechanics of Fibrillar Collagen in Human Aorta via Atomic Force Microscopy Testing: Implications on Tissue Mechanics at Macroscopic Scale" Advanced Nanobiomed Research vol. 2,5 (2022): 85-96.	Cryosectioned human aorta (20 µm); spherical tip (radius= 2 µm) and sharp tip (radius= 2 nm)	Maximum 81.9 kPa with spherical tip; maximum 7.26 MPa with sharp tip
This thesis.	Cryosectioned whole muscle and DMM (7 µm); a SCANASYST-FLUID tip (radius= 20 nm)	150-1,300 kPa

Table 2: Literature modulus values for tissue and ECM scaffolds

Furthermore, since DMM retained a stiffer microenvironment, its use as a regenerative biomaterial may be compromised as muscle progenitor cells aberrantly proliferate on stiffer substrates. Furthermore, stiffness is known to alter mesenchymal differentiation, with stiffer substrates supporting osteoblastic pathways at the expense of adipogenic, chondrogenic, and myogenic pathways.[225,226] Interestingly, we observed a rougher microenvironment in old DMM, which conflicts with the known decrease in collagen tortuosity with age.[6,227] However, an overall dysregulation in the structure of the basal lamina does occur with old age.[41] These data confirm that pathological changes occurred in the old muscle ECM.

To determine whether the age-dependent changes we observed in DMM collagen were AGE specific cross-links we tested levels of AGEs in our samples and detected an increase in the number of AGEs in old whole muscle when normalized to hydroxyproline. We did not observe this increase in AGEs when normalizing to wet weight and protein. This observation suggested that AGE crosslinks might be concentrated in the ECM, leading us to choose collagen for normalization. A known difficulty in measuring AGE content is that most AGEs reside in the irreducible matrix, and as such a normalization factor (e.g., hydroxyproline) that accounts for the matrix components would account for this.[228] Interestingly, when we measured the amount of mechanically soluble hydroxyproline, it was reduced at both 2 months and 20 months of age. Since we did not detect a reduction at 2 months in the harsher proteinase K digestion, we suspected that collagen cross-linking at 20 months was greater than 2 months. We observed this same effect with hydroxyproline in the DMM; however, there was no increase in AGEs with age. In our homogenization schema, it is possible that in DMM, where the intracellular components are removed, the AGEs are in the pellet and thus are not measurable. To test this theory, we treated DMM with ALT-711, an AGE-specific cross-link breaker, and showed that there was no longer a reduction in hydroxyproline with age.[229] When we measured AGEs in the ALT-711 treated DMM, there was a reduction in the 1-month and 20-month samples compared to no treatment, showing that ALT-711 is effective in reducing elevated levels of AGEs. All of this together emphasizes that there were AGE cross-links in the DMM below our assay's detection limits and that ALT-711 effectively reduced them in the aged DMM. Impressively, ALT-711 treatment was also a viable method at reducing AGEs in human-derived DMM, pointing to its clinical relevance. Reducing AGEs on aged DMM could restore the supple microenvironment of younger muscle ECM while eliminating the harmful effects of aberrant RAGE signaling. Furthermore, if successful this would open the gateway for using readily available old human muscle in decellularization applications. However, future studies are needed to characterize this treatment on aged DMM in promoting skeletal muscle regeneration.

Materials and Methods

Animal Model: 1-month, 2-month, and 20-month-old male *C57BL/6J* mice were selected to represent an immature, young adult, and old adult mouse. The gastrocnemius muscle was used for all experiments (one n is one muscle). Gastrocnemius muscles were large enough to perform multiple assays. All surgical procedures were performed under an IACUC-approved protocol at VCU (AD10000675, 1 March 2019). Briefly, the mice were euthanized with CO_2 asphyxiation followed by cervical dislocation. The skin covering the limbs was bluntly dissected, and the gastrocnemius muscles

excised, taking care to remove the overlying biceps femoris and underlying soleus and plantaris. The Achilles tendon was also removed before experimental use.

Decellularization: Gastrocnemius from 1-month, 2-month, and 20-month-old male C57Bl/6 mice were used as a model of skeletal muscle aging. The gastrocnemius was isolated and frozen at −80 °C until decellularization. On the day of decellularization, the muscle was thawed and cut into quarters, and each quarter of the muscle was put into its own well of a 24-well plate and decellularized at 4 °C on a plate shaker (Figure 16). The quarters were treated with three 10 min DI water washed, 0.25% trypsin for 6 h, 0.1% Triton X-100 for 24 h, 0.2% sodium deoxycholate for 24 h, DNase for 1 h, and 0.1% peracetic acid for 24 hours. There were three 15 min DI water washing steps between all steps, and five 15 min 1×PBS washes after the peracetic acid step. All volumes were 1.5 mL, except the DNAse was 0.5 mL. To create a DMM gel, the DMM was lyophilized and cryomilled to create a DMM powder. This powder was digested with pepsin (2300units/mg powder) in 0.01M HCl for 6 hours, pH and salt balanced with NaOH and 10xPBS, and gelled at 37 °C for 1 h. Decellularization was confirmed by running the pre-gel on the picogreen dsDNA assay.[230] The gelation rate was determined by measuring optical density at 550 nm in a 96-well plate every 2 min at 37 °C for 1 h (n = 12 for all groups). The results were then curve-fitted using Matlab to extract the gelation rate [99]. Matlab code is available upon reasonable request.

Histological Evaluation: Whole muscle was processed with formalin-fixed paraffin-embedded (FFPE) tissue processing. Briefly, the tissue was fixed in 10% neutral-buffered formalin and then processed through increasing gradients of ethanol, cleared with xylenes, and infiltrated with paraffin wax. The samples were then embedded in paraffin wax, and 7 µm sections were taken, floated on a warm water bath, and picked up onto charged glass slides, dried, stained, and cover slipped. Before staining, the sections were deparaffinized with xylenes and rehydrated with decreasing gradients of ethanol. DMM was processed with cryosectioning, where the tissue was embedded in Optimal Cutting Temperature (OCT) compound, frozen at −80°C, sectioned in a microtome at 7 µm onto charged glass slides, and kept at −80°C until staining. Before staining, the OCT was washed out with DI water. Hemotoxylin and Eosin (H&E) and Masson's Trichrome (Weigert's Iron Hematoxylin, Biebrich Scarlet-Acid Fuchsin, and Aniline Blue) were applied to assess the muscle (3 representative 10× images per sample) and DMM (3 representative 10× images per sample) morphometrically. Additionally, 40× pictures were taken to represent the whole muscle in Figure 5. Masson's Trichrome and Picrosirius Red were used to qualify and quantify, respectfully, the collagen content of whole muscle and DMM. Two 50× images per sample

were quantified in the whole muscle Picrosirius Red sections, and three 10× images for DMM. The regions were selected based on representation (whether the image reflected the natural variation in the muscle or not) and usability for data analysis (e.g., regions where the muscles were cut longitudinally were not included, as it is not possible to measure the diameter). The Zen Pro software (Carl Zeiss Meditec AG, Jena, Germany) was used to perform the histomorphometry. Minimum Feret diameter was found for the whole muscle by using the linear measurement tool on Zen Pro to measure the minimum diameter of the myofibers.[198,231] The distance between myofibers was found using the linear measurement tool on Zen Pro. The collagen area was measured with the polygon contour tool for whole muscle in the Picrosirius red section. For decellularized muscle, the white area from the Picrosirius red images was measured using automatic thresholding using Zen Pro, and this was subtracted from the total area to find the area of red stain. Porosity of H&E stained DMM was found by measuring the empty spaces in 3 random 10× images per sample (Zeiss AxioVision Microscope; Carl Zeiss Microscopy LLC, White Plains, New York, USA), and then the data was presented as a percentage of these spaces to the total area of the image, averaged per sample. The same process was applied to the Picrosirius Red samples, except the red areas (collagen-stained) were quantified and reported as a percentage of the total area of the image, averaged per sample.

Scanning Electron Microscopy: Scanning Electron Microscopy (SEM) was used on tissue that is cryosectioned at 30 μm, washed with DI water to remove the OCT, lyophilized, and sputter-coated with platinum. The sections were imaged with SEM (Hitachi SU-70 FE-SEM, Hitachi, Ltd., Tokyo, Japan) with 5.0kV at × 350 and × 20.0k to characterize the ultrastructure. Zen Pro software (Carl Zeiss Meditec AG) was used to quantify the thickness of the endomysium and the porosity on x350 images. The porosity was found by measuring the total open pore area and dividing that area by the total area using the Zen Pro linear measurement tool for endomysium thickness, and using the contour polygon area tool.

Collagen Cross-linking: Collagen cross-linking was determined by assessing collagen's resistance to Proteinase K digestion. Briefly, the samples were homogenized in NP-40 lysis buffer with a 6.0 mm zirconium bead in the beadbug homogenizer, then incubated in 800 U/mL Proteinase K (P8107S, New England Biolabs, Ipswich, Massachusetts, USA) for 1 h at 37 °C. A protease inhibitor cocktail was added, the samples were centrifuged at 13,000 rpm (17,949 g) (Centrifuge 5427 R, Eppendorf, Hamburg, Germany) for 3 min, and the supernatants hydrolyzed for 24 h with 5N HCl at 120 °C before being run on the hydroxyproline assay (6017, Chondrex, Woodinville, Washington, USA). The

supernatants were also assessed with Western blotting, where the rabbit anti-Collagen I antibody (ab34710, Abcam, Cambridge, UK) was used, and the results were normalized to total protein (926-11016, LI-COR Biosciences, Lincoln, Nebraska, USA). This Western blotting approach was also applied to the pregel of the processed DMM gel. Other samples were hydrolyzed without homogenization to determine the total hydroxyproline amount (DMM was normalized to dry weight before decellularization).

Atomic Force Microscopy: Atomic Force Microscopy was used on tissue that is cryosectioned at 7 μm. The OCT was removed with DI water, and the section was hydrated with 1×PBS for the experiment's duration. The Dimension FastScan AFM from Bruker along with the SCANASYST-FLUID tip (20 nm radius) was used to gather topographical and modulus measurements from the sections under 1×PBS. Each tip was calibrated under 1×PBS using thermal tuning followed by ramping (5 curves, 200 nm ramp height, 0.20 V ramp set point) to determine the k value. Then, the samples were probed using peakforce quantitative nanomechanical mapping under fluid (1×PBS) with a 2 μm × 2 μm scan size at 400 samples/line for topographic images. The same image was taken again but at 128 samples/line to gather individual force curves (16,384 per image). The modulus was extracted from each force curve by applying the 2-point JKR model with taking into account positive adhesion forces (Poisson's ratio was assumed to be 0.5). The incalculable force curves were removed using MatLab (code available upon reasonable request) and the data averaged, then the histograms of the modulus and height values were plotted using GraphPad Prism (GraphPad Prism 5.04, GraphPad Software, San Diego, California, USA).

AGEs: Muscle samples were minced and homogenized with the Minute™ Total Protein Extraction Kit for Muscles (using the Denaturing Buffer) and ran on an AGE ELISA (STA-817, Cell Biolabs, San Diego, California, USA) to determine AGE levels. For DMM, homogenization was done with a 6.0 mm zirconium bead in a beadbug homogenizer (BeadBug™ Cat #: 31-212, Genesee Scientific, San Diego, California, USA) at 4000 rpm for 60 seconds 20 times while keeping the tubes on ice for at least 5 min between runs, to pulverize the tough ECM, followed by centrifugation at 13,000 rpm (17,949 g) (Centrifuge 5427 R, Eppendorf, Hamburg, Germany) for 3 min. For human DMM, homogenization was done with NP-40 lysis buffer with a 2 mL tenbroeck glass-pot homogenizer followed by centrifugation at 13,000 rpm (17,949 g) (Centrifuge 5427 R, Eppendorf, Hamburg, Germany) for 3 min. The Pierce™ BCA Protein Assay Kit (23,225 and 23227, Thermo Fisher Scientific, Waltham, Massachusetts, USA) and hydroxyproline assays were used for normalization purposes. To reduce AGE cross-links, DMM

was incubated with 10 mM of the AGE-cross-link breaker ALT-711 (Alagebrium Chloride A3166 TCI America, Portland, Oregon, USA) in 1xPBS for 5 days at 37 °C. The DMM was then washed 3 times with DI water for 5 min each, then frozen at −80 °C until analysis.

Western Blotting: 30 mg of gastrocnemius muscles were homogenized in NP-40 lysis buffer (BP-119, Boston BioProducts, Ashland, Massachusetts, USA) with a PI cocktail and 25mM NaF with a 6.0 mm zirconium bead in a beadbug homogenizer (BeadBug™ Cat #: 31-212, Genesee Scientific, San Diego, California, USA) at 4000 rpm for 60 s 5 times while keeping the tubes on ice for at least 5 min between runs. The homogenate was centrifuged 9703 rpm (10,000 g) (Centrifuge 5427 R, Eppendorf, Hamburg, Germany) for 10 min, and the supernatant was used for Western blotting. Briefly, the supernatant was run on the BCA assay. Equal amounts of protein were denatured with Laemmli buffer at 100 °C for 10 min, then electrophoresed on polyacrylamide gels, transferred to a PVDF low fluorescence membrane, blocked for 1 h at room temperature, and stained overnight with primary antibodies (mouse anti-PAX7 (ab55494 Abcam, Cambridge, UK), mouse anti-MYOD (MA1-41017, Thermo Fisher, Waltham, Massachusetts, USA), mouse anti-Myogenin (ab1835, Abcam, Cambridge, UK), mouse anti-Myosin Heavy Chain clone A4.1025 (05-716, Sigma Aldrich, St. Louis, Missouri, USA), mouse Anti-Myosin (Skeletal, Fast) clone MY-32 (M4276, Sigma-Aldrich, St. Louis, Missouri, USA,) rabbit anti-M Cadherin (ab87374, Abcam, Cambridge, UK), rabbit anti-ITGA7 (PA5-37435, Thermo Fisher, Waltham, Massachusetts, USA), rabbit anti-RAGE (ab37647, Abcam, Cambridge, UK) or rabbit anti-GAPDH (14C10) (2118S Cell Signaling Technology, Danvers, Massachusetts, USA,). The membranes were then incubated with secondary antibodies (926-68073, 926-32210, and 926-32211, LI-COR Biosciences, Lincoln, Nebraska, USA) for 40 min at room temperature, then they were imaged on the LI-COR Odyssey and quantified. 1-month and 2-month samples were run on the same gel, and 20-month samples were run on a separate gel. Each blot was analyzed separately and results were normalized to GAPDH levels. The normalization factor for samples on one blot was determined by identifying the highest GAPDH signal and dividing each GAPDH signal intensity by the highest GAPDH signal, producing a value of 1 for the strongest signal and less than 1 relative to that stronger signal. Target protein signals were divided by the normalization factor to obtain the normalized signal. An advantage of this normalization method is that it is not affected by variations in housekeeping proteins as seen in old age.[232]

Statistical Analysis: Data are represented as mean ± standard error of the mean. Statistical analysis is performed using a one-way analysis of variance (ANOVA) followed by a two-tailed Tukey's correction

to determine significance using $\alpha = 0.05$. Groups not sharing letters are statistically significant. Outliers were removed using Grubb's test ($\alpha = 0.05$). All statistical analyses are performed using GraphPad Prism (GraphPad Prism 5.04, GraphPad Software, San Diego, California, USA) and JMP Pro (JMP Pro 15, SAS Institute, Cary, North Carolina, USA).

Conclusions

Skeletal muscle aging elevates the amount of intramuscular collagen, AGE cross-linking, and stiffness at a clinically relevant age that could be deleterious to regeneration. Our data shows that these aging alterations are preserved in DMM, providing an obstacle for the clinical translation of DMM since older muscle is available in greater frequency. Interestingly, these changes are also retained in a more processed DMM gel, indicating that age still affects DMM at every level of reduction. However, ALT-711 shows efficacy in reversing AGE cross-linking in DMM, providing a pathway for future biological studies at improving aged DMM.

Chapter 4. S100b Treatment Overcomes RAGE Signaling Deficits in Myoblasts on Advanced Glycation End-product Cross-linked Collagen and Promotes Myogenic Differentiation

Abstract

Advanced glycation end products (AGEs) stochastically accrue in skeletal muscle and on collagen over an individual's lifespan, stiffening the muscle stem cell (MuSC) microenvironment while promoting proinflammatory, anti-regenerative signaling via the receptor for advanced glycation end products (RAGE). We developed a novel in vitro model of this phenomenon by cross-linking a 3D collagen scaffold with AGEs and investigated how myoblasts responded. AGEs promoted excess proliferation in myoblasts, and this effect was successfully countered by RAGE inhibition. Additionally, the differentiation and fusion of myoblasts were disrupted by AGEs, and this was associated with reductions in integrins and suppression of RAGE. Surprisingly, S100b (RAGE agonist) treatment recovered myotube formation. Our results provide novel insights into the role of the AGE-RAGE axis in skeletal muscle aging, and future work is warranted on the potential application of S100b as a pro-regenerative factor in aged skeletal muscle.

Introduction

The aging of skeletal muscle is fueled by deterministic and stochastic events that culminate in sarcopenia, a muscle-wasting disease typified by the loss of muscle mass and force.[233] Sarcopenia is associated with a decrease in skeletal muscle's capacity to regenerate, suggesting that the satellite cell niche is compromised by the aging process.[233] Satellite cells are Pax7+ multipotent adult stem cells that are located adjacent to the muscle fibers underneath the basal lamina.[51,234] Injury activates these cells causing them to proliferate, enter into the myogenic program, differentiate, and fuse to form new muscle fibers or fuse to existing muscle fibers while also self-renewing to maintain a reservoir of satellite cells.[55,235] In aging, satellite cell number decreases while myogenic transcription factors that regulate differentiation, MyoD and MyoG, increase. These data suggest that factors in the satellite cell niche are aberrantly activating them while preventing self-renewal.[16,61,214,236] The extracellular matrix (ECM) makes up half of the satellite cell's niche (the other half being the skeletal muscle fiber) and thus is influential over the self-renewal and differentiation of these cells.[51,56,237]

A hallmark of aged skeletal muscle ECM is the upregulation of collagens that produce a fibrotic phenotype.[79] Advanced glycation end-products (AGEs) are a non-enzymatic modification to proteins that follow the Maillard reaction and may be a major driver of this phenomenon.[25,238] AGEs are formed when sugars stochastically interact with proteins, using a sugar monomer or metabolite that binds to a protein (usually at a cysteine group) to form an Amadori product (pre-AGE).[238] This product then stabilizes over the course of a few days to form a mature AGE. Skeletal muscle ECM is a prime location for these AGEs to accumulate, especially since collagens are long-lived and contain cysteine/lysine groups.[238] The non-enzymatic modifications to the ECM result in a matrix that is stiffer and more resistant to degradation by matrix metalloproteases and other enzymes.[238] During the aging process, the number and activity of satellite cells were impacted by modifications to the ECM such as basement membrane remodeling, loss of fibronectin, and increased laminin,[3,15,16,239] but none of these studies explored the role of ECM glycations.

We developed and characterized an *in vitro* system modeling aged glycated collagen, and tested the response of myoblasts to our system using C2C12s, a well-characterized immortalized mouse myoblast cell line, and human primary myoblasts. Additionally, we probed the AGE-RAGE axis with known RAGE inhibitors FPS-ZM1 and Azeliragon, and with the RAGE agonist S100b. We hypothesized that AGE cross-links would dysregulate myogenesis and that this would be RAGE dependent.

Materials and Methods

AGE-Collagen preparation: RCT collagen tape (ACE Surgical Supply, Brockton, MA) was punched into 48-well-sized pieces with a 10 mm biopsy punch (Acuderm, Fort Lauderdale, FL) and placed in a 48-well plate (Greiner Bio-One International GmbH). AGE formation was induced on the collagen in a dose-dependent manner with 0, 25, 40, 100, or 250 mM ribose (Millipore Sigma, St. Louis, MO) in a solution of 1X PBS with 44 mM NaHCO3 (Sigma-Aldrich, St. Louis, MO) and 25 mM HEPES (Sigma-Aldrich, St. Louis, MO) buffer for 5 days. After 5 days, the membranes were washed 3 times for 5 minutes with 5 mL of DI water in 6-well plates and frozen at -80°C for long-term storage. Prior to use membranes were lyophilized overnight. To confirm that D-ribose was washed out of the collagen, the collagen was digested in collagenase type 1A (Sigma-Aldrich, St. Louis, MO) and ran on a colorimetric ribose assay.[240,241]

Collagen cross-linking and AGE analysis: Collagen cross-linking was determined by assessing collagen's resistance to Proteinase K digestion. Briefly, the samples were homogenized in NP-40 lysis buffer with a 6.0 mm zirconium bead in a beadbug homogenizer, then incubated in 800 U/mL Proteinase K (P8107S, New England Biolabs, Ipswich, MA, USA) for 1 h at 37 °C. A protease inhibitor cocktail (Sigma-Aldrich, St. Louis, MO) was added, the samples were centrifuged at 13,000 rpm (17,949 g) (Centrifuge 5427 R, Eppendorf, Hamburg, Germany) for 3 min, and the supernatants hydrolyzed for 24 h with 5N HCl at 120 °C before and then were ran on a hydroxyproline assay (6017, Chondrex, Woodinville, WA, USA). The results were normalized to wet weight.

For AGE analysis the collagen samples were homogenized in 400 µL 1xPBS in a beadbug homogenizer (BeadBug™ Cat #: 31-212, Genesee Scientific, San Diego, CA, USA) at 4000 rpm for 60 seconds 5 times while keeping the tubes on ice for at least 5 min between runs. After mechanical homogenization, collagenase type III (STEMCELL Technologies Inc., Vancouver, Canada) (100 µL, 4000 U/mL in 1xPBS) was added to the homogenate and incubated at 37ºC for 1 hour. Then EDTA (Sigma-Aldrich, St. Louis, MO, USA) (0.5 M, 10 µL) was added to the collagenase-treated samples to quench the digest followed by centrifugation at 13,000 rpm (17,949 g) (Centrifuge 5427 R, Eppendorf, Hamburg, Germany) for 3 minutes. The supernatant was used for the assays. The supernatants were run on an AGE ELISA (STA-817, Cell Biolabs, San Diego, CA, USA) and results were normalized to wet weight, hydroxyproline, and protein with the Pierce™ BCA Protein Assay Kit (23,225 and 23227, Thermo Fisher Scientific, Waltham, MA, USA).

Scanning Electron Microscopy: Scanning Electron Microscopy (SEM) was used on lyophilized collagen samples that were sputter-coated with platinum. The samples were imaged with SEM (Hitachi SU-70 FE-SEM, Hitachi, Ltd., Tokyo, Japan) with 5.0kV at × 350 and × 20.0k to characterize the ultrastructure.

Atomic Force Microscopy: Atomic Force Microscopy was used on tissue that is cryosectioned at 7 µm. The OCT was removed with DI water, and the section was hydrated with 1×PBS for the experiment's duration. The Dimension FastScan AFM from Bruker along with the SCANASYST-FLUID tip (20 nm radius) was used to gather topographical images from the sections under 1×PBS.

Bulk Mechanical Testing: Compressive and tensile mechanical properties were assessed using a Bose ElectroForce 3200 Series III Axial-Torsion System equipped with a 250 g load cell as previously described.[242–245] The compressive properties were assessed via unconfined compression using a 25 mm platen to load 10 mm diameter biopsies. The height of each sample was measured prior to testing

and all tests were performed with hydrated constructs fully immersed in PBS at room temperature. Constructs were pre-loaded with 0.05 g to ensure contact with the surface, and then loaded to 50% compression at a strain rate of 0.5% strain/sec, assuming quasi-static loading.[242,243] The compressive modulus was calculated based on the slope of the most linear region of the stress-strain curve between 10-30% strain with a linear regression fit of R^2>0.99. For tensile tests, 10 mm biopsies were cut into rectangles with dimensions of ~1-2 mm wide by 8-10 mm in length. Prior to testing, rectangles were fully hydrated in PBS and dimensions were measured. The rectangles were secured between grips and loaded to failure at a strain rate of 0.5%/s, assuming quasi-static loading and ensuring failure occurred between the grips.[244,245] The tensile modulus is the slope of the linear region of the stress-strain curve as determined by a linear regression fit ensuring an R^2>0.99. The strain at failure and the ultimate tensile strength (UTS) are the maximum stress point.

Mass Spectrometry Analysis: Three collagen samples (control with no AGEs) were sent to UVA's mass spectrometry core, and the samples were initially solubilized (mostly) using a Bead Beater with stainless steel balls before acetone precipitation to produce a protein pellet. The pellet was re-solubilized in digestion buffer using heat and sonication. The protein did not all go into solution so each sample was divided into a soluble fraction and insoluble pellet. The soluble fraction (10ug) and insoluble pellet were digested (and ran by MS) separately. The sample were reduced with DTT for 30 minutes at RT, then alkylated using iodoacetamide for 30 minutes at RT, followed by overnight digestion with 0.5 ug trypsin (insoluble – second overnight trypsin digestion). The samples were cleaned up using C18 tips. The LC-MS system consisted of a Thermo Orbitrap Exploris 480 mass spectrometer system with an Easy Spray ion source connected to a Thermo 3 µm C18 Easy Spray column (through pre-column). 1 µg of the extract (soluble and insoluble separately) was injected and the peptides eluted from the column by an acetonitrile/0.1 M acetic acid gradient at a flow rate of 0.3 µL/min over 2.0 hours. The nanospray ion source was operated at 1.9 kV. The digest was analyzed using the rapid switching capability of the instrument acquiring a full scan mass spectrum to determine peptide molecular weights followed by product ion spectra (Top10 HCD) to determine amino acid sequence in sequential scans. This mode of analysis produces approximately 25000 MS/MS spectra of ions ranging in abundance over several orders of magnitude. Not all MS/MS spectra are derived from peptides. The data were analyzed by database searching using the Sequest search algorithm against Uniprot Bovine.

Cell culture: Collagen (0 mM) and AGE-Collagen (100 and 250 mM) collagen membranes were prepared as described previously. The scaffolds were pre-wetted in 48-well plates with 250 µL of growth

media (α-MEM+10% FBS+1%Pen/Strep for C2C12s, Cook Myocyte Basal Media+10%Myotonic Growth Supplement+1%Pen/Strep for human primary myoblasts) which was removed prior to seeding. C2C12s (originally derived from female mice) or male human primary myoblasts were seeded onto the collagen membranes at 15,000 cells/cm^2 in 50 µL of growth media.[246] The collagen was placed in a 37°C incubator for 2 hours to promote cell attachment. After 2 hours, 200 µL of growth media was added. After 24 hours, the collagen scaffolds were moved to new wells with fresh media (250 µL) using sterile forceps, to prevent any cells that attached to the bottom of the plate from influencing the experiment. Following this the media was changed every 48 hours. The RAGE inhibitors FPS-ZM1 (Cayman Chemical Company, Ann Arbor, Michigan, USA) and Azeliragon (MedChem Express, Monmouth Junction, NJ, USA) were delivered in DMSO (Fisher Scientific, Hampton, NH, USA), and all DMSO concentration was kept at 0.1%. The RAGE agonist S100b (Boster Bio, Pleasanton, CA, USA) was delivered in 20mM Tris-HCl buffer (pH 8.0) containing 1mM DTT and 10% glycerol. S100b's vehicle was kept at 0.1% concentration in the growth media. When myoblasts were cultured with the inhibitors and agonist, the cells were incubated with the respective inhibitors/agonist for 30 minutes at 37°C to allow for receptor binding before the cells were seeded onto the scaffolds. After then, all media changes included the inhibitors/agonist.

DNA quantification: Total DNA was analyzed either on day 2, day 4 or day 6. On the day of harvest, the collagen/wells were washed twice with 1 mL of 1xPBS, and submerged in 250 µL of 0.05% Triton X-100. The samples were frozen at -20°C until the day of assay. On the day of assay, the samples were sonicated at a minimum amplitude of 40, for 5 seconds per well. The samples were lightly centrifuged (2,000 g) for 1 minute, and the supernatant was used with the QuantiFluor® dsDNA System (Promega, Madison, WI, USA) to determine dsDNA levels.

Fluorescent imaging: On the day of harvest, the collagen was washed twice with 1 mL of 1xPBS, and fixed with 250 µL of 4% paraformaldehyde for 15 minutes at room temperature. The samples were stored at 4°C until the day of assay. On the day of assay, the samples were washed two times with 1mL of 1xPBS and then were permeabilized in 0.1% Triton X-100 in 1xPBS for 15 minutes. The samples were washed two more times with 1mL of 1xPBS. 200 µL of staining solution (Invitrogen™ Alexa Fluor™ 594 Phalloidin (Invitrogen, Waltham, MA, USA) and Hoechst 33258 (Invitrogen, Waltham, MA, USA)) was added to the samples and allowed to incubate at room temperature for 45 minutes. The collagen was washed 3 more times with 1 mL of 1xPBS, and imaged with a 10x objective to visualize the phalloidin (actin) and Hoechst (nuclei) in order to assess the myoblast density and

morphology. Myotubes with 3 nuclei or more were counted to assess the total myotube number. To reduce error, 3 representative 10x images per sample were used for the RAGE inhibitor and agonist experiments.

Protein analysis: The collagen was homogenized in NP-40 lysis buffer (BP-119, Boston BioProducts, Ashland, MA, USA) with a protease inhibitor cocktail and 25 mM sodium fluoride with a 6.0 mm zirconium bead in a beadbug homogenizer (BeadBugTM Cat #: 31-212, Genesee Scientific, San Diego, CA, USA) at 4000 rpm for 60 s 5 times. The tubes were kept on ice for at least 5 minutes between runs. The homogenate was centrifuged at 9703 rpm (10,000× g) (Centrifuge 5427 R, Eppendorf, Hamburg, Germany) for 5 min, and the supernatant was used for dot blotting according to the Bio-Rad manufacturer protocol, which uses a 0.45 μM nitrocellulose membrane. Following overnight staining with primary antibodies, the membranes were then incubated with secondary antibodies (926-68073, 926-32210, and 926-32211, LI-COR Biosciences, Lincoln, NE, USA) for 40 min at room temperature, then they were imaged on the LI-COR Odyssey and quantified. Target protein signals were divided by the total protein signal, and included RAGE, phospho p38, phospho JNK, phospho Nf-kB, phospho Erk1/2, Myf5, MyoG, MyHC, integrins β1, β3, α2, α7, and αV.

Statistical Analysis: Each variable was tested using n = 6 unless otherwise specified. Data are presented as mean ± SEM with the analysis done using GraphPad Prism 6.0 (GraphPad, La Jolla, CA, USA). Outliers were removed according to Grubb's test (α-0.05). Analysis comparing only two groups was performed by unpaired Student's t-test (one-paired or two-paired), whereas analysis comparing more than two groups using one-way analysis of variance with Tukey's posthoc test. All p values < 0.05 were considered significant.

Results

AGEs were created on collagen in a dose-dependent manner, with 250 mM producing significantly more AGEs than all other doses (Figure 17A). Concomitantly, soluble hydroxyproline decreased in a dose-dependent manner, with doses 40 mM and above reduced compared to 0 and 25 mM (Figure 17B). Further, 250 mM was reduced compared to 40 mM. We verified that hydroxyproline normalized AGE levels accurately by demonstrating that AGE-collagen digested with collagenase 1A (less specific to collagen) and collagenase 3 (highly specific for collagen) both had similar levels of AGEs per hydroxyproline, despite collagenase 3 releasing more hydroxyproline (Figure 18A-H). AGEs and hydroxyproline were measured using the 250mM concentration over 5 days and demonstrated a time-

dependent increase in AGEs per hydroxyproline (Figure 17C). Additionally, soluble hydroxyproline was lowest on day 5 compared to all other days (Figure 17D). We confirmed that no residual D-ribose remained in the collagen after washing with 5 mL of DI water (Figure 19A). Mass spectrometry analysis of the control collagen revealed it was 82.4% collagen type I, with a trace amount of keratin (~8%), collagen III (2%), and Pancreatic trypsin inhibitor (2%) (Figure 20A-B). A sample from each D-ribose dose was selected and imaged by SEM. There were no appreciable differences to the collagen at x350 and the ultrastructure at x20k due to AGE induction (Figure 17E).

Next, we performed an AFM analysis to verify the SEM results. Collagen fibers were visualized in AFM topographical images at all doses, and no qualitative differences were observed (Figure 17F). We performed bulk mechanical testing on 0, 100, and 250 mM collagens. Tensile modulus and ultimate strain were increased at 250 mM compared to 0 mM (Figure 17G,I). Ultimate tensile strength was increased at 250 mM compared to 0 and 100 mM (Figure 17H). Interestingly, the compressive modulus was elevated in both 100 and 250 mM compared to 0 mM (Figure 17J).

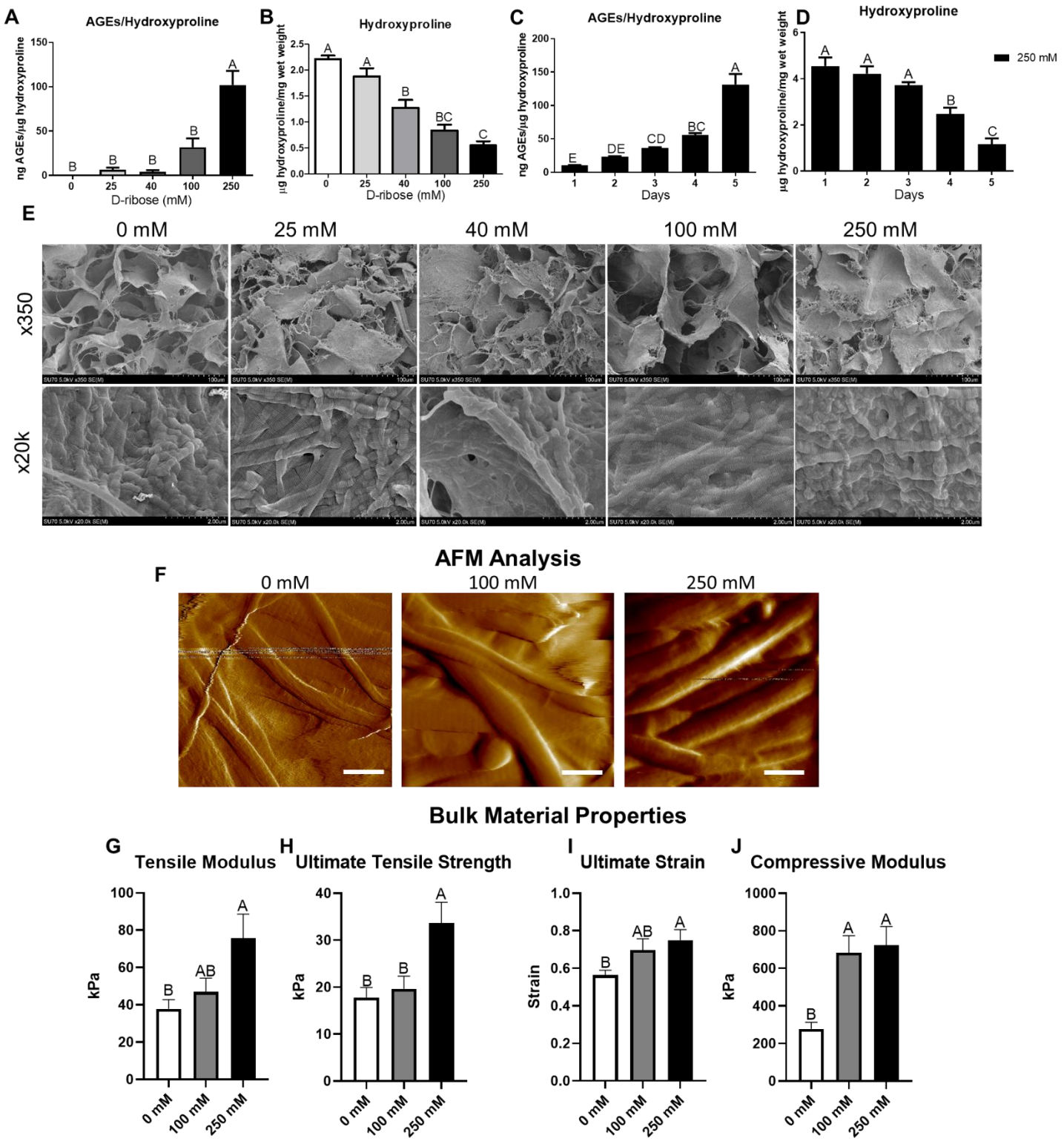

Figure 17. AGE cross-links were successfully induced onto collagen, which resulted in increased mechanical properties. A) AGEs were induced on collagen in a dose-dependent method, and 250 mM formed more AGEs than all other doses. B) Soluble hydroxyproline decreased in a dose dependent

manner. C) 250mM of D-ribose formed AGEs in a time-dependent manner, with highest AGE formation at 5 days. D) Additionally, soluble hydroxyproline was lowest at day 5. E) There were no appreciable differences to the collagen according to SEM at x350 and to the ultrastructure at x20k due to AGE induction. F) Collagen fibers were visualized by AFM and no differences were seen. G-H) Bulk tensile modulus and ultimate strain were increased by 250 mM D-ribose treatment. I) Ultimate tensile strength was higher in 250 mM. J) Bulk compressive modulus was increased in 100 and 250 mM collagen.

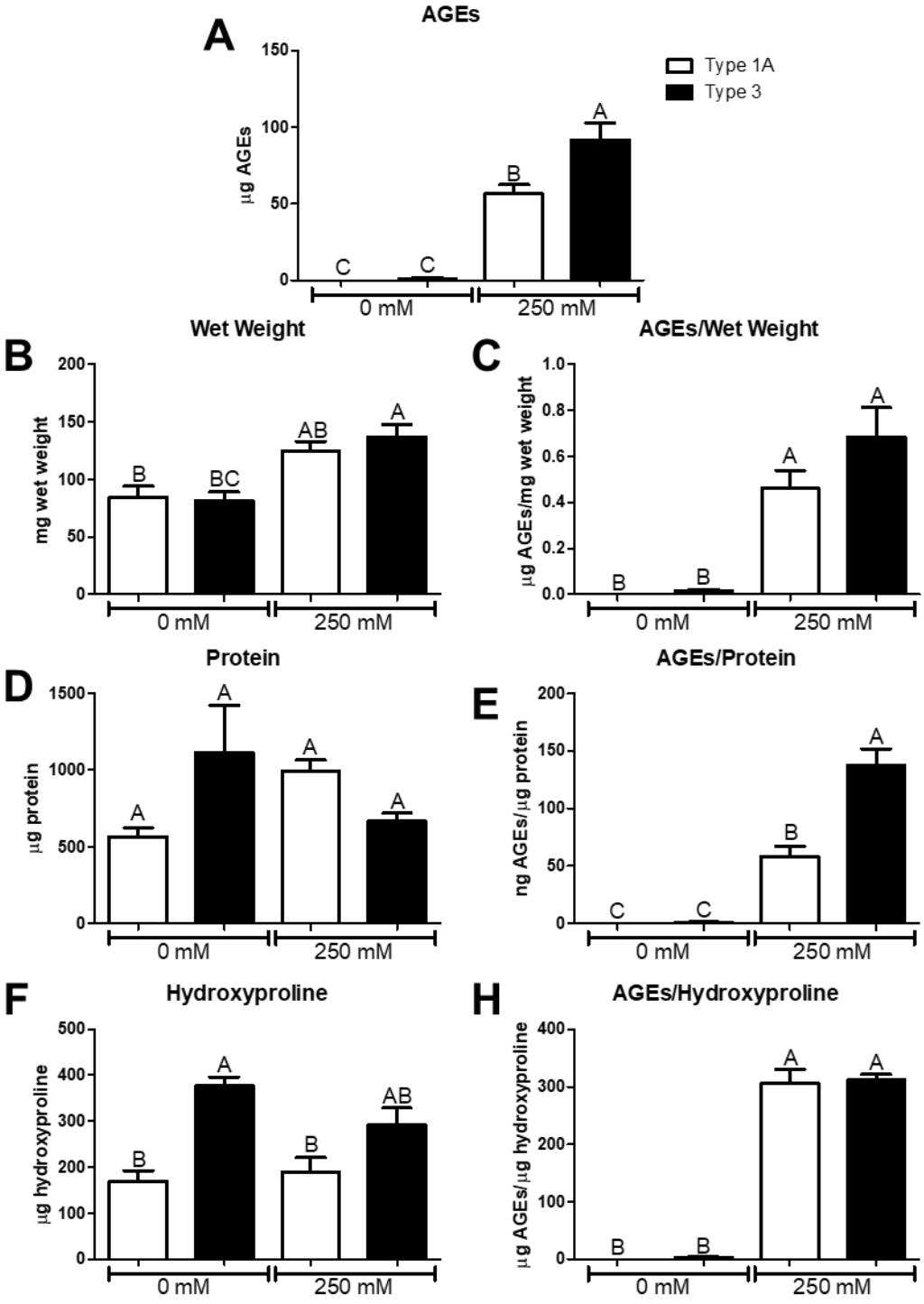

Figure 18: Hydroxyproline performs well for normalizing AGEs despite varying collagenase treatment. A-H) Collagenase 3 extracts more AGEs and hydroxyproline that collagenase 1A, and AGE levels from both extracts correlate with hydroxyproline normalization.

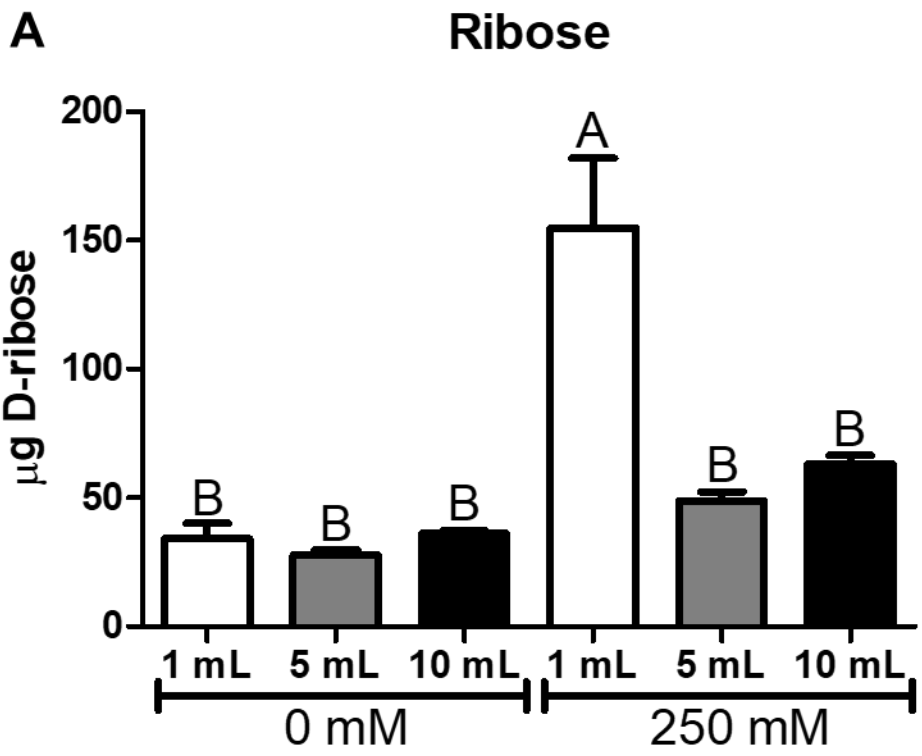

Figure 19: Washing with 5 mL of DI H20 removes residual D-ribose from AGE-collagen.

A

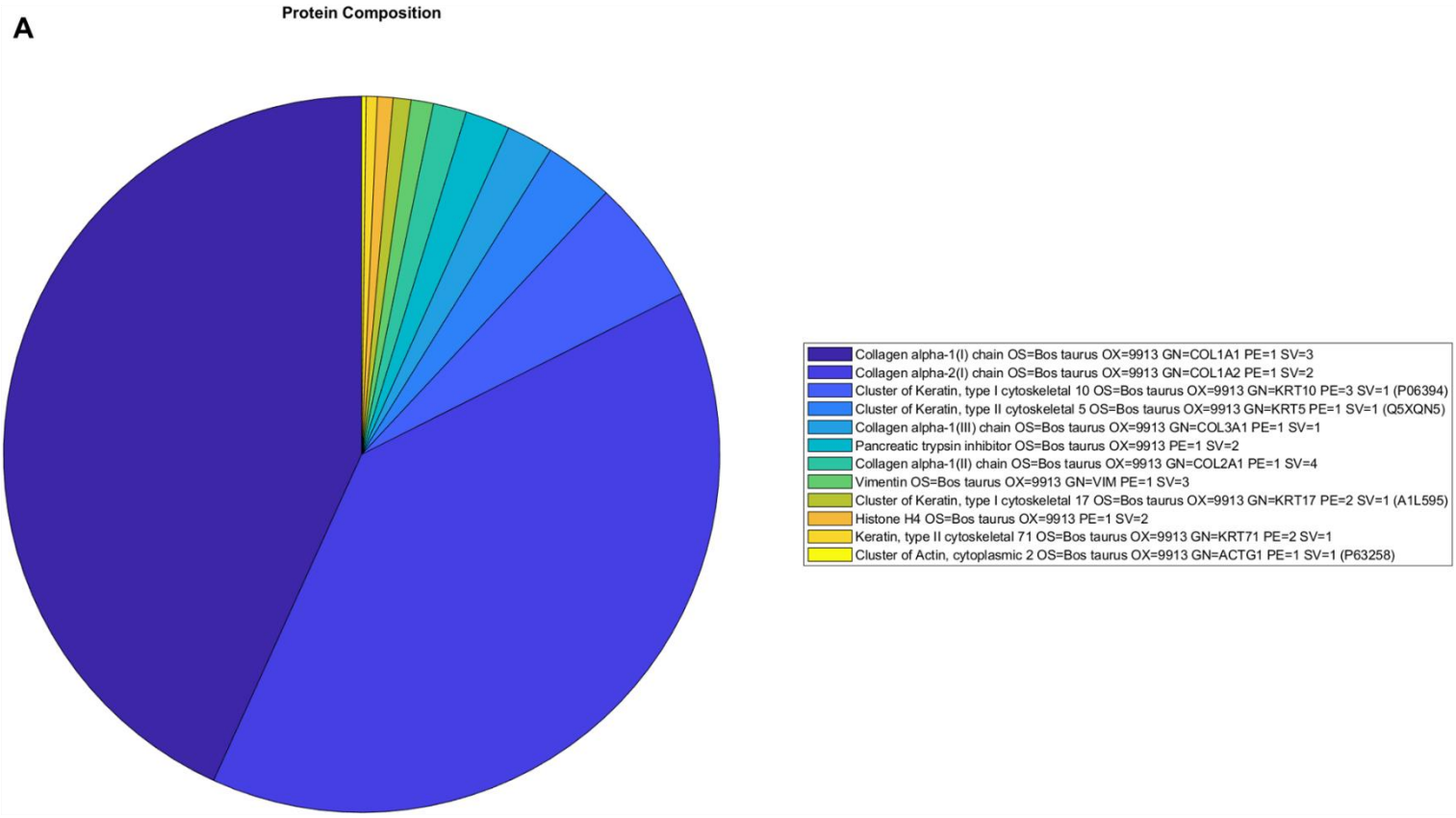

B

Protein	Percentage
Collagen alpha-1(I) chain OS=Bos taurus OX=9913 GN=COL1A1 PE=1 SV=3	43.2161
Collagen alpha-2(I) chain OS=Bos taurus OX=9913 GN=COL1A2 PE=1 SV=2	39.1960
Cluster of Keratin, type I cytoskeletal 10 OS=Bos taurus OX=9913 GN=KRT10 PE=3 SV=1 (P06394)	5.6281
Cluster of Keratin, type II cytoskeletal 5 OS=Bos taurus OX=9913 GN=KRT5 PE=1 SV=1 (Q5XQN5)	3.1156
Collagen alpha-1(III) chain OS=Bos taurus OX=9913 GN=COL3A1 PE=1 SV=1	2.1106
Pancreatic trypsin inhibitor OS=Bos taurus OX=9913 PE=1 SV=2	2.0101
Collagen alpha-1(II) chain OS=Bos taurus OX=9913 GN=COL2A1 PE=1 SV=4	1.5075
Vimentin OS=Bos taurus OX=9913 GN=VIM PE=1 SV=3	1.0050
Cluster of Keratin, type I cytoskeletal 17 OS=Bos taurus OX=9913 GN=KRT17 PE=2 SV=1 (A1L595)	0.8040
Histone H4 OS=Bos taurus OX=9913 PE=1 SV=2	0.7035
Keratin, type II cytoskeletal 71 OS=Bos taurus OX=9913 GN=KRT71 PE=2 SV=1	0.5025
Cluster of Actin, cytoplasmic 2 OS=Bos taurus OX=9913 GN=ACTG1 PE=1 SV=1 (P63258)	0.2010

Figure 20: Mass spectrometry confirms purity of collagen type 1 scaffold. A-B) Mass spectrometry analysis on collagen reveals high levels of collagen, with trace amounts of keratin and pancreatic trypsin inhibitor.

After characterizing the AGE-collagen scaffolds, we cultured C2C12s and human primary myoblasts on them to test the effect of AGEs on myoblast proliferation, differentiation, and fusion. C2C12s grown

on AGE-collagen resulted in dose-dependent increases in DNA, especially on day 6 (Figure 21A). Curiously, DNA for human primary myoblasts did not increase at any time point, indicating that this effect may be cell line dependent (Figure 21B). When C2C12s were stained and imaged for actin and DNA on day 6, we noted increased nuclear and cellular density at 250 mM compared to 0 mM (Figure 21C).

C2C12s were then grown in differentiation conditions for 12 days to induce myotube formation on the collagen scaffolds. Cells were imaged by staining for actin and DNA at days 6 and 12. AGEs blunted myotube formation on day 12 (Figure 22A-B). When quantified, the 250 mM group demonstrated reduced myotube formation at day 12 (Figure 22C). Next, we measured myogenic differentiation markers Myf5, MyoG, and MyHC. All differentiation markers were significantly reduced by AGEs at day 12, however, MyoG was only reduced by 250 mM collagen scaffolds (Figure 22D-F). On day 6, Myf5 was reduced by 100 mM scaffolds, but not by 250 mM. MyoG was suppressed by AGEs at day 6 by both 100 and 250 mM collagen scaffolds. Curiously, MyHC was increased in the 250 mM group on day 6, but myotube numbers demonstrated that these values did not correlate fully with fiber formation. To determine if AGEs were regulating the integrin profile, we measured integrins α2, α7, αV, β1, and β3. AGEs suppressed integrin levels at day 12 in all integrins measured, however, integrin α7 was only suppressed at 250 mM (Figure 22G-K). Interestingly, integrin α7 was reduced by AGEs at day 6, and integrin β1 showed an inverted bi-phasic response to AGEs at day 6.

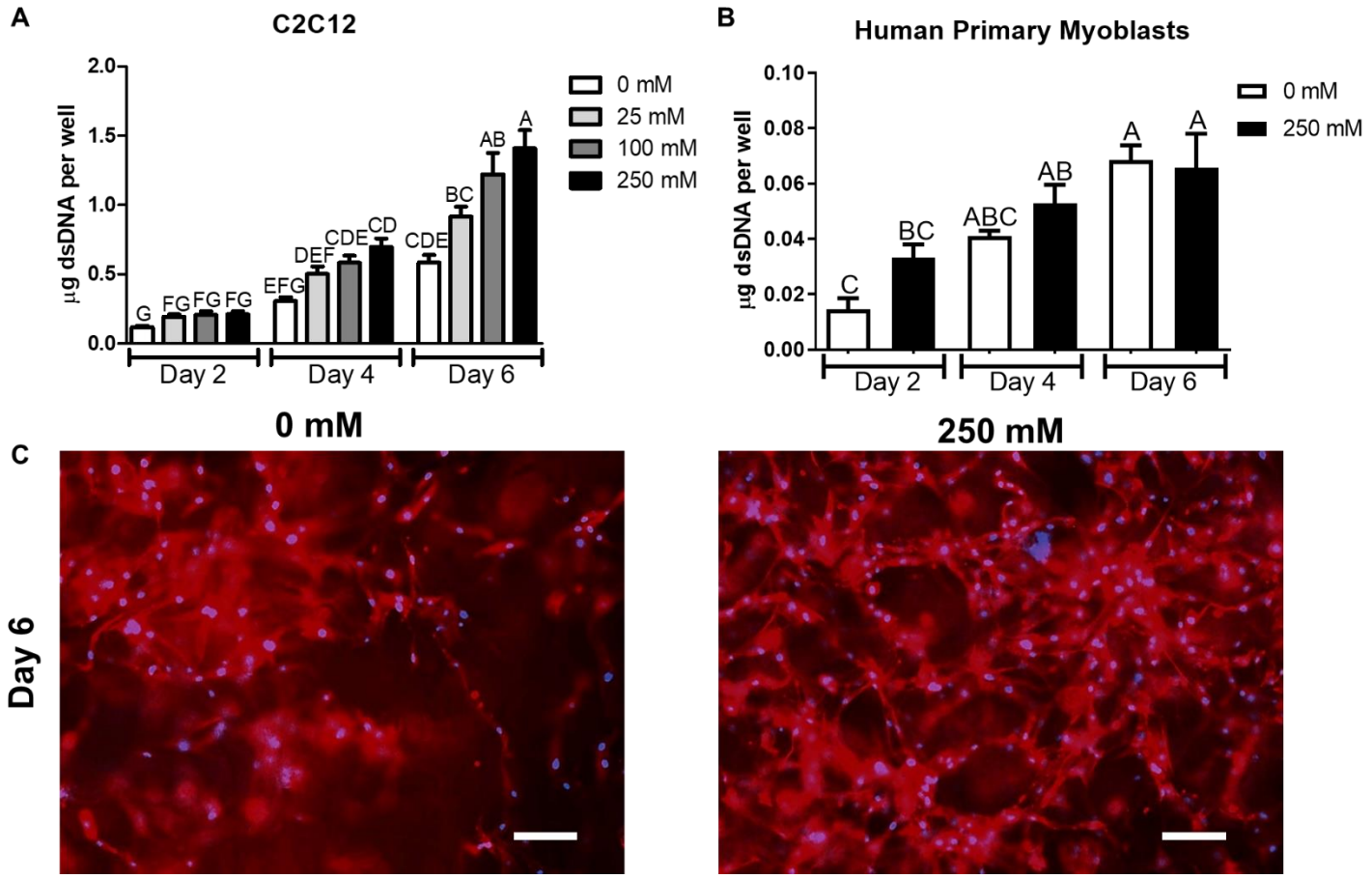

Figure 21. AGE cross-links promote proliferation in C2C12 myoblasts. A) C2C12s show dose dependent increases in DNA based on D-ribose treatment. B) Human primary myoblasts did not increase in DNA. C) C2C12s present increased nuclear and cellular density at day 6 on 250 mM D-ribose treated collagen compared to 0 mM (scale bar is 100 µm).

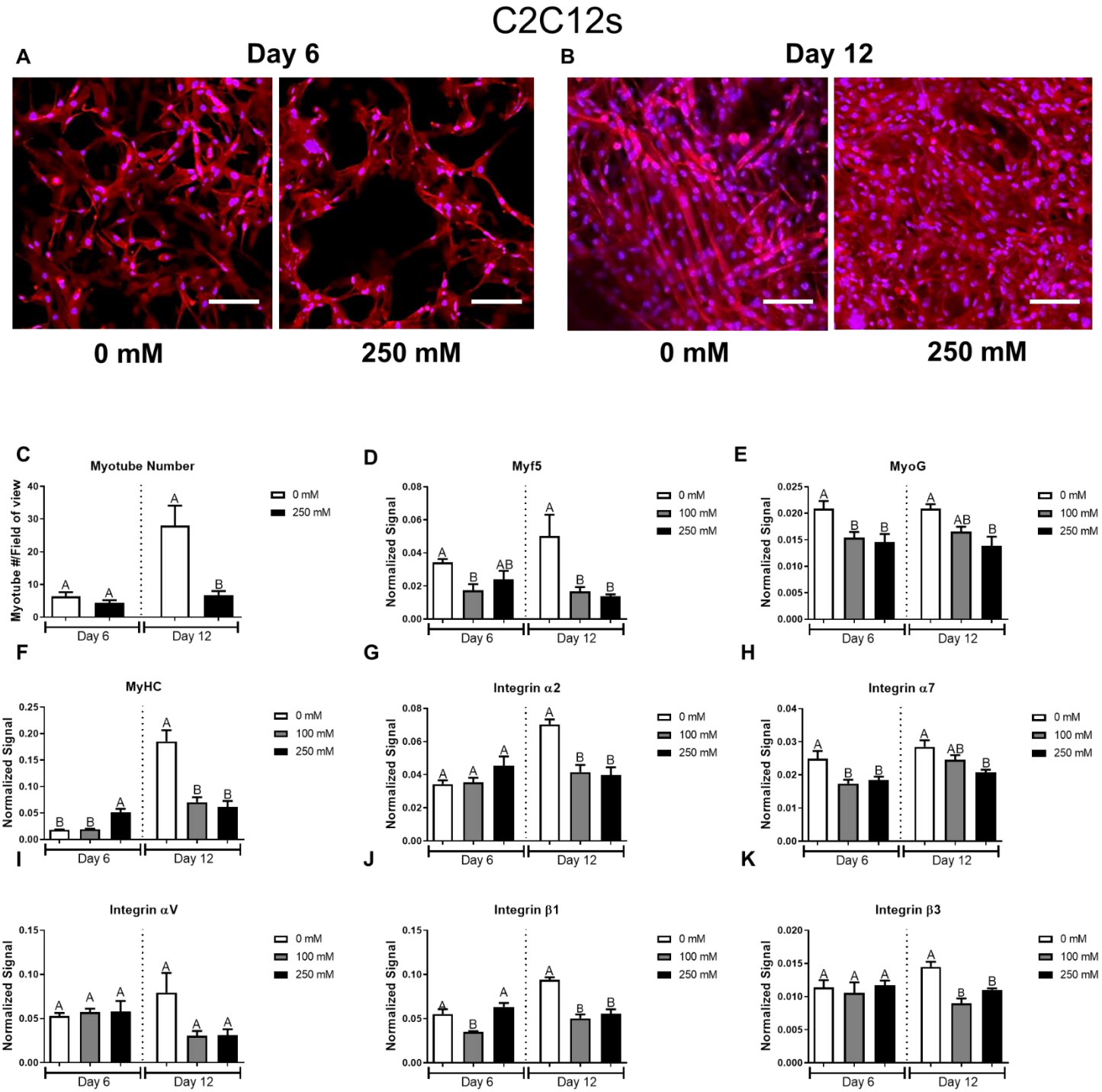

Figure 22. AGEs cause differentiation and fusion deficits in C2C12 myoblasts, and this is associated with integrin signaling. A-B) C2C12s increased in density from day 6-12 and AGEs prevented normal fusion (scale bar=100 μm). C) Quantification revealed lower myotube number due to AGEs at day 12. D-F) AGEs reduced the myogenic differentiation factors Myf5, MyoG, and MyHC at day 12, however MyoG was only reduced by 250 mM scaffolds. (Figure 22D-F). G-K) We measured integrins α2, α7,

αV, β1, and β3. AGEs reduced integrin levels at day 12 in all integrins, but integrin α7 was only affected at 250 mM.

To confirm that the C2C12 data was a real effect and not cell-line specific, we cultured human primary myoblasts on the 250 mM AGE-collagen scaffolds for 12 days. We observed slower growth on 0 and 250 mM collagen scaffolds compared to C2C12s and this was shown in our stained samples. We also used actin and DNA staining to assay myotube formation and determined that AGEs disrupted myotube formation on day 12 (Figure 23A-C). All differentiation markers (Myf5, MyoG, and MyHC) were reduced by AGEs at day 12 (Figure 23D-F). Additionally, AGEs reduced Myf5 and MyHC on day 6. While AGEs reduced integrin levels in the entire integrin panel (α2, α7, αV, β1, and β3), integrin α7 was only suppressed at day 6 (Figure 23G-K).

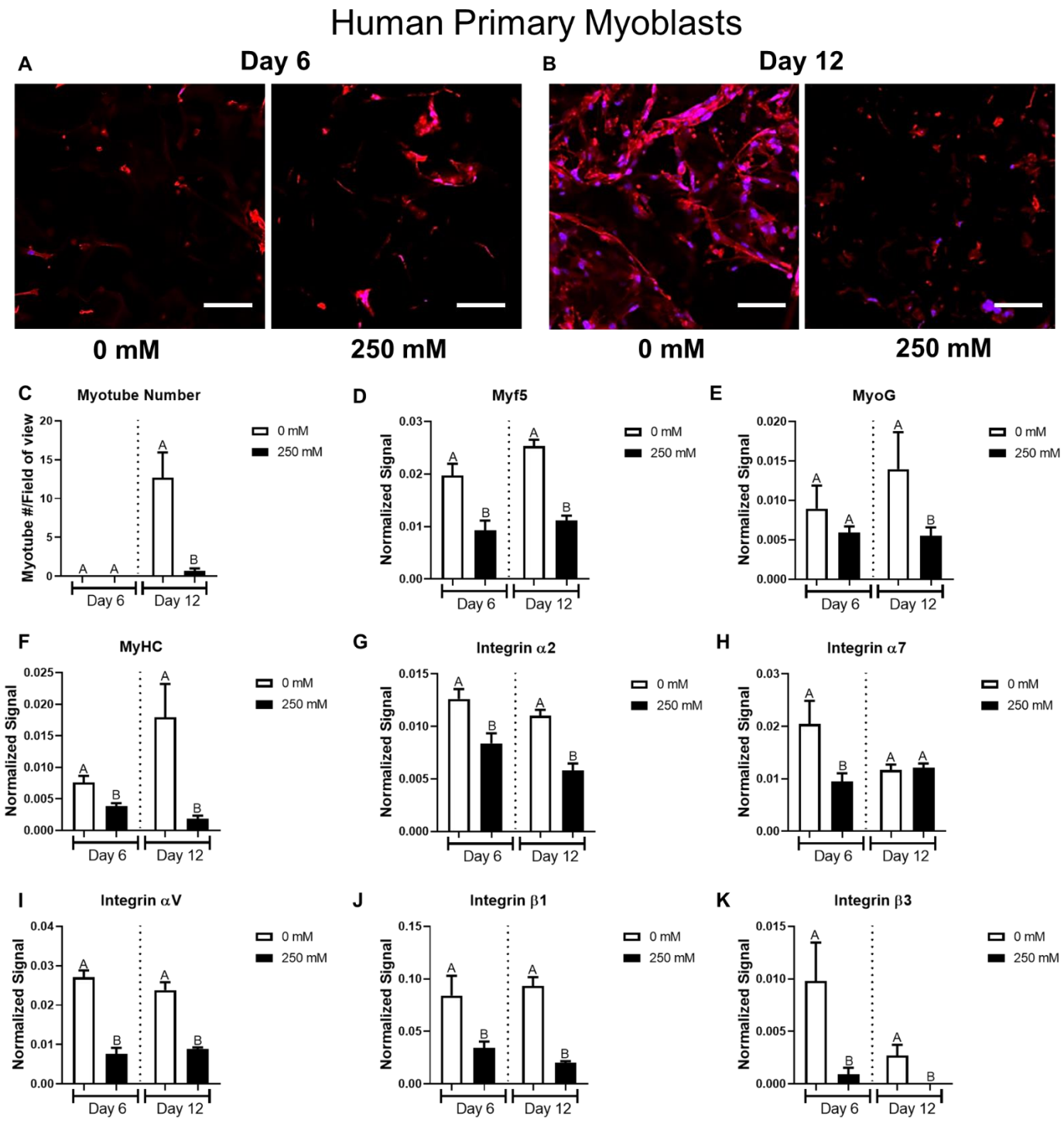

Figure 23. AGEs cause differentiation and fusion deficits in human primary myoblasts, and this is associated with integrin signaling. A-B) Human primary myoblasts increased in density from day 6-12 in the 0 mM group and AGEs prevented normal fusion (scale bar=100 μm). C) Quantification revealed lower myotube number due to AGEs at day 12. D-F) AGEs reduced the myogenic differentiation factors

Myf5, MyoG, and MyHC at day 12. G-K) We measured integrins α2, α7, αV, β1, and β3. AGEs reduced integrin levels at day 12 in all integrins, except for integrin α7.

Next, we investigated the role of RAGE in our system. We measured RAGE levels produced by C2C12s, and surprisingly RAGE was reduced by AGEs at day 12 and was unchanged at day 6 (Figure 24A). This effect was also observed in human primary myoblasts (Figure 24B). The RAGE pathway members Nf-κB, JNK, Erk1/2, and P38 were investigated. Phospho Nf-κB was unaffected by AGEs in C2C12s, but it was reduced by AGEs in human primary myoblasts at day 6 (Figure 24C-D). Phospho JNK was not altered by AGEs in C2C12s or human primary myoblasts (Figure 24E-F). Phospho Erk1/2 produced by C2C12s was not different in the presence of AGEs; however, AGEs reduced Erk1/2 at day 12 in human primary myoblasts (Figure 24G-H). Phospho P38 was the only factor to mirror RAGE in C2C12s, with reduced levels in the 250 mM group at day 12 (Figure 24I). However, AGEs did not change Phospho P38 in human primary myoblasts (Figure 24J).

To understand why RAGE was reduced in late differentiation, we challenged C2C12 myoblasts with FPS-ZM1, Azeliragon, and S100b throughout the culturing process. Aberrant proliferation was successfully recovered by 20 μM FPS-ZM1 and 1 μM Azeliragon, while S100b did not have an effect (Figure 25A-C). Both FPS-ZM1 and Azeliragon suppressed myotube formation at medium and high doses (Figure 25D-G). Impressively, the RAGE agonist S100b restored myotube formation on AGE-collagen to control levels at 10 nM (Figure 25H-I).

We probed for RAGE, the early differentiation factor Myf5, and the late differentiation factor MyoG in C2C12s treated with the RAGE inhibitors and agonist. FPS-ZM1 reduced RAGE production to a similar level as produced by myoblasts grown on AGE scaffolds, and Azeliragon did not have an effect on RAGE amount (Figure 26A, Figure 27A). Surprisingly, S100b reduced RAGE levels in the control group down to the level produced by myoblasts grown on AGE scaffolds (Figure 26B). In control and AGE scaffolds, Myf5 was reduced by FPS-ZM1 at the highest concentration (20μM) to levels that were similar between control and AGE scaffolds (Figure 26C), while Azeliragon had no effect (Figure 27B). S100b treatment recovered Myf5 levels in myoblasts grown on AGE scaffolds to levels that were similar to the control group at 1 nM and 10 nM (Figure 26D). FPS-ZM1 reduced MyoG in myoblasts cultured on control and AGE scaffolds that resulted in similar levels between control and AGE groups at a 20 μM concentration (Figure 26E). MyoG was unaffected by Azeliragon (Figure 27C). Interestingly, S100b reduced MyoG at a 10 nM concentration in myoblast grown on control scaffolds compared to 0 and 1 nM. Moreover, MyoG protein remained unchanged in myoblasts cultured on AGE scaffolds.

Consequently, this resulted in similar levels between control and AGE groups at 10 nM concentrations (Figure 26F).

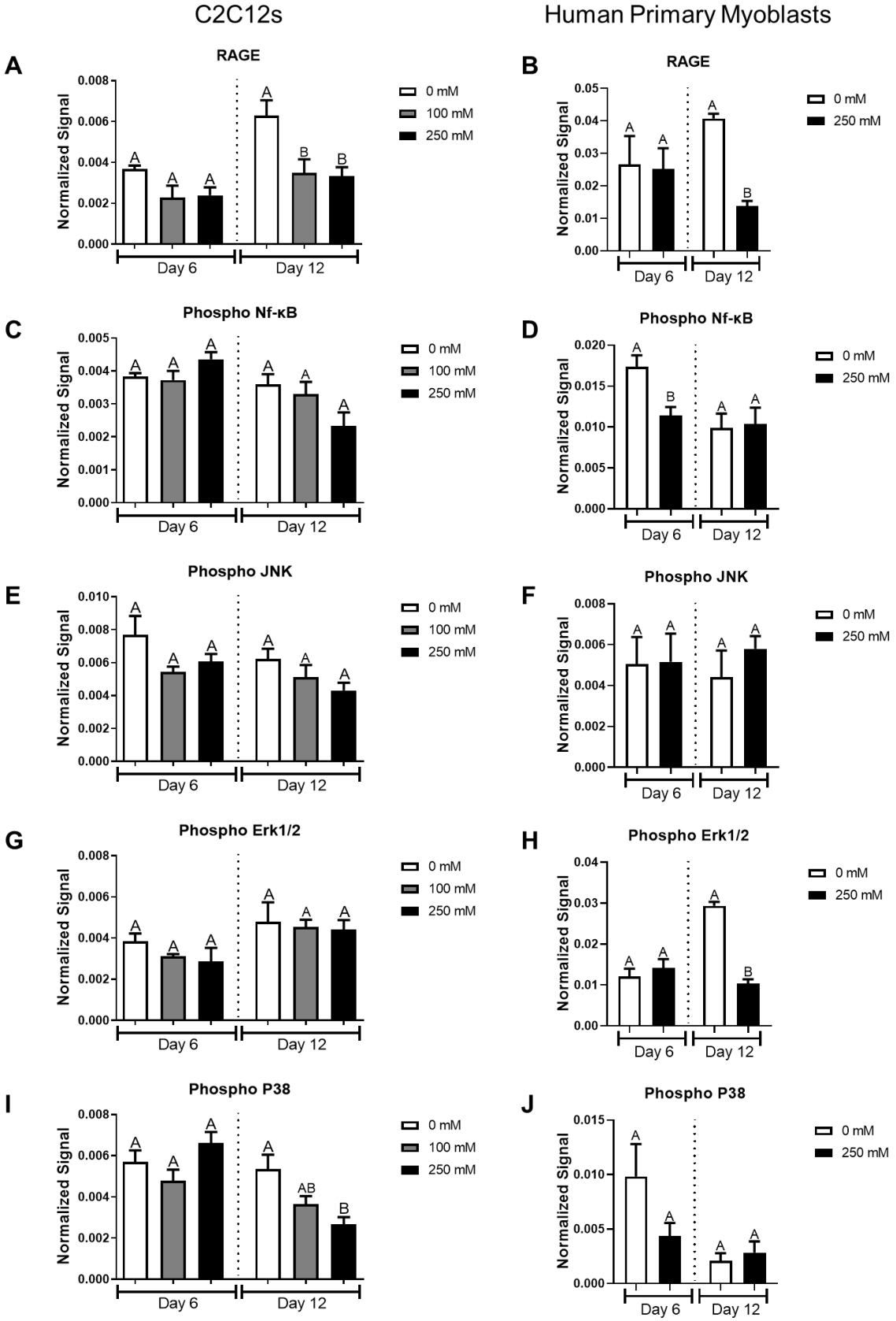
C2C12s
Human Primary Myoblasts
A
RAGE
Normalized Signal
0 mM
100 mM
250 mM
Day 6
Day 12
B
RAGE
C
Phospho Nf-κB
D
Phospho Nf-κB
E
Phospho JNK
F
Phospho JNK
G
Phospho Erk1/2
H
Phospho Erk1/2
I
Phospho P38
J
Phospho P38

Figure 24. AGEs suppress RAGE in chronic cell culture conditions. A-B) AGE cross-links reduce RAGE at day 12 in C2C12s and human primary myoblasts. C-D) The RAGE pathway was investigated. Phospho Nf-κB was unaltered by AGEs in C2C12s, but AGEs reduced it in human primary myoblasts at day 6. E-F) Phospho JNK was not affected by AGEs in C2C12s or human primary myoblasts. G-H) Phospho Erk1/2 in C2C12s did not change due to AGEs. AGEs reduced Erk1/2 in human primary myoblasts at day 12. I-J) Phospho P38 was reduced by 250 mM scaffolds in C2C12s at day 12. AGEs did not alter Phospho P38 in human primary myoblasts.

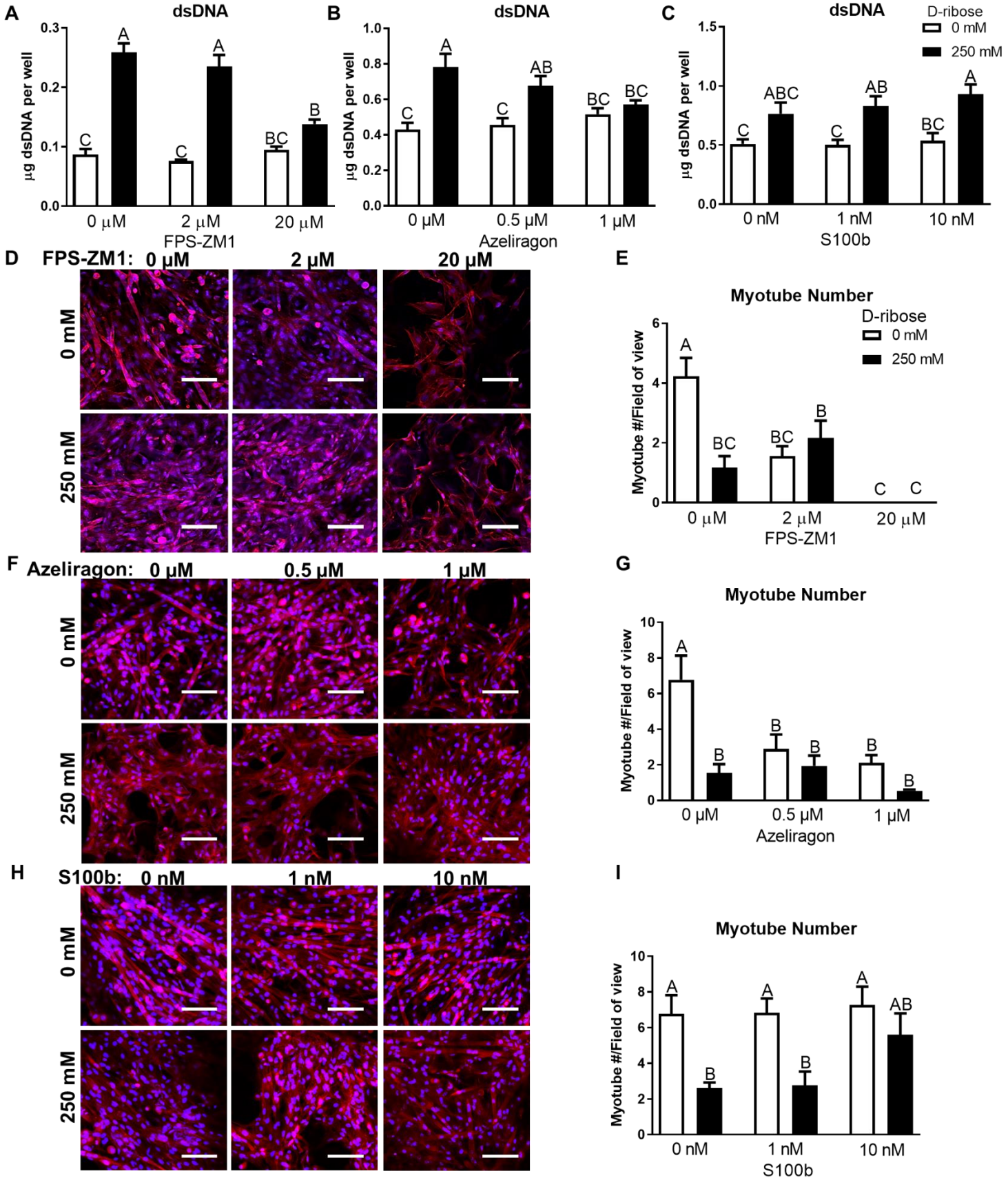
A
dsDNA
μg dsDNA per well
0 μM
2 μM
20 μM
FPS-ZM1
B
dsDNA
0 μM
0.5 μM
1 μM
Azeliragon
C
dsDNA
D-ribose
0 mM
250 mM
0 nM
1 nM
10 nM
S100b
D FPS-ZM1: 0 μM 2 μM 20 μM
0 mM
250 mM
E
Myotube Number
Myotube #/Field of view
F Azeliragon: 0 μM 0.5 μM 1 μM
G
Myotube Number
H S100b: 0 nM 1 nM 10 nM
I
Myotube Number

Figure 25. RAGE agonists reduced myoblastic proliferation and fusion, while RAGE agonist S100b restored myotube formation on AGE-collagen. A-C) Excess proliferation was ameliorated by 20 μM FPS-ZM1 and 1 μM Azeliragon, but S100b did not have an effect. D-G) FPS-ZM1 and Azeliragon prevented myotube formation at middle and high doses. H-I) S100b recovered myotube formation on AGE-collagen at 10 nM. Scale bar=100 μm.

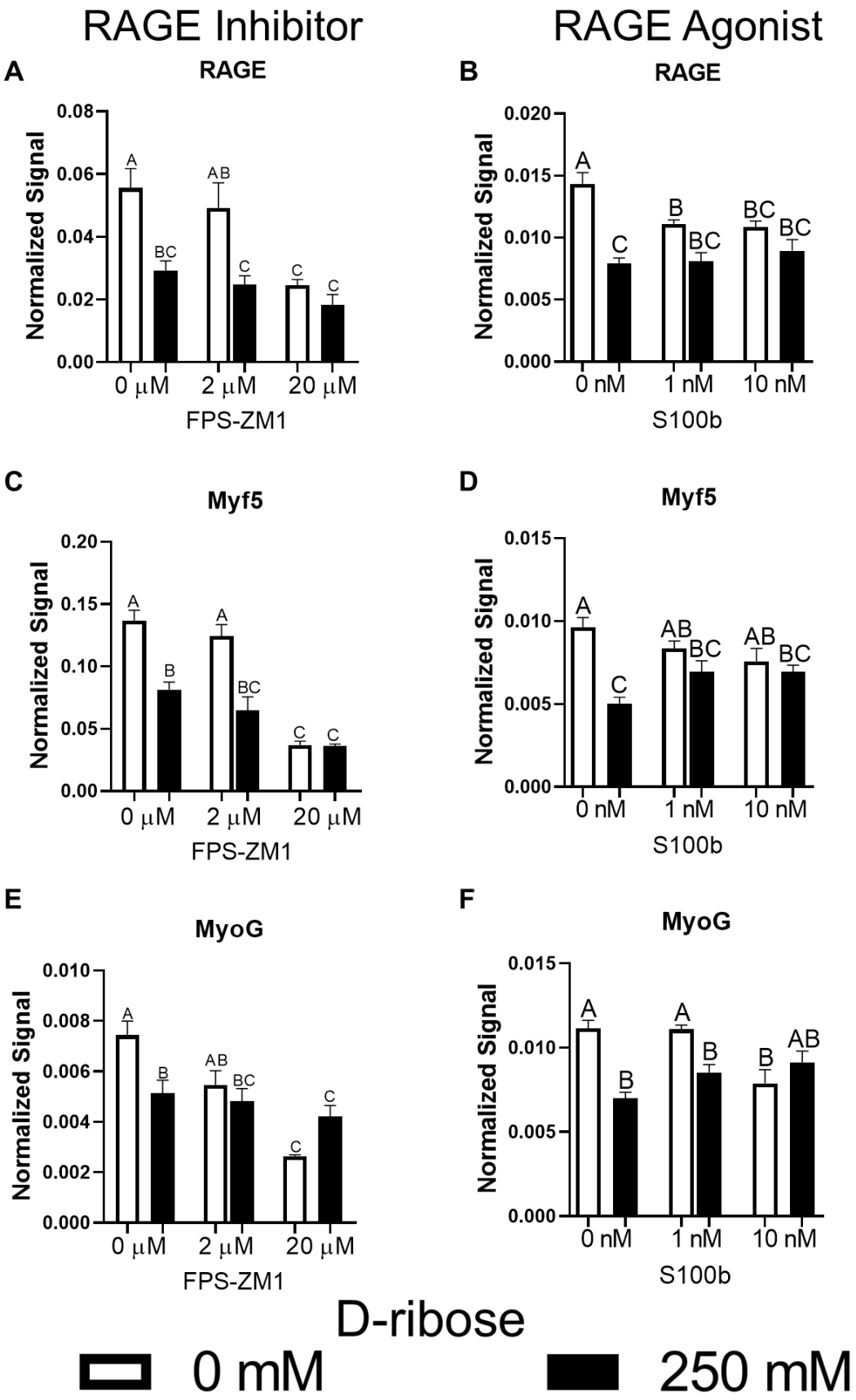
RAGE Inhibitor
RAGE Agonist
A
RAGE
Normalized Signal
0.08
0.06
0.04
0.02
0.00
A
BC
AB
C
C
C
0 μM
2 μM
20 μM
FPS-ZM1
B
RAGE
Normalized Signal
0.020
0.015
0.010
0.005
0.000
A
C
B
BC
BC
BC
0 nM
1 nM
10 nM
S100b
C
Myf5
Normalized Signal
0.20
0.15
0.10
0.05
0.00
A
B
A
BC
C
C
0 μM
2 μM
20 μM
FPS-ZM1
D
Myf5
Normalized Signal
0.015
0.010
0.005
0.000
A
C
AB
BC
AB
BC
0 nM
1 nM
10 nM
S100b
E
MyoG
Normalized Signal
0.010
0.008
0.006
0.004
0.002
0.000
A
B
AB
BC
C
C
0 μM
2 μM
20 μM
FPS-ZM1
F
MyoG
Normalized Signal
0.015
0.010
0.005
0.000
A
B
A
B
B
AB
0 nM
1 nM
10 nM
S100b
D-ribose
0 mM
250 mM

Figure 26. The RAGE inhibitor FPS-ZM1 and the RAGE agonist S100b reduced RAGE and differentiation factors, however S100b also elevated Myf5 and MyoG on AGE-collagen. A-B) FPS-ZM1 and RAGE reduce RAGE. C-D) Myf5 was reduced by FPS-ZM1 to AGE levels. S100b treatment slightly decreased Myf5 levels in the control group while slightly increasing levels in the AGE group, resulting in no significant difference. E-F) FPS-ZM1 reduced MyoG to AGE levels. Curiously, S100b lowered MyoG to AGE-collagen levels while elevating MyoG on AGE-collagen to control levels.

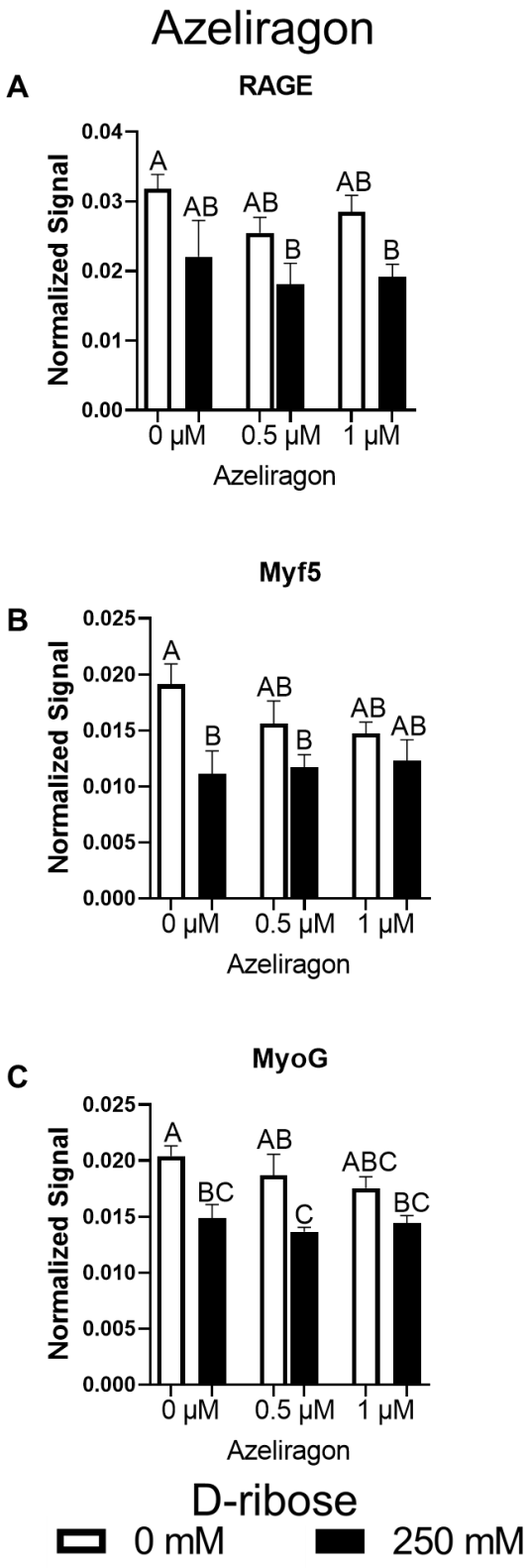

Figure 27: A-C) Azeliragon treatment minorly reduced RAGE, Myf5 and MyoG on control collagen.

Challenges

Culturing myoblasts on a 3D collagen surface for the purposes of measuring proliferation, differentiation, and fusion presented several challenges. First, the myoblasts grew much slower on collagen when compared to TCPS (data not shown). As such, we optimized the timepoints and discovered that day 6 was best for measuring proliferation, rather than an earlier timepoint. Next, the myoblasts presented increased apoptosis in classic differentiation conditions (serum starvation). We hypothesized that the slower growth rate did not allow the myoblasts to reach the appropriate confluence before differentiation induction. To circumvent this, we employed full media conditions and relied on myoblast contact to initiate differentiation. Further, as a result the process was prolonged, and we had to measure fusion at day 12, rather than day 6.

Discussion

We successfully created a three-dimensional *in vitro* model of AGE cross-linked collagen and used this to demonstrate that myoblasts were sensitive to AGE cross-links. As far as we know, we are the first to demonstrate that insoluble AGEs exert an aging phenotype onto myoblasts. All other reports on the impact of AGEs on myoblasts were performed with a soluble delivery of AGEs in the form of AGE-BSA, methylglyoxal, or other forms.[247–249] Unlike soluble AGEs, which only exert a biological impact through receptor signaling, AGEs cross-linked on collagen mechanically stiffen the microenvironment, which can promote deleterious outcomes.[21] However, it is not clear how myoblasts respond to AGEs cross-linked to collagen. In one scenario, AGEs could act as a ligand that signals through RAGE, or an alternate scenario could be that increased stiffness (non-RAGE pathway) disrupted myoblast signaling. These two potential outcomes prompted our AGE study.

When characterized, our system showed evidence of cross-linking in the presence of increased AGEs. An increase in insoluble hydroxyproline and stronger mechanics in the presence of AGEs coupled with the absence of ultrastructural changes indicates that our collagen system was laden with AGE cross-links independent of other age-dependent collagen alterations.[25] *In vivo*, collagen aging involves increases in total amount, geometric randomness, and cross-linking.[238] All three of these age-dependent collagen alterations impact collagen's function and mechanics. Here, we isolated collagen cross-linking with AGEs by keeping the collagen amount and orientation identical.

Impressively, AGE cross-linked collagen supported C2C12 proliferation (i.e., DNA levels) at 2-3 times the level of control collagen. While stiffer microenvironments promote myoblast proliferation, AGEs

disrupt proliferation by promoting apoptotic pathways,[247,250] producing a unique dichotomy that our study aimed to elucidate. To determine if mechanics were the sole reason for increased proliferation, we treated C2C12s with RAGE inhibitors (FPS-ZM1 and Azeliragon) and a RAGE agonist (S100b). FPS-ZM1 allosterically blocks RAGE by binding to the V domain of the receptor.[251] While the exact antagonistic mechanism of Azeliragon is unclear, it was also shown to block RAGE-ligand binding and has undergone human clinical trials.[252] Both of the RAGE inhibitors reduced proliferation back to control levels, indicating that AGE-RAGE signaling is important for this effect. The RAGE ligand, S100b did not affect proliferation, indicating that AGEs promote proliferation through a ligand-specific RAGE pathway.

In order to study differentiation, we cultured myoblasts in full media conditions and relied on myoblast contact to promote differentiation and fusion. The 3D microenvironment of the collagen significantly slowed proliferation, and this combined with the lack of optical visibility made it difficult to optimize our system.[253] Once we determined optimal conditions on days 6 and 12 (unreported data), we investigated early and late differentiation/fusion thereafter. AGEs decidedly suppressed myotube formation, and this result was true across cell types. Additionally, early and late differentiation markers were reduced by AGEs. The full-scale suppression of myogenic differentiation by stiff microenvironments has been well-characterized, and interestingly soluble AGE delivery produced a similar effect.[17,146,225,247–249,254,255] Our system is the first to investigate this duality that more accurately represents *in vivo* collagen aging in skeletal muscle.

Integrin signaling is essential for myogenic differentiation and is necessary for late differentiation.[256] Additionally, integrin αvβ3 levels were highly expressed in early differentiation but were downregulated in late differentiation.[257] In cases where integrin αvβ3 was reduced to low levels, differentiation was blunted.[257] Integrin α2β1 is known to bind to collagen, and while it is not normally a major integrin player for myoblasts, we investigated it since the myoblasts were grown on collagen.[258] Integrin β1 is known to be a promiscuous integrin subunit, and in skeletal muscle, it dimerizes with α1, α3, α4, α5, α6, α7, α9, and αv.[259] Satellite cells expressed integrin β1, and its presence was proven to be essential to maintaining the satellite cell niche.[218] Further, restoring β1 signaling ameliorated myogenic deficits in aged muscle. In our system, all integrins were downregulated in C2C12s with AGEs at day 12.[218] In human primary myoblasts, this held true except for integrin α7, which was only reduced at day 6. There are several consequences to these results. First, reductions in integrin α2β1 indicated that the myoblasts were losing sensitivity to the collagen surface in the presence of AGEs, which could be caused by physical blockage of cell attachment sites on collagen.[260] Additionally, the broad reduction

of multiple integrins indicated that the myoblasts may have been desensitized to the increased mechanical stiffness caused by AGEs in addition to reducing myogenic differentiation.

While our integrin panel revealed insights into how mechanics may be modulating the myoblasts, we also investigated the role that the AGE-RAGE axis played in our system. Surprisingly, RAGE levels were reduced by AGEs at day 12 in both C2C12s and human primary myoblasts, and AGEs did not alter RAGE at day 6. We are the first to report that, contrary to dogma, AGEs cross-linked on collagen reduced RAGE in myoblasts in a chronic culturing set-up. Interestingly, there is one report of soluble AGE delivery to myoblasts where RAGE mRNA was reduced, albeit not significantly.[247] All other reports, that we are aware of, demonstrated that AGE delivery increased RAGE levels in myoblasts.[22,146] Only phospho-P38 in C2C12s and phospho-Erk1/2 in human primary myoblasts mirrored the reduction in RAGE at day 12, which could have been due to the chronic AGE exposure in our system. All the RAGE pathway members investigated are known to play broad, important roles in many pathways related to cell cycle and differentiation, and this may have created additional noise in our measurements.[261–266]

To test whether AGEs acted as ligands to bind RAGE, we used the RAGE inhibitors FPS-ZM1 and Azeliragon to better understand if RAGE signaling played a key role in our system.[267,268] Despite reductions in RAGE protein levels, it is possible that pronounced receptor signaling was still functioning. Surprisingly, treatment with both RAGE inhibitors was able to suppress myotube formation, even at lower doses. Further, FPS-ZM1 reduced RAGE, Myf5, and MyoG to AGE levels at 20 μM. Azeliragon exerted a more modest effect on protein levels, but the data supported the idea that RAGE signaling plays an important role in myogenesis, and this has been reported elsewhere.[22–24] Since inhibiting RAGE mimicked the AGE effect on myoblasts, we hypothesized that RAGE stimulation would recover myoblasts on AGE-collagen. We treated C2C12s with S100b, a RAGE ligand, and demonstrated that myotube formation increased back to control levels at the 10 nM dose. Additionally, S100b recovered the myogenic differentiation factors Myf5 and MyoG back to control levels at 10 nM concentrations.

It was previously reported that when S100b binds RAGE in low-density myoblasts, proliferation was stimulated via Erk1/2 and myogenic differentiation was promoted via P38 MAPK.[24] However, when S100b was delivered to high-density myoblasts, which occurred during chronic S100b treatment, proliferation was stimulated while differentiation was inhibited because S100b blocked RAGE and engaged basic fibroblast growth factor (bFGF) receptor 1 (FGFR1) signaling.[24] This dual S100b effect provides a possible explanation for our data. We saw deficits in both Erk1/2 and P38 signaling caused

by AGEs, and since S100b is known to promote pro-myogenic RAGE-dependent signaling through these pathways, that could explain why myotube formation increased. Conversely, since the controls did not experience these deficits, S100b may have blocked RAGE and engaged bFGF/FGFR1 signaling, causing the slight deficits in RAGE and myogenic differentiation observed in our system.

Altogether, our results indicated that our collagen scaffolds rich in AGE cross-links pathologically promoted myoblast proliferation in a RAGE-dependent manner while disrupting myoblast differentiation and fusion via RAGE. Impressively, while mechanically stiffer substrates, like our AGE-collagen, are known to promote myoblast proliferation while suppressing differentiation, our data suggested that RAGE could change myoblast sensitivity to substrate stiffness.

Conclusions

We developed a novel aging-relevant 3D glycated collagen system to investigate how mechanics and the AGE-RAGE axis exert an aging phenotype on skeletal muscle progenitor cells. AGE cross-linked collagen promoted myoblast proliferation while disrupting myoblast differentiation and fusion. When challenged with RAGE inhibitors, excess proliferation by AGEs was prevented, but differentiation was also suppressed. Interestingly, AGEs lowered RAGE levels in late differentiation and treatment with the RAGE agonist S100b restored fusion deficits. Our data provide novel insights into the role of the AGE-RAGE axis in skeletal muscle aging, and future study into S100b as a skeletal muscle regenerative treatment in an aging context is warranted.

Chapter 5. Human adipose-derived stromal cells delivered on decellularized muscle improve muscle regeneration and regulate RAGE and P38 MAPK

Abstract

Our goal in this chapter was to determine if AGEs were produced in response to muscle trauma, and if they would impede commonly used cell delivery methods. This information is valuable considering the difficulties associated with tissue regeneration in severe laceration or blast injuries that remove bulk muscle. Volumetric muscle loss (VML) is the acute loss of muscle mass due to trauma. Such injuries occur primarily in the extremities and are debilitating, as there is no clinical treatment to restore muscle function. Pro-inflammatory advanced glycation end-products (AGEs) and the soluble receptor for advanced glycation end-products (RAGE) are known to increase in acute trauma patient's serum and are correlated with increased injury severity. However, it is unclear whether AGEs and RAGE increase in muscle post-trauma. To test this, we used decellularized muscle matrix (DMM), a pro-myogenic, non-immunogenic extracellular matrix biomaterial derived from skeletal muscle. We delivered adipose-derived stromal cells (ASCs) and primary myoblasts to support myogenesis and immunomodulation (N=8 rats/group). DMM non-seeded and seeded grafts were compared to empty defect and sham controls. 56 days after surgery muscle force was assessed, histology characterized, and protein levels for AGEs, RAGE, p38 MAPK, and myosin heavy chains were measured. Overall, our data showed improved muscle regeneration in ASC-treated injury sites and a regulation of RAGE and p38 MAPK signaling, while myoblast-treated injuries resulted in minor improvements. Taken together, these results suggested that ASCs combined with DMM provides a pro-myogenic microenvironment with immunomodulatory capabilities and indicates further exploration of RAGE signaling in VML.

Introduction

Skeletal muscle makes up 40% of the body by mass, and is a highly regenerative tissue due to its reservoir of muscle satellite stem cells (MuSCs). Extremity trauma, such as the type incurred during warfare, car accidents, tumor resection, and other blunt trauma can result in volumetric muscle loss (VML) injury. In VML injuries, the MuSC pool is depleted through the loss of muscle volume, infringing on muscle's inherent regenerative capacity.[269,270] In addition, extracellular matrix (ECM) accounts for ~10% of the skeletal muscle mass and coats muscle fibers and MuSCs.[271] Loss of the ECM eliminates

a key element in muscle regeneration. Indeed, when the ECM is present following injury, muscle's regenerative capacity remains intact.[272,273] A strategy to overcome a loss of both the MuSC pool and the ECM is to implant a muscle-derived ECM seeded with muscle-derived stem cells.[274] Our lab has previously established a method to decellularize skeletal muscle, removing the cellular components that would induce an aberrant immune response, and using this as a platform for new cell ingrowth in the injury area.[180,184] Other research groups have also explored the use of decellularized tissues in VML injuries and most have determined that decellularized matrices result in functional fibrosis and not in regeneration, owing a lack luster regeneration to an inability to support MuSC pool expansion.[275–277] However, our research showed that our DMM preparation is capable of supporting MuSCs and nascent muscle fiber formation within the graft area.[180]

Regenerative medicine strategies often use cellular therapies to enhance tissue regeneration, where the stem and progenitor cells used are typically derived from a single source. These cell therapies have focused on myoblasts, satellite cells, mesoangioblasts, pericytes, and mesenchymal stem cells.[278,279] Stem cell-based therapies represent a promising VML treatment option because they have the ability to self-renew and differentiate into various types of functional progeny, including skeletal myoblasts.[280] Muscle satellite cells are tissue resident stem cells in skeletal muscle and are the primary cell type to regenerate new muscle fibers. In uninjured muscle, these cells reside underneath the basal lamina in a quiescent state. Following injury, mitogenic signals activate them into a proliferating state, whereby parent satellite cells give rise to daughter cells often referred to as myogenic precursor cells (or myoblasts), and their activation initiates the myogenic program.[4] While these cells are the gold standard for muscle regeneration studies, few have been able to effectively deliver satellite cells to VML injuries without eliminating the inherent ability of satellite cells to proliferate and self-renew, a key advantage in their use.

While satellite cells are crucial for effective muscle regeneration and functional recovery, the number of cells harvested from muscle is far less than other mesenchymal tissues. This may require the addition of other mesenchymal stem cells to regenerate enough tissue for VML. ASCs (Adipose-Derived Stromal Cells) are a potent source of mesenchymal stem cells, but their ability to enhance muscle regeneration has been limited.[281–283] ASCs have been shown to support muscle repair, and our preliminary data demonstrate expression of myogenic genes, indicating their potential to enter the myogenic program.[284] Despite the work done to characterize an optimal biomaterial delivery system, the current solutions available for VML have had mixed results with low rates of improvement and the

risk of adverse immune responses.[278] Thus, the field continues to investigate a variety of potential scaffolds, cells, and molecular signaling solutions.

The challenge with current scaffold options is that some natural polymers are easily degraded, and synthetic materials risk stimulation of a foreign body response.[285–287] This study will use DMM which has been shown to provide a suitable cellular environment and remains within the wound site to allow the native tissue to reform in a VML injury.[180,184]

Use of ASCs provides an alternative solution with potential to acquire an appropriate number of cells capable of contributing to muscle regeneration. We have data that indicate an ability for ASCs to enter the myogenic program, and these findings were supported by others[288–290]. In other recent studies, ASCs cultured with myoblast-conditioned media increased levels of myogenic differentiation[291] or co-cultured with muscle satellite cells stimulated ASC fusion into multinucleated myotubes[292]. In addition, ASCs were implanted into a muscle defect with an angiotensin inhibitor that stimulated ASC fusion into new myofibers[293], suggesting that ASCs can communicate and fuse with muscle progenitors and aiding in regeneration of new muscle fibers in VML injuries.

For the current study, we hypothesized that delivering either ASCs or early stage myoblasts to the injury site using DMM would improve muscle regeneration. In addition to satellite cells, it has been shown that ASCs participate in the myogenic process. Moreover, these cells are easy to harvest from liposuction procedures, making their use in the clinic relevant for skeletal muscle tissue engineering. We used human ASCs or human myoblasts to test this hypothesis in an athymic rat gastrocnemius defect model as step toward clinical translation in humans.

Materials and Methods

Decellularized muscle preparation. All animal studies were performed in accordance with approved VCU protocols (IACUC #AD10000675). Male Sprague Dawley rats weighing 250-300g (Envigo, Huntingdon, United Kingdom) were euthanized using CO_2. Gastrocnemius muscles were isolated bilaterally frozen at -80^{o}C, and shipped to MTF Biologics (Edison, NJ) to be decellularized. Decellularization was performed via a proprietary method composed of multiple saline, detergent, and disinfection soaks using American Association of Tissue Banking and Food and Drug Administration approved protocols developed by MTF. The rat tissue was processed aseptically and without any terminal sterilization. Frozen decellularized muscle matrices (DMM) were shipped back to Virginia Commonwealth University (VCU) and were kept frozen at -80^{o}C until surgery.

Cell culture. Human myoblasts (Cook Myosite, NJ) were subcultured in myoblast growth media (Cook Myosite) and passaged at 50% confluence. Cells were maintained in subculture until passage 3 and were used for DMM seeding. Human ASCs were subcultured in αMEM supplemented with 10% fetal bovine serum (FBS), 1% penicillin/streptomycin (P/S), and 1% L-glutamine. Cells were maintained in subculture and passaged at 70% confluence to be seeded onto DMM scaffolds. Cell seeding on DMM was first optimized for cell response data using both murine myoblasts and human ASCs. Murine myoblasts (C2C12, ATCC) were cultured on DMM using DMEM supplemented with 10% FBS and 1% P/S, and hASCs were cultured as described above. An optimal seeding density of 50,000 cells/cm^2 was determined. Seeding density was checked using Live/Dead Viability staining (Thermo Scientific, L3224). Live/Dead staining was prepared by diluting 20 µL of 2 mM EthD-1 into 10mL of 1x PBS followed by a dilution of 5 µL of 4 mM calcein AM stock solution into the 4 µM EthD-1 solution. 100 µL of Live/Dead stain was then added to each cell seeded sample and incubated at room temperature for 30 minutes. Labeled cells were imaged using a Zeiss AXIO Observer.Z1 fluorescence microscope. Prior to surgery, DMM was seeded with 2,000,000 cells/scaffold and allowed to subculture for 24 hours. At surgery, seeded DMM scaffolds were prepared by washing in 1x PBS just prior to implantation.

Volumetric muscle loss surgery. Fourty male *Foxn1^{RNU}* (RNU) rats (250-300g, ~4 months old) were obtained from Envigo (Huntingdon, United Kingdom) and were divided into five groups (N=8 rats/group unless specified): sham surgery (n=6); empty defect surgery, DMM surgery, DMM+hASC surgery, and DMM+h-myoblast surgery. All rats were given ad libitum access to standard pellet and water and provided environmental enrichment. Animals were housed individually. All surgical procedures were performed under an approved protocol at VCU (IACUC #AD10000675) as previously described[8]. Briefly, rats were anesthetized using 4% isoflurane/400ml/minute O_2 and prepared for surgery. Rats were transferred to the operating table, and anesthesia was continued at 1-3% isoflurane in O_2. An oblique anterolateral incision extending from the patella to the calcaneus was made. After an incision in the biceps femoris muscle to expose the gastrocnemius was made, the left lateral gastrocnemius muscle was isolated, and a 1.5x1 cm defect was cut in the lateral gastrocnemius, taking care to preserve the sural and tibial nerve. At the end of surgery, biceps femoris was sutured closed using 5-0 nylon and skin was stapled closed thereafter.

Sham surgeries were performed as described except when the left lateral gastrocnemius was exposed, no incision was made to create a defect. Instead, biceps femoris and skin were closed without a defect. Empty defect surgeries were performed as described and left untreated, closing the biceps femoris and skin following tissue harvest. Rats that received DMM, DMM+ASC, or DMM+myoblast were sutured into muscle defects, using a modified Kessler technique and taking care to orient the anisotropic features in the direction of the muscle fibers. One rat from the empty defect group and one from the DMM+ASC group died or was euthanized (due to significant weight loss) prior to the end of the study. All remaining rats were euthanized at 8 weeks following muscle physiology tests.

Ultrasound Imaging. Rats were anesthetized with isoflurane (4% with 400ml/minute O_2) and hindlimbs shaved. Ultrasound gel was applied to an L15-7io Broadband compact linear array transducer from Philips (Massachusetts, USA), and the transducer was applied to the gastrocnemius muscle to visualize the injury area (cross-sectional orientation). Suture landmarks identified the edges of the injury. A cross-section from the injury site's center was used for analysis. We applied Heckmatt's Scale to grade the ultrasound images qualitatively.[294] The grading criteria are as follows: Grade I- normal, darker muscle, normal fascia thickness/brightness, and the tibia/fibula will be clearly visible; Grade II- brighter muscle, thicker/brighter fascia, and the tibia/fibula will be clearly visible; Grade III- markedly brighter muscle, much thicker/brighter fascia, and less visible tibia/fibula; Grade IV- very bright muscle, considerably thicker/brighter fascia, and no visible tibia/fibula. Three independent, blinded observers scored each image. The three independent ordinal scores for each image were averaged together, and the resulting data was treated parametrically by applying one-way ANOVA with Tukey's post test (α=0.05).

Muscle physiology. Peak tetanic force, peak twitch force, maximum rate of contraction, force-time curve integration, and maximum relaxation were measured. Rats were chosen at random and anesthetized using a vaporizer at 4% isoflurane/400ml/minute O_2. Following induction of general anesthesia, the sciatic nerve was isolated, and sural and peroneal branches ligated. Sciatic nerve was then stimulated using platinum electrodes connected to a Grass stimulator model SD9 (Astro-Med, Inc., Westwarwick, RI) at 2-msec duration and 2-msec delay at varying voltages and frequencies. The knee and ankle joints were immobilized, and the Achilles tendon was cut from its insertion and connected to a MLT500/A force transducer (ADInstruments, Inc., Colorado Springs, CO) with 2-0 silk sutures. Output

was collected digitally using LabChart 8 software (ADInstruments). Optimal muscle length, stimulating voltage, and tetanic frequency were determined. During muscle lengthening, muscle was stimulated to tetanus for 3 seconds at each interval. Once optimal length was determined, tetanic contraction was stimulated at 3 second intervals until peak tetanic force dropped, indicating fatigue. Immediately following this force drop, 3 separate submaximal stimulations were measured. Those stimulations were used for muscle physiology assessments. Peak tetanic force was measured at maximum force for optimal frequency. Peak twitch force was measured at the peak of the submaximal force-time curve. Measurements in injured and treated limbs were the result of total force output from the posterior crural muscles (medial gastrocnemius, lateral gastrocnemius, soleus, and plantaris).

Histology. Whole gastrocnemius muscles were removed and fixed in 10% neutral buffer formalin, dehydrated, and embedded in paraffin. Muscles were cross-sectioned approximately 0.5 cm from the margins. Sections (5 μm) were placed on Histobond slides (VWR, Radnor, PA), deparaffinized and rehydrated, and stained with Masson's trichrome using Weighert's haematoxylin (Sigma-Aldrich, St. Louis, MO), Biebrich's scarlet-acid fuschin (Sigma-Aldrich), and aniline blue (Sigma-Aldrich). Coverslips were mounted with xylene-based mounting media and allowed to dry flat before imaging.

Histomorphometry. Histomorphometry was used to quantify the percent of centrally located nuclei, myofiber diameter, and ratio of muscle to collagen. Histological sections stained with Masson's trichrome were imaged using a 10x and 40x objective, and were assessed as previously reported.[180] Healthy muscle from sham operated animals was used as a positive control. Histological analysis was performed on each muscle (n = 6 for sham, n = 7 for Empty, n = 7 for DMM-ASC, n = 8 for DMM, n = 8 for DMM-Myo) in 3 different locations within the graft area. Field sizes of 650x870μm and 165x220μm were used for histomorphometry. DMM locations were identified by first locating the zone of injury using injury margins. Once the zone was established, images were taken from three locations within the injury site, one at the margin, a second within the middle of the graft, and a third within an additional area of the graft away from the margins.

Nanostring. Gene expression of 817 total RNAs were measured using the NanoString fluorescent RNA hybridization and counting method. The custom panel measured genes related to muscle and nerve expression from the mouse genome matching at least 90% homology to the rat genome of interest. Samples were diluted to 55 ng/uL and checked for 260/280 purity using spectrophotometry. Fourteen genes were used as reference genes while ten others were used as housekeeping normalization genes. Counting was performed using the nCounter® Digital Analyzer while raw data analysis was accomplished using nSolver™ Analysis Software 4.0. Background thresholding was used to eliminate potential noise caused by low count (<20) genes followed by housekeeping normalization using geometric means. Genes found outside of the normalization factor range of 0.1-10 were flagged for QC. Fold change from each group was calculated against sham. Genes were considered differentially expressed if their log2 fold change was greater than |± 2| and p-value ≤ 0.05.

	Host Species	Antibody, clone	Cat. No.	Company
1	Mouse	αMyHC, A4.1025	05-716	Sigma Aldrich, St. Louis
2	Mouse	αMyHC Fast, MY-32	M4276	DHSB, Iowa City, Iowa
3	Mouse	αMyHC-I, BA-D5	BA-D5	DHSB, Iowa City, Iowa
4	Rabbit	αRAGE	ab37647	Abcam, Cambridge, UK
5	Rabbit	αP-38 MAPK	9212S	Cell Signaling, Danvers, MA
6	Mouse	αpP-38 MAPK (Thr180/Tyr182), 28B10	9216S	Cell Signaling
7	Rabbit	αGAPDH, 14C10	2118S	Cell Signaling

Table 3. List of antibodies used for western blotting.

Western blot. 30 mg of gastrocnemius muscles were homogenized in NP-40 lysis buffer (BP-119, Boston BioProducts, Ashland, MA, USA) with a PI cocktail and 25 mM NaF with a 6.0 mm zirconium bead in a beadbug homogenizer (BeadBug™ Cat #: 31-212, Genesee Scientific, San Diego, CA, USA) at 4000 rpm for 60 s 5 times while keeping the tubes on ice for at least 5 min between runs. The homogenate was

centrifuged 9703 rpm (10,000 g) (Centrifuge 5427 R, Eppendorf, Hamburg, Germany) for 10 min, and the supernatant was used for Western blotting. Briefly, the supernatant was run on the BCA assay. Equal amounts of protein were denatured with Laemmli buffer at 100 °C for 10 min, then electrophoresed on polyacrylamide gels, transferred to a PVDF low fluorescence membrane, blocked for 1 h at room temperature, and stained overnight with primary antibodies listed in Table 3. The membranes were then incubated with secondary antibodies (926-68073, 926-32210, and 926-32211, LI-COR Biosciences, Lincoln, NE, USA) for 40 min at room temperature, then they were imaged on the LI-COR Odyssey and quantified. Each blot was analyzed separately and results were normalized to GAPDH levels. The normalization factor for samples on one blot was determined by identifying the highest GAPDH signal and dividing each GAPDH signal intensity by the highest GAPDH signal, producing a value of 1 for the strongest signal and less than 1 relative to that stronger signal. Target protein signals were divided by the normalization factor to obtain the normalized signal.

AGEs. Muscle samples were minced and homogenized with the Minute™ Total Protein Extraction Kit for Muscles (using the Denaturing Buffer) and ran on an AGE ELISA (Cell Biolabs, STA-817) to determine AGE levels. For DMM, homogenization was done with a 6.0 mm zirconium bead in a beadbug homogenizer (Genesee Scientific, BeadBug™ Cat #: 31-212) at 4,000 rpm for 60 seconds 20 times while keeping the tubes on ice for at least 5 minutes between runs, to pulverize the tough ECM, followed by centrifugation at 13,000 rpm (17,949 g) (Eppendorf, Centrifuge 5427 R) for 3 minutes. The Pierce™ BCA Protein Assay Kit (Thermo Fisher Scientific, 23225 and 23227) and hydroxyproline assays were used for normalization purposes.

Statistical analysis. Each variable was tested using N = 8 independent animals. The animal number was chosen based on a power analysis using an alpha of 0.05 and a power of 80% (delta=5, sigma=3, m=1) to reveal a minimum of n=7 per group to yield statistical significance. Data are presented as mean ± SEM with analysis done using GraphPad Prism 6.0 (GraphPad, La Jolla, CA). Analysis comparing more than 2 groups used one-way analysis of variance with Tukey post hoc test to determine differences between rat treatments, while comparisons of 2 groups used the Students unpaired t-test. For Heckmatt's Scoring, the three independent ordinal scores for each image were averaged together,

and the resulting data was treated parametrically by applying one-way ANOVA with Tukey's post hoc test (α=0.05). All *p* values <0.05 were considered significant.

Results

Gene Analysis for VML Injuries Treated with DMM

The effect of DMM in injury sites was compared to injuries with no treatment and sham operated controls. Over 700 genes were assessed using muscle lysates isolated from the VML injury sites. Heat maps demonstrated unique gene profiles between DMM and Empty Defects (Figure 28A). Volcano plots were examined to isolate genes that demonstrated a log 2-fold change (Figure 28B). Evidence showed that Empty Defects had an increased number of fibrotic gene markers compared to DMM. Moreover, one of the primary genes that was isolated during this analysis showed upregulated levels for MAP3K, Jun, cMyc (Figure 28C). These were mapped using a pathway analysis, and indicated increased inflammatory stimulants that were possibly regulated by RAGE and related to p38 MAPK (Figure 28D).

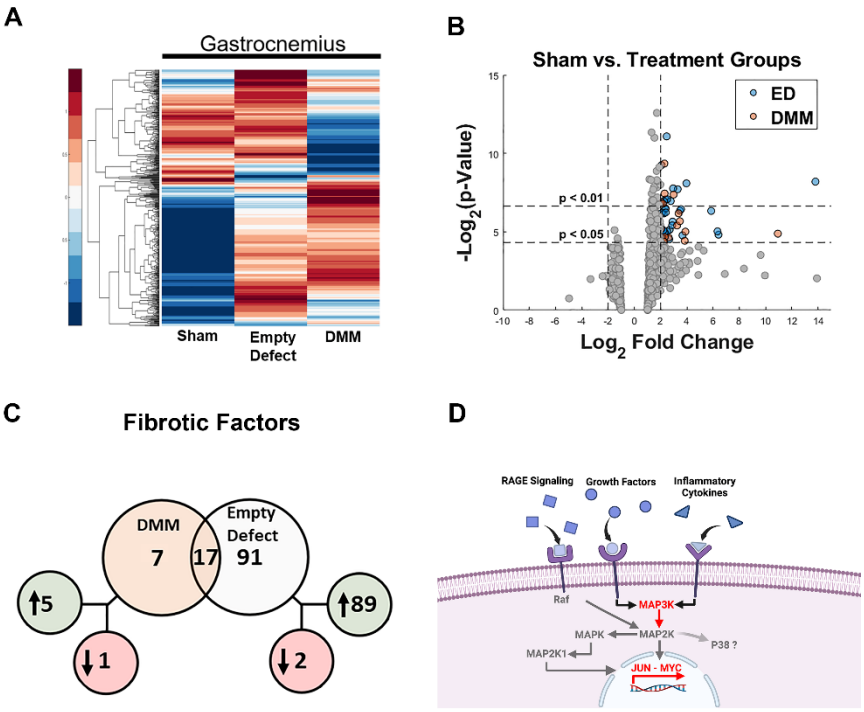

Figure 28. Gene expression analysis of VML injury sites. Nanostring analysis demonstrated unique changes between Sham v. Empty and Sham v. DMM (A). Gene targets were identified using volcano plots (B) and Venn diagrams (C). Venn diagram demonstrated shared genes (overlapping circles) versus unshared genes (separate circles). Genes in green were upregulated while genes in red were downregulated. These genes of interest in addition to pathway analysis suggested increased inflammatory pathways which possibly included RAGE (D).

Cell Seeding onto DMM

To assess cellularization of DMM, we seeded murine myoblasts (C2C12s) or hASCs onto DMM and stained the cells using Live/Dead. These first studies demonstrated that myoblasts and hASCs could be successfully grown on DMM. We then determined mRNA levels in myoblasts and hASCs cultured on DMM versus TCPS. mRNA levels in myoblasts showed increased levels for Myod (Figure 29B) and Myog (Figure 29C). All other myogenic markers were unchanged (Figure 29D-F). hASCs cultured on DMM demonstrated elevated levels of MYF5 (Figure 29G) and levels for ITGA7 (Figure 29K) were detectable when compared to TCPS. All other measured genes were not different between DMM and TCPS.

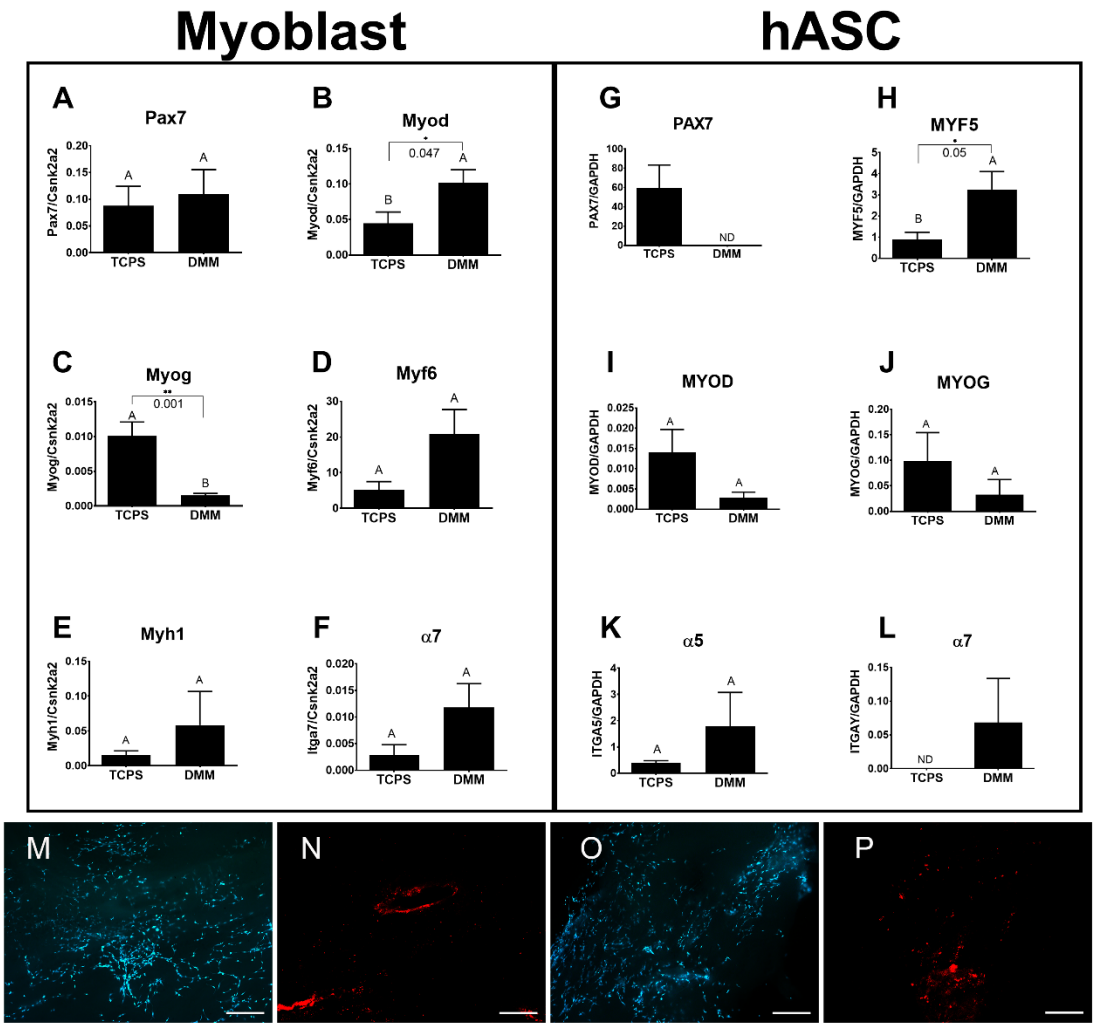

Figure 29. Gene expression analysis and live/dead staining for myoblasts and ASCs cultured on DMM. Myoblasts and ASCs were seeded onto DMM and assessed for markers of differentiation. No change in Pax7 was detected (A) while Myod (B) and Myog (C) increased compared to TCPS. Late markers for Myf6 (D), Myh1 (E), and α7 (F) were not different from TCPS. ASCs cultured on DMM did not express PAX7 (G), but did express higher levels of MYF5 (H). No change in MYOD (I), MYOG (J), or α5 (K) were detected. α7 (L) was detected in ASCs cultured on DMM while it was not detected on TCPS. Myoblasts and hASCs were seeded onto DMM and stained for Live/Dead (M, N, O, P). Letters not shared indicate a significant difference ($p < 0.05$, unpaired t-test). Expression not detected was marked as N.D. Data shown are means ± SEM of 6 samples from a representative experiment. Each DMM was randomly selected from a different donor. Experiments were repeated to ensure validity. Scale bar size is 500 µm.

Muscle force.

Muscle force decreased in VML injured muscles by 23% in empty defect sites, 22% in DMM and ASC treated sites, and 12% in myoblast treated sites when compared to sham animals (Figure 30A). This produced a significant decrease if muscle maximum tetanic force output in the VML injured muscles compared to sham surgeries. In addition, neither DMM treatment nor cell treatment significantly improved muscle force. Integration of force-time curves as well as the maximum and minimum slopes were calculated with no differences amongst any groups (Figure 30B-D).

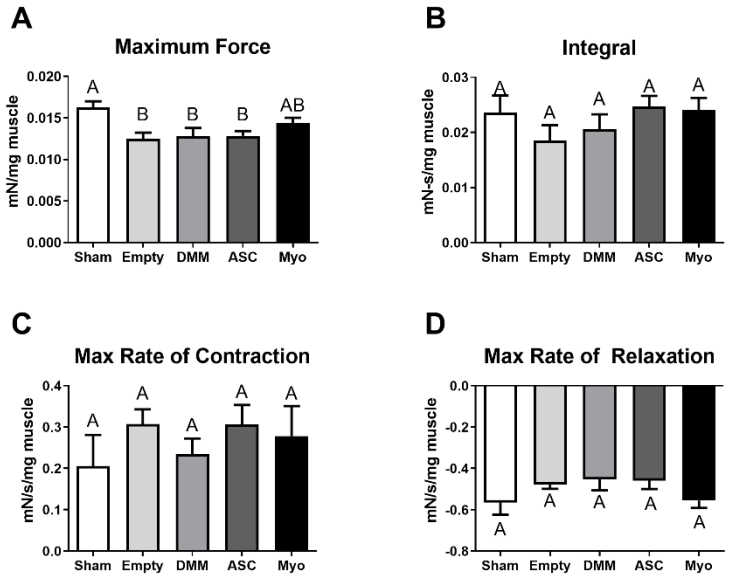

Figure 30. Muscle force analysis demonstrates no overall improvements after cell treatment. Maximum muscle force output from the posterior crural muscles was analyzed and showed reduced force in injured limbs but no improvements were detected in treated injury sites (A). Force-time integration (B), max rate of contraction (C), and max rate of relaxation (D) also showed no differences amongst treatment groups and no groups were different from sham surgeries. Letters not shared indicate a significant difference ($p < 0.05$, Tukey). Data shown are means ± SEM of 8 animals.

Magnetic Resonance Imaging.

Magnetic resonance imaging was used to characterize fibrotic areas over the time course of healing. Heckmatt's scores demonstrated no change in echogenicity at 2 weeks, increased echogenicity by 4 weeks in myoblast treated injury sites (Figure 31B), and echogenicity was unchanged after 8 weeks of healing (Figure 31C). Of note, echogenicity was on average elevated in all injury sites compared to sham animals although this was not statistically different.

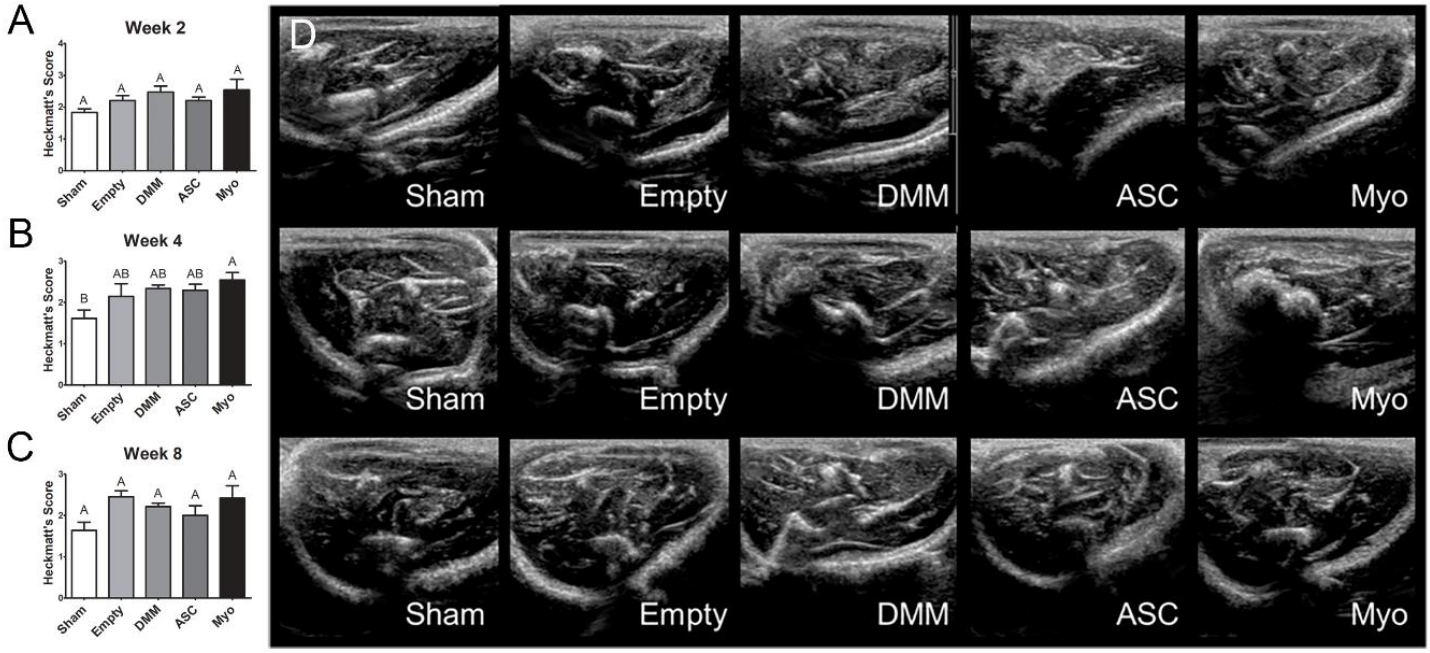

Figure 31. Echogenicity assessment using a Heckmatt's score. Muscles were evaluated for echogenicity and scored at weeks 2 (A), 4 (B), and 8 (C). Representative images of each group are shown in panel (D). Letters not shared indicate a significant difference ($p < 0.05$, Tukey). Data shown are means ± SEM of 8 animals.

Histological assessment.

VML injured sites treated with DMM with or without cells showed areas of regeneration (Figure 32). The number of muscle fibers and Feret fiber diameters were first characterized with no differences amongst the groups (Figure 32F,G). Feret's fiber diameter was plotted as a histogram, showing that sham animals had larger muscle fibers than injured animals with a rightward shift in the distribution (Figure 32H,I). As previously shown in prior research[8], DMM supported de novo fiber formation within the graft area with centrally located nuclei within the graft area. Empty defect sites also showed areas of centrally located nuclei that were similar in number to DMM, but it should be noted these areas were located at the margins of the injury with no grafted area. In contrast, DMM treated sites showed newly regenerated fibers within the graft area, away from the margins. ASCs delivered to VML injuries improved the number of regenerated fibers compared to empty injury sites, but were not different from DMM or myoblast delivery (Figure 32J). Collagen was assessed using the aniline blue stain, and showed increased collagen within all injured muscles compared to sham animals (Figure 32K).

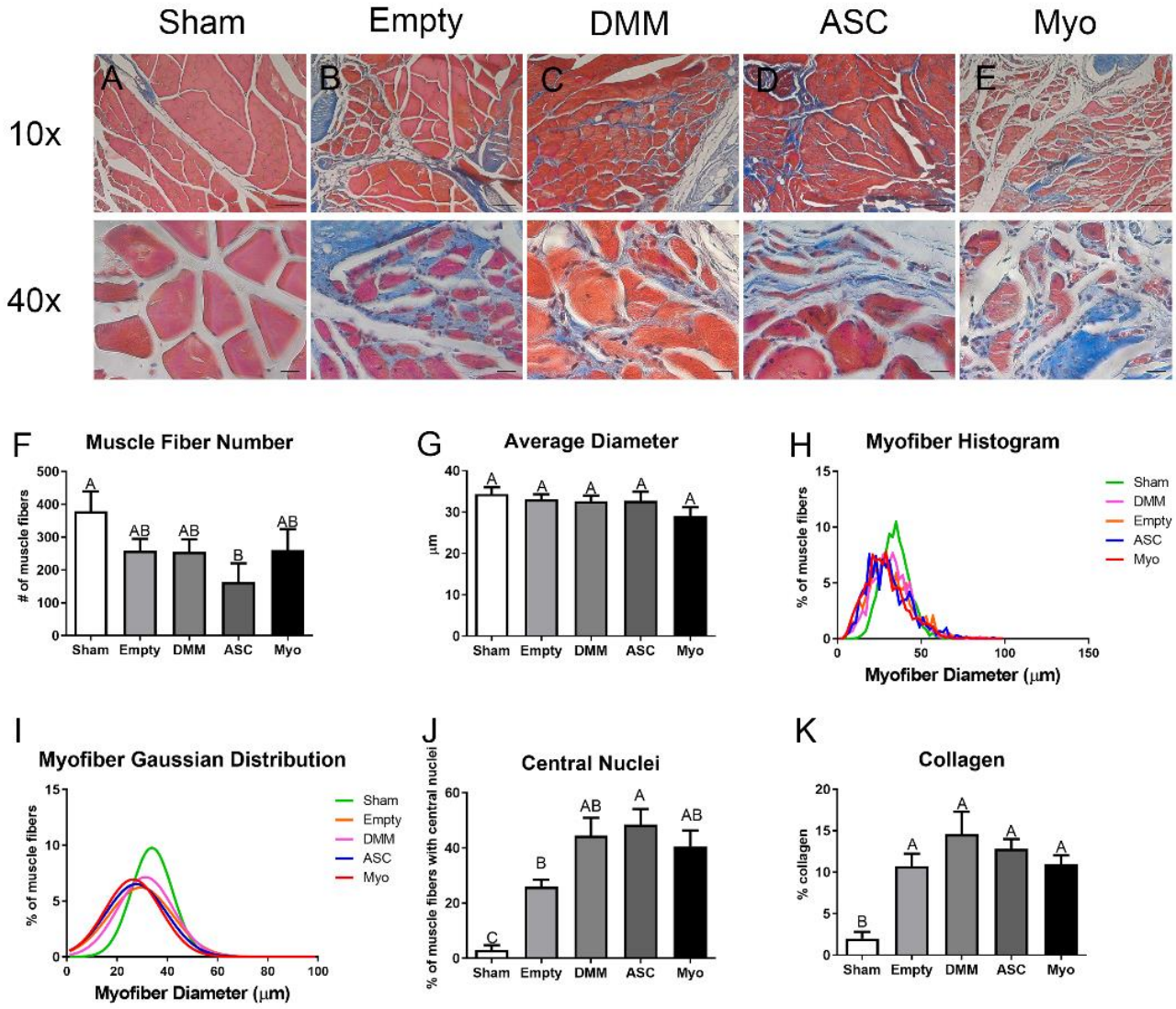

Figure 32. Histological staining and morphometric analysis for VML injuries treated with myoblasts and ASCs. Representative images demonstrate a normal appearance of muscle in sham operated animals (A), while a response to injury and treatment is represented in (B,C,D,E). Histomorphometry showed a similar number of muscle fibers (F) and a similar Feret's diameter (G). Histograms reveal a slight leftward shift in Feret's diameter (H,I). Increased central nuclei were detected in all groups compared to sham while ASC treated injuries showed the largest increase (J). Lastly, increased collagen levels were determined relative to sham for all injury sites (K). Letters not shared indicate a significant

difference ($p < 0.05$, Tukey). Data shown are means ± SEM of 8 animals. Scale bars for 10x and 40x images are 100 μm and 20 μm, respectively.

Myofibrillar assessment.

Human myoblasts and ASCs behaved differently when delivered to muscle injuries. Myoblasts delivered to VML injuries did not affect myosin heavy chain levels when compared to either empty defects or sham animals. In contrast, ASCs delivered to VML injuries increased levels of mixed myosins, which included both slow and fast twitch MyHC (Figure 33A). Those myosins were parsed using more specific antibodies for fast, neonatal, and slow myosin, demonstrating a significant increase in fast myosin that was over 4-fold higher that sham and over 7-fold higher than empty defect surgeries (Figure 33B). Neonatal myosins were unchanged regardless of treatment, but levels in ASC-treated sites were noteworthy with a 3-fold increase over sham and a 9-fold increase over empty defects (Figure 33C). Lastly, slow myosin heavy chains were unchanged regardless of treatment (Figure 33D).

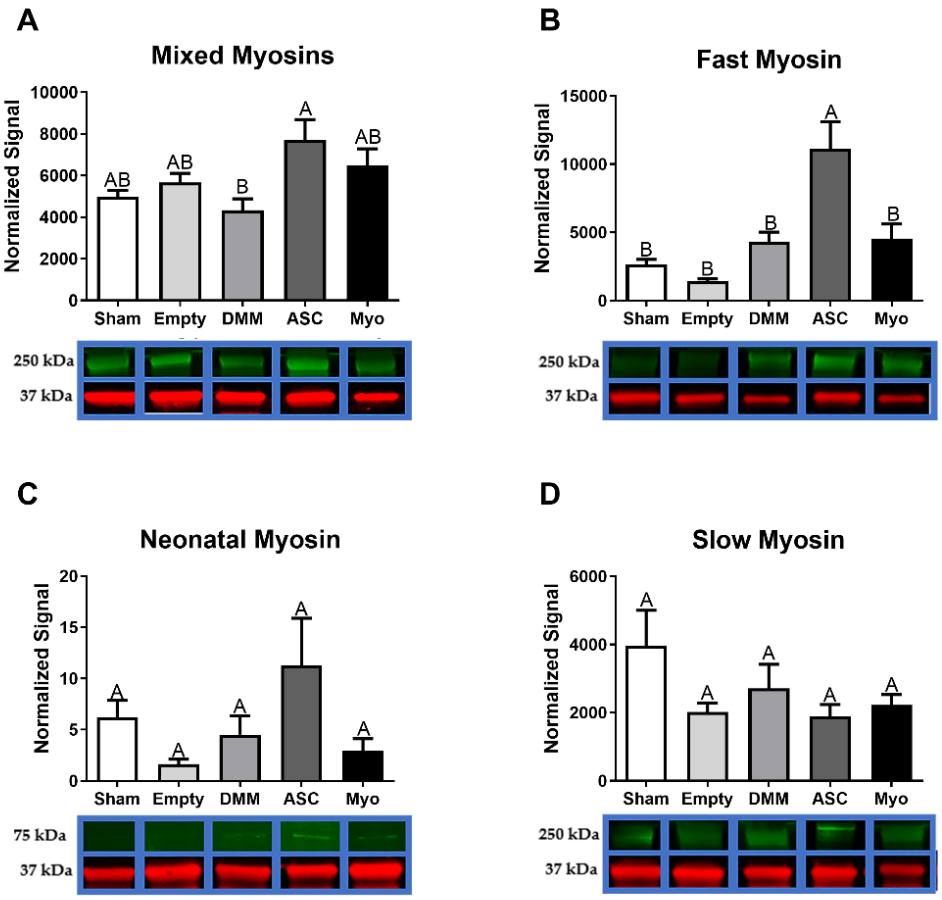

Figure 33. ASC treated DMM support increased fast myosin levels. Myosin heavy chains were analyzed for a mixed population of slow and fast myosins (A), fast myosin heavy chain (B), neonatal myosin (C), and slow myosin heavy chain (D). Protein levels for mixed slow and fast twitch myosin heavy chain were elevated in ASC treated injuries, and DMM was treated animals was lowest. Fast twitch MyHC showed increased levels only in ASC treated animals. Neonatal and slow myosin levels were unaffected. Data shown are means ± SEM of 8 animals. Western blot bands are representative bands where green represents the target antibody and red represents GAPDH for normalization. Western blots were repeated to ensure validity. Letters not shared indicated a significant difference ($p < 0.05$, Tukey).

AGEs and RAGE.

Previously, we showed that AGE crosslinks were associated with age-related fibrosis.[25] Whether this was also the case in VML injuries had not yet been determined. Collagen levels were assessed using hydroxyproline assays. Whilst no significant differences in collagen were detected amongst all

groups, average levels were more consistently elevated in DMM, ASC, and myoblast treated injury sites (Figure 34A). Interestingly, AGEs were normalized to hydroxyproline and showed a reduction in all treated injury sites using DMM with or without cells (Figure 34B). RAGE levels showed an increase in ASC treated injuries compared to empty, DMM, and myoblast groups (Figure 34C), and p38 MAPK was most elevated in DMM treated VML injuries while levels were reduced in ASC and myoblast groups compared to DMM (Figure 34D).

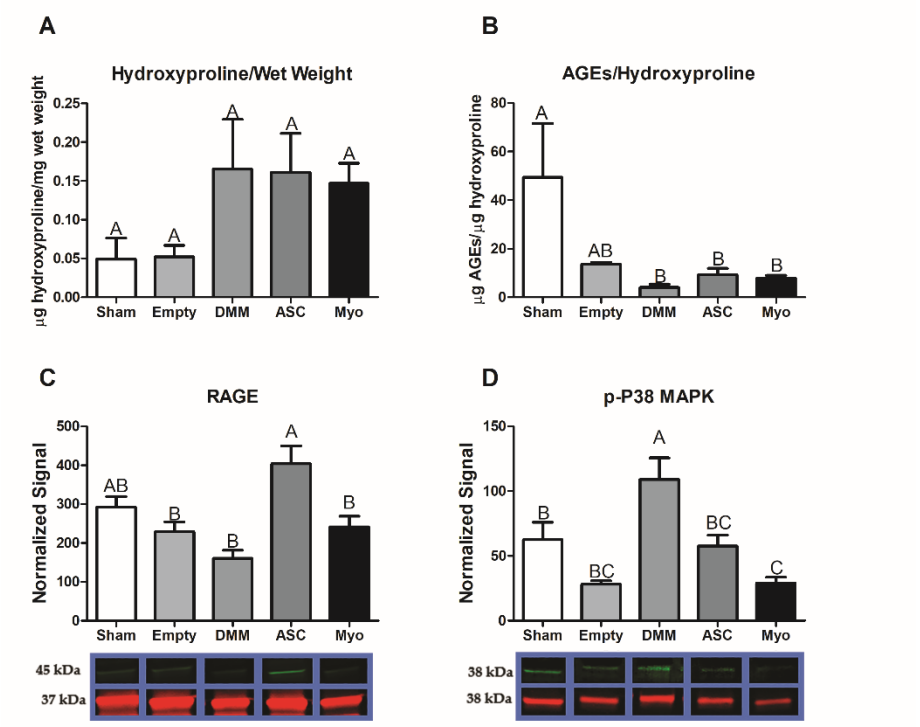

Figure 34. AGEs do not mediate fibrosis and RAGE is activated normally in VML injuries. Collagen levels measured by hydroxyproline were unchanged across all groups (A). AGEs were normalized to hydroxyproline and showed reduced levels in DMM, ASC, and myoblast treated groups (B). RAGE levels were higher in ASC treated injuries, but similar to sham (C). p38 MAPK was elevated in DMM treated sites (D). Data shown are means ± SEM of 8 animals. Hydroxyproline, AGE ELISA, and Western blots were repeated to ensure validity. Western blot bands are representative bands where green represents the target antibody and red represents GAPDH for normalization. Letters not shared indicated a significant difference ($p < 0.05$, Tukey).

Challenges

Optimizing cell attachment to the DMM presented a challenge. We attempted a simple seeding procedure (like plating TCPS), but the cells only coated the surface and did not penetrate the DMM. To overcome this, we seeded the cells at a high concentration, and allowed the cells to penetrate for 24 hours. As a result, the cells had increased attachment and penetration into the DMM.

Discussion

In this study, we first assessed differences in gene expression amongst DMM-treated VML sites, ED VML sites, and sham operated animals and determined that MAPK signaling was strongly affected including inflammatory associated pathways. These initial studies helped to identify specific pathways related to our injury model. DMM scaffolds were then seeded with human ASCs or myoblasts to determine if delivery of stem cells or progenitor cells would improve muscle regeneration in a VML model. While functional differences were unremarkable, differences in centrally located nuclei were elevated in ASC delivered cells versus DMM and empty defect animals. In contrast, myoblast delivered injury sites were unchanged compared to DMM and lower than empty defect animals. Western blotting confirmed the observed increase in central nuclei in ASC treated injuries, showing increased fast twitch myosin heavy chain. In addition, collagen levels were quantified using Masson's Trichrome staining and showed increased collagen across all injury sites. We hypothesized that increased fibrosis was related to aberrant AGE/RAGE signaling based on our initial gene analysis of VML wounds treated with DMM. Interestingly, AGE cross-links were downregulated in injured animals while RAGE signaling increased in ASC treated sites. These data correlated with increased regenerative markers in ASC treated injury sites, suggesting that RAGE signaling occurred in a normal physiologic manner. Downstream p38MAPK signaling was assessed and found to be lower in DMM and myoblast treated animals but similar to empty and sham in ASC, further confirming normal RAGE signaling. This is significant because other studies indicated that muscle trauma aberrantly increases RAGE signaling, contributing to a prolonged immune response; however, our data show a different effect in a rodent VML model.[22,295] Overall, our data suggest that ASCs improved levels of muscle regenerative markers compared to myoblasts and that RAGE signaling also appears to be involved in ASC-mediated regeneration.

ASCs are an abundant source of multipotent mesenchymal stromal cells with myogenic potential. These cells are capable of expressing several myogenic factors including Pax7, Myf5, MyoD, and myogenin. Indeed, Di Rocco et al. showed that a small population of ASCs was capable of

sporadically converting into a myogenic lineage, suggesting an inherent myogenic potential.[280] Moreover, this same group demonstrated that ASCs injected into an ischemic injury model fused with existing muscle fibers, supporting the idea that ASCs are suitable stem cell source for muscle regeneration studies. Prior studies also compared ASCs and myoblasts to each other to determine any differences in their regenerative potential when seeded onto decellularized bladder matrix.[296] While the study did not remark about ASCs versus myoblasts, they demonstrated histological evidence that ASCs and myoblasts were identified in the decellularized matrix.

We first demonstrated that ASCs and myoblasts could be cultured on DMM, and that ASCs expressed myogenic markers when seeded on DMM *in vitro*. We then determined whether ASCs or myoblasts would change the muscle's response to VML injury, and showed that regenerative markers were unaffected by myoblast seeding whereas ASCs showed improvements in regeneration when assessing MyHC II, centrally located nuclei, and RAGE signaling.

Myosin heavy chains follow a re-expression pattern during muscle regeneration that is important when analyzing de novo muscle fiber growth in a scaffold area.[297] In cardiotoxin-induced injury models, neonatal MyHC was detected within 2-3 days after injury and persisted for up to 3 weeks.[298] The switch from neonatal to adult fast myosins is independent of innervation and is a likely cause for the increase observed in ASC treated sites.[299] Since, cardiotoxin injuries are a fully regenerative model, it is not surprising for us to detect neonatal MyHC in injured critical-sized muscle injury 8 weeks after implantation. Moreover, only in the presence of nerve is slow myosin upregulated and fast downregulated, suggesting that while we showed elevated levels of neonatal and fast myosins in ASC treated sites they likely remained denervated.

We explored the role of advanced glycation end-products in our VML injury model and its involvement in fibrosis. Previously, we showed that AGEs were associated with fibrosis in older muscle.[25] Those data coupled with our pathway analysis (Figure 19) led us to hypothesize that fibrosis development in VML was also associated with AGEs. Other research showed that AGEs were elevated following chronic muscle injury with long-term RAGE signaling triggered by high concentrations of RAGE ligands producing a deleterious effect.[295] We first tested AGE cross-link levels and determined that AGEs per collagen were suppressed in all VML groups. Moreover, AGEs levels in whole muscle lysates were lower in DMM treated sites, but were at sham levels for all other groups. This suggested that RAGE ligands were not chronically elevated as shown in prior literature studies, where RAGE ligands were explored in myopathies.[146,255]

Interestingly, RAGE was elevated in ASC treated injury sites compared to all other groups. These data coupled with low AGEs and elevated levels of regenerative markers suggested normal physiologic RAGE signaling in the newly regenerating areas. This is supported by studies that demonstrated delayed regeneration in an acute injury model using Ager knockout mice compared to other studies that explored chronic pathologic conditions.[295] These opposing effects were ascribed to the levels of RAGE ligands available to activate the receptor. In addition, RAGE is highly dependent on its co-activators that help direct a particular signaling pathway. We explored whether p38 MAPK was involved given its known role in AGE/RAGE/p38 MAPK signaling, and determined that p38 MAPK was elevated in DMM and ASC treated injury sites compared to empty defect while myoblast treated sites were similar to empty.[23]

P38 MAPK plays a critical role in muscle regeneration.[300] It was first described as a transducer of the response to environmental stress conditions, and in muscle was found to regulate muscle fiber formation via satellite cell differentiation, slow myosin heavy chain gene repression, and is involved in muscle pathologies.[300–302] When taken into context with our observed increase in fast MyHC, centrally located nuclei, and RAGE signaling, use of p38 MAPK as a marker of regeneration in a VML model becomes more intriguing. As a disease mechanism, cell delivery reduced p38 levels and this could aid in regeneration.[303] As a repressor of slow myosin heavy chain gene expression, p38 MAPK could explain the increases observed in fast myosin heavy chain protein levels in DMM, ASC, and Myo treated injuries compared to empty sites, but more study would be needed to fully elucidate the role of p38 MAPK in a VML model.

Conclusions

Prior research has shown that cell delivery to a VML injury site is essential to assist in muscle regeneration, improving the number of de novo muscle fibers within the injury. Our results demonstrated that our DMM was sufficient to improve muscle fiber regeneration and DMM was enhanced by ASCs but not myoblasts. We also determined that AGE/RAGE is not involved in late-stage healing and fibrosis following VML injury, indicating that AGE crosslinks do not adversely affect skeletal muscle ECM. p38 MAPK plays a critical role in muscle regeneration, and its levels were higher in DMM treated muscles without cells compared to untreated and cell treated injury sites. We theorize this response is due to an enhanced myogenic capacity of ASC seeded DMM, and RAGE and p38 MAPK appeared to be regulated independent of one another. In addition, RAGE appeared to function in a pro-myogenic

fashion, which was reported to occur under normal physiologic conditions. This could mean that DMM mitigates pro-inflammatory responses and promotes a pro-myogenic environment.

Chapter 6. Glycations on Decellularized Muscle Matrix Reduce Regeneration and Increase Inflammation in a Sprague-Dawley Volumetric Muscle Injury Model

Abstract

Volumetric muscle loss (VML) caused by a traumatic injury results in long-term loss of muscle function. Treatments that use autologous grafts risk donor site complication as well as harvest site morbidity. An alternative solution is to use allogenic tissue sources to harvest muscle for decellularization. These decellularized muscle matrices (DMM) have shown promise and deliver muscle-specific factors in a biocompatible scaffold. One complication is that allogenic tissue usually comes from aged donors, and prior work from our lab demonstrated higher advanced glycation end product (AGE) cross-links within muscle from aged donors compared to young donors. The objective of this study was to determine whether increased AGE cross-links reduced the regenerative capacity of DMM. We hypothesized that increased AGEs would reduce DMM-mediated muscle regeneration in a VML rodent model. In this study, we removed 35% of the gastrocnemius and attempted to regenerate it with either AGE-laden DMM or DMM alone with comparison to a sham operation and empty defect. To assess graft performance, we measured muscle function, histomorphometry, and protein content. AGEs reduced important muscle morphometrics such as muscle area, fiber number, and fiber diameter but increased collagen area. Also, AGEs reduced key extracellular matrix (ECM) remodeling proteins and increased inflammatory proteins. In conclusion, our data supports the idea that AGEs reduce the myogenic potential of DMM and that old age should be carefully considered when sourcing muscle for DMM.

Introduction

Skeletal muscle extracellular matrix (ECM) plays a pivotal role in muscle development and regeneration via muscle-specific cues.[304,305] Decellularized muscle matrix (DMM), a processed skeletal muscle ECM, preserves pro-myogenic characteristics by retaining an aligned architecture and chemical components of the ECM to promote muscle regeneration.[180] In addition, removing the cellular content and elements in decellularized scaffolds eliminates an immunogenic response while not altering the intrinsic structural benefits of the native acellular framework, enabling these scaffolds to promote regeneration.[172] These characteristics make skeletal muscle-derived ECM a bio-scaffold solution that can support muscle

regeneration, where muscle stem cells (MuSCs), fibroblasts, macrophages, and other support cells interact with muscle ECM to regulate regeneration.[306] However, the age of the DMM donor has not been adequately explored for use in muscle regeneration.[25]

The Organ Procurement and Transplantation Network reported that 33% of donated tissues came from donors 50+ in age (Based on OPTN data as of March 13, 2023). Considering donor age and muscle injuries that might occur in individuals 65 and older, our goal for this study was to explore the role of ECM from aging donors on the regenerative capacity of DMM.[26,307] Previously, we determined that increased connective tissue in old mouse muscle was related to advanced glycation end products (AGEs), a type of collagen cross-link, and treatment with ALT-711, a glycosylated protein cross-link breaker, reduced AGEs in aged DMM.[25] AGEs are chemical cross-links that form on ECM via the Maillard reaction, and are found in skeletal muscle aging.[238] AGEs preferentially accrue on collagen fibers due to repeating arginine and lysine residues that potentiate the Maillard reaction via a stochastic interaction of monosaccharides with proteins.[25] These cross-links are the final derivative of the Maillard reaction and are also implicated in the receptor for advanced glycation end-product (RAGE) activity.[22] Further, the glycation cross-links result in a stiffening of the collagenous matrix, underscoring the premise that AGE accumulation in the ECM has deleterious effects on regeneration.[85]

To test the effect of AGEs on muscle regeneration, we used an established volumetric muscle loss (VML) injury in a rodent model.[180] VML is caused by severe laceration, gunshot, blast, and tumor resection wounds, and has been found to overwhelm muscle regeneration, resulting in loss of long-term muscle function and increased risk of comorbidities.[277,308] Current treatment plans include physical therapy as well as muscle flap transfers; however, these clinical procedures are unable to address functional losses and cannot restore adequate muscle strength.[180] Most treatments result in suboptimal recovery, and, in extreme cases, result in donor-site morbidity relating to functional loss and volume deficiency at the harvest site.[180] To avoid autologous site complications, we used established DMM scaffolds to encourage muscle regeneration.[180,184,309]

To model aged rat ECM, we used D-ribose sugar to create AGE cross-links in young DMM and hypothesized that increased AGEs would reduce DMM-mediated muscle regeneration in a Sprague Dawley gastrocnemius VML model. VML injuries promote a pathophysiology that enhances fibrogenesis and inflammation, which involves a plethora of cells that respond to the injury site.[275] The aim of the present study is to use of a VML model appropriate to help understand how AGEs might limit

a bio-scaffold's regenerative capacity, and to test the extent to which RAGE might be involved due to its role in muscle differentiation, fibrosis, and inflammation during muscle regeneration.

Materials and Methods

2.1 Decellularization and D-Ribose Incubation: The decellularization process relies on the complete removal of all cellular elements within the cell, including DNA and associated organelles [175]. SAS Sprague-Dawley rats (250–300 g) were obtained from Charles River (Wilmington, MA, USA), euthanized with CO_2, and the skin was bluntly dissected from the hindlimbs following a VCU-approved protocol (IACUC #AD10000675). The biceps femoris muscles were removed, and the gastrocnemius muscles were extracted at the Achilles tendon and proximal to the posterior knee joint. Care was taken to separate and remove the plantaris and soleus muscles from the gastrocnemius. The gastrocnemius muscles were frozen at -80ºC and thawed in a 37ºC water bath before decellularization. Both heads of the gastrocnemius muscle were butterflied to a several mm thickness to allow for thorough penetration of the decellularization solutions. Gastrocnemius muscles were then decellularized in 50 mL Pyrex Low Form Griffin Beakers (Corning Inc., Corning, NY, USA) with constant stirring using a proprietary method that included enzymes and cationic, anionic, and zwitterionic detergent treatments. Peracetic acid (Sigma-Aldrich, St. Louis, MO, USA) was used for sterility purposes at the very end of the decellularization process. DMMs were then frozen at -80ºC, lyophilized overnight, and placed back in the freezer at -80ºC. For AGE formation, DMMs were placed in 100- and 250-mM D-ribose (Sigma-Aldrich, St. Louis, MO, USA) solution (2.22 mL/mg dry weight) in 6-well plates for 5 days at 37°C with 5% CO_2, and excess D-ribose was removed with 3 5-minute 10 mL DI water washes. DMM that was used in the VML model (see section 2.3) were kept in 0.9% saline at 37°C with 5% CO_2 overnight after AGE induction to avoid additional freeze-thaw cycles.

DMM Characterization: Following the decellularization process, DMMs or control muscle were homogenized in 0.05% Triton X-100 with a 6.0 mm zirconium bead in a beadbug homogenizer (BeadBug™ Cat #: 31-212, Genesee Scientific, San Diego, CA, USA) at 4000 rpm for 60 s 3 times. The resulting homogenate was centrifuged for 30 seconds on a table-top centrifuge (g=2,000), and the supernatant was electrophoresed on a 1% agarose gel (Sigma-Aldrich, St. Louis, MO, USA) and stained with ethidium bromide to compare DMM DNA fragmentation from DMM to a control whole muscle (WM) control biopsy. Once DNA removal was confirmed, a sample of DMM was fixed in 10% neutral buffered formalin (VWR, Radnor, PA, USA), processed histologically, and stained with Masson's trichrome stain and Hoechst stain (Sigma-Aldrich, St. Louis, MO, USA). Masson's trichrome

was used to differentiate between collagen and muscle morphology, and Hoechst stain was used as an additional tool to assess DNA presence.

VML Surgery: SAS Sprague-Dawley rats (250–300 g) were obtained from Charles River (Wilmington, MA, USA) and were divided into sham, empty defect, DMM (DMM+ 0 mM D-ribose), and AGE (DMM+ 250 mM D-ribose) experimental groups (N = 8 rats/group). All rats were given ad libitum access to standard pellets and water and provided environmental enrichment, as well as housed individually. All surgical procedures were performed under a VCU-approved protocol (IACUC #AD10000675). The VML surgeries were performed as described previously.[180] Briefly, rats were anesthetized, the skin was bluntly dissected above the right biceps femoris, and the biceps was then partially transected and resected to expose the gastrocnemius. The right gastrocnemius muscle was carefully separated from the soleus and plantaris. A 1.5 cm × 1 cm defect was cut in the lateral gastrocnemius, taking care to preserve the nerve. Sham surgeries were performed as described except when gastrocnemius was exposed, no muscle was removed. In grafted groups, the DMM or AGE-DMM was aligned to the muscle grain and sutured to the gastrocnemius with a horizontal mattress knot at the proximal and distal ends. The biceps femoris was sutured closed and the skin was stapled once the VML defect was created. All animals received IP injections of 2 mL 0.9% saline with 1% DMSO (Thermo Fisher Scientific, Waltham, MA, USA) to develop the model for future RAGE inhibitor treatments (e.g., DMSO is the delivery vehicle for the RAGE inhibitors FPS-ZM1 and Azeliragon). Injections were done one day before surgery and seven days after, followed by 3 times a week for the remainder of the study. All but one AGE animal survived. After 8 weeks, the animals were placed under anesthesia and muscle force testing was done using the Aurora Scientific 1305A 3-in-1 Whole Animal System for Rats (Aurora Scientific, Aurora, ON, Canada). Briefly, the right hindlimbs were secured to the foot pedal, and two needle electrodes was placed subcutaneously approximately 1 inch apart along the posterior-lateral line of the gastrocnemius, and the posterior hindlimb muscles were stimulated at 150 Hz to achieve tetany. Force transducers recorded the resulting torque produced on the foot pedal by plantar flexion. The animals were euthanized under anesthesia by cervical dislocation after the muscle force testing. The gastrocnemius muscles (right and left) were isolated, taking care to preserve any fibrosis or remaining DMM material on the injured muscles. Top-down gross morphological images were taken of all gastrocnemius muscles next to a surgical ruler. The right gastrocnemius muscles were then bisected perpendicular to the muscle grain, and the top half was used for histology and the bottom half was used for AGE and protein analysis. The top half was sliced a few mm thick against the muscle grain at the center of the injury and at the edge (25% of the distance between the proximal and distal sutures, measured from

the proximal suture line) of the injury, and these 2 slices were fixed in 10% neutral buffered formalin (VWR, Radnor, PA, USA). The bottom half of the muscle was frozen at -80ºC until homogenization. On the day of homogenization, 40 mg of the muscle in the injury area was biopsied and used for the assays.

AGE Analysis: For DMM analysis (after AGE induction) 30 mg of minced DMM was homogenized in 400 µL 1xPBS in a beadbug homogenizer (BeadBug™ Cat #: 31-212, Genesee Scientific, San Diego, CA, USA) at 4000 rpm for 60 seconds 5 times while keeping the tubes on ice for at least 5 min between runs. After mechanical homogenization, collagenase type III (STEMCELL Technologies Inc., Vancouver, Canada) (100 µL, 4000 U/mL in 1xPBS) was added to the homogenate and incubated at 37ºC for 1 hour. Then EDTA (Sigma-Aldrich, St. Louis, MO, USA) (0.5 M, 10 µL) was added to the collagenase-treated samples to quench the digest followed by centrifugation at 13,000 rpm (17,949 g) (Centrifuge 5427 R, Eppendorf, Hamburg, Germany) for 3 minutes. The supernatant was used for the assays.

Muscle biopsies taken from the injury area were minced and the Denaturing Buffer from the Minute™ Total Protein Extraction Kit for Muscles was added to 10 mg of minced muscle, and homogenization was done with a 6.0 mm zirconium bead in a beadbug homogenizer (BeadBug™ Cat #: 31-212, Genesee Scientific, San Diego, CA, USA) at 4000 rpm for 60 seconds 20 times while keeping the tubes on ice for at least 5 min between runs, followed by centrifugation at 13,000 rpm (17,949 g) (Centrifuge 5427 R, Eppendorf, Hamburg, Germany) for 3 minutes and the supernatant was used for the assays.

The supernatants were run on an AGE ELISA (STA-817, Cell Biolabs, San Diego, CA, USA) to determine AGE levels. The Pierce™ BCA Protein Assay Kit (23,225 and 23227, Thermo Fisher Scientific, Waltham, MA, USA) and hydroxyproline assays were used for normalization purposes. The supernatants were hydrolyzed for 24 h with 5N HCl at 120 °C before being run on the hydroxyproline assay (Chondrex, Woodinville, WA, USA).[25]

Histology: The middle and edge slices of gastrocnemius muscle were removed from the fixative 24 hours after fixation, dehydrated with increasing concentrations of ethanol followed by xylene, and embedded in paraffin blocks. Microtome sections (5 µm) were taken from each histological site, and placed on Histobond slides (VWR, Radnor, PA, USA) and were deparaffinized with xylene to allow for proper staining. They were then rehydrated, and stained with Masson's trichrome using Wiegert's hematoxylin (Sigma-Aldrich, St. Louis, MO, USA), Biebrich's scarlet-acid Fuchsia (Sigma-Aldrich, St. Louis, MO, USA), and aniline blue (Sigma-Aldrich, St. Louis, MO, USA). Coverslips were mounted with

xylene-based mounting media and allowed to dry flat before imaging. Stitching images were taken of the entire histological section using a 10x objective.

Histomorphometry: The Zen Pro software (Carl Zeiss Meditec AG, Jena, Germany) was used to perform the histomorphometry. Healthy muscle from the sham-operated animals was used as a positive control. Since the sections were stained with Masson's trichrome, the red features were muscle fibers, the blue features were collagen, and the dark purple features were nuclei. Due to the dynamic nature of skeletal muscle injuries, we employed a conservative method to determine the injury border (the border parallel to the muscle fibers). We based this method on the gross morphology of the contralateral muscle. Since the injured muscles presented a smaller muscle width due to muscle loss at the injury site, we overlayed the contralateral muscle belly outline onto the injured muscle, and measured 1 cm (the original injury was 1.5 cm into the muscle) into the injured muscle starting at the contralateral muscle belly for both the middle and edge histological sites. We subtracted any part of the 1 cm that was empty space and used the resulting distance to determine the distance into the injury we needed to measure on the histology. Histomorphometry was applied to all of the muscle tissue within this distance. Histomorphometry was used to quantify the area of total muscle, healthy muscle, regenerative muscle, collagen, and fat present. Each parameter was identified using the following: peripherally located nuclei indicated healthy muscle, centrally located nuclei indicated regenerative muscle, blue staining was collagen, and fat was identified by large vacuous white space with a surrounding membrane and nucleus. Additionally, muscle fiber diameter was measured using the minimum Feret diameter method.

Protein Analysis: In total, 30 mg of biopsied muscle was homogenized in NP- 40 lysis buffer (BP-119, Boston BioProducts, Ashland, MA, USA) with a PI cocktail and 25 mM NaF with a 6.0 mm zirconium bead in a beadbug homogenizer (BeadBugTM Cat #: 31-212, Genesee Scientific, San Diego, CA, USA) at 4000 rpm for 60 s 5 times. The tubes were kept on ice for at least 5 min between runs. The homogenate was centrifuged at 9703 rpm (10,000× g) (Centrifuge 5427 R, Eppendorf, Hamburg, Germany) for 10 min, and the supernatant was used for dot blotting according to Bio-Rad manufacturer protocol, which utilizes a 0.45 µM nitrocellulose membrane. Following overnight staining with primary antibodies, the membranes were then incubated with secondary antibodies (926-68073, 926-32210, and 926-32211, LI-COR Biosciences, Lincoln, NE, USA) for 40 min at room temperature, then they were imaged on the LI-COR Odyssey and quantified. Target protein signals normalized by the total

protein signal, and included RAGE, phosphorylated p38, Pax7, MyoD, Myf5, MyoG, neonatal myosin, as well as myosin heavy chains.

Mass Spectrometry Analysis: 3 random samples per group were selected from Sham, DMM, and AGE, and 40 µL of the protein isolate from the protein analysis section were sent to UVA's mass spectrometry core, and the samples were solubilized using a Bead Beater with stainless steel balls before acetone precipitation to produce a protein pellet. The pellet was re-solubilized in digestion buffer using heat and sonication. The sample were reduced with DTT for 30 minutes at RT, then alkylated using iodoacetamide for 30 minutes at RT, followed by overnight digestion with 0.5 ug trypsin. The samples were cleaned up using beads and C18 tips. The LC-MS system consisted of a Thermo Orbitrap Exploris 480 mass spectrometer system with an Easy Spray ion source connected to a Thermo 3 µm C18 Easy Spray column (through pre-column). 1 µg of the extract was injected and the peptides eluted from the column by an acetonitrile/0.1 M acetic acid gradient at a flow rate of 0.3 µL/min over 2.0 hours. The nanospray ion source was operated at 1.9 kV. The digest was analyzed using the rapid switching capability of the instrument acquiring a full scan mass spectrum to determine peptide molecular weights followed by product ion spectra (Top10 HCD) to determine amino acid sequence in sequential scans. This mode of analysis produces approximately 25000 MS/MS spectra of ions ranging in abundance over several orders of magnitude. Not all MS/MS spectra are derived from peptides. The data were analyzed by database searching using the Sequest search algorithm against Uniprot Rat.

Statistical Analysis: Each variable was tested using N = 8 independent animals unless specified. Data are presented as mean ± SEM with the analysis done using GraphPad Prism 6.0 (GraphPad, La Jolla, CA, USA). Outliers were removed according to Grubb's test (α-0.05). Analysis comparing only two groups was performed by unpaired Student's t-test, whereas analysis comparing more than two groups using one-way analysis of variance with Tukey's posthoc test. All p values $\leq$ 0.05 were considered significant.

Results

Masson's trichrome stain revealed a collagenous matrix in DMM, and no nuclei were observed at 100x magnification (Figure 35A-B, Figure 36A). Despite elevated background Hoechst staining compared to no stain controls, nuclei were not observed at 100x magnification, confirming the absence of the nuclear element (Figure 36B). Agarose gel electrophoresis of DMM stained with ethidium bromide indicated no DNA presence in the DMMs compared to whole muscle control (Figure

36C). We successfully created AGEs in DMM at 250 mM, and this translated into reduced soluble hydroxyproline (Figure 36D-E) as previously shown [25]. Total AGEs and AGEs per wet weight increased in a D-ribose dose-dependent manner, while wet weight remained the same (Figure 37A-C). Further, the protein data had a similar trend to the hydroxyproline data (Figure 37D-E).

Over 8 weeks, animal body weights increased from 300 to 400 grams, and there were no differences amongst the groups (Figure 38). The gross morphology of the gastrocnemius after 8 weeks showed a volumetric deficit in the empty group (Figure 39A). Although muscle weight and muscle width decreased with VML injury, DMM treatment with and without AGEs did not recover these parameters (Figure 39B-C). Interestingly, the AGE group had a larger width than the empty group, though not as large as sham (Figure 39C). The maximum tetanic force was reduced in Empty from sham, validating our VML model (Figure 39D). The maximum tetanic force did not differ in DMM and AGE-treated injuries compared to sham and Empty. Max rate of relaxation decreased in the Empty group, while there was not a difference in other force-time analysis outcomes (Figure 40). Graft area was measured in the gross morphological images, and more graft material was observed in the AGE group compared to DMM (Figure 39E). Muscle biopsies in the injury site had elevated soluble hydroxyproline in DMM compared to AGE, which is inversely correlated to collagen cross-linking (Figure 39F). However, the number of AGEs per hydroxyproline was not different in the AGE group compared to DMM, despite an elevated mean (Figure 39I). Interestingly, as we have reported previously, AGEs were higher in sham compared to the grafted groups, which may be due to the increase of injury-related nascent collagen.[309]

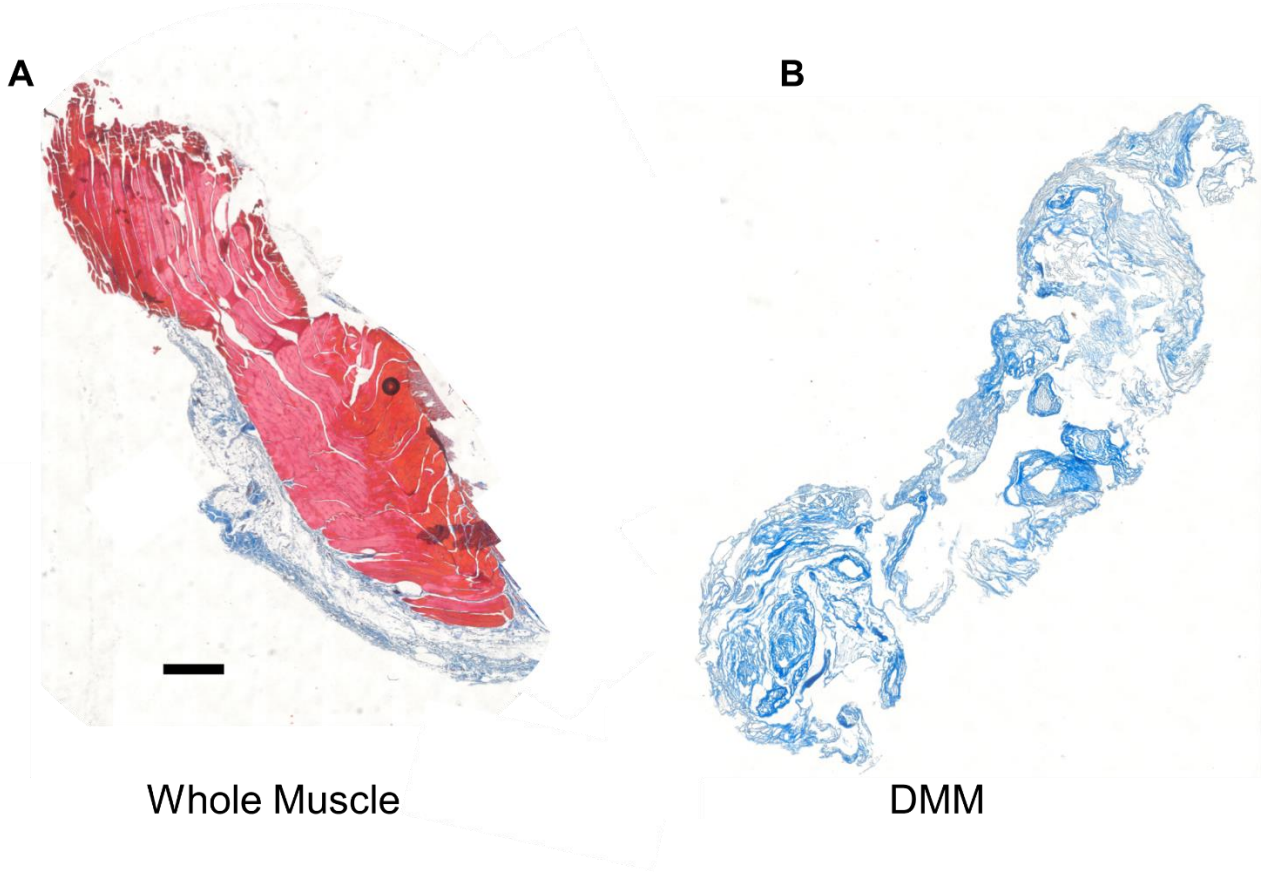

Figure 35: Whole histological sections show absence of muscle tissue in DMM. A) Whole muscle stained with Masson's trichrome (red=muscle, blue=collagen). B) DMM stained with Masson's trichrome showed lack of muscle tissue. (Scale bar= 500 mm)

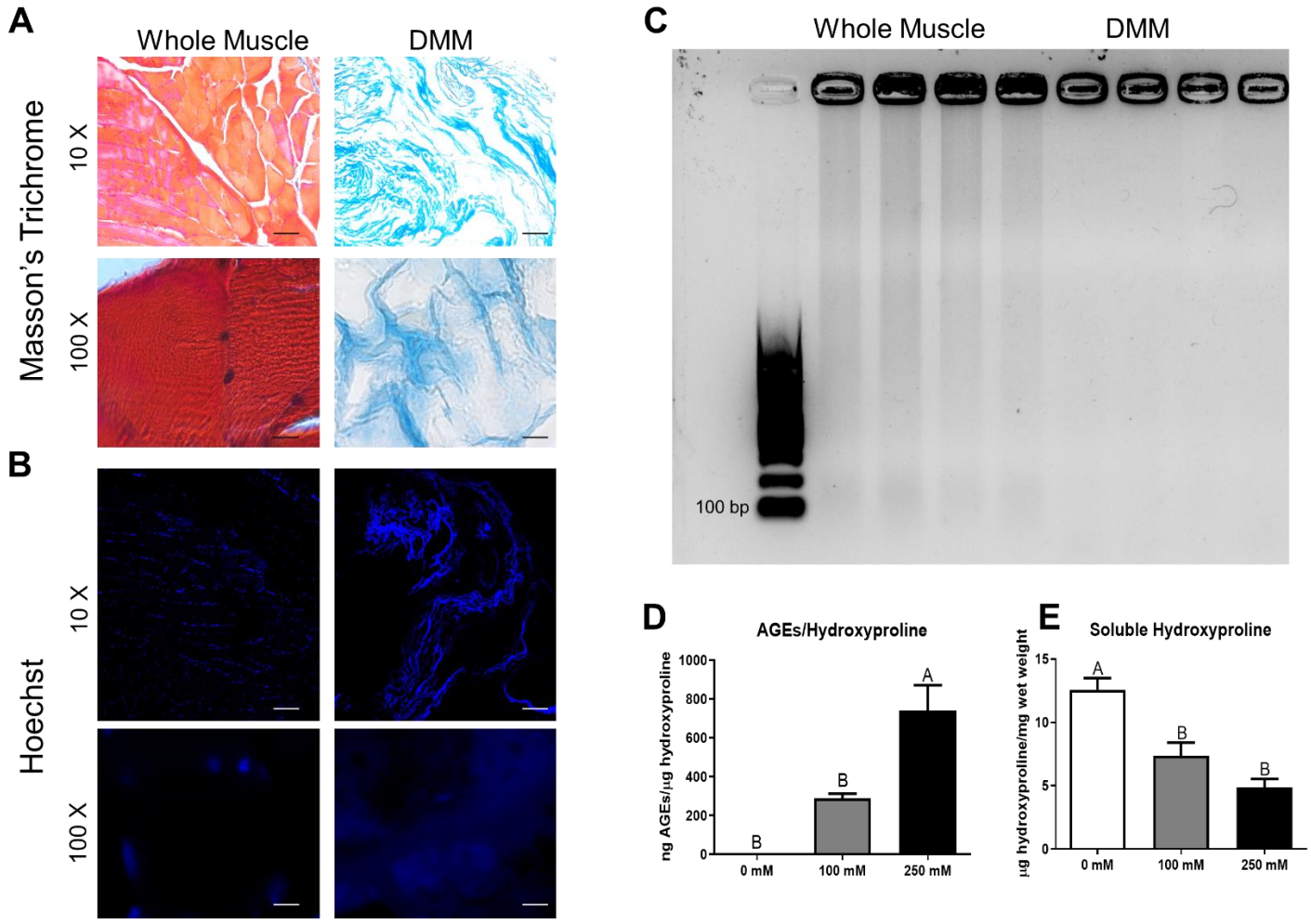

Figure 36: Decellularizing whole muscle into DMM produced a collagenous scaffold free of the nuclear element, and allows for AGE formation. A-B) Whole muscle and DMM were stained with Masson's Trichrome (red=muscle, blue= collagen, dark purple= nuclei) (A) and Hoechst nuclear stain (B) visualized at 10x (scale bar=100 µm) and 100x (scale bar=10 µm). DMM did not retain the nuclear or cytoplasmic elements. C) Whole muscle and DMM DNA extracts were ran on an agarose gel and DNA was visualized with ethidium bromide (lowest ladder band is 100 bp), with DMM having an absence of genomic DNA. D-E) DMM was incubated with 0, 100, and 250 mM D-ribose for 5 days, and AGE and hydroxyproline levels were assayed. AGEs/hydroxyproline was higher with 250 mM D-ribose, and soluble hydroxyproline was reduced with 100 and 250 mM D-ribose.

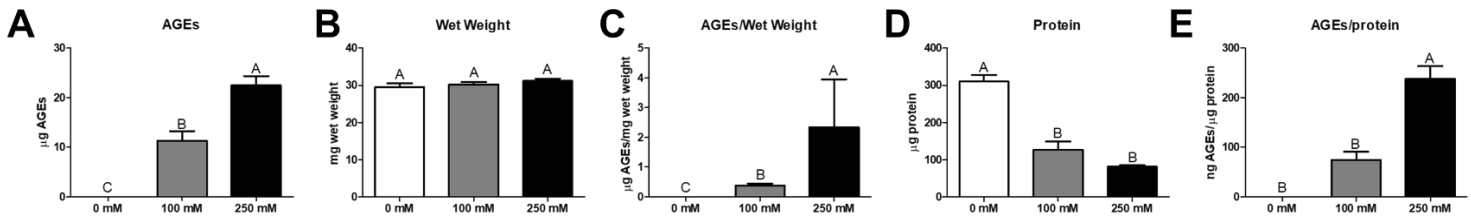

Figure 37: D-ribose incubation increased AGEs in DMM when normalized by wet weight and protein. A) AGEs, without normalization, increased in DMM at 100 and 250 mM D-ribose. B) The wet weight of the DMM biopsy after D-ribose incubation was consistent. C) AGEs normalized to wet weight increased in DMM at 100 and 250 mM D-ribose. D) Extracted protein levels decreased with D-ribose incubation. E) AGEs per protein was increased in the 250 mM D-ribose group only.

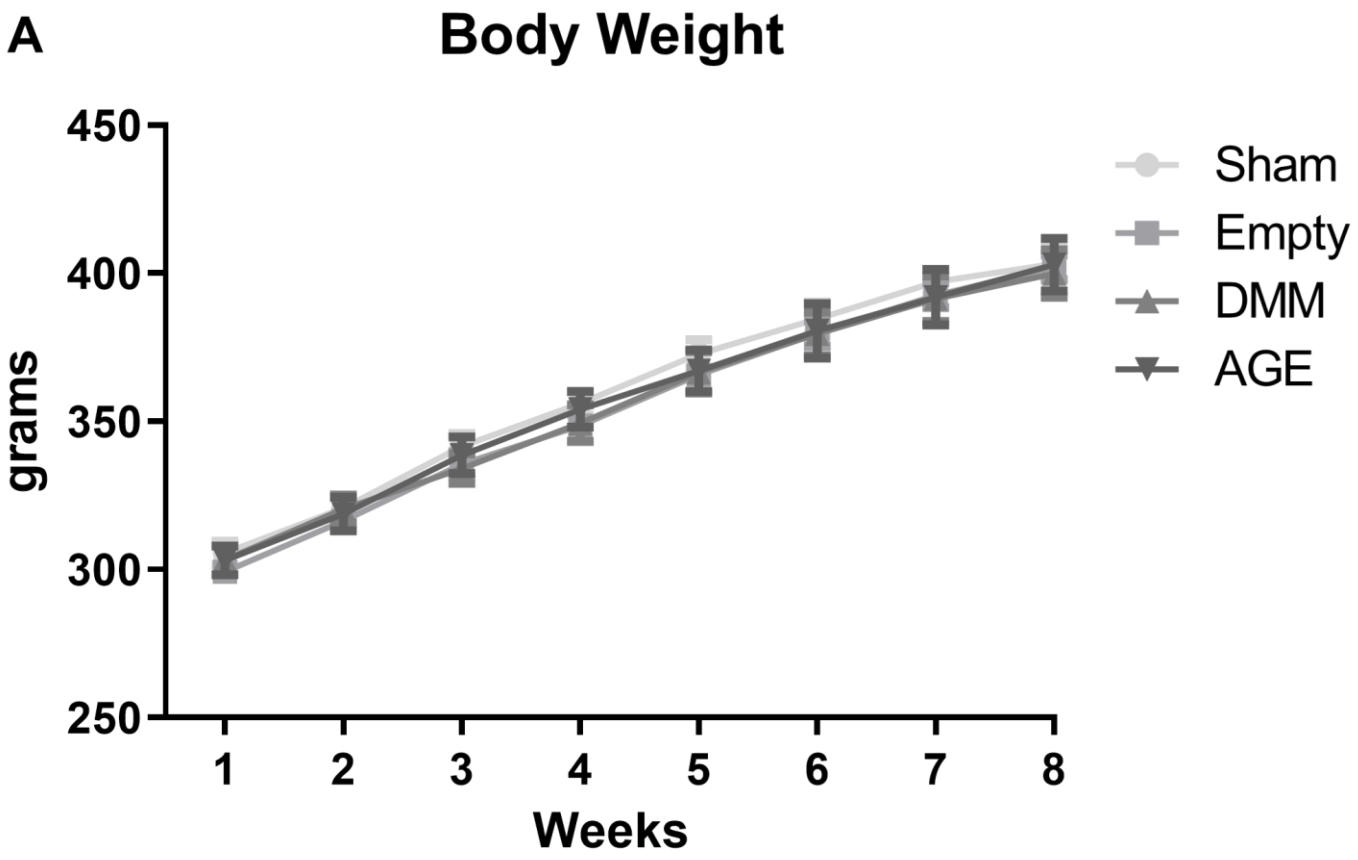

Figure 38: Body weight increased throughout the study, and there was no group effect.

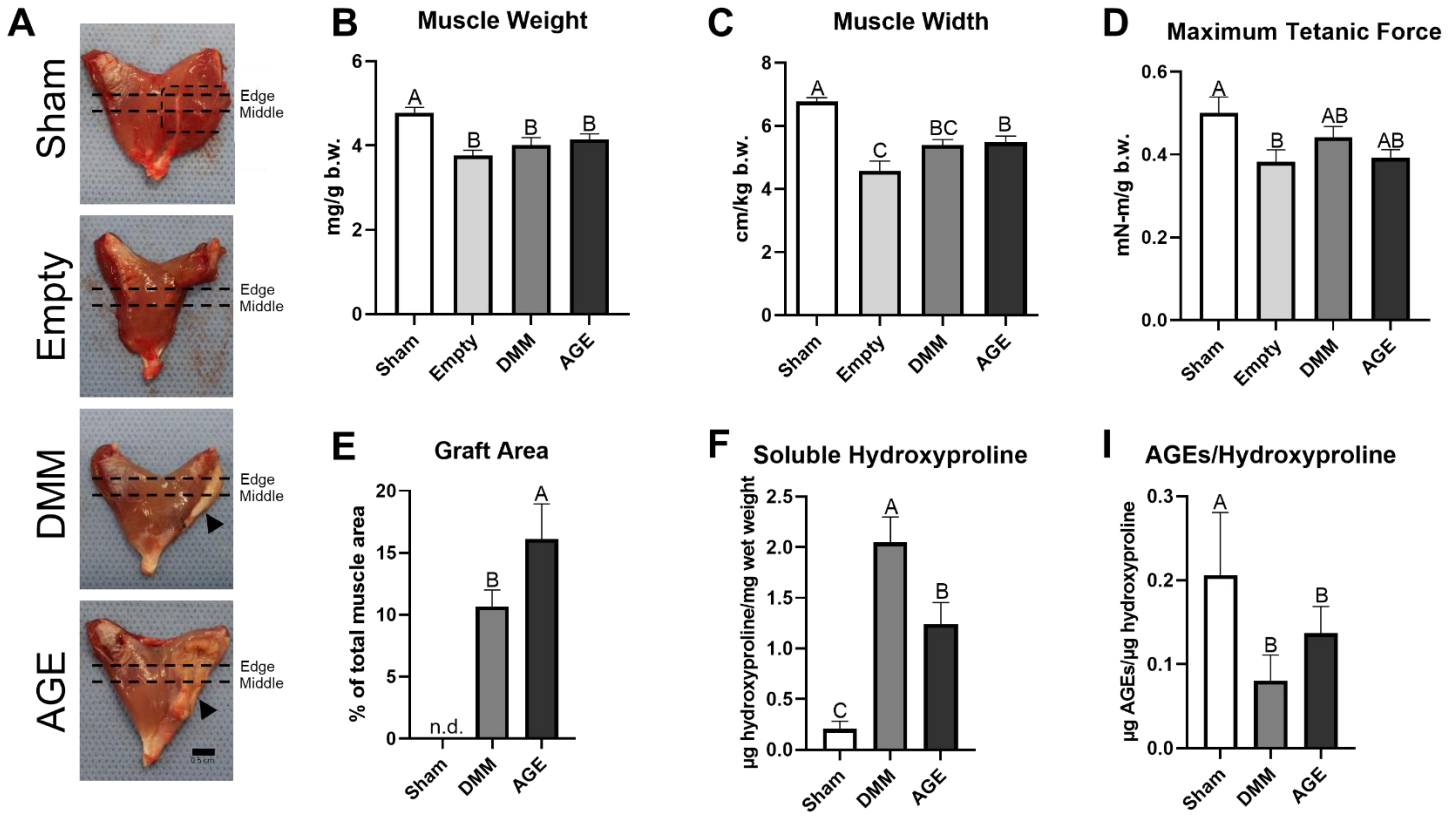

Figure 39: VML injury produced pronounced muscle mass and force deficits, while AGEs produced higher graft area associated with increased collagen cross-linking. A) Gross morphological images on explanted gastrocnemii were taken 8-weeks post-surgery (original injury area outlined on Sham; the edge and middle histological cuts are shown; implant area indicated by the black arrow; scale bar is 0.5 cm). Empty showed reductions in muscle mass, while this was not the case with DMM and AGE. AGE had more visible graft material than DMM. B-C) Muscle weight and width were measured and normalized to total body weight, and both parameters were reduced in all injury groups. D) Maximum tetanic force, which is the peak of the tetanic force curve, was measured and Empty had reduced force compared to Sham. E) Graft area, as visualized on the gross morphological images, was quantified, and the AGE group had increased graft compared to DMM. F-I) Soluble hydroxyproline and AGEs were measured in muscle tissue biopsies, and AGE had significantly less soluble hydroxyproline than DMM, but had similar AGE levels to DMM.

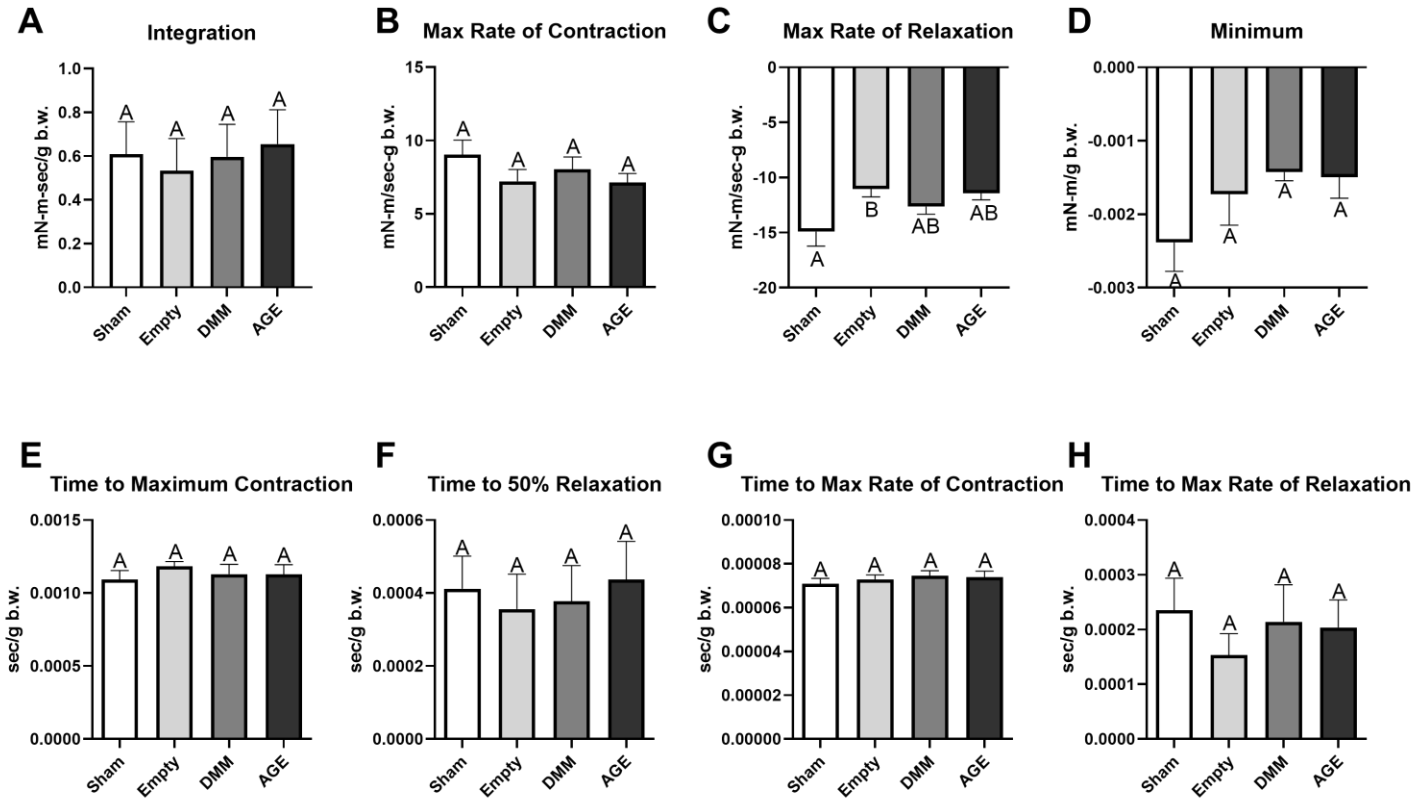

Figure 40: Tetanic muscle force curve analysis showed differenced in max rate of relaxation. A-B) There was no difference in integration and max rate of contraction. C) Max rate of relaxation was decreased in the Empty group compared to sham. D-H) There was no difference in minimum, time to maximum contraction, time to 50% relaxation, time to max rate of contraction, and time to max rate of relaxation.

Histological cross-sections were taken at the center and edge of the defect (locations shown in Figure 41B). Masson's trichrome staining showed increased collagen levels in DMM and AGE groups and evidence of muscle fiber regeneration (Figure 41A). Histomorphometry was analyzed and the total muscle area at the edge and center was lower in DMM and AGE compared to the sham (Figure 41C). Total muscle fiber number was reduced at the edge in AGE only compared to sham, while both AGE and DMM had reduced total muscle fiber number compared to sham at the middle (Figure 41D). Curiously, there was a reduction in total muscle fiber diameter in DMM and AGE at the edge only (Figure 41E). AGE-treated animals possessed higher levels of collagen area compared to DMM and sham, and this was true both at the edge and middle (Figure 41F). Further, DMM had more collagen area than sham at both locations (Figure 41F). Healthy muscle area was reduced in DMM and AGE

relative to sham at the edge and middle (Figure 41G). Healthy muscle fiber number was reduced in DMM and AGE at both histological sites (Figure 41H). Healthy muscle fiber diameter was reduced in AGE at the middle compared to the other groups (Figure 41I). Curiously, fat content measured from the edge and middle of the defect was higher in DMM compared to sham and AGE (Figure 41J). DMM and AGE animals displayed more de novo muscle at the edge compared to the sham, confirming active regeneration (Figure 41K). Interestingly, regenerative area was only increased in DMM compared to sham at the middle (Figure 41K). When the middle and edge of the graft were compared, regeneration was qualitatively reduced in the middle of the injury compared to the edge. Regenerative muscle fiber number was increased in DMM compared to sham at the edge and middle (Figure 41L). The regenerative muscle fiber diameter was significantly increased in DMM and AGE at both the edge and middle (Figure 41M). Histograms and the gaussian curve for the muscle fiber diameter data communicated similar group differences (Figure 42).

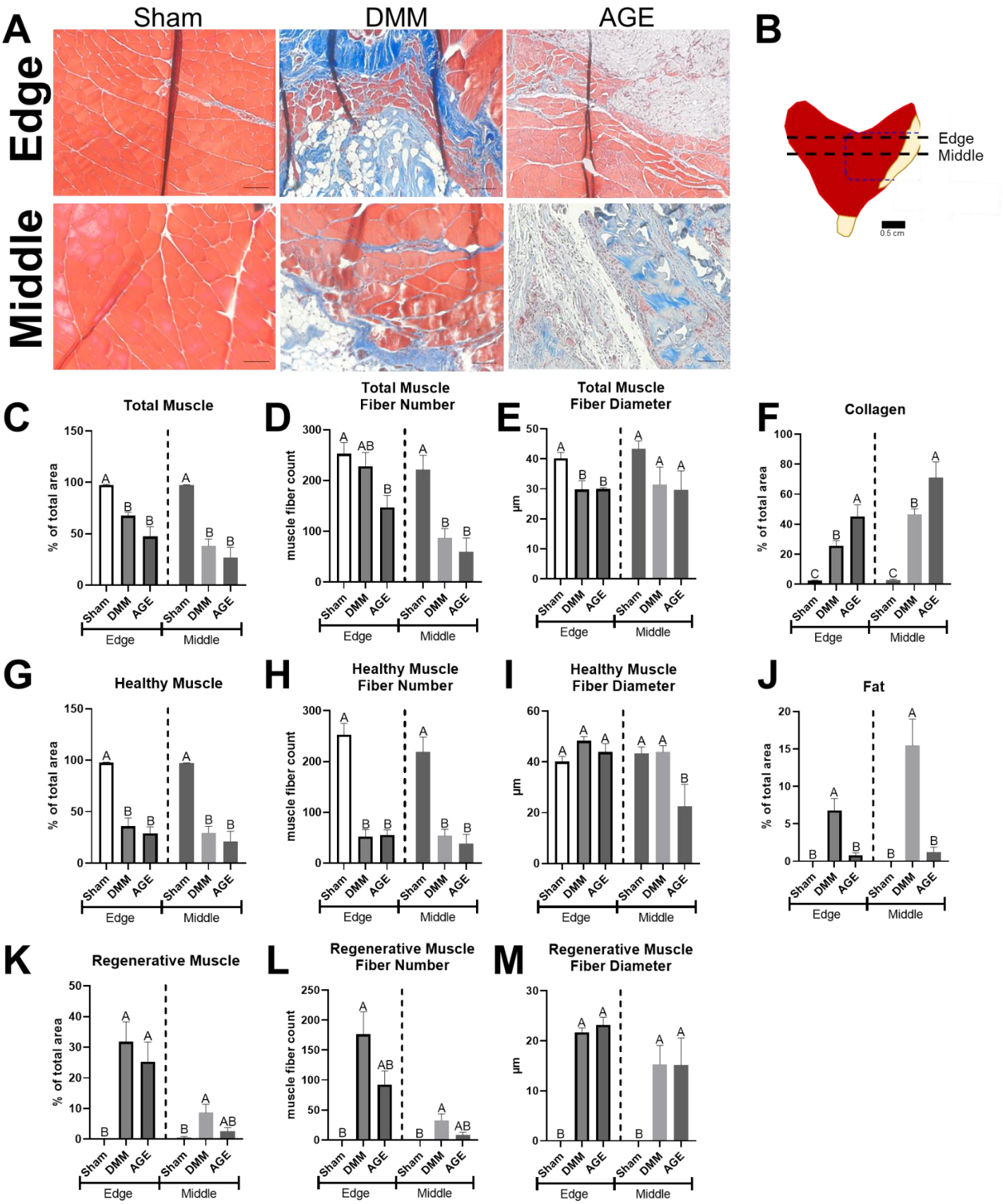
A
Sham
DMM
AGE
Edge
Middle
B
Edge
Middle
0.5 cm
C
Total Muscle
% of total area
D
Total Muscle Fiber Number
muscle fiber count
E
Total Muscle Fiber Diameter
µm
F
Collagen
% of total area
G
Healthy Muscle
% of total area
H
Healthy Muscle Fiber Number
muscle fiber count
I
Healthy Muscle Fiber Diameter
µm
J
Fat
% of total area
K
Regenerative Muscle
% of total area
L
Regenerative Muscle Fiber Number
muscle fiber count
M
Regenerative Muscle Fiber Diameter
µm
Sham
DMM
AGE
Edge
Middle

Figure 41: Histological cross-sections were taken at the center and edge of the defect, and revealed that the AGE group had higher collagen and reduced regeneration compared to DMM. A) Masson's trichrome (red=muscle, blue=collagen, scale bar= 100 μm) visualized the injury site, and increased collagen levels were observed in DMM and AGE groups, along with evidence of muscle fiber regeneration. B) A schematic showing where the edge and middle were cut (black dashed lines) and the original injury area (blue dashed line); scale bar is 0.5 cm. C) Total muscle area at the edge and middle was reduced in DMM and AGE compared to sham. D) Total muscle fiber number was lower at the edge in AGE compared to the sham control, while both grafted groups were reduced in total muscle fiber number relative to sham at the middle. E) Total muscle fiber diameter was reduced in DMM and AGE at the edge only. F) The AGE group had elevated levels of collagen area compared to DMM and sham both at the edge and middle. Also, DMM presented elevated collagen area compared to sham at both locations. G) DMM and AGE groups had lower healthy muscle area relative to sham at the edge and middle. H) Healthy muscle fiber number was lower in grafted groups at both histological sites. I) Interestingly, healthy muscle fiber diameter was lower in AGE at the middle compared to sham and DMM. J) Fat area was higher in DMM compared to sham and AGE at both locations. K) DMM and AGE had more regenerative muscle area at the edge compared to the sham, confirming active regeneration. Also, regenerative area was increased in DMM only compared to sham at the middle. L) Regenerative muscle fiber number was elevated in DMM compared to sham at the edge and middle, although it was not different from the AGE group. M) Regenerative muscle fiber diameter was higher in DMM and AGE at both the edge and middle.

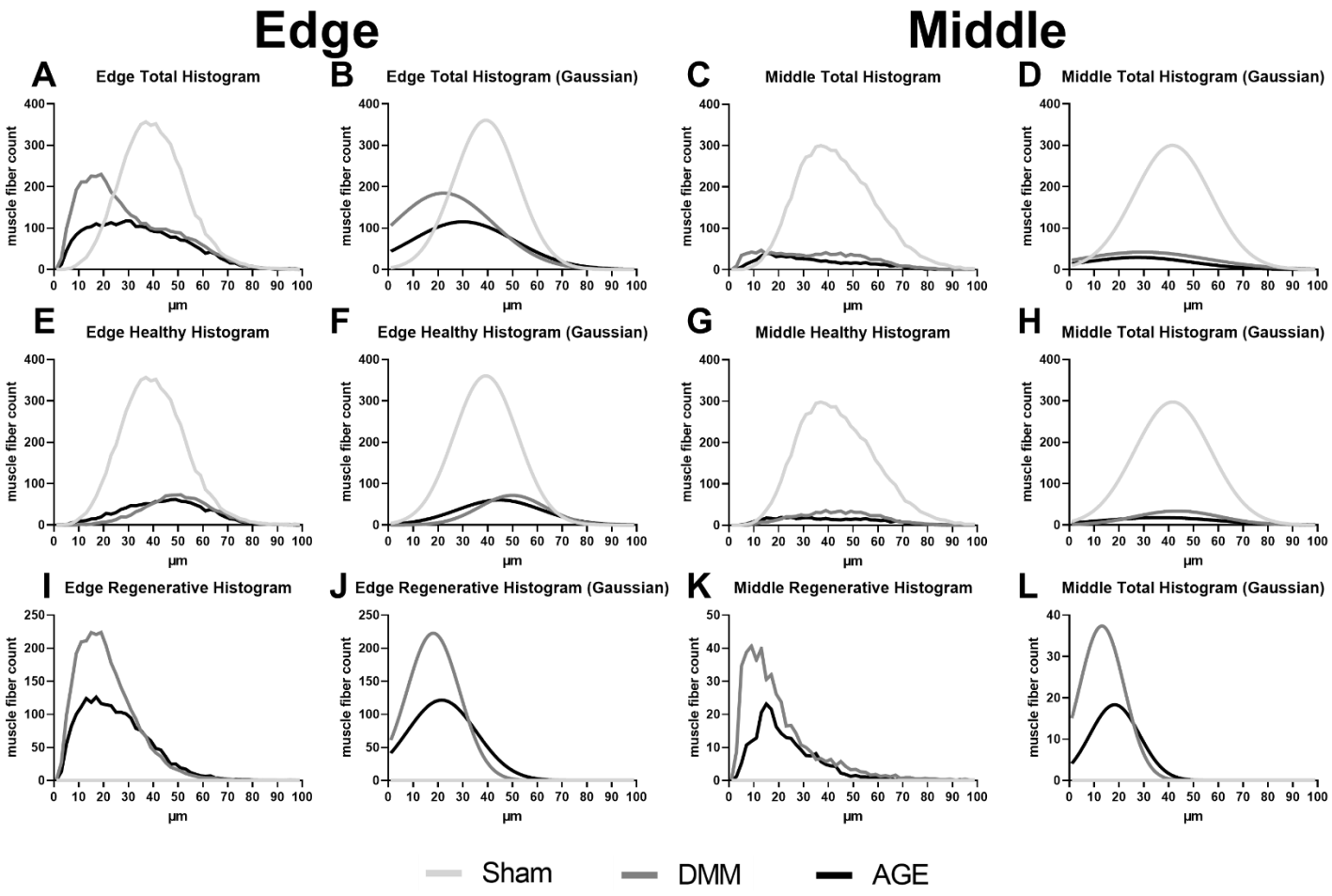

Figure 42: Muscle fiber diameter histograms clearly show that injury groups have reduced spread and amplitude from sham, and DMM shows a higher amplitude for regenerative fibers. A-B) Total muscle fiber histogram at the edge showed that the AGE group was reduced from DMM and sham, while DMM was also reduced from sham. C-D) Both DMM and AGE had reduced total muscle fiber histogram at the middle. E-H) Healthy muscle histograms showed a reduced amplitude for DMM and AGE compared to sham at the edge and the middle. I-L) Regenerative muscle fiber histogram was reduced in AGE compared to DMM at the edge and middle.

The presence of various muscle differentiation and maturation markers was measured in sham, DMM, and AGE groups. Pax7 and MyoD were higher in DMM and AGE compared to sham (Figure 43A-B). AGE muscles displayed more Myf5 compared to DMM and sham (Figure 43C). Myogenin (MyoG) was higher in DMM and AGE compared to Sham (Figure 43D). The MyoG/Myf5 ratio, which is positively correlated with myogenic differentiation, was increased in the DMM group compared to AGE (Figure 43E). Neonatal myosin, fast-twitch MyHC, and slow-twitch MyHC were elevated in grafted groups relative to sham, but AGEs did not have an effect compared to DMM (Figure 43F-H). The total amount of RAGE was highest in sham compared to VML treated injuries (as was previously shown) and significantly elevated in the AGE group compared to DMM alone, where RAGE was barely detectable (Figure 43I).[309] Phosphorylated p38 MAPK, a downstream member of the RAGE pathway, was not different between DMM and AGE groups (Figure 43J).

Mass spectrometry analysis was performed on 3 randomized protein samples per group. 1994 unique proteins were discovered and quantified. When presented as a heatmap, the DMM and AGE groups were similar but differed from sham (Figure 44A). The data was presented with a present/absent criterion on a Venn diagram, and all groups shared 1631 proteins, while DMM and AGE shared more proteins (210) than either group shared with sham (Figure 44B). Interestingly, the AGE group had 38 unique proteins compared to only 9 in DMM. Next, a fisher's exact test was employed to determine which proteins were significantly regulated by AGEs compared to the DMM group. 111 proteins were found to be significant, and these were displayed as a Volcano plot with 58 proteins upregulated and 53 downregulated in the AGE group (Figure 44C). Further, 15 muscle-specific proteins were pulled from the 111, and 13 were significantly downregulated by AGEs (Figure 44D). Finally, all three groups were analyzed with an analysis of variance followed by the Benjamini-Hochberg multiple test correction, and the significant proteins in either DMM or AGE were matched to GO pathway terminology (biological process and cellular component), and graphed on pie charts (Figure 44E). The immune system process was increased in the AGE group compared to DMM, and the extracellular region was decreased in the AGE group compared to DMM.

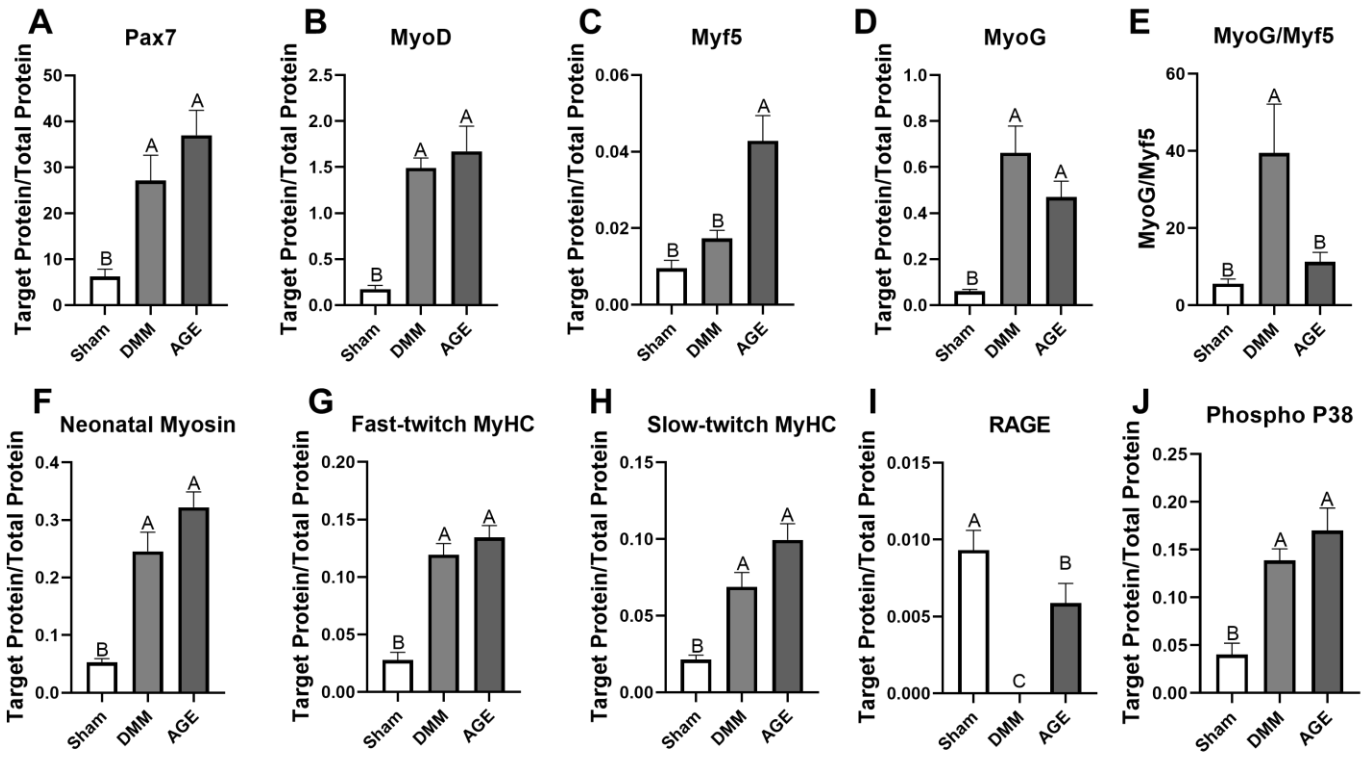

Figure 43: AGEs show an early differentiation phenotype and higher RAGE levels compared to DMM. A-B) Pax7 and MyoD were elevated in grafted groups compared to sham. C) The AGE group had more Myf5 relative to sham and DMM. D) Myogenin (MyoG) was increased in DMM and AGE. E) The MyoG/Myf5 ratio was increased in DMM relative to the AGE group, indicating a later differentiation phenotype in DMM. F-H) Neonatal myosin, fast-twitch MyHC, and slow-twitch MyHC were increased in injury groups. I) Sham had higher RAGE levels than DMM and AGE, and AGE had higher levels than DMM. J) Phosphorylated p38 MAPK, a member of the RAGE pathway, was increased in DMM and AGE, however levels did not differ between DMM and AGE.

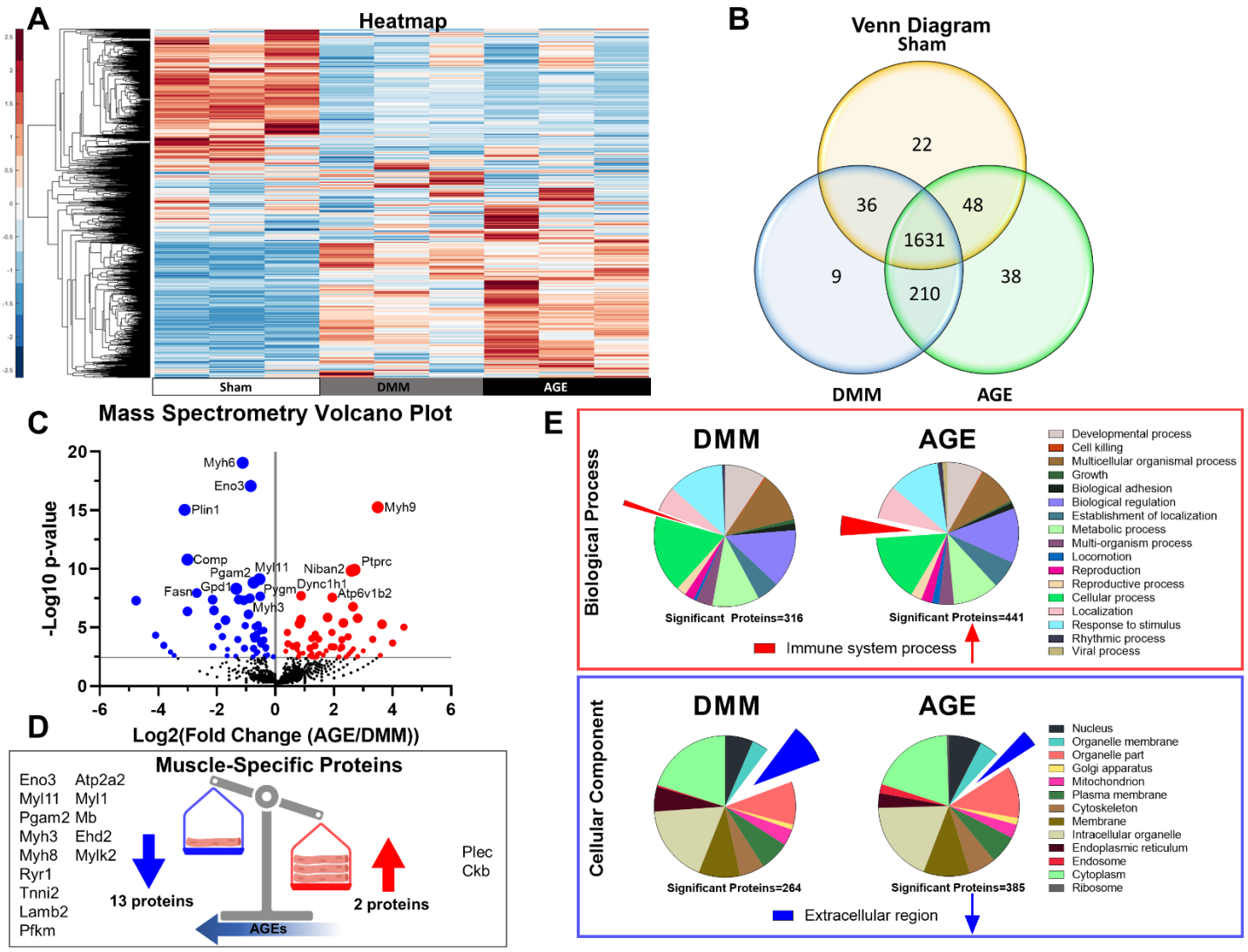

Figure 44: Mass spectrometry analysis showed critical differences between AGE and DMM, including suppression of muscle markers, increased immune system involvement, and decreased extracellular region by AGEs. A) 1994 unique proteins were analyzed and presented as a heatmap, and DMM and AGE groups were differed from sham. B) Venn diagram analysis showed all groups shared 1631 proteins, and DMM and AGE shared more proteins (210) than with sham. C) 111 proteins were significantly regulated by AGEs compared to DMM, and these were displayed on a volcano plot. D) Further, 15 muscle-specific proteins were found, with 13 being significantly downregulated by AGEs. E) Significant proteins in either DMM or AGE were matched to GO pathway terminology (biological process and cellular component), and graphed. The immune system process was larger in the AGE group compared to DMM, and the extracellular region was smaller in the AGE group compared to DMM.

Fisher's exact test was used again to compare AGE and DMM groups, and proteins matching to the immune system process and extracellular region GO terms were sorted for and visualized via volcano plots (Figure 45A-B). A total of 11 proteins were significantly regulated by AGEs under the immune system process umbrella, and 8 of these were increased. 20 proteins in the extracellular region category were regulated by AGEs, and 15 of them were downregulated. Of note, the immune-associated proteins receptor-type tyrosine-protein phosphatase C (Ptprc), Coronin-1A (Coro1a), Complement component C6 (C6 protein), Actin-related protein 2 (Actr2), Monocyte differentiation antigen CD14 (Cd14), H-2 class II histocompatibility antigen gamma chain (Cd74), Protein NDRG1 (Ndrg1), Sphingosine-1-phosphate lyase 1 (Sgpl1), and Myosin-9 (Myh9) were all upregulated by AGEs (Figure 6C-E,I-K,O-Q). Further, the extracellular-associated proteins Collagen I alpha-2 chain (Col1a2), Adipocyte enhancer-binding protein 1 (Aebp1), Laminin subunit beta-2 (Lamb2), Cartilage oligomeric matrix protein (Comp), Olfactomedin-like protein 1 (Olfml1), Fibromodulin (Fmod), C-type lectin domain family 11 member A (Clec11a), Thrombospondin-4 (Thbs4), and Carboxylesterase 1D (Ces1d) were reduced by AGEs (Figure 6F-H,L-N,R-T).

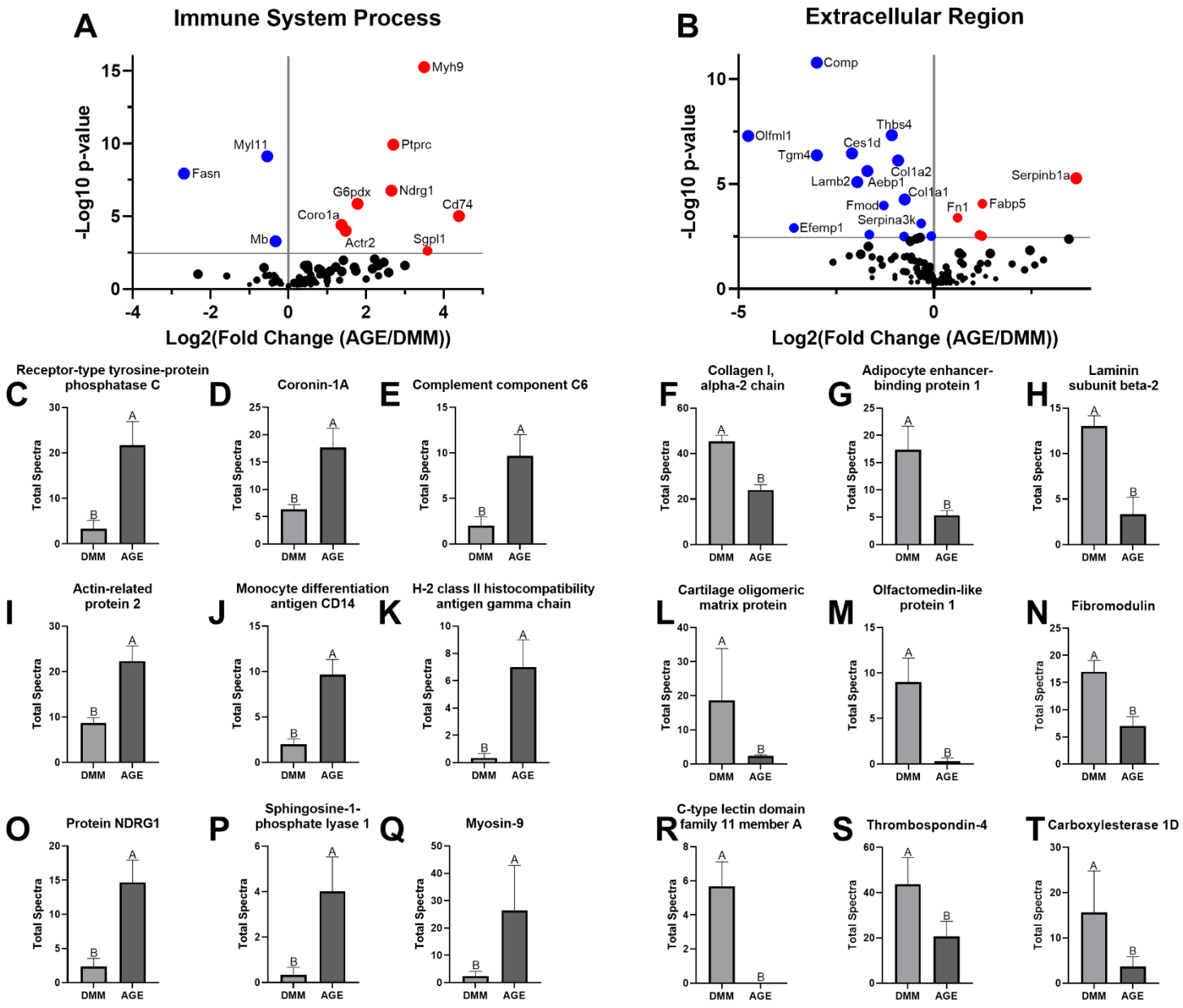

Figure 45: Proteins matching to the immune system process and extracellular region GO terms were investigated. A) 11 proteins were regulated by AGEs under the immune system process GO term, and 8 were increased. B) 20 proteins in the extracellular region GO term were impacted by AGEs, with 15 of them were downregulated. C-E,I-K,O-Q)Specifically, the immune-associated proteins receptor-type tyrosine-protein phosphatase C (Ptprc), Coronin-1A (Coro1a), Complement component C6 (C6 protein), Actin-related protein 2 (Actr2), Monocyte differentiation antigen CD14 (Cd14), H-2 class II histocompatibility antigen gamma chain (Cd74), Protein NDRG1 (Ndrg1), Sphingosine-1-phosphate lyase 1 (Sgpl1), and Myosin-9 (Myh9) were all increased by AGEs. F-H,L-N,R-T)

Additionally, the extracellular-associated proteins Collagen I alpha-2 chain (Col1a2), Adipocyte enhancer-binding protein 1 (Aebp1), Laminin subunit beta-2 (Lamb2), Cartilage oligomeric matrix protein (Comp), Olfactomedin-like protein 1 (Olfml1), Fibromodulin (Fmod), C-type lectin domain family 11 member A (Clec11a), Thrombospondin-4 (Thbs4), and Carboxylesterase 1D (Ces1d) were lowered by AGEs.

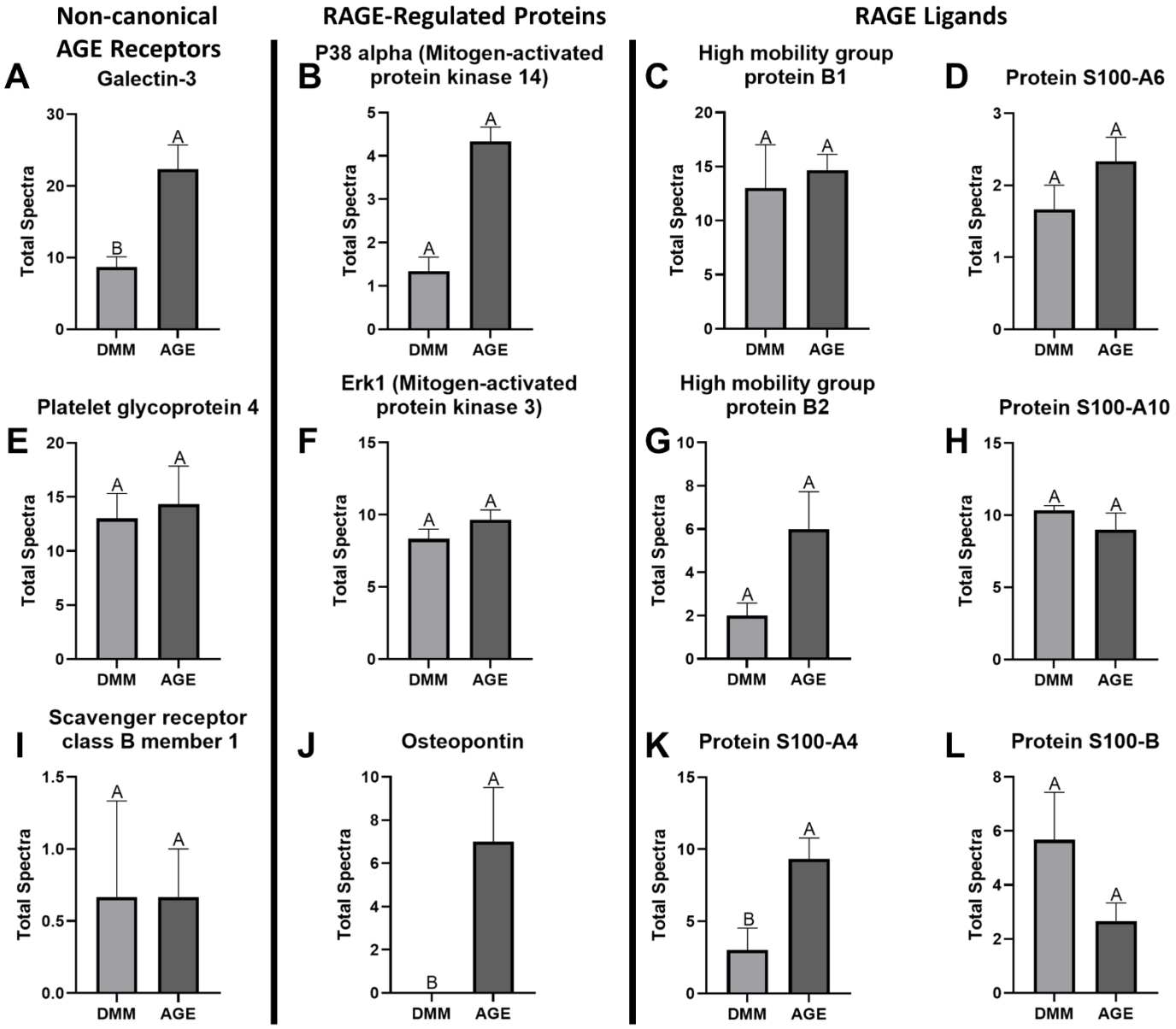

Figure 46: AGE and RAGE-specific protein analysis. A) Galectin-3, an AGE receptor, was increased in the AGE group. E,I) Platelet glycoprotein 4 and Scavenger receptor class B member 1, two more AGE receptors, were detected but not regulated by AGEs. B) The RAGE pathway member P38α, or

Mitogen-activated protein kinase 14, was detected at elevated levels in the AGE group, but not at a statistically different level. F,J) There was no change in Erk1 (Mitogen-activated protein kinase 3), while osteopontin was significantly increased in the AGE group. C-D,G-H,K-L) The RAGE ligands High mobility group protein B1, High mobility group protein B2, Protein S100-A4, Protein S100-A6, Protein S100-A10, and Protein S100-B were present, but only Protein S100-A4 showed a significant increase in the AGE group. .

Next, we focused on AGE and RAGE-specific proteins. Galectin-3, a non-canonical AGE receptor, was increased in the AGE group (Figure 46A). Platelet glycoprotein 4 and Scavenger receptor class B member 1, two more non-canonical AGE receptors, were detected but did not differ significantly in the presence of AGEs (Figure 46E,I). Next, we investigated RAGE-pathway related proteins. P38α, or Mitogen-activated protein kinase 14, was detected at higher levels with AGEs, but the difference was not statistically noteworthy (Figure 46B). There was no difference detected in Erk1 (Mitogen-activated protein kinase 3), and osteopontin was significantly increased by AGEs (Figure 46F,J). The RAGE ligands High mobility group protein B1, High mobility group protein B2, Protein S100-A4, Protein S100-A6, Protein S100-A10, and Protein S100-B were detected, but only Protein S100-A4 showed a significant difference, with higher levels due to AGEs (Figure 46C-D,G-H,K-L).

Challenges

The decellularization protocol we relied on in chapter 3 was not sufficient for the much larger rat gastrocnemius muscles. We went through an extended optimization process, whereby we increased the solution volumes, length of time, and concentration of the components involved. Ultimately, we landed on a 7-day protocol that decellularized the muscles in beakers with constant stirring. Additionally, we incorporated the zwitterionic detergents CHAPS and SB-16 to enhance the process. Our novel decellularization process produced a rat gastrocnemius DMM large enough to repair a 1.5x1.0 cm VML injury.

Discussion

The goal of this study was to ascertain whether AGEs on DMM could be used as a model of old muscle ECM and to determine the role of glycations in DMM-mediated regeneration. We developed a model of aged DMM by inducing AGE cross-links on young DMM, observing a higher number of collagen cross-links than the control DMM. The increased AGE counts per hydroxyproline were similar to aged DMM.[25] As such, we have established a model of skeletal muscle aging that solely captures AGE-

crosslinking. The advantage of this model is that we can make declarative statements about AGEs alone by removing other known confounding aging variables such as increases in total collagen content, pathological increases in laminin, decreased fibronectin, and decreased ECM growth factor presence.[15,25,239,310]

We selected a challenging 1.5 × 1 cm full-thickness gastrocnemius defect in a Sprague Dawley rat as our VML model since it was previously characterized by our group to produce a sufficient deficit to test DMM's regenerative capacity.[180] We confirmed our model by demonstrating that muscle weight, width, and tetanic force were all reduced in untreated animals (empty defect). As we have previously shown, DMM treatment somewhat recovered tetanic force. Interestingly, AGEs did not negatively affect muscle force, and this could be due to the development of functional fibrosis to transmit muscle force that is comparable to non-glycated DMM.[276] Furthermore, our model is limited by the measurement of all posterior crural muscles instead of isolating the lateral head of the gastrocnemius, and these additional muscles are likely contributing to overall force output.

AGEs tightly regulate collagen degradation and deposition, preventing collagen degradation via cross-linking and challenging the immune system to promote a pro-inflammatory environment that perpetuates fibrosis.[238,311–313] Supporting this, more collagen was measured in AGE-treated DMM compared to non-glycated DMM with 45% at the edge and up to 71% in the middle. Collagen is synthesized by fibroblasts, fibroadipogenic progenitor cells (FAPs), and myoblasts.[314] Collagen-specific AGE crosslinks using methylglyoxal changed the way cardiac fibroblasts interpreted collagen fibers, promoting a myofibroblast phenotype mediated via TGF-β signaling.[315] These results support the idea that AGE-treated DMM could be influencing fibroblasts in our model.[316] FAPs are a mesenchymal-like cell population that have the capacity to differentiate down either an adipogenic or myofibroblast lineage to support muscle regeneration, increase fat, or increase fibrosis.[316,317] Interestingly, total fat was highest in DMM while AGE-treated DMM suppressed total fat formation near sham levels. Prior work demonstrated that substrate stiffness increased α-smooth muscle actin to enhance myofibroblast differentiation in FAPs, indicating that FAPs are sensitive to surface stiffness.[318] AGEs stiffen the ECM and could be pushing the FAPs to a more fibrotic phenotype, but more study is needed to determine this.

Muscle regeneration is dependent on ECM, MuSCs, fibroblasts, FAPs, and macrophages and understanding how AGE cross-links in muscle ECM regulate different cell populations is an important step in developing regenerative bio-scaffolds.[306,319] We measured muscle fiber counts in regenerating

muscle and determined that AGEs reduced the number of de novo muscle fibers within the injury site during muscle regeneration compared to DMM. Moreover, Feret diameter in regenerating fibers was no different between AGE and DMM treated injuries, suggesting that AGEs were suppressing muscle fiber formation. This is an important finding and leads to an unanswered question – do AGE-crosslinks exert a unique effect on muscle regeneration different from soluble AGEs? Current studies in AGE-related research have focused on soluble AGEs and not ECM-based cross-links since it is much more difficult to deliver AGE cross-links *in vivo*. To further answer this question, we measured Feret diameter in healthy muscle fibers (peripherally located nuclei) as well and found that muscle fiber diameters were smaller in injury sites exposed to AGE cross-links compared to DMM-treated sites and those fibers from DMM sites were similar to sham. This was another critical finding in this study since soluble AGEs have been implicated in age-associated sarcopenia.[320–322]

Muscle regeneration is tightly regulated by activation and differentiation of MuSCs. Pax7 maintains the MuSC pool and is essential for myogenesis and encourages myogenic commitment.[323,324] In adults, MuSCs are Pax7 positive when quiescent, but upon activation, they express Myf5 and MyoD.[325] Myf5 plays a role in the burst of myoblast proliferation during myogenesis before late-stage differentiation.[326] In chronic muscle injury environments such as facioscapulohumeral muscular dystrophy 1A and denervation, Myf5 is upregulated along with other myogenic transcription factors.[327,328] The chronic muscle fiber turnover in these states causes MuSC over-activation and limits self-renewal. Classically, it is thought that the myogenic genes are upregulated in old age through a process known as homeostatic decompensation.[236,329] Reports showed that Myf5 increases in aged muscle; however, in conditions where myogenic cells are “stuck” in a Myf5 positive state, MyoG and MyHC are occluded, blocking proper differentiation.[330]

In our model, Pax7 and MyoD levels were higher in DMM and AGE, indicating that MuSCs were activated. Interestingly, AGEs increased Myf5 levels while DMM was similar to sham, suggesting that AGEs could be stimulating proliferation of MuSCs. Contrary to our hypothesis, MyoG and MyHCs were similar between AGE and DMM treatments. This could be possible because we assayed a muscle biopsy that contains a mixture of progenitor cells and muscle fibers. Thus, while we measured nascent, fast-twitch, and slow-twitch muscle fibers, total protein from these biopsies were likely comparable to our histological results from total muscle where there were no differences between total fiber counts or total muscle area between DMM and AGE treated injury sites. These results suggested that our dot blots were not sensitive enough to detect differences in myosin proteins.[297,299]

The receptor for AGEs (RAGE) is involved in multiple cell types during myogenesis, including myoblasts, fibroblasts, macrophages, and Schwann cells.[68,331–333] Despite the lack of AGE levels in explanted injury sites, the AGE group measured positive for RAGE expression, while RAGE was barely detectable in DMM. It is not surprising that RAGE is present at baseline levels in sham muscle due to its expression in fibroblasts, macrophages, and other cell types. Prior research in our lab showed that the RAGE protein was suppressed in VML injuries compared to sham.[309] This supports that AGE delivery had a tangible effect on RAGE, and may still be present at 8 weeks. Thus, increased RAGE in AGE-treated VML potentially demonstrates an AGE/RAGE axis, and which cell types regulates RAGE expression in this context still needs to be determined. RAGE is known to be expressed in activated myoblasts, and the RAGE ligands S100b and HMGB1 exert proliferative and pro-myogenic pathways via RAGE-P38-MyoG signaling.[24,71,295] RAGE is then downregulated in late differentiation, and is not detected after myoblasts fuse into muscle fibers.[22] In our study, elevated Myf5 levels in the presence of AGEs indicated that MuSCs are preferentially activated over self-renewed. It is possible that elevated levels of RAGE are due to the same phenomena, but more study is needed to prove this.

To perform a more sensitive and unbiased analysis of the proteomic profile produced by AGE delivery, we used mass spectrometry analysis. As expected, DMM and AGE treated muscle had a much different proteomic profile compared to sham, supporting the idea that our challenging VML model was not yet resolved at 8 weeks. Our Venn diagram analysis highlighted this, where injured muscle was an order of magnitude higher compared to sham. We parsed this further and determined that AGEs supported 38 unique proteins whereas DMM only had 9. Moreover, we determined that 111 proteins were significantly regulated by AGEs, and we found that AGEs specifically suppressed muscle-specific proteins (Myh3 and Myh8), which supports the histological reductions in regenerative muscle we measured in the AGE group. Additionally, we explored the GO terminology under the Biological Process and Cellular Component genres to capture if AGEs regulated specific categories. Interestingly, the immune system response was elevated, matching a known effect of AGEs. Further, the extracellular region was negatively impacted.

Several immune-specific proteins were clearly upregulated by AGEs further supporting the fact that AGE cross-links regulated the innate immune response and promoted an inflammatory environment. Major innate immune system markers included those for macrophages (Cd14, Actr2, Cd74) and mast cells (NDRG).[334–338] Macrophages are essential in skeletal muscle regeneration, but in VML injuries are strongly activated contributing to fibrosis.[319] Furthermore, adaptive immune cell markers such as

the B and T cell markers PTPRC, Coronin-1A, and the T-cell promoting protein Sphingosine-1-phosphate lyase 1 were increased by AGEs.[339–341] We previously showed that adaptive immunity regulates skeletal muscle regeneration by comparing immunocompromised to immunointact rats.[184] Finally, myosin-9 was increased due to AGEs, and this is a marker of immune cell migration.[342]

The ECM plays a complex spatiotemporal regulatory role in muscle repair and regeneration that can reestablish healthy ECM following injury, or in the case of chronic inflammatory environments, promotes aberrant fibrosis. Counterintuitively, AGEs negatively regulated the fibrotic markers of the ECM. Reduced collagen type I indicated that while overall collagen levels were elevated collagen synthesis was suppressed. Further, this supports that elevated collagen area in the AGE group, as seen in the histology, is from decreased graft remodeling rather than increased collagen synthesis. However, more study is needed to prove this. Prior literature indicated that AGEs disrupt ECM synthesis in fibroblasts, which could explain the reduction in fibrotic factors.[343] Additionally, VML injuries in aged animals produce less collagen, and the reductions in ECM components we measured could indicate that AGEs promote an aged regeneration phenotype.[183] Adipocyte enhancer-binding protein 1 (AEBP1) and cartilage oligomeric matrix protein (COMP), which were reduced in the AGE group, are also markers of fibrosis in non-muscle tissue and their role in skeletal muscle remains largely unclear.[344,345] Carboxylesterase 1D (Ces1d) is an enzyme that plays a role in lipid metabolism and inflammation and loss of this enzyme increases inflammation.[346] In our model, Ces1d was reduced by AGEs, providing further evidence that AGEs enhanced the inflammatory response. Laminin, osteolectin, fibromodulin, and thrombosponin-4 were all detected at lower levels in the AGE group. These 4 proteins are known to be pro-regenerative ECM proteins, and reductions in their levels could be associated with the reduced number of regenerating muscle fibers measured in Figure 41.[347–351] It was also noteworthy that olfactomedin-like protein 1, which is primarily found in nerves, was reduced by AGEs and could indicate abrogated recovery of the nerve-muscle connection.[352]

Aside from RAGE, galectin-3 acts as a separate extracellular receptor for AGEs that is present on most innate immune cells, and plays an important role in the immune response and is associated with musculoskeletal diseases.[353,354] While endogenous galectin-3 also plays a role in normal skeletal muscle regeneration, its levels in AGE treated muscle were more than double DMM, suggesting its role was beyond that of repair or regeneration.[355,356] However, more study is needed to discern which cell types are responsible for galectin-3 increases. We next investigated RAGE-pathway members to determine the extent to which the AGE/RAGE axis was involved. We detected P38α and Erk1; however

they were not significantly regulated by AGEs. AGEs enhanced osteopontin levels, which is known to be regulated by RAGE signaling and is associated with increased fibrosis.[357] Moreover, osteopontin increases in skeletal muscle with aging and is partly responsible for age-related reductions in skeletal muscle regeneration.[358] Further, we investigated known RAGE ligands, and several were detected. Interestingly, only S100-A4 was increased by AGEs, suggesting that AGEs could promote a positive RAGE signaling feed-back loop with S100-A4.[359]

Conclusions

The presence of AGEs in DMM supports a fibrotic environment and appears to dysregulate myogenesis. AGE cross-linked DMM exhibited reduced performance in a challenging VML model. Specifically, AGEs increased fibrosis and collagen cross-linking in the injury, while maintaining elevated RAGE and Myf5 levels that suggest MuSC dysregulation. Also, muscle regeneration and specific ECM remodeling factors were reduced by AGEs. Our data support that AGE accumulation on muscle ECM derived from older donors may cause reduced efficacy compared to DMM from younger donors. Future work investigating how to mitigate the effects of AGEs is needed.

Chapter 7. Conclusions and Future Directions

Summary

Overall, this thesis provides critical insight into the role of AGE cross-links in skeletal muscle regeneration. AGEs are previously thought to inhibit muscle regeneration through stiffening the MuSC microenvironment and by signaling through the receptor for advanced glycation end-products (RAGE). It is known that stiffer substrates promote myoblast proliferation at the expense of differentiation, while soluble AGEs inhibit both proliferation and differentiation. We are the first to report that AGE cross-linked 3D collagen substrates, which are stiffer and rich with AGE adducts, promote proliferation at the expense of differentiation in a RAGE-dependent manner. These data reveal that AGE cross-links have a unique RAGE-dependent regulatory role over myoblasts and do not act like soluble AGEs. Further, we report that AGE cross-links negatively regulate RAGE in late differentiation, and serve to suppress myogenesis by downregulating RAGE, rather than over-stimulating RAGE signaling. Dogma supports that RAGE is upregulated in myoblasts by soluble AGEs, and soluble AGE-RAGE signaling is antiproliferative and dysregulates differentiation. We provide strong evidence of a unique, non-canonical RAGE mechanism for AGE cross-links. Next, we investigated the role of AGE cross-links in VML injury by inducing AGE cross-links on DMM before implantation into VML injuries. We proved that AGE-DMM reduces muscle regeneration in a VML model, and downregulates ECM synthesis while promoting inflammation. Further, the AGE receptors RAGE and Galectin-3 were upregulated by AGE cross-links.

Future Directions: The AGE-RAGE axis in myogenesis

Despite over two decades of research, much is left to uncover on the role of AGE-RAGE in skeletal muscle regeneration. Myoblasts, the primary expressor of RAGE in skeletal muscle, are regulated in their proliferation and differentiation by canonical RAGE ligand signaling. However, it is generally agreed that AGEs overstimulate RAGE, resulting in the disruption of myoblast proliferation and differentiation.[22] These classical AGE *in vitro* and *in vivo* studies rely on their soluble delivery via AGE-BSA, Methylglyoxal, or other form such as CML. In the context of skeletal muscle aging, soluble AGEs do play a role, however, AGE cross-links accrue with age on muscular ECM proteins such as the collagens. Until this thesis, it has not been studied what role AGE cross-links play on myoblasts independent of soluble AGEs. Our data provides novel insight into how AGE cross-links exert a pro-proliferative, anti-differentiative effect on myoblasts that is RAGE dependent during proliferation, and

inversely RAGE dependent in differentiation. It is well known that stiffness is positively correlated with proliferation in myoblasts, however it is not clear how our finding of a RAGE-dependent effect synergizes with the stiffness effect.[360,361] Perhaps there is an AGE integrin-RAGE interplay. Other groups have reported that integrin αVβ3 is tightly regulated with RAGE in cultured podocytes, as evidenced by their co-precipitation.[362] Impressively, treatment with the αV-integrin antagonist cilengestide blocked AGE-BSA signaling in their study, indicating that signaling is strongly shared between RAGE and integrin αVβ3. In this thesis, we observed that both integrin αV and β3 were decreased along with RAGE, and this could indicate a mechano-RAGE coupling. Interestingly, if RAGE and integrins are this tightly co-regulated, it would obfuscate the question on whether the mechanics or AGE-RAGE signaling have a larger role in our data. However, more study is needed to determine this.

Curiously, our data showed that RAGE was reduced by AGE cross-links in late differentiation. It is known that ADAM10, a disintegrin and sheddase, cleaves full-length RAGE into the decoy receptor sRAGE (soluble RAGE).[363] Further, the authors discovered that HMBG1 binding to RAGE promoted RAGE cleavage. RAGE cleavage could explain the reductions of RAGE seen in our studies, and it makes sense that AGE binding could act like HMBG1 and promote this process. Additionally, it is a well-known receptor phenomenon for a receptor to become tolerant of its ligand over time, resulting in a reduced ligand effect. This is classically observed in G protein-coupled receptors, where they are reduced in number by endocytosis when chronically exposed to their ligands.[364] While the exact mechanism may differ, the principle can still apply to RAGE. Ironically, while reduced RAGE may be a protective effect against over-stimulation by AGEs, its reduction precludes the possibility for canonical RAGE signaling, resulting in reduced myoblast function. All in all, it is clear that negative RAGE regulation by AGEs is harmful for myoblast differentiation and fusion, and is a rich area for future study.

Future Directions: Key RAGE ligand players

Canonical RAGE signaling for myoblasts relies on two key players, HMGB1 and S100b. S100b has varied roles based on myoblast density, but it is essentially understood to promote proliferation and the transition from proliferation to differentiation via P38 MAPK signaling.[24] HMGB1 binds RAGE and promotes myogenin through P38 MAPK, resulting in the shutdown of proliferation with enhanced differentiation and fusion.[71] Interestingly, RAGE begins to be expressed upon myoblast activation, and increases in amount until it reaches a peak at late differentiation/early fusion, and tapers off entirely once fusion is complete.[23,24] S100b plays an important role in early differentiation, while HMGB1 takes over later in the process. In our data, we observed a stark deficit in

RAGE by late differentiation in the presence of AGE cross-links. Surprisingly, there was not a change in RAGE due to AGEs in early differentiation. Since we delivered AGE cross-links to myoblasts in a chronic fashion, we hypothesized that restoring canonical RAGE signaling from the onset of the culturing process would restore myoblast fusion. When we delivered S100b, myoblast fusion was restored in the presence of AGE cross-links. Further, AGE cross-links acted more as an inhibitor of canonical RAGE signaling than an activator of RAGE. More study is warranted *in vivo* to determine if AGE cross-links can be overcome via RAGE ligand delivery. Additionally, it is not known if HMGB1 treatment would have the same outcome as S100b.

Future Directions: AGE cross-links and mechano-transduction

AGE cross-links are notoriously difficult to study since their cellular impact can be exerted through both mechanical and receptor signaling mechanisms. Our model did not completely decouple mechanics from receptor signaling, though we were able to isolate RAGE through inhibition and activation. While we measured increased stiffness due to AGE cross-links, the focus of the hypothesis did not address many standard mechano-transduction signaling factors such as focal adhesion kinase and YAP/TAZ nuclear localization.[318,365] However, our data did present as a classical stiffness effect on myoblasts, and even though we could explain the data through RAGE inhibition and activation, it is possible that RAGE is working with mechano-transduction in its effect. Interestingly, analysis of mass spectrometry data from our *in vivo* VML study revealed upregulation of sphingosine-1-phosphate lyase 1 by AGE cross-links, which has been known to degrade the stiffness-associated sphingosine-1-phosphate.[366,367] This singular piece of data suggests that stiffness did not play a large role in AGE cross-links' impact *in vivo*. However, more study is needed to fully appreciate AGE's mechanical role in skeletal muscle regeneration.

Future Directions: Muscle-nerve communication

While it is known that AGEs play a role in peripheral nerve neuropathy, it is not well characterized if AGEs promote a denervated phenotype in aged muscle, or how much they contribute to the atrophic environment in sarcopenic muscle. Studies elucidating the role of AGE-cross-linked collagen on motor nerve health need to be developed. Muscle and nerve signaling and their relation to the ECM has been particularly difficult to study due to the plastic sensitivity of innervation and inability to study it ex vivo. To date, the current standard for studying muscle-nerve interactions and endplate remodeling is in animal models. There is currently no in vitro model that accurately re-creates muscle innervation. Development of such a model would greatly improve reproducibility while reducing the noise, expense, and animal sacrifice currently required. Further, while there has been increased interest in

understanding the specialized endplate ECM, few papers have been published on the non-myelinating Schwann cells that cover each endplate and are known to protectively regulate the intra-synaptic ECM. It is unknown if AGEs cross-link within the synaptic cleft or how cross-linking this specialized ECM effects acetylcholine transmission. Hence, this area of research is relatively unexplored, leaving a possible future topic in ECM modifications and muscle to nerve signaling during aging and other diseases that increase AGE cross-links. In addition, whether modifications to laminin change neural pathfinding and synapse formation is still unclear and interrogating these types of questions might lead to new discoveries in endplate development, motor nerve pathfinding, and endplate stability in the neuromuscular junction.

Conclusions

Overall, this thesis provides novel insight into the role of AGE cross-linked collagen on myoblast function and skeletal muscle regeneration. AGE cross-links promote myoblast proliferation and hinder differentiation in a RAGE-dependent manner. Further, the AGE effect was restored with S100b delivery, hinting that S100b could be a viable promotor of skeletal muscle regeneration in circumstances with high AGE levels. It is still an open question as to how tied in mechano-transduction is to this process. Also, whether reductions in RAGE are due to RAGE cleavage needs to be explored. AGE cross-links on DMM promoted inflammation and hindered regeneration in a VML model, and evidence showed that AGEs upregulated RAGE and Galectin 3. Further study is needed to ascertain which cell types express RAGE, and what role Galectin 3 plays in the transduction of the AGE cross-link effect. Also, the data in this thesis beckons for further study into the clinical relevance of AGE cross-links on DMM.

References

1. Hamerman D. Aging and the musculoskeletal system. *Ann Rheum Dis*. 1997;56(10):578-585. doi:10.1136/ard.56.10.578

2. Bernet JD, Doles JD, Hall JK, Kelly Tanaka K, Carter TA, Olwin BB. p38 MAPK signaling underlies a cell-autonomous loss of stem cell self-renewal in skeletal muscle of aged mice. *Nat Med*. 2014;20(3):265-271. doi:10.1038/nm.3465

3. Rayagiri SS, Ranaldi D, Raven A, et al. Basal lamina remodeling at the skeletal muscle stem cell niche mediates stem cell self-renewal. *Nat Commun*. 2018;9(1):1075. doi:10.1038/s41467-018-03425-3

4. Yin H, Price F, Rudnicki MA. Satellite Cells and the Muscle Stem Cell Niche. *Physiol Rev*. 2013;93(1):23. doi:10.1152/PHYSREV.00043.2011

5. Bentzinger CF, Wang YX, von Maltzahn J, Soleimani VD, Yin H, Rudnicki MA. Fibronectin regulates Wnt7a signaling and satellite cell expansion. *Cell Stem Cell*. 2013;12(1):75-87. doi:10.1016/j.stem.2012.09.015

6. Stearns-Reider KM, D'Amore A, Beezhold K, et al. Aging of the skeletal muscle extracellular matrix drives a stem cell fibrogenic conversion. *Aging Cell*. 2017;16(3):518-528. doi:10.1111/acel.12578

7. Bentzinger Cf, von Maltzahn J, Rudnicki MA. Extrinsic regulation of satellite cell specification. *Stem Cell Res Ther*. 2010;1(3):27. doi:10.1186/scrt27

8. Carlson BM, Faulkner JA. Muscle transplantation between young and old rats: age of host determines recovery. *Am J Physiol*. 1989;256(6 Pt 1). doi:10.1152/AJPCELL.1989.256.6.C1262

9. Shavlakadze T, McGeachie J, Grounds MD. Delayed but excellent myogenic stem cell response of regenerating geriatric skeletal muscles in mice. *Biogerontology*. 2010;11(3):363-376. doi:10.1007/S10522-009-9260-0

10. Conboy IM, Conboy MJ, Wagers AJ, Girma ER, Weismann IL, Rando TA. Rejuvenation of aged progenitor cells by exposure to a young systemic environment. *Nature 2004 433:7027*. 2005;433(7027):760-764. doi:10.1038/nature03260

11. Mezzogiorno A, Coletta M, Zani BM, Cossu G, Molinaro M. Paracrine stimulation of senescent satellite cell proliferation by factors released by muscle or myotubes from young mice. *Mech Ageing Dev*. 1993;70(1-2):35-44. doi:10.1016/0047-6374(93)90057-X

12. Chakkalakal J, Brack A. Extrinsic Regulation of Satellite Cell Function and Muscle Regeneration Capacity during Aging. *J Stem Cell Res Ther*. 2012;Suppl 11(S11):001. doi:10.4172/2157-7633.S11-001

13. Barberi L, Scicchitano BM, De Rossi M, et al. Age-dependent alteration in muscle regeneration: the critical role of tissue niche. *Biogerontology*. 2013;14(3):273-292. doi:10.1007/S10522-013-9429-4

14. Grounds MD. Therapies for sarcopenia and regeneration of old skeletal muscles: more a case of old tissue architecture than old stem cells. *Bioarchitecture*. 2014;4(3):81-87. doi:10.4161/BIOA.29668

15. Lukjanenko L, Jung MJ, Hegde N, et al. Loss of fibronectin from the aged stem cell niche affects the regenerative capacity of skeletal muscle in mice. *Nat Med*. 2016;22(8):897. doi:10.1038/NM.4126

16. Chakkalakal J V, Jones KM, Albert Basson M, Brack AS. The aged niche disrupts muscle stem cell quiescence. doi:10.1038/nature11438

17. Wood LK, Kayupov E, Gumucio JP, Mendias CL, Claflin DR, Brooks S V. Intrinsic stiffness of extracellular matrix increases with age in skeletal muscles of mice. *J Appl Physiol (1985)*. 2014;117(4):363-369. doi:10.1152/japplphysiol.00256.2014

18. Maillard LC. Condensation des acides amines en presence de la glycerine; Cycloglycylglycine et polypeptides. *C R Hebd Seances Acad Sci*. 1911;153:1078-1080.

19. KAWAMURA S. Seventy Years of the Maillard Reaction. In: *The Maillard Reaction in Foods and Nutrition*. Vol 215. ACS Symposium Series. AMERICAN CHEMICAL SOCIETY; 1983:1-3. doi:doi:10.1021/bk-1983-0215.ch001

20. Suzuki A, Yabu A, Nakamura H. Advanced glycation end products in musculoskeletal system and disorders. *Methods*. Published online 2020. doi:https://doi.org/10.1016/j.ymeth.2020.09.012

21. Svensson RB, Smith ST, Moyer PJ, Magnusson SP. Effects of maturation and advanced glycation on tensile mechanics of collagen fibrils from rat tail and Achilles tendons. *Acta Biomater*. 2018;70:270-280. doi:https://doi.org/10.1016/j.actbio.2018.02.005

22. Riuzzi F, Sorci G, Sagheddu R, Chiappalupi S, Salvadori L, Donato R. RAGE in the pathophysiology of skeletal muscle. *J Cachexia Sarcopenia Muscle*. 2018;9(7):1213. doi:10.1002/JCSM.12350

23. Riuzzi F, Sorci G, Sagheddu R, Donato R. HMGB1-RAGE regulates muscle satellite cell homeostasis through p38-MAPK- and myogenindependent repression of Pax7 transcription. *J Cell Sci*. 2012;125(6):1440-1454. doi:10.1242/JCS.092163/258339/AM/HMGB1-RAGE-REGULATES-MUSCLE-SATELLITE-CELL

24. Riuzzi F, Sorci G, Beccafico S, Donato R. S100B Engages RAGE or bFGF/FGFR1 in Myoblasts Depending on Its Own Concentration and Myoblast Density. Implications for Muscle Regeneration. *PLoS One*. 2012;7(1):e28700. doi:10.1371/JOURNAL.PONE.0028700

25. Olson LC, Nguyen TM, Heise RL, Boyan BD, Schwartz Z, McClure MJ. Advanced Glycation End Products Are Retained in Decellularized Muscle Matrix Derived from Aged Skeletal Muscle. *International Journal of Molecular Sciences 2021, Vol 22, Page 8832*. 2021;22(16):8832. doi:10.3390/IJMS22168832

26. Vollset SE, Goren E, Yuan CW, et al. Fertility, mortality, migration, and population scenarios for 195 countries and territories from 2017 to 2100: a forecasting analysis for the Global Burden of Disease Study. *The Lancet*. 2020;396(10258):1285-1306. doi:10.1016/S0140-6736(20)30677-2

27. Miljkovic N, Lim JY, Miljkovic I, Frontera WR. Aging of Skeletal Muscle Fibers. *Ann Rehabil Med*. 2015;39(2):155. doi:10.5535/ARM.2015.39.2.155

28. Doherty TJ. Invited review: Aging and sarcopenia. *J Appl Physiol (1985)*. 2003;95(4):1717-1727. doi:10.1152/japplphysiol.00347.2003

29. Larsson L, Degens H, Li M, et al. Sarcopenia: Aging-related loss of muscle mass and function. *Physiol Rev*. 2019;99(1):427-511. doi:10.1152/physrev.00061.2017

30. Walston JD. Sarcopenia in older adults. *Curr Opin Rheumatol*. 2012;24(6):623-627. doi:10.1097/BOR.0b013e328358d59b

31. ARTHUR W. ON THE RELATIONSHIP BETWEEN STRENGTH OF GRIP AND CERTAIN MENTAL AND SENSORY CHARACTERS. *Biometrika*. 1924;16(3-4):299-327. doi:10.1093/BIOMET/16.3-4.299

32. Berg BN. Muscular Dystrophy in Aging Rats. *J Gerontol*. 1956;11(2):134-139. doi:10.1093/GERONJ/11.2.134

33. Siparsky PN, Kirkendall DT, Garrett WE, Jr. Muscle Changes in Aging: Understanding Sarcopenia. *Sports Health*. 2014;6(1):36. doi:10.1177/1941738113502296

34. Gillies AR, Lieber RL. Structure and function of the skeletal muscle extracellular matrix. *Muscle Nerve*. 2011;44(3):318-331. doi:10.1002/mus.22094

35. Unoki H, Yamagishi S ichi. Advanced Glycation End Products and Insulin Resistance. *Curr Pharm Des*. 2008;14(10):987-989. doi:10.2174/138161208784139747

36. Ahmad K, Lee E, Moon J, Park SY, Choi I. Multifaceted Interweaving Between Extracellular Matrix, Insulin Resistance, and Skeletal Muscle. *Cells*. 2018;7(10):148. doi:10.3390/cells7100148

37. Ahmad K, Shaikh S, Lee EJ, Lee YH, Choi I. Consequences of Dicarbonyl Stress on Skeletal Muscle Proteins in Type 2 Diabetes. *Curr Protein Pept Sci*. 2019;21(9):878-889. doi:10.2174/1389203720666191119100759

38. Seynnes O, Schiaffino S, Blottner D, Csapo R, Gumpenberger M, Wessner B. Skeletal Muscle Extracellular Matrix – What Do We Know About Its Composition, Regulation, and Physiological Roles? A Narrative Review. *Front Physiol*. 2020;11:253. doi:10.3389/fphys.2020.00253

39. Chazaud B. Inflammation during skeletal muscle regeneration and tissue remodeling: Application to exercise-induced muscle damage management. *Immunol Cell Biol*. 2016;94(2):140-145. doi:10.1038/icb.2015.97

40. Etienne J, Liu C, Skinner CM, Conboy MJ, Conboy IM. Skeletal muscle as an experimental model of choice to study tissue aging and rejuvenation. *Skeletal Muscle 2020 10:1*. 2020;10(1):1-16. doi:10.1186/S13395-020-0222-1

41. Kragstrup TW, Kjaer M, Mackey AL, Wenzel Kragstrup T. Structural, biochemical, cellular, and functional changes in skeletal muscle extracellular matrix with aging. Published online 2011. doi:10.1111/j.1600-0838.2011.01377.x

42. Rowe RWD. Morphology of perimysial and endomysial connective tissue in skeletal muscle. *Tissue Cell*. 1981;13(4):681-690. doi:10.1016/S0040-8166(81)80005-5

43. Gao Y, Waas AM, Faulkner JA, Kostrominova TY, Wineman AS. Micromechanical modeling of the epimysium of the skeletal muscles. *J Biomech*. 2008;41(1):1-10. doi:10.1016/j.jbiomech.2007.08.008

44. Purslow PP, Trotter JA. The morphology and mechanical properties of endomysium in series-fibred muscles: variations with muscle length. *J Muscle Res Cell Motil*. 1994;15(3):299-308. doi:10.1007/BF00123482

45. Bowman W. On the minute structure and movements of voluntary muscle. *R and JR Taylor*. 1840;Part II(Philosophical Transactions):457-501. https://wellcomecollection.org/works/f6wb4mbj

46. Hu P, Geles KG, Paik JH, DePinho RA, Tjian R. Codependent Activators Direct Myoblast-Specific MyoD Transcription. *Dev Cell*. 2008;15(4):534-546. doi:10.1016/j.devcel.2008.08.018

47. Mauro A, Sten-Knudsen O. THE ROLE OF THE SARCOLEMMA IN MUSCLE PHYSIOLOGY. *Acta Med Scand*. 1952;142(266 S):715-724. doi:10.1111/j.0954-6820.1952.tb13422.x

48. Kovanen V, Suominen H, Heikkinen E. Collagen of slow twitch and fast twitch muscle fibres in different types of rat skeletal muscle. *Eur J Appl Physiol Occup Physiol*. 1984;52(2):235-242. doi:10.1007/BF00433399

49. Sanes JR. The Basement Membrane/Basal Lamina of Skeletal Muscle *. *Journal of Biological Chemistry*. 2003;278(15):12601-12604. doi:10.1074/JBC.R200027200

50. Grzelkowska-Kowalczyk K. The Importance of Extracellular Matrix in Skeletal Muscle Development and Function. *Composition and Function of the Extracellular Matrix in the Human Body*. Published online June 15, 2016. doi:10.5772/62230

51. Mauro A. SATELLITE CELL OF SKELETAL MUSCLE FIBERS . *J Biophys Biochem Cytol*. 1961;9(2):493-495. doi:10.1083/jcb.9.2.493

52. Aziz A, Sebastian S, Dilworth JJ. The Origin and Fate of Muscle Satellite Cells. *Stem Cell Rev Rep*. 2012;8(2):609-622. doi:10.1007/s12015-012-9352-0

53. Mayer U. Integrins: Redundant or important players in skeletal muscle? *Journal of Biological Chemistry*. 2003;278(17):14587-14590. doi:10.1074/jbc.R200022200

54. Hantaü D, Gautron J, Labat-Robert J. Immunolocalization of Fibronectin and other Macromolecules of the Intercellular Matrix in the Striated Muscle Fiber of the Adult Rat. *Top Catal*. 1983;3(5):381-391. doi:10.1016/S0174-173X(83)80019-3

55. Florian Bentzinger C, Wang YX, Rudnicki MA. Building muscle: Molecular regulation of myogenesis. *Cold Spring Harb Perspect Biol*. 2012;4(2). doi:10.1101/cshperspect.a008342

56. Kuang S, Gillespie MA, Rudnicki MA. Niche Regulation of Muscle Satellite Cell Self-Renewal and Differentiation. *Cell Stem Cell*. 2008;2(1):22-31. doi:10.1016/j.stem.2007.12.012

57. S K, K K, F LG, MA R. Asymmetric self-renewal and commitment of satellite stem cells in muscle. *Cell*. 2007;129(5):999-1010. doi:10.1016/J.CELL.2007.03.044

58. JB M. Myogenic programs of mouse muscle cell lines: expression of myosin heavy chain isoforms, MyoD1, and myogenin. *J Cell Biol*. 1990;111(3):1149-1159. doi:10.1083/JCB.111.3.1149

59. Wehrle U, Düsterhöft S, Pette D. Effects of chronic electrical stimulation on myosin heavy chain expression in satellite cell cultures derived from rat muscles of different fiber-type composition. *Differentiation*. 1994;58(1):37-46. doi:10.1046/J.1432-0436.1994.5810037.X

60. Stern-Straeter J, Bonaterra GA, Kassner SS, et al. Characterization of human myoblast differentiation for tissue-engineering purposes by quantitative gene expression analysis. *J Tissue Eng Regen Med*. 2011;5(8):e197-e206. doi:10.1002/TERM.417

61. Carlson BM, Carlson BM. Denervation and the Aging of Skeletal Muscle. Accessed April 12, 2021. http://citeseerx.ist.psu.edu/viewdoc/summary?doi=10.1.1.375.7242

62. Dedkov EI, Kostrominova TY, Borisov AB, Carlson BM. MyoD and myogenin protein expression in skeletal muscles of senile rats. *Cell Tissue Res*. 2003;311:401-416. doi:10.1007/s00441-002-0686-9

63. Musarò A, Cusella De Angelis MG, Germani A, Ciccarelli C, Molinaro M, Zani BM. Enhanced Expression of Myogenic Regulatory Genes in Aging Skeletal Muscle. *Exp Cell Res*. 1995;221(1):241-248. doi:10.1006/EXCR.1995.1372

64. Neeper M, Schmidt AM, Brett J, et al. Cloning and expression of a cell surface receptor for advanced glycosylation end products of proteins. *Journal of Biological Chemistry*. 1992;267(21):14998-15004. doi:10.1016/S0021-9258(18)42138-2

65. Oczypok EA, Perkins TN, Oury TD. All the “RAGE” in lung disease: The receptor for advanced glycation endproducts (RAGE) is a major mediator of pulmonary inflammatory responses. *Paediatr Respir Rev*. 2017;23:40-49. doi:10.1016/J.PRRV.2017.03.012

66. D’Agati V, Schmidt AM. RAGE and the pathogenesis of chronic kidney disease. *Nature Reviews Nephrology 2010 6:6*. 2010;6(6):352-360. doi:10.1038/nrneph.2010.54

67. SF Yan SDYRRAS. Tempering the wrath of RAGE: an emerging therapeutic strategy against diabetic complications, neurodegeneration, and inflammation. *Ann Med*. 2009;41(6):408-422. doi:10.1080/07853890902806576

68. Sagheddu R, Chiappalupi S, Salvadori L, Riuzzi F, Donato R, Sorci G. Targeting RAGE as a potential therapeutic approach to Duchenne muscular dystrophy. *Hum Mol Genet*. 2018;27(21):3734-3746. doi:10.1093/HMG/DDY288

69. Chiappalupi S, Sorci G, Vukasinovic A, et al. Targeting RAGE prevents muscle wasting and prolongs survival in cancer cachexia. *J Cachexia Sarcopenia Muscle*. 2020;11(4):929-946. doi:10.1002/JCSM.12561

70. Beccafico S, Riuzzi F, Puglielli C, et al. Human muscle satellite cells show age-related differential expression of S100B protein and RAGE. doi:10.1007/s11357-010-9197-x

71. Sorci G, Riuzzi F, Arcuri C, Giambanco I, Donato R. Amphoterin Stimulates Myogenesis and Counteracts the Antimyogenic Factors Basic Fibroblast Growth Factor and S100B via RAGE Binding Downloaded from. *Mol Cell Biol*. 2004;24(11):4880-4894. doi:10.1128/MCB.24.11.4880-4894.2004

72. Rauvala H, Rouhiainen A. RAGE as a Receptor of HMGB1 (Amphoterin): Roles in Health and Disease. *Curr Mol Med*. 2007;7(8):725-734. doi:10.2174/156652407783220750

73. Wu SE, Chiu YL, Kao TW, Chen WL. Elevated level of the soluble receptor for advanced glycation end-products involved in sarcopenia: an observational study. *BMC Geriatrics 2021 21:1*. 2021;21(1):1-9. doi:10.1186/S12877-021-02487-1

74. Peng Y, Kim JM, Park HS, et al. AGE-RAGE signal generates a specific NF-κB RelA “barcode” that directs collagen I expression. *Scientific Reports 2016 6:1*. 2016;6(1):1-10. doi:10.1038/srep18822

75. Verzár F. Aging of the Collagen Fiber. *Int Rev Connect Tissue Res*. 1964;2:243-300. doi:10.1016/B978-1-4831-6751-0.50012-4

76. Shoulders MD, Raines RT. COLLAGEN STRUCTURE AND STABILITY. *Annu Rev Biochem*. 2009;78:929. doi:10.1146/ANNUREV.BIOCHEM.77.032207.120833

77. Lodish H, Berk A, Zipursky SL, Matsudaira P, Baltimore D, Darnell J. Collagen: The Fibrous Proteins of the Matrix. Published online 2000. Accessed July 5, 2021. https://www.ncbi.nlm.nih.gov/books/NBK21582/

78. Haus JM, Carrithers JA, Trappe SW, Trappe TA. Collagen, cross-linking, and advanced glycation end products in aging human skeletal muscle. Published online 2007. doi:10.1152/japplphysiol.00670.2007.-We

79. Schaub MC. The Ageing of Collagen in the Striated Muscle. *Gerontology*. 1963;8(1):16-35. doi:10.1159/000211204

80. G G, K F, PE W, DJ W. Age-related changes in collagen gene expression in the muscles of mdx dystrophic and normal mice. *Neuromuscul Disord*. 1994;4(3):183-191. doi:10.1016/0960-8966(94)90019-1

81. MA H, BK P. Age-related changes in collagenous and noncollagenous proteins of skeletal muscle of a short-lived species of reptile. *Gerontology*. 1978;24(5):343-347. doi:10.1159/000212269

82. Hindle AG, Horning M, Mellish JAE, Lawler JM. Diving into old age: muscular senescence in a large-bodied, long-lived mammal, the Weddell seal (Leptonychotes weddellii). *Journal of Experimental Biology*. 2009;212(6):790-796. doi:10.1242/JEB.025387

83. CARMICHAEL DJ, LAWRIE RA. Bovine collagen. I. Changes in collagen solubility with animal age. *Int J Food Sci Technol*. 1967;2(4):299-311. doi:10.1111/J.1365-2621.1967.TB01354.X

84. Dickerson JWT, Widdowson EM. Chemical changes in skeletal muscle during development. *Biochemical Journal*. 1960;74(2):247. doi:10.1042/BJ0740247

85. Lacraz G, Rouleau AJ, Couture V, et al. Increased Stiffness in Aged Skeletal Muscle Impairs Muscle Progenitor Cell Proliferative Activity. *PLoS One*. 2015;10(8). doi:10.1371/JOURNAL.PONE.0136217

86. C D, P M, B D, S C, F L, JP D. Effects of jump training on passive mechanical stress and stiffness in rabbit skeletal muscle: role of collagen. *Acta Physiol Scand*. 2003;178(3):215-224. doi:10.1046/J.1365-201X.2003.01109.X

87. Verzár F. The Stages and Consequences of Ageing of Collagen. *Gerontology*. 1969;15(2-3):233-239. doi:10.1159/000211689

88. Herchenhan A, Uhlenbrock F, Eliasson P, et al. Lysyl Oxidase Activity Is Required for Ordered Collagen Fibrillogenesis by Tendon Cells * □ S. *Journal of Biological Chemistry*. 2015;290:16440-16450. doi:10.1074/jbc.M115.641670

89. Heinemeier KM, Schjerling P, Heinemeier J, Magnusson SP, Kjaer M. Lack of tissue renewal in human adult Achilles tendon is revealed by nuclear bomb 14C. *The FASEB Journal*. 2013;27(5):2074. doi:10.1096/FJ.12-225599

90. Elliott B, Youl Moon H, Levinger I, et al. Skeletal Muscle Fiber Size and Gene Expression in the Oldest-Old With Differing Degrees of Mobility. *Frontiers in Physiology | www.frontiersin.org*. 2019;10:313. doi:10.3389/fphys.2019.00313

91. Wessner B, Liebensteiner M, Nachbauer W, Csapo R. Age-specific response of skeletal muscle extracellular matrix to acute resistance exercise: A pilot study. *https://doi.org/101080/1746139120181526974*. 2018;19(3):354-364. doi:10.1080/17461391.2018.1526974

92. Smith LR, Hammers DW, Sweeney HL, Barton ER. Increased collagen cross-linking is a signature of dystrophin-deficient muscle. *Muscle Nerve*. 2016;54(1):71. doi:10.1002/MUS.24998

93. Lawrence MM, Abbott C, Peelor FF, Lopes EBP, Griffin TM, Miller BF. Determining Resistance to Protein Turnover in Aged Skeletal Muscle Collagen Using a Novel Stable Isotope Timecourse Approach. *The FASEB Journal*. 2020;34(S1):1-1. doi:10.1096/FASEBJ.2020.34.S1.01802

94. LM S, NA F, LV T. Advanced glycation end-product accumulation and associated protein modification in type II skeletal muscle with aging. *J Gerontol A Biol Sci Med Sci*. 2007;62(11):1204-1210. doi:10.1093/GERONA/62.11.1204

95. Gulati AK, Reddi AH, Zalewski AA. Distribution of fibronectin in normal and regenerating skeletal muscle. *Anat Rec*. 1982;204(3):175-183. doi:10.1002/ar.1092040302

96. Kovanen V, Suominen H, Risteli J, Risteli L. Type IV collagen and laminin in slow and fast skeletal muscle in rats--effects of age and life-time endurance training. *Coll Relat Res*. 1988;8(2):145-153. doi:10.1016/S0174-173X(88)80026-8

97. Kiss AA, Somlyai-Popovics N, Kiss M, Boldogkői Z, Csiszár K, Mink M. Type IV Collagen Is Essential for Proper Function of Integrin-Mediated Adhesion in Drosophila Muscle Fibers. *International Journal of Molecular Sciences 2019, Vol 20, Page 5124*. 2019;20(20):5124. doi:10.3390/IJMS20205124

98. Kanazawa Y, Ikegami K, Sujino M, et al. Effects of aging on basement membrane of the soleus muscle during recovery following disuse atrophy in rats. *Exp Gerontol*. 2017;98:153-161. doi:10.1016/J.EXGER.2017.08.014

99. B B, M D, S R, RE S, A S. Age-associated changes of extracellular matrix collagen impair lung cancer cell migration. *FASEB J*. 2009;23(5):1510-1520. doi:10.1096/FJ.08-122648

100. JF T, LA R, LT F. Decreased interaction of fibronectin, type IV collagen, and heparin due to nonenzymatic glycation. Implications for diabetes mellitus. *Biochemistry*. 1987;26(4):1014-1020. doi:10.1021/BI00378A006

101. AK P, TM G, RA M, IM C, JE S. Stimulatory effects of advanced glycation endproducts (AGEs) on fibronectin matrix assembly. *Matrix Biol*. 2017;59:39-53. doi:10.1016/J.MATBIO.2016.07.003

102. Ohlendieck K. Proteomic Profiling of Fast-To-Slow Muscle Transitions during Aging. *Front Physiol*. 2011;2. doi:10.3389/FPHYS.2011.00105

103. SD Z, RJ M, RK V, DP T. Age and training alter collagen characteristics in fast- and slow-twitch rat limb muscle. *J Appl Physiol (1985)*. 1993;75(4):1670-1674. doi:10.1152/JAPPL.1993.75.4.1670

104. R N, T S, M L, et al. The decline in skeletal muscle mass with aging is mainly attributed to a reduction in type II muscle fiber size. *Exp Gerontol*. 2013;48(5):492-498. doi:10.1016/J.EXGER.2013.02.012

105. L L, L E. Effects of age on enzyme-histochemical fibre spectra and contractile properties of fast- and slow-twitch skeletal muscles in the rat. *J Neurol Sci*. 1986;76(1):69-89. doi:10.1016/0022-510X(86)90143-7

106. DT K, WE G. The effects of aging and training on skeletal muscle. *Am J Sports Med*. 1998;26(4):598-602. doi:10.1177/03635465980260042401

107. L L, J K. Isometric and dynamic endurance as a function of age and skeletal muscle characteristics. *Acta Physiol Scand*. 1978;104(2):129-136. doi:10.1111/J.1748-1716.1978.TB06259.X

108. M B, RI C. The transformation of myosin in cross-innervated rat muscles. *J Physiol*. 1971;213(2):455-474. doi:10.1113/JPHYSIOL.1971.SP009393

109. Evans WJ, Lexell J. Human Aging, Muscle Mass, and Fiber Type Composition. *The Journals of Gerontology: Series A*. 1995;50A(Special_Issue):11-16. doi:10.1093/GERONA/50A.SPECIAL_ISSUE.11

110. MC G, E S. The distribution of satellite cells and their relationship to specific fiber types in soleus and extensor digitorum longus muscles. *Anat Rec*. 1982;202(3):329-337. doi:10.1002/AR.1092020305

111. H S, U H. The number of nuclei in adult rat muscles with special reference to satellite cells. *Anat Rec*. 1977;189(2):169-175. doi:10.1002/AR.1091890204

112. MH S. A quantitative ultrastructural analysis of satellite cells in denervated fast and slow muscles of the mouse. *Anat Rec*. 1983;207(4):593-604. doi:10.1002/AR.1092070407

113. AL M, M K, N C, et al. Assessment of satellite cell number and activity status in human skeletal muscle biopsies. *Muscle Nerve*. 2009;40(3):455-465. doi:10.1002/MUS.21369

114. S O, I N, SM C. Muscle fiber type differentiation and satellite cell populations in normally grown and neonatally denervated muscles in the rat. *Acta Neuropathol*. 1984;65(2):90-98. doi:10.1007/BF00690462

115. Bentzinger CF, von Maltzahn J, Dumont NA, et al. Wnt7a stimulates myogenic stem cell motility and engraftment resulting in improved muscle strength. *Journal of Cell Biology*. 2014;205(1):97-111. doi:10.1083/jcb.201310035

116. Verdijk LB, Snijders T, Drost M, Delhaas T, Kadi F, Loon LJC van. Satellite cells in human skeletal muscle; from birth to old age. *Age (Omaha)*. 2014;36(2):545. doi:10.1007/S11357-013-9583-2

117. LB V, R K, G S, K M, HH S, LJ van L. Satellite cell content is specifically reduced in type II skeletal muscle fibers in the elderly. *Am J Physiol Endocrinol Metab*. 2007;292(1). doi:10.1152/AJPENDO.00278.2006

118. Horwath O, Moberg M, Larsen FJ, Philp A, Apró W, Ekblom B. Influence of sex and fiber type on the satellite cell pool in human skeletal muscle. *Scand J Med Sci Sports*. 2021;31(2):303-312. doi:10.1111/SMS.13848

119. Deschenes M, Gaertner J, O'Reilly S. The Effects of Sarcopenia on Muscles with Different Recruitment Patterns and Myofiber Profiles. *Curr Aging Sci*. 2014;6(3):266-272. doi:10.2174/1874609813066660035

120. B R, L L. Detection of an aging-related increase in advanced glycation end products in fast- and slow-twitch skeletal muscles in the rat. *Biogerontology*. 2013;14(3):293-301. doi:10.1007/S10522-013-9430-Y

121. Yang X, Arber S, William C, et al. Patterning of Muscle Acetylcholine Receptor Gene Expression in the Absence of Motor Innervation. *Neuron*. 2001;30(2):399-410. doi:10.1016/S0896-6273(01)00287-2

122. Sanes JR, Lichtman JW. Induction, assembly, maturation and maintenance of a postsynaptic apparatus. *Nature Reviews Neuroscience 2001 2:11*. 2001;2(11):791-805. doi:10.1038/35097557

123. Patton BL, Miner JH, Chiu AY, Sanes JR. Distribution and Function of Laminins in the Neuromuscular System of Developing, Adult, and Mutant Mice. *Journal of Cell Biology*. 1997;139(6):1507-1521. doi:10.1083/JCB.139.6.1507

124. Rogers RS, Nishimune H. THE ROLE OF LAMININS IN THE ORGANIZATION AND FUNCTION OF NEUROMUSCULAR JUNCTIONS. *Matrix Biol*. 2017;57-58:86. doi:10.1016/J.MATBIO.2016.08.008

125. Yu WM, Yu H, Chen ZL. Laminins in Peripheral Nerve Development and Muscular Dystrophy. *Molecular Neurobiology 2007 35:3*. 2007;35(3):288-297. doi:10.1007/S12035-007-0026-X

126. Tricaud N. Myelinating Schwann Cell Polarity and Mechanically-Driven Myelin Sheath Elongation. *Front Cell Neurosci*. 2018;0:414. doi:10.3389/FNCEL.2017.00414

127. Gordon T. Peripheral Nerve Regeneration and Muscle Reinnervation. *Int J Mol Sci*. 2020;21(22):1-24. doi:10.3390/IJMS21228652

128. Willadt S, Nash M, Slater CR. Age-related fragmentation of the motor endplate is not associated with impaired neuromuscular transmission in the mouse diaphragm. *Scientific Reports 2016 6:1*. 2016;6(1):1-8. doi:10.1038/srep24849

129. Bao Z, Cui C, Chow SKH, Qin L, Wong RMY, Cheung WH. AChRs Degeneration at NMJ in Aging-Associated Sarcopenia–A Systematic Review. *Front Aging Neurosci*. 2020;0:454. doi:10.3389/FNAGI.2020.597811

130. Bodine SC, Baehr LM. Skeletal muscle atrophy and the E3 ubiquitin ligases MuRF1 and MAFbx/atrogin-1. *https://doi.org/101152/ajpendo002042014*. 2014;307(6):E469-E484. doi:10.1152/AJPENDO.00204.2014

131. Fu XQ, Peng J, Wang AH, Luo ZG. Tumor necrosis factor alpha mediates neuromuscular synapse elimination. *Cell Discovery 2020 6:1*. 2020;6(1):1-14. doi:10.1038/s41421-020-0143-5

132. Monaco CMF, Gingrich MA, Hawke TJ. Considering Type 1 Diabetes as a Form of Accelerated Muscle Aging. *Exerc Sport Sci Rev*. 2019;47(2):98-107. doi:10.1249/JES.0000000000000184

133. Mesinovic J, Zengin A, Courten B De, Ebeling PR, Scott D. Sarcopenia and type 2 diabetes mellitus: a bidirectional relationship . *Diabetes Metab Syndr Obes*. 2019;12:1057-1072. doi:10.2147/DMSO.S186600

134. Popescu S, Timar B, Baderca F, et al. Age as an independent factor for the development of neuropathy in diabetic patients. *Clin Interv Aging*. 2016;11:313-318. doi:10.2147/CIA.S97295

135. TJ H, SA P, L C, et al. Insulin prevents depolarization of the mitochondrial inner membrane in sensory neurons of type 1 diabetic rats in the presence of sustained hyperglycemia. *Diabetes*. 2003;52(8):2129-2136. doi:10.2337/DIABETES.52.8.2129

136. Dobretsov M, Romanovsky D, Stimers JR. Early diabetic neuropathy: Triggers and mechanisms. *World Journal of Gastroenterology : WJG*. 2007;13(2):175. doi:10.3748/WJG.V13.I2.175

137. M B, G N. Peripheral neuropathies and aging. *Geriatr Psychol Neuropsychiatr Vieil*. 2018;16(4):409-413. doi:10.1684/PNV.2018.0768

138. Almurdhi MM, Reeves ND, Bowling FL, Boulton AJM, Jeziorska M, Malik RA. Reduced Lower-Limb Muscle Strength and Volume in Patients With Type 2 Diabetes in Relation to Neuropathy, Intramuscular Fat, and Vitamin D Levels. *Diabetes Care*. 2016;39(3):441-447. doi:10.2337/DC15-0995

139. Andersen H, Nielsen S, Mogensen CE, Jakobsen J. Muscle Strength in Type 2 Diabetes. *Diabetes*. 2004;53(6):1543-1548. doi:10.2337/DIABETES.53.6.1543

140. Abe T, Loenneke JP, Thiebaud RS, Fukunaga T. Age-related site-specific muscle wasting of upper and lower extremities and trunk in Japanese men and women. *Age (Omaha)*. 2014;36(2):813. doi:10.1007/S11357-013-9600-5

141. Abe T, Sakamaki M, Yasuda T, et al. Age-Related, Site-Specific Muscle Loss in 1507 Japanese Men and Women Aged 20 to 95 Years. *J Sports Sci Med*. 2011;10(1):145. Accessed September 22, 2021. /pmc/articles/PMC3737910/

142. H M, A K, M A, et al. Advanced glycation end-products are a risk for muscle weakness in Japanese patients with type 1 diabetes. *J Diabetes Investig*. 2017;8(3):377-382. doi:10.1111/JDI.12582

143. H M, A K, M I, et al. Association of accumulated advanced glycation end-products with a high prevalence of sarcopenia and dynapenia in patients with type 2 diabetes. *J Diabetes Investig*. 2019;10(5):1332-1340. doi:10.1111/JDI.13014

144. Piasecki M, Ireland A, Jones DA, McPhee JS. Age-dependent motor unit remodelling in human limb muscles. *Biogerontology*. 2016;17(3):485. doi:10.1007/S10522-015-9627-3

145. Ling SM, Conwit RA, Ferrucci L, Metter EJ. Age-Associated Changes in Motor Unit Physiology: Observations From the Baltimore Longitudinal Study of Aging. *Arch Phys Med Rehabil*. 2009;90(7):1237. doi:10.1016/J.APMR.2008.09.565

146. Chiu CY, Yang R Sen, Sheu ML, et al. Advanced glycation end-products induce skeletal muscle atrophy and dysfunction in diabetic mice via a RAGE-mediated, AMPK-down-regulated, Akt pathway. *J Pathol*. 2016;238(3):470-482. doi:10.1002/PATH.4674

147. Singh VP, Bali A, Singh N, Jaggi AS. Advanced Glycation End Products and Diabetic Complications. *Korean J Physiol Pharmacol*. 2014;18(1):1. doi:10.4196/KJPP.2014.18.1.1

148. Wilson NM, Wright DE. Experimental motor neuropathy in diabetes. *Handb Clin Neurol*. 2014;126:461-467. doi:10.1016/B978-0-444-53480-4.00030-8

149. Dyck PJ, Kratz KM, Karnes JL, et al. The prevalence by staged severity of various types of diabetic neuropathy, retinopathy, and nephropathy in a population-based cohort. *Neurology*. 1993;43(4):817-817. doi:10.1212/WNL.43.4.817

150. Feldman EL, Nave KA, Jensen TS, Bennett DLH. New Horizons in Diabetic Neuropathy: Mechanisms, Bioenergetics, and Pain. *Neuron*. 2017;93(6):1296-1313. doi:10.1016/J.NEURON.2017.02.005

151. Muramatsu K. Diabetes Mellitus-Related Dysfunction of the Motor System. *International Journal of Molecular Sciences 2020, Vol 21, Page 7485*. 2020;21(20):7485. doi:10.3390/IJMS21207485

152. Ramji N, Toth C, Kennedy J, Zochodne DW. Does diabetes mellitus target motor neurons? *Neurobiol Dis*. 2007;26(2):301-311. doi:10.1016/J.NBD.2006.11.016

153. YC EB, PATS C, GLF L, et al. Reaching task performance is associated to neuromuscular junction adaptations in rats with induced diabetes mellitus. *Braz J Med Biol Res*. 2020;53(7). doi:10.1590/1414-431X20208763

154. NE C, MA C, K D, A L. Effects of aminoguanidine on peripheral nerve function and polyol pathway metabolites in streptozotocin-diabetic rats. *Diabetologia*. 1992;35(10):946-950. doi:10.1007/BF00401423

155. Cameron NE, Gibson TM, Nangle MR, Cotter MA. Inhibitors of Advanced Glycation End Product Formation and Neurovascular Dysfunction in Experimental Diabetes. *Ann N Y Acad Sci*. 2005;1043(1):784-792. doi:10.1196/ANNALS.1333.091

156. Y N, R W, M B, M T, C HI, S Y. Neuropathy induced by exogenously administered advanced glycation end-products in rats. *J Diabetes Investig*. 2010;1(1-2):40-49. doi:10.1111/J.2040-1124.2009.00002.X

157. Öztürk G, Şekeroğlu MR, Erdoğan E, Öztürk M. The effect of non-enzymatic glycation of extracellular matrix proteins on axonal regeneration in vitro. *Acta Neuropathologica 2006 112:5*. 2006;112(5):627-632. doi:10.1007/S00401-006-0124-2

158. Duran-Jimenez B, Dobler D, Moffatt S, et al. Advanced Glycation End Products in Extracellular Matrix Proteins Contribute to the Failure of Sensory Nerve Regeneration in Diabetes. *Diabetes*. 2009;58(12):2893-2903. doi:10.2337/DB09-0320

159. Gumy LF, Bampton ETW, Tolkovsky AM. Hyperglycaemia inhibits Schwann cell proliferation and migration and restricts regeneration of axons and Schwann cells from adult murine DRG. *Molecular and Cellular Neuroscience*. 2008;37(2):298-311. doi:10.1016/J.MCN.2007.10.004

160. Sango K, Horie H, Saito H, et al. Diabetes is not a potent inducer of neuronal cell death in mouse sensory ganglia, but it enhances neurite regeneration in vitro. *Life Sci*. 2002;71(20):2351-2368. doi:10.1016/S0024-3205(02)02040-4

161. H S, K S, H H, et al. Enhanced neural regeneration from transected vagus nerve terminal in diabetic mice in vitro. *Neuroreport*. 1999;10(5):1025-1028. doi:10.1097/00001756-199904060-00024

162. Nishida N, Yamagishi SI, Mizukami H, Yagihashi S. Impaired nerve fiber regeneration in axotomized peripheral nerves in streptozotocin-diabetic rats. *J Diabetes Investig*. 2013;4(6):533-539. doi:10.1111/JDI.12115

163. H Y, M T, Y T, et al. Impaired regeneration and no amelioration with aldose reductase inhibitor in crushed unmyelinated nerve fibers of diabetic rats. *Neuroreport*. 1999;10(11):2405-2409. doi:10.1097/00001756-199908020-00034

164. Sango K, Mizukami H, Horie H, Yagihashi S. Impaired Axonal Regeneration in Diabetes. Perspective on the Underlying Mechanism from In Vivo and In Vitro Experimental Studies. *Front Endocrinol (Lausanne)*. 2017;0(FEB):12. doi:10.3389/FENDO.2017.00012

165. Eckersley L. Role of the Schwann cell in diabetic neuropathy. *Int Rev Neurobiol*. 2002;50:293-321. doi:10.1016/S0074-7742(02)50081-7

166. Ota K, Nakamura J, Li W, et al. Metformin prevents methylglyoxal-induced apoptosis of mouse Schwann cells. *Biochem Biophys Res Commun*. 2007;357(1):270-275. doi:10.1016/J.BBRC.2007.03.140

167. Xu S, Bao W, Men X, et al. Interleukin-10 Protects Schwann Cells against Advanced Glycation End Products-Induced Apoptosis via NF-κB Suppression. *Experimental and Clinical Endocrinology & Diabetes*. 2019;128(02):89-96. doi:10.1055/A-0826-4374

168. Sekido H, Suzuki T, Jomori T, Takeuchi M, Yabe-Nishimura C, Yagihashi S. Reduced cell replication and induction of apoptosis by advanced glycation end products in rat Schwann cells. *Biochem Biophys Res Commun*. 2004;320(1):241-248. doi:10.1016/J.BBRC.2004.05.159

169. Fukunaga M, Miyata S, Liu BF, et al. Methylglyoxal induces apoptosis through activation of p38 MAPK in rat Schwann cells. *Biochem Biophys Res Commun*. 2004;320(3):689-695. doi:10.1016/J.BBRC.2004.06.011

170. Kim KM, Jang HC, Lim S. Differences among skeletal muscle mass indices derived from height-, weight-, and body mass index-adjusted models in assessing sarcopenia. *Korean J Intern Med*. 2016;31(4):643-650. doi:10.3904/kjim.2016.015

171. Csapo R, Gumpenberger M, Wessner B. Skeletal Muscle Extracellular Matrix – What Do We Know About Its Composition, Regulation, and Physiological Roles? A Narrative Review. *Front Physiol*. 2020;11:253. doi:10.3389/FPHYS.2020.00253

172. Urciuolo A, De Coppi P. Decellularized Tissue for Muscle Regeneration. *International Journal of Molecular Sciences* . 2018;19(8). doi:10.3390/ijms19082392

173. Gilpin A, Yang Y. Decellularization Strategies for Regenerative Medicine: From Processing Techniques to Applications. Published online 2017. doi:10.1155/2017/9831534

174. Zhang J, Hu ZQ, Turner NJ, et al. Perfusion-decellularized skeletal muscle as a three-dimensional scaffold with a vascular network template. *Biomaterials*. 2016;89:114-126. doi:10.1016/j.biomaterials.2016.02.040

175. Porzionato A, Sfriso MM, Pontini A, et al. Decellularized Human Skeletal Muscle as Biologic Scaffold for Reconstructive Surgery. *International Journal of Molecular Sciences* . 2015;16(7). doi:10.3390/ijms160714808

176. Kasukonis B, Kim J, Brown L, et al. Codelivery of Infusion Decellularized Skeletal Muscle with Minced Muscle Autografts Improved Recovery from Volumetric Muscle Loss Injury in a Rat Model. *Tissue Eng Part A*. 2016;22(19-20):1151-1163. doi:10.1089/ten.tea.2016.0134

177. Wolf MT, Dearth CL, Sonnenberg SB, Loboa EG, Badylak SF. Naturally derived and synthetic scaffolds for skeletal muscle reconstruction. *Adv Drug Deliv Rev*. 2015;84:208-221. doi:10.1016/j.addr.2014.08.011

178. Urciuolo A, Urbani L, Perin S, et al. Decellularised skeletal muscles allow functional muscle regeneration by promoting host cell migration. *Sci Rep*. 2018;8(1):8398. doi:10.1038/s41598-018-26371-y

179. Perniconi B, Coletti D, Aulino P, et al. Muscle acellular scaffold as a biomaterial: Effects on C2C12 cell differentiation and interaction with the murine host environment. *Front Physiol*. 2014;5(SEP). doi:10.3389/fphys.2014.00354

180. McClure MJ, Cohen DJ, Ramey AN, et al. Decellularized Muscle Supports New Muscle Fibers and Improves Function Following Volumetric Injury. *Tissue Eng Part A*. 2018;24(15-16):1228-1241. doi:10.1089/ten.tea.2017.0386

181. Chaturvedi V, Dye DE, Kinnear BF, Van Kuppevelt TH, Grounds MD, Coombe DR. Interactions between Skeletal Muscle Myoblasts and their Extracellular Matrix Revealed by a Serum Free Culture System. Published online 2015. doi:10.1371/journal.pone.0127675

182. Kim JT, Kasukonis BM, Brown LA, Washington TA, Wolchok JC. Recovery from volumetric muscle loss injury: A comparison between young and aged rats. *Exp Gerontol*. 2016;83:37-46. doi:10.1016/j.exger.2016.07.008

183. Kim JT, Kasukonis B, Dunlap G, Perry R, Washington T, Wolchok JC. Regenerative Repair of Volumetric Muscle Loss Injury is Sensitive to Age. *Tissue Eng Part A*. 2020;26(1-2):3-14. doi:10.1089/ten.tea.2019.0034

184. McClure MJ, Olson LC, Cohen DJ, et al. Rnu (Foxn1^{rnu}-nude) rats demonstrate an improved ability to regenerate muscle in a volumetric muscle injury compared to sprague dawley rats. *Bioengineering*. 2021;8(1). doi:10.3390/bioengineering8010012

185. Giacomello E, Crea E, Torelli L, et al. Age dependent modification of the metabolic profile of the tibialis anterior muscle fibers in C57BL/6J mice. *Int J Mol Sci*. 2020;21(11):3923. doi:10.3390/ijms21113923

186. Agbulut O, Destombes J, Thiesson D, Butler-Browne G. Age-related appearance of tubular aggregates in the skeletal muscle of almost all male inbred mice. *Histochem Cell Biol*. 2000;114(6):477-481. doi:10.1007/s004180000211

187. Cundy T, Reid IR, Grey A. Metabolic bone disease. *Clinical Biochemistry: Metabolic and Clinical Aspects: Third Edition*. Published online January 1, 2014:604-635. doi:10.1016/B978-0-7020-5140-1.00031-6

188. J S, C C. Skeletal muscle fiber types in the adult mouse. *Acta Neurol Scand*. 1976;54(1):45-56. doi:10.1111/J.1600-0404.1976.TB07619.X

189. RS S, WJ K, RS H, AC F, JD M, GE C. Fiber type composition of four hindlimb muscles of adult Fisher 344 rats. *Histochem Cell Biol*. 1999;111(2):117-123. doi:10.1007/S004180050341

190. Real-Martinez A, Brull A, Huerta J, et al. Low survival rate and muscle fiber-dependent aging effects in the McArdle disease mouse model. *Scientific Reports 2019 9:1*. 2019;9(1):1-14. doi:10.1038/s41598-019-41414-8

191. Verzijl N, DeGroot J, Thorpe SR, et al. Effect of collagen turnover on the accumulation of advanced glycation end products. *Journal of Biological Chemistry*. 2000;275(50):39027-39031. doi:10.1074/jbc.M006700200

192. Graber TG, Kim JH, Grange RW, et al. C57BL/6 life span study: age-related declines in muscle power production and contractile velocity. doi:10.1007/s11357-015-9773-1

193. Hill C, James RS, Cox ValM, Seebacher F, Tallis J. Age-related changes in isolated mouse skeletal muscle function are dependent on sex, muscle, and contractility mode. *American Journal of Physiology-Regulatory, Integrative and Comparative Physiology*. 2020;319(3):R296-R314. doi:10.1152/ajpregu.00073.2020

194. Uchitomi R, Hatazawa Y, senoo N, et al. Metabolomic Analysis of skeletal Muscle in Aged Mice. doi:10.1038/s41598-019-46929-8

195. Saulnier PJ, Wheelock KM, Howell S, et al. Advanced Glycation End Products Predict Loss of Renal Function and Correlate With Lesions of Diabetic Kidney Disease in American Indians With Type 2 Diabetes. *Diabetes*. 2016;65(12):3744-3753. doi:10.2337/db16-0310

196. Flurkey K, Currer JM, Harrison DE. Mouse Models in Aging Research. *The Mouse in Biomedical Research*. 2007;3:637-672. doi:10.1016/B978-012369454-6/50074-1

197. Yuan R, Peters LL, Paigen B. Mice as a Mammalian Model for Research on the Genetics of Aging. *ILAR journal / National Research Council, Institute of Laboratory Animal Resources*. 2011;52(1):4. doi:10.1093/ILAR.52.1.4

198. Valentine MS, Link PA, Herbert JA, et al. Inflammation and Monocyte Recruitment Due to Aging and Mechanical Stretch in Alveolar Epithelium are Inhibited by the Molecular Chaperone 4-Phenylbutyrate. *Cell Mol Bioeng*. 2018;11(6):495. doi:10.1007/S12195-018-0537-8

199. Cousin W, Ho ML, Desai R, et al. Regenerative Capacity of Old Muscle Stem Cells Declines without Significant Accumulation of DNA Damage. *PLoS One*. 2013;8(5):e63528. doi:10.1371/JOURNAL.PONE.0063528

200. VL F, RA A, TA B, SJ S. Bone development and age-related bone loss in male C57BL/6J mice. *Bone*. 2003;33(3):387-398. doi:10.1016/S8756-3282(03)00199-6

201. Linn SC, Mustonen AM, Silva KA, et al. Nail Abnormalities Identified in an Aging Study of 30 Inbred Mouse Strains. *Exp Dermatol*. 2019;28(4):383. doi:10.1111/EXD.13759

202. Sugiyama Y, Naito K, Goto K, et al. Effect of aging on the tendon structure and tendon-associated gene expression in mouse foot flexor tendon. *Biomed Rep*. 2019;10(4):238-244. doi:10.3892/BR.2019.1200

203. Tarrant JC, Savickas P, Omodho L, Spinazzi M, Radaelli E. Spontaneous Incidental Brain Lesions in C57BL/6J Mice: *https://doi.org/101177/0300985819859878*. 2019;57(1):172-182. doi:10.1177/0300985819859878

204. Gehwolf R, Wagner A, Lehner C, et al. Pleiotropic roles of the matricellular protein Sparc in tendon maturation and ageing. *Scientific Reports 2016 6:1*. 2016;6(1):1-15. doi:10.1038/srep32635

205. Huang H, Skelly JD, Ayers DC, Song J. Age-dependent Changes in the Articular Cartilage and Subchondral Bone of C57BL/6 Mice after Surgical Destabilization of Medial Meniscus. *Scientific Reports 2017 7:1*. 2017;7(1):1-9. doi:10.1038/srep42294

206. Menees KB, Earls RH, Chung J, et al. Sex- and age-dependent alterations of splenic immune cell profile and NK cell phenotypes and function in C57BL/6J mice. *Immunity & Ageing 2021 18:1*. 2021;18(1):1-13. doi:10.1186/S12979-021-00214-3

207. Kim KA, Jeong JJ, Yoo SY, Kim DH. Gut microbiota lipopolysaccharide accelerates inflamm-aging in mice. *BMC Microbiology 2016 16:1*. 2016;16(1):1-9. doi:10.1186/S12866-016-0625-7

208. CV M, DM G, CE F. Reproductive senescence in female C57BL/6J mice: ovarian impairments and neuroendocrine impairments that are partially reversible and delayable by ovariectomy. *Endocrinology*. 1984;115(5):1653-1662. doi:10.1210/ENDO-115-5-1653

209. Chen H, Wang X, Han J, et al. AKT and its related molecular feature in aged mice skin. *PLoS One*. 2017;12(6):e0178969. doi:10.1371/JOURNAL.PONE.0178969

210. Kovanen V, Suominen H, Peltonen L. Effects of aging and life-long physical training on collagen in slow and fast skeletal muscle in rats - A morphometric and immuno-histochemical study. *Cell Tissue Res*. 1987;248(2):247-255. doi:10.1007/BF00218191

211. Petrany MJ, Swoboda CO, Sun C, et al. Single-nucleus RNA-seq identifies transcriptional heterogeneity in multinucleated skeletal myofibers. *Nat Commun*. 2020;11(1). doi:10.1038/S41467-020-20063-W

212. Donalies M, Cramer M, Ringwald M, Starzinski-Powitz A. Expression of M-cadherin, a member of the cadherin multigene family, correlates with differentiation of skeletal muscle cells. *Proceedings of the National Academy of Sciences*. 1991;88(18):8024 LP - 8028. doi:10.1073/pnas.88.18.8024

213. Marti M, Montserrat N, Pardo C, et al. M-cadherin-mediated intercellular interactions activate satellite cell division. *J Cell Sci*. 2013;126(22):5116-5131. doi:10.1242/jcs.123562

214. Sajko P, Kubínová L, Cvetko E, Kreft M, Wernig A, Er I. *Frequency of M-Cadherin-Stained Satellite Cells Declines in Human Muscles During Aging*. Vol 52.; 2004. http://www.jhc.org

215. Moore R, Walsh FS. The cell adhesion molecule M-cadherin is specifically expressed in developing and regenerating, but not denervated skeletal muscle. *Development*. 1993;117(4):1409-1420.

216. Boppart MD, Mahmassani ZS. Integrin signaling: linking mechanical stimulation to skeletal muscle hypertrophy. *American Journal of Physiology-Cell Physiology*. 2019;317(4):C629-C641. doi:10.1152/ajpcell.00009.2019

217. Sarathy A, Wuebbles RD, Fontelonga TM, et al. SU9516 Increases α7β1 Integrin and Ameliorates Disease Progression in the mdx Mouse Model of Duchenne Muscular Dystrophy. *Molecular Therapy*. 2017;25(6):1395-1407. doi:10.1016/j.ymthe.2017.03.022

218. Rozo M, Li L, Fan CM. Targeting β1-Integrin Signaling Enhances Regeneration in Aged and Dystrophic Muscle in Mice. *Nat Med*. 2016;22(8):889. doi:10.1038/NM.4116

219. Garg K, Mahmassani ZS, Dvoretskiy S, et al. Laminin-111 Improves the Anabolic Response to Mechanical Load in Aged Skeletal Muscle. Anderson RM, ed. *The Journals of Gerontology: Series A*. 2021;76(4):586-590. doi:10.1093/gerona/glaa308

220. Snow LM, McLoon LK, Thompson L V. Adult and developmental myosin heavy chain isoforms in soleus muscle of aging Fischer Brown Norway rat. *Anatomical Record - Part A Discoveries in Molecular, Cellular, and Evolutionary Biology*. 2005;286(1):866-873. doi:10.1002/ar.a.20218

221. Ballak SB, Degens H, de Haan A, Jaspers RT. Aging related changes in determinants of muscle force generating capacity: A comparison of muscle aging in men and male rodents. *Ageing Res Rev*. 2014;14(1):43-55. doi:10.1016/j.arr.2014.01.005

222. Haus JM, Carrithers JA, Miller BI, Trappe TA. Intramuscular collagen cross-linking in aging men and women. *The FASEB Journal*. 2007;21(6):LB118-LB118. doi:https://doi.org/10.1096/fasebj.21.6.LB118

223. Rahman N, O'neill E, Irnaten M, Wallace D, O'brien C. Corneal Stiffness and Collagen Cross-Linking Proteins in Glaucoma: Potential for Novel Therapeutic Strategy. doi:10.1089/jop.2019.0118

224. Pavan P, Monti E, Bondí M, et al. Alterations of Extracellular Matrix Mechanical Properties Contribute to Age-Related Functional Impairment of Human Skeletal Muscles. *International Journal of Molecular Sciences Article*. doi:10.3390/ijms21113992

225. Olivares-Navarrete R, Lee EM, Smith K, Hyzy SL, Doroudi M, Williams JK. Substrate Stiffness Controls Osteoblastic and Chondrocytic Differentiation of Mesenchymal Stem Cells without Exogenous Stimuli. *PLoS One*. 2017;12(1):170312. doi:10.1371/journal.pone.0170312

226. Rowlands AS, George PA, Cooper-White JJ. Directing osteogenic and myogenic differentiation of MSCs: Interplay of stiffness and adhesive ligand presentation. *Am J Physiol Cell Physiol*. 2008;295(4):1037-1044. doi:10.1152/ajpcell.67.2008

227. Imayama S, Braverman IM. *A Hypothetical Explanation for the Aging of Skin Chronologic Alteration of the Three-Dimensional Arrangement of Collagen and Elastic Fibers in Connective Tissue Materials and Methods Normal Male Wistar and Sprague-Dawley Rats from Na-Tional Institute on Aging (National Institute for Health*. Vol 134.; 1989.

228. Rabbani N, Thornalley PJ. Hidden complexities in the measurement of fructosyl-lysine and advanced glycation end products for risk prediction of vascular complications of diabetes. *Diabetes*. 2015;64(1):9-11. doi:10.2337/db14-1516

229. Dhar A, Udumula MP, Medapi B, et al. Pharmacological evaluation of novel alagebrium analogs as methylglyoxal scavengers in vitro in cardiac myocytes and in vivo in SD rats. *Int J Cardiol*. 2016;223:581-589. doi:10.1016/j.ijcard.2016.08.243

230. Johnson TD, DeQuach JA, Gaetani R, et al. Human versus porcine tissue sourcing for an injectable myocardial matrix hydrogel. *Biomater Sci*. 2014;2014(5):60283D. doi:10.1039/C3BM60283D

231. Briguet A, Courdier-Fruh I, Foster M, Meier T, Magyar JP. Histological parameters for the quantitative assessment of muscular dystrophy in the mdx-mouse. *Neuromuscular Disorders*. 2004;14(10):675-682. doi:10.1016/J.NMD.2004.06.008

232. Vigelsø A, Dybboe R, Hansen CN, Dela F, Helge JW, Grau AG. GAPDH and β-actin protein decreases with aging, making Stain-Free technology a superior loading control in Western blotting of human skeletal muscle. *https://doi.org/101152/japplphysiol008402014*. 2015;118(3):386-394. doi:10.1152/JAPPLPHYSIOL.00840.2014

233. von Haehling S, Morley JE, Anker SD. An overview of sarcopenia: facts and numbers on prevalence and clinical impact. *J Cachexia Sarcopenia Muscle*. 2010;1(2):129. doi:10.1007/S13539-010-0014-2

234. Berberoglu MA, Gallagher TL, Morrow ZT, et al. Satellite-like cells contribute to pax7-dependent skeletal muscle repair in adult zebrafish. *Dev Biol*. 2017;424(2):162. doi:10.1016/J.YDBIO.2017.03.004

235. Sabourin LA, Rudnicki MA. The molecular regulation of myogenesis. *Clin Genet*. 2000;57(1):16-25. doi:10.1034/j.1399-0004.2000.570103.x

236. Carlson BM. Denervation and the Aging of Skeletal Muscle. *Basic and Applied Myology*. 2004;14(3):135-139.

237. Yin H, Price F, Rudnicki MA. Satellite cells and the muscle stem cell niche. *Physiol Rev*. 2013;93(1):23-67. doi:10.1152/physrev.00043.2011

238. Olson LC, Redden JT, Schwartz Z, Cohen DJ, McClure MJ. Advanced Glycation End-Products in Skeletal Muscle Aging. *Bioengineering (Basel)*. 2021;8(11). doi:10.3390/BIOENGINEERING8110168

239. Nederveen JP, Joanisse S, Thomas ACQ, et al. Age-related changes to the satellite cell niche are associated with reduced activation following exercise. *The FASEB Journal*. 2020;34(7):8975-8989. doi:10.1096/FJ.201900787R

240. Roe JH, Rice EW. A PHOTOMETRIC METHOD FOR THE DETERMINATION OF FREE PENTOSES IN ANIMAL TISSUES*. Published online 1948. doi:10.1016/S0021-9258(18)57423-8

241. Alzoubi KH, Ismail ZB, Al-Essa MK, Alshogran OY, Abutayeh RF, Abu-Baker N. Pharmacokinetic evaluation of D-ribose after oral and intravenous administration to healthy rabbits. *Clin Pharmacol*. 2018;10:73. doi:10.2147/CPAA.S167150

242. Guex AG, Puetzer JL, Armgarth A, et al. Highly porous scaffolds of PEDOT:PSS for bone tissue engineering. *Acta Biomater*. 2017;62:91-101. doi:10.1016/J.ACTBIO.2017.08.045

243. Gouldin AG, Brown ME, Puetzer JL. An inducible model for unraveling the effects of advanced glycation end-product accumulation in aging connective tissues. *Connect Tissue Res*. 2022;63(4):406-424. doi:10.1080/03008207.2021.1991333

244. Puetzer JL, Ma T, Sallent I, Gelmi A, Stevens MM. Driving Hierarchical Collagen Fiber Formation for Functional Tendon, Ligament, and Meniscus Replacement. *Biomaterials*. 2021;269. doi:10.1016/J.BIOMATERIALS.2020.120527

245. Bates ME, Troop L, Brown ME, Puetzer JL. Temporal application of lysyl oxidase during hierarchical collagen fiber formation differentially effects tissue mechanics. *Acta Biomater*. 2023;160. doi:10.1016/J.ACTBIO.2023.02.024

246. Blau HM, Chiu CP, Webster C. Cytoplasmic activation of human nuclear genes in stable heterocaryons. *Cell*. 1983;32(4):1171-1180. doi:10.1016/0092-8674(83)90300-8

247. Adachi N, Kanazawa I, Tanaka K ichiro, et al. Insulin-Like Growth Factor-I Protects Against the Detrimental Effects of Advanced Glycation End Products and High Glucose in Myoblastic C2C12 Cells. *Calcif Tissue Int*. 2019;105(1):89-96. doi:10.1007/S00223-019-00537-W/FIGURES/5

248. Takata T, Sakasai-Sakai A, Takeuchi M. Impact of intracellular toxic advanced glycation end-products (TAGE) on murine myoblast cell death. *Diabetol Metab Syndr*. 2020;12(1):1-8. doi:10.1186/S13098-020-00561-Z/FIGURES/2

249. Pinto-Junior DC, Silva KS, Michalani ML, et al. Advanced glycation end products-induced insulin resistance involves repression of skeletal muscle GLUT4 expression. *Scientific Reports 2018 8:1*. 2018;8(1):1-11. doi:10.1038/s41598-018-26482-6

250. van Santen VJB, Klein-Nulend J, Bakker AD, Jaspers RT. Stiff matrices enhance myoblast proliferation, reduce differentiation, and alter the response to fluid shear stress in vitro. *Cell Biochem Biophys*. 2022;80(1):161-170. doi:10.1007/S12013-021-01050-4

251. Deane R, Singh I, Sagare AP, et al. A multimodal RAGE-specific inhibitor reduces amyloid β-mediated brain disorder in a mouse model of Alzheimer disease. *J Clin Invest*. 2012;122(4):1377-1392. doi:10.1172/JCI58642

252. Burstein AH, Sabbagh M, Andrews R, Valcarce C, Dunn I, Altstiel L. Development of Azeliragon, an Oral Small Molecule Antagonist of the Receptor for Advanced Glycation Endproducts, for the Potential Slowing of Loss of Cognition in Mild Alzheimer's Disease. *J Prev Alzheimers Dis*. 2018;5(2):1-6. doi:10.14283/JPAD.2018.18

253. Hu LY, Mileti CJ, Loomis T, et al. Skeletal muscle progenitors are sensitive to collagen architectural features of fibril size and cross linking. *Am J Physiol Cell Physiol*. 2021;321(2):C330-C342. doi:10.1152/AJPCELL.00065.2021/ASSET/IMAGES/LARGE/AJPCELL.00065.2021_F005.JPEG

254. Trensz F, Lucien F, Couture V, et al. Erratum: Increased microenvironment stiffness in damaged myofibers promotes myogenic progenitor cell proliferation [Skelet Muscle., 5 (2015) (5)]. *Skelet Muscle*. 2016;6(1):1-16. doi:10.1186/s13395-016-0109-3

255. MH B, AT J, G R, et al. Methylglyoxal and Advanced Glycation End products: Insight of the regulatory machinery affecting the myogenic program and of its modulation by natural compounds. *Sci Rep*. 2017;7(1). doi:10.1038/S41598-017-06067-5

256. McClure MJ, Ramey AN, Rashid M, Boyan BD, Schwartz Z. Integrin-α7 signaling regulates connexin 43, M-cadherin, and myoblast fusion. *Am J Physiol Cell Physiol*. 2019;316(6):C876-C887. doi:10.1152/AJPCELL.00282.2018

257. Blaschuk KL, Guérin C, Holland PC. Myoblast αvβ3 Integrin Levels Are Controlled by Transcriptional Regulation of Expression of the β3 Subunit and Down-regulation of β3 Subunit Expression Is Required for Skeletal Muscle Cell Differentiation. *Dev Biol*. 1997;184(2):266-277. doi:10.1006/DBIO.1997.8527

258. Ozeki N, Jethanandani P, Nakamura H, Ziober BL, Kramer RH. Modulation of satellite cell adhesion and motility following BMP2-induced differentiation to osteoblast lineage. *Biochem Biophys Res Commun*. 2007;353(1):54. doi:10.1016/J.BBRC.2006.11.110

259. Cachaço AS, Pereira CS, Pardal RG, Bajanca F, Thorsteinsdóttir S. Integrin repertoire on myogenic cells changes during the course of primary myogenesis in the mouse. *Developmental Dynamics*. 2005;232(4):1069-1078. doi:10.1002/DVDY.20280

260. McCarthy AD, Uemura T, Etcheverry SB, Cortizo AM. Advanced glycation endproducts interfere with integrin-mediated osteoblastic attachment to a type-I collagen matrix. *International Journal of Biochemistry and Cell Biology*. 2004;36(5):840-848. doi:10.1016/j.biocel.2003.09.006

261. Xie SJ, Li JH, Chen HF, et al. Inhibition of the JNK/MAPK signaling pathway by myogenesis-associated miRNAs is required for skeletal muscle development. *Cell Death & Differentiation 2018 25:9*. 2018;25(9):1581-1597. doi:10.1038/s41418-018-0063-1

262. Perdiguero E, Ruiz-Bonilla V, Gresh L, et al. Genetic analysis of p38 MAP kinases in myogenesis: fundamental role of p38α in abrogating myoblast proliferation. *EMBO J*. 2007;26(5):1245. doi:10.1038/SJ.EMBOJ.7601587

263. Wu Z, Woodring PJ, Bhakta KS, et al. p38 and Extracellular Signal-Regulated Kinases Regulate the Myogenic Program at Multiple Steps. *Mol Cell Biol*. 2000;20(11):3951. doi:10.1128/MCB.20.11.3951-3964.2000

264. Guttridge DC, Albanese C, Reuther JY, Pestell RG, Albert S. Baldwin Jr. NF-κB Controls Cell Growth and Differentiation through Transcriptional Regulation of Cyclin D1. *Mol Cell Biol*. 1999;19(8):5785. doi:10.1128/MCB.19.8.5785

265. Bakkar N, Wang J, Ladner KJ, et al. IKK/NF-κB regulates skeletal myogenesis via a signaling switch to inhibit differentiation and promote mitochondrial biogenesis. *J Cell Biol*. 2008;180(4):787. doi:10.1083/JCB.200707179

266. ERK1/2 is required for myoblast proliferation but is dispensable for muscle gene expression and cell fusion - Jones - 2001 - Journal of Cellular Physiology - Wiley Online Library. Accessed June 12, 2023. https://onlinelibrary.wiley.com/doi/10.1002/1097-4652(200101)186:1%3C104::AID-JCP1015%3E3.0.CO;2-0

267. Hong Y, Shen C, Yin Q, Sun M, Ma Y, Liu X. Effects of RAGE-Specific Inhibitor FPS-ZM1 on Amyloid-β Metabolism and AGEs-Induced Inflammation and Oxidative Stress in Rat Hippocampus. *Neurochem Res*. 2016;41(5):1192-1199. doi:10.1007/S11064-015-1814-8

268. Burstein AH, Sabbagh M, Andrews R, Valcarce C, Dunn I, Altstiel L. Development of Azeliragon, an Oral Small Molecule Antagonist of the Receptor for Advanced Glycation Endproducts, for the Potential Slowing of Loss of Cognition in Mild Alzheimer's Disease. *J Prev Alzheimers Dis*. 2018;5(2):1-6. doi:10.14283/JPAD.2018.18

269. Fischer JP, Elliott RM, Kozin SH, Levin LS. Free function muscle transfers for upper extremity reconstruction: a review of indications, techniques, and outcomes. *J Hand Surg Am*. 2013;38(12):2485-2490. doi:10.1016/J.JHSA.2013.03.041

270. Corona BT, Rivera JC, Owens JG, Wenke JC, Rathbone CR. Volumetric muscle loss leads to permanent disability following extremity trauma. *J Rehabil Res Dev*. 2015;52(7):785-792. doi:10.1682/JRRD.2014.07.0165

271. Carraro E, Rossi L, Maghin E, Canton M, Piccoli M. 3D in vitro Models of Pathological Skeletal Muscle: Which Cells and Scaffolds to Elect? *Front Bioeng Biotechnol*. 2022;10. doi:10.3389/FBIOE.2022.941623

272. Turner NJ, Badylak SF. Regeneration of skeletal muscle. *Cell Tissue Res*. 2012;347(3):759-774. doi:10.1007/S00441-011-1185-7

273. Karalaki M, Fili S, Philippou A, Koutsilieris M. Muscle regeneration: cellular and molecular events. *In Vivo*. 2009;23(5):779-796. Accessed June 14, 2023. https://pubmed.ncbi.nlm.nih.gov/19779115/

274. Vandusen KW, Syverud BC, Williams ML, Lee JD, Larkin LM. Engineered skeletal muscle units for repair of volumetric muscle loss in the tibialis anterior muscle of a rat. *Tissue Eng Part A*. 2014;20(21-22):2920-2930. doi:10.1089/TEN.TEA.2014.0060

275. Corona BT, Wenke JC, Ward CL. Pathophysiology of Volumetric Muscle Loss Injury. *Cells Tissues Organs*. 2016;202(3-4):180-188. doi:10.1159/000443925

276. Corona BT, Wu X, Ward CL, McDaniel JS, Rathbone CR, Walters TJ. The promotion of a functional fibrosis in skeletal muscle with volumetric muscle loss injury following the transplantation of muscle-ECM. *Biomaterials*. 2013;34(13):3324-3335. doi:10.1016/J.BIOMATERIALS.2013.01.061

277. Greising SM, Rivera JC, Goldman SM, Watts A, Aguilar CA, Corona BT. Unwavering Pathobiology of Volumetric Muscle Loss Injury. *Sci Rep*. 2017;7(1):1-14. doi:10.1038/s41598-017-13306-2

278. Liu J, Saul D, Böker KO, Ernst J, Lehman W, Schilling AF. Current Methods for Skeletal Muscle Tissue Repair and Regeneration. *Biomed Res Int*. 2018;2018. doi:10.1155/2018/1984879

279. Pantelic MN, Larkin LM. Stem Cells for Skeletal Muscle Tissue Engineering. *Tissue Eng Part B Rev*. 2018;24(5):373-391. doi:10.1089/TEN.TEB.2017.0451

280. Di Rocco G, Iachininoto MG, Tritarelli A, et al. Myogenic potential of adipose-tissue-derived cells. *J Cell Sci*. 2006;119(Pt 14):2945-2952. doi:10.1242/JCS.03029

281. Park JK, Ki MR, Lee EM, et al. Losartan improves adipose tissue-derived stem cell niche by inhibiting transforming growth factor-β and fibrosis in skeletal muscle injury. *Cell Transplant*. 2012;21(11):2407-2424. doi:10.3727/096368912X637055

282. Mizuno H. The Potential for Treatment of Skeletal Muscle Disorders with Adipose-Derived Stem Cells. *Curr Stem Cell Res Ther*. 2010;5(2):133-136. doi:10.2174/157488810791268573

283. Carlson ME, Conboy IM. Loss of stem cell regenerative capacity within aged niches. *Aging Cell*. 2007;6(3):371. doi:10.1111/J.1474-9726.2007.00286.X

284. Huang H, Liu J, Hao H, et al. Preferred M2 Polarization by ASC-Based Hydrogel Accelerated Angiogenesis and Myogenesis in Volumetric Muscle Loss Rats. *Stem Cells Int*. 2017;2017. doi:10.1155/2017/2896874

285. Mariani E, Lisignoli G, Borzì RM, Pulsatelli L. Biomaterials: Foreign Bodies or Tuners for the Immune Response? *Int J Mol Sci*. 2019;20(3). doi:10.3390/IJMS20030636

286. Chung L, Maestas DR, Housseau F, Elisseeff JH. Key players in the immune response to biomaterial scaffolds for regenerative medicine. *Adv Drug Deliv Rev*. 2017;114:184-192. doi:10.1016/J.ADDR.2017.07.006

287. Han WM, Jang YC, García AJ. Engineered matrices for skeletal muscle satellite cell engraftment and function. *Matrix Biology*. 2017;60-61:96-109. doi:10.1016/j.matbio.2016.06.001

288. Mizuno H. The potential for treatment of skeletal muscle disorders with adipose-derived stem cells. *Curr Stem Cell Res Ther*. 2010;5(2):133-136.

289. de la Garza-Rodea AS, van der Velde-van Dijke I, Boersma H, et al. Myogenic properties of human mesenchymal stem cells derived from three different sources. *Cell Transplant*. 2012;21(1):153-173. doi:10.3727/096368911X580554

290. Choi YS, Vincent LG, Lee AR, et al. The alignment and fusion assembly of adipose-derived stem cells on mechanically patterned matrices. *Biomaterials*. 2012;33(29):6943-6951. doi:10.1016/j.biomaterials.2012.06.057

291. STERN-STRAETER J, BONATERRA GA, JURITZ S, et al. Evaluation of the effects of different culture media on the myogenic differentiation potential of adipose tissue- or bone marrow-derived human mesenchymal stem cells. *Int J Mol Med*. 2014;33(1):160-170. doi:10.3892/ijmm.2013.1555

292. Di Rocco G, Iachininoto MG, Tritarelli A, et al. Myogenic potential of adipose-tissue-derived cells. *J Cell Sci*. 2006;119(Pt 14):2945-2952. doi:10.1242/jcs.03029

293. Park JK, Ki MR, Lee EM, et al. Losartan improves adipose tissue-derived stem cell niche by inhibiting transforming growth factor-β and fibrosis in skeletal muscle injury. *Cell Transplant*. 2012;21(11):2407-2424. doi:10.3727/096368912X637055

294. Heckmatt JZ, Leeman S, Dubowitz V. Ultrasound imaging in the diagnosis of muscle disease. *J Pediatr*. 1982;101(5):656-660. doi:10.1016/S0022-3476(82)80286-2

295. Riuzzi F, Beccafico S, Sagheddu R, et al. Levels of S100B protein drive the reparative process in acute muscle injury and muscular dystrophy. *Sci Rep*. 2017;7(1). doi:10.1038/S41598-017-12880-9

296. Kesireddy V. Evaluation of adipose-derived stem cells for tissue-engineered muscle repair construct-mediated repair of a murine model of volumetric muscle loss injury. *Int J Nanomedicine*. 2016;11:1461-1473. doi:10.2147/IJN.S101955

297. Schiaffino S, Rossi AC, Smerdu V, Leinwand LA, Reggiani C. Developmental myosins: Expression patterns and functional significance. *Skelet Muscle*. 2015;5(1):1-14. doi:10.1186/S13395-015-0046-6/FIGURES/1

298. Ciciliot S, Schiaffino S. Regeneration of mammalian skeletal muscle. Basic mechanisms and clinical implications. *Curr Pharm Des*. 2010;16(8):906-914. doi:10.2174/138161210790883453

299. d'ALBIS A, COUTEAUX R, JANMOT C, ROULET A, MIRA J -C. Regeneration after cardiotoxin injury of innervated and denervated slow and fast muscles of mammals. *Eur J Biochem*. 1988;174(1):103-110. doi:10.1111/J.1432-1033.1988.TB14068.X

300. Keren A, Tamir Y, Bengal E. The p38 MAPK signaling pathway: a major regulator of skeletal muscle development. *Mol Cell Endocrinol*. 2006;252(1-2):224-230. doi:10.1016/J.MCE.2006.03.017

301. Sharlo KA, Mochalova EP, Belova SP, Lvova ID, Nemirovskaya TL, Shenkman BS. The role of MAP-kinase p38 in the m. soleus slow myosin mRNA transcription regulation during short-term functional unloading. *Arch Biochem Biophys*. 2020;695:108622. doi:10.1016/J.ABB.2020.108622

302. Brennan CM, Emerson CP, Owens J, Christoforou N. p38 MAPKs - roles in skeletal muscle physiology, disease mechanisms, and as potential therapeutic targets. *JCI Insight*. 2021;6(12). doi:10.1172/JCI.INSIGHT.149915

303. Segalés J, Perdiguero E, Muñoz-Cánoves P. Regulation of Muscle Stem Cell Functions: A Focus on the p38 MAPK Signaling Pathway. *Front Cell Dev Biol*. 2016;4(AUG). doi:10.3389/FCELL.2016.00091

304. Urciuolo A, Quarta M, Morbidoni V, et al. Collagen VI regulates satellite cell self-renewal and muscle regeneration. *Nat Commun*. 2013;4(May). doi:10.1038/ncomms2964

305. Reed RK, Rubin K. Transcapillary exchange: Role and importance of the interstitial fluid pressure and the extracellular matrix. *Cardiovasc Res*. 2010;87(2):211-217. doi:10.1093/cvr/cvq143

306. Ceafalan LC, Popescu BO, Hinescu ME. Cellular Players in Skeletal Muscle Regeneration. *Biomed Res Int*. 2014;2014. doi:10.1155/2014/957014

307. Ardeljan AD, Hurezeanu R. Sarcopenia. *StatPearls*. Published online July 4, 2022.

308. Recovery from volumetric muscle loss injury: A comparison between young and aged rats | Elsevier Enhanced Reader. Accessed June 3, 2021. https://reader.elsevier.com/reader/sd/pii/S0531556516301954?token=D5A96EBADCAC40CC9752C95CD473E2C884106E03F1EB0479CB753BADD193BCB9C26DCAB03E6CEF07DB7CB62B6F294C1E&originRegion=us-east-1&originCreation=20210604033416

309. Olson LC, Redden JT, Gilliam LS, et al. Human Adipose-Derived Stromal Cells Delivered on Decellularized Muscle Improve Muscle Regeneration and Regulate RAGE and P38 MAPK. *Bioengineering*. 2022;9(9):426. doi:10.3390/BIOENGINEERING9090426/S1

310. Chen WJ, Lin IH, Lee CW, Chen YF. Aged Skeletal Muscle Retains the Ability to Remodel Extracellular Matrix for Degradation of Collagen Deposition after Muscle Injury. *Int J Mol Sci*. 2021;22(4):1-14. doi:10.3390/IJMS22042123

311. Van Der Lugt T, Weseler AR, Gebbink WA, Vrolijk MF, Opperhuizen A, Bast A. Dietary Advanced Glycation Endproducts Induce an Inflammatory Response in Human Macrophages in Vitro. *Nutrients*. 2018;10(12). doi:10.3390/NU10121868

312. Mulrennan S, Baltic S, Aggarwal S, et al. The role of receptor for advanced glycation end products in airway inflammation in CF and CF related diabetes. *Sci Rep*. 2015;5. doi:10.1038/SREP08931

313. Yang W, Hu P. Skeletal muscle regeneration is modulated by inflammation. *J Orthop Translat*. 2018;13:25-32. doi:10.1016/J.JOT.2018.01.002

314. Chapman MA, Mukund K, Subramaniam S, Brenner D, Lieber RL. Three distinct cell populations express extracellular matrix proteins and increase in number during skeletal muscle fibrosis. *Am J Physiol Cell Physiol*. 2017;312(2):C131-C143. doi:10.1152/AJPCELL.00226.2016

315. Yuen A, Laschinger C, Talior I, et al. Methylglyoxal-modified collagen promotes myofibroblast differentiation. *Matrix Biology*. 2010;29(6):537-548. doi:10.1016/J.MATBIO.2010.04.004

316. Sastourné-Arrey Q, Mathieu M, Contreras X, et al. Adipose tissue is a source of regenerative cells that augment the repair of skeletal muscle after injury. *Nature Communications 2023 14:1*. 2023;14(1):1-17. doi:10.1038/s41467-022-35524-7

317. Johnson CD, Zhou LY, Kopinke D. A Guide to Examining Intramuscular Fat Formation and its Cellular Origin in Skeletal Muscle. *J Vis Exp*. 2022;2022(183). doi:10.3791/63996

318. Loomis T, Hu LY, Wohlgemuth RP, Chellakudam RR, Muralidharan PD, Smith LR. Matrix stiffness and architecture drive fibro-adipogenic progenitors' activation into myofibroblasts. *Scientific Reports 2022 12:1*. 2022;12(1):1-15. doi:10.1038/s41598-022-17852-2

319. Kiran S, Dwivedi P, Kumar V, Price RL, Singh UP. Immunomodulation and Biomaterials: Key Players to Repair Volumetric Muscle Loss. *Cells*. 2021;10(8). doi:10.3390/CELLS10082016

320. Egawa T, Kido K, Yokokawa T, Fujibayashi M, Goto K, Hayashi T. Involvement of receptor for advanced glycation end products in microgravity-induced skeletal muscle atrophy in mice. *Acta Astronaut*. 2020;176:332-340. doi:10.1016/J.ACTAASTRO.2020.07.002

321. Yabuuchi J, Ueda S, Yamagishi S ichi, et al. Association of advanced glycation end products with sarcopenia and frailty in chronic kidney disease. *Sci Rep*. 2020;10(1). doi:10.1038/S41598-020-74673-X

322. Dalal M, Ferrucci L, Sun K, Beck J, Fried LP, Semba RD. Elevated serum advanced glycation end products and poor grip strength in older community-dwelling women. *J Gerontol A Biol Sci Med Sci*. 2009;64(1):132-137. doi:10.1093/GERONA/GLN018

323. Sincennes MC, Brun CE, Lin AYT, et al. Acetylation of PAX7 controls muscle stem cell self-renewal and differentiation potential in mice. *Nature Communications 2021 12:1*. 2021;12(1):1-15. doi:10.1038/s41467-021-23577-z

324. Kassar-Duchossoy L, Giacone E, Gayraud-Morel B, Jory A, Gomès D, Tajbakhsh S. Pax3/Pax7 mark a novel population of primitive myogenic cells during development. *Genes Dev*. 2005;19(12):1426. doi:10.1101/GAD.345505

325. Olguín HC, Pisconti A. Marking the tempo for myogenesis: Pax7 and the regulation of muscle stem cell fate decisions. *J Cell Mol Med*. 2012;16(5):1013-1025. doi:10.1111/J.1582-4934.2011.01348.X

326. Ustanina S, Carvajal J, Rigby P, Braun T. The myogenic factor Myf5 supports efficient skeletal muscle regeneration by enabling transient myoblast amplification. *Stem Cells*. 2007;25(8):2006-2016. doi:10.1634/STEMCELLS.2006-0736

327. Ansseau E, Laoudj-Chenivesse D, Marcowycz A, et al. DUX4c Is Up-Regulated in FSHD. It Induces the MYF5 Protein and Human Myoblast Proliferation. *PLoS One*. 2009;4(10):e7482. doi:10.1371/JOURNAL.PONE.0007482

328. Zammit PS, Carvajal JJ, Golding JP, et al. Myf5 expression in satellite cells and spindles in adult muscle is controlled by separate genetic elements. *Dev Biol*. 2004;273(2):454-465. doi:10.1016/J.YDBIO.2004.05.038

329. Musarò A, Cusella De Angelis MG, Germani A, Ciccarelli C, Molinaro M, Zani BM. Enhanced expression of myogenic regulatory genes in aging skeletal muscle. *Exp Cell Res*. 1995;221(1):241-248. doi:10.1006/excr.1995.1372

330. Zhang P, Li W, Wang L, et al. Salidroside inhibits myogenesis by modulating p-Smad3-induced Myf5 transcription. *Front Pharmacol*. 2018;9(MAR):209. doi:10.3389/FPHAR.2018.00209/BIBTEX

331. Riuzzi F, Sorci G, Sagheddu R, Chiappalupi S, Salvadori L, Donato R. RAGE in the pathophysiology of skeletal muscle. Published online 2018. doi:10.1002/jcsm.12350

332. Jang M, Oh SW, Lee Y, Kim JY, Ji ES, Kim P. Targeting extracellular matrix glycation to attenuate fibroblast activation. *Acta Biomater*. 2022;141:255-263. doi:10.1016/J.ACTBIO.2022.01.040

333. WADA R, YAGIHASHI S. Role of Advanced Glycation End Products and Their Receptors in Development of Diabetic Neuropathy. *Ann N Y Acad Sci*. 2005;1043(1):598-604. doi:10.1196/ANNALS.1338.067

334. Durieux J -J, Vita N, Popescu O, et al. The two soluble forms of the lipopolysaccharide receptor, CD14: Characterization and release by normal human monocytes. *Eur J Immunol*. 1994;24(9):2006-2012. doi:10.1002/eji.1830240911

335. Wei P, Dong M, Bi Y, et al. Identification and validation of a signature based on macrophage cell marker genes to predict recurrent miscarriage by integrated analysis of single-cell and bulk RNA-sequencing. *Front Immunol*. 2022;13:6770. doi:10.3389/FIMMU.2022.1053819/BIBTEX

336. Zhu ZB, Atkinson TP, Hovanky KT, et al. High prevalence of complement component C6 deficiency among African-Americans in the South-eastern USA. *Clin Exp Immunol*. 2001;119(2):305-310. doi:10.1046/J.1365-2249.2000.01113.X

337. Noer JB, Talman MLM, Moreira JMA. HLA class II histocompatibility antigen γ chain (CD74) expression is associated with immune cell infiltration and favorable outcome in breast cancer. *Cancers (Basel)*. 2021;13(24). doi:10.3390/CANCERS13246179/S1

338. Fang BA, Kovačević Ž, Park KC, et al. Molecular functions of the iron-regulated metastasis suppressor, NDRG1, and its potential as a molecular target for cancer therapy. *Biochimica et Biophysica Acta (BBA) - Reviews on Cancer*. 2014;1845(1):1-19. doi:10.1016/J.BBCAN.2013.11.002

339. Al Barashdi MA, Ali A, McMullin MF, Mills K. Protein tyrosine phosphatase receptor type C (PTPRC or CD45). *J Clin Pathol*. 2021;74(9):548. doi:10.1136/JCLINPATH-2020-206927

340. Yee CSK, Sanal O, Chou JS, et al. Coronin-1A Oligomerization Is Critical For Host Defense Against Viral Pathogens. *Journal of Allergy and Clinical Immunology*. 2014;133(2):AB94. doi:10.1016/j.jaci.2013.12.351

341. Aoki M, Aoki H, Ramanathan R, Hait NC, Takabe K. Sphingosine-1-Phosphate Signaling in Immune Cells and Inflammation: Roles and Therapeutic Potential. *Mediators Inflamm*. 2016;2016. doi:10.1155/2016/8606878

342. Chen W, Wang W, Sun X, et al. NudCL2 regulates cell migration by stabilizing both myosin-9 and LIS1 with Hsp90. *Cell Death & Disease 2020 11:7*. 2020;11(7):1-15. doi:10.1038/s41419-020-02739-9

343. Liao H, Zakhaleva J, Chen W. Cells and tissue interactions with glycated collagen and their relevance to delayed diabetic wound healing. Published online 2009. doi:10.1016/j.biomaterials.2008.11.038

344. Gerhard GS, Hanson A, Wilhelmsen D, et al. AEBP1 expression increases with severity of fibrosis in NASH and is regulated by glucose, palmitate, and miR-372-3p. *PLoS One*. 2019;14(7). doi:10.1371/JOURNAL.PONE.0219764

345. Posey KL, Coustry F, Hecht JT. Cartilage oligomeric matrix protein: COMPopathies and beyond. *Matrix Biol*. 2018;71-72:161. doi:10.1016/J.MATBIO.2018.02.023

346. Szafran BN, Borazjani A, Scheaffer HL, et al. Carboxylesterase 1d Inactivation Augments Lung Inflammation in Mice. *ACS Pharmacol Transl Sci*. 2022;5(10):919-931. doi:10.1021/ACSPTSCI.2C00098/ASSET/IMAGES/LARGE/PT2C00098_0008.JPEG

347. Holmberg J, Durbeej M. Laminin-211 in skeletal muscle function. *Cell Adh Migr*. 2013;7(1):111-121. doi:10.4161/cam.22618

348. Liu L, Daniel AB, James AB, et al. Comparative label-free mass spectrometric analysis of temporal changes in the skeletal muscle proteome after impact trauma in rats. *Am J Physiol Endocrinol Metab*.

2020;318(6):E1022-E1037. doi:10.1152/AJPENDO.00433.2019/ASSET/IMAGES/LARGE/ZH10052083430008.JPEG

349. Lee EJ, Ahmad SS, Lim JH, et al. Interaction of fibromodulin and myostatin to regulate skeletal muscle aging: An opposite regulation in muscle aging, diabetes, and intracellular lipid accumulation. *Cells*. 2021;10(8):2083. doi:10.3390/CELLS10082083/S1

350. Yin H, Cui C, Han S, et al. Fibromodulin Modulates Chicken Skeletal Muscle Development via the Transforming Growth Factor-β Signaling Pathway. *Animals (Basel)*. 2020;10(9):1-11. doi:10.3390/ANI10091477

351. Stenina-Adognravi O, Plow EF. Thrombospondin-4 in tissue remodeling. *Matrix Biol*. 2019;75-76:300. doi:10.1016/J.MATBIO.2017.11.006

352. Tomarev SI, Nakaya N. Olfactomedin Domain-Containing Proteins: Possible Mechanisms of Action and Functions in Normal Development and Pathology. *Mol Neurobiol*. 2009;40(2):122. doi:10.1007/S12035-009-8076-X

353. Noriega B, Zenker D;, Croes HE;, et al. Receptor Mediated Effects of Advanced Glycation End Products (AGEs) on Innate and Adaptative Immunity: Relevance for Food Allergy. *Nutrients 2022, Vol 14, Page 371*. 2022;14(2):371. doi:10.3390/NU14020371

354. Janelle-Montcalm A, Boileau C, Poirier F, et al. Extracellular localization of galectin-3 has a deleterious role in joint tissues. *Arthritis Res Ther*. 2007;9(1):R20. doi:10.1186/AR2130

355. Cerri DG, Rodrigues LC, Alves VM, et al. Endogenous Galectin-3 is Required for Skeletal Muscle Repair. *bioRxiv*. Published online October 1, 2020:2020.10.01.322461. doi:10.1101/2020.10.01.322461

356. Ji X, Jiang X, Yang F, Yu J, Xue M, Bao Z. Galectin-3 regulates skeletal muscle loss via TGFβ1-Smad2/3 signaling activation in mice. *Archives of Medical Science*. Published online March 26, 2023. doi:10.5114/AOMS/161626

357. Palanissami G, Paul SFD. RAGE and Its Ligands: Molecular Interplay Between Glycation, Inflammation, and Hallmarks of Cancer—a Review. *Hormones and Cancer 2018 9:5*. 2018;9(5):295-325. doi:10.1007/S12672-018-0342-9

358. Paliwal P, Pishesha N, Wijaya D, Conboy IM. Age dependent increase in the levels of osteopontin inhibits skeletal muscle regeneration. *Aging*. 2012;4(8):553-566. doi:10.18632/AGING.100477

359. Herwig N, Belter B, Wolf S, Haase-Kohn C, Pietzsch J. Interaction of extracellular S100A4 with RAGE prompts prometastatic activation of A375 melanoma cells. *J Cell Mol Med*. 2016;20(5):825. doi:10.1111/JCMM.12808

360. Engler AJ, Griffin MA, Sen S, Bönnemann CG, Sweeney HL, Discher DE. Myotubes differentiate optimally on substrates with tissue-like stiffness: Pathological implications for soft or stiff microenvironments. *Journal of Cell Biology*. 2004;166(6):877-887. doi:10.1083/jcb.200405004

361. Boontheekul T, Hill EE, Kong HJ, Mooney DJ. Regulating Myoblast Phenotype Through Controlled Gel Stiffness and Degradation. *Tissue Eng*. 2007;13(7):1431-1442. doi:10.1089/ten.2006.0356

362. Kim EY, Dryer SE. RAGE and αVβ3-integrin are essential for suPAR signaling in podocytes. *Biochimica et Biophysica Acta (BBA) - Molecular Basis of Disease*. 2021;1867(10):166186. doi:10.1016/J.BBADIS.2021.166186

363. Raucci A, Cugusi S, Antonelli A, et al. A soluble form of the receptor for advanced glycation endproducts (RAGE) is produced by proteolytic cleavage of the membrane-bound form by the sheddase a disintegrin and metalloprotease 10 (ADAM10). *The FASEB Journal*. 2008;22(10):3716-3727. doi:10.1096/FJ.08-109033

364. González-Maeso J, Sealfon SC. Hormone Signaling Via G Protein–Coupled Receptors. *Endocrinology: Adult and Pediatric, Sixth Edition*. 2010;1:83-105. doi:10.1016/B978-1-4160-5583-9.00005-8

365. Abaricia JO, Shah AH, Olivares-Navarrete R. Substrate stiffness induces neutrophil extracellular trap (NET) formation through focal adhesion kinase activation. *Biomaterials*. 2021;271:120715. doi:10.1016/j.biomaterials.2021.120715

366. Ko P, Kim D, You E, et al. Extracellular Matrix Rigidity-dependent Sphingosine-1-phosphate Secretion Regulates Metastatic Cancer Cell Invasion and Adhesion. *Sci Rep*. 2016;6. doi:10.1038/SREP21564

367. Serra M, Saba JD. Sphingosine 1-phosphate lyase, a key regulator of sphingosine 1-phosphate signaling and function. *Adv Enzyme Regul*. 2010;50(1):349. doi:10.1016/J.ADVENZREG.2009.10.024

Vita

Lucas Christian Olson was born on March 16, 1994 in Rockford, Illinois. He moved to Montpelier, VA in 1998, and has been in the Greater Richmond Virginia area ever since. He graduated from Patrick Henry High School in 2012. He earned his Bachelors of Science in Biomedical Engineering from Virginia Commonwealth University in Richmond, Virginia in 2016. He earned his Masters of Science in Gerontology from Virginia Commonwealth University in Richmond, Virginia in 2022. He is receiving a Doctor of Philosophy in Biomedical Engineering from Virginia Commonwealth University in 2022.